K. Sato • Y. Iwasa (Eds.)

Groundwater Hydraulics

Springer

Springer Japan KK

Kuniaki Sato, Yoshiaki Iwasa (Eds.)

Groundwater Hydraulics

With 132 Figures

Springer

Kuniaki Sato
Professor
Geosphere Research Institute, Saitama University
255, Shimo-Okubo, Sakura-ku,
Saitama 338-8570, Japan

Yoshiaki Iwasa
President
Institute of Earth Science and Technology
3-1-14, Kitahama, Chuo-ku,
Osaka 541-0041, Japan

ISBN 978-4-431-67966-0 ISBN 978-4-431-53959-9 (eBook)
DOI 10.1007/978-4-431-53959-9

Printed on acid-free paper

Originally published by Springer-Verlag Tokyo Berlin Heidelberg New York in 2000

springeronline.com

SPIN: 11527541

PREFACE

Subsurface water constitutes an essential part of the hydrological cycle in nature and plays an important role in water-resources management. Numerical methods have advanced rapidly in groundwater hydrology and hydraulics, and a basic knowledge of groundwater and modeling elements is required for researchers and engineers to solve the problems they face.

This book contains the essentials of groundwater hydraulics: properties of porous media and aquifers, mathematical modeling of isothermal and thermal groundwater flow, hydraulic dispersion and two-phase flow in coastal aquifers, numerical methods, groundwater investigation, and management of groundwater resources — all of which one needs in order to become a real specialists. Examples and exercises are provided at the end of each chapter to reinforce and review the material that has just been presented creating a textbook for students and engineers. Readers, who want more advanced information, can refer to the recommended technical sources.

Several fields of science and technology are related to or concerned with groundwater: geohydrology or hydrogeology for a macroscopic view of the hydrological cycle and geography, groundwater hydraulics based on engineering dynamics, fluid dynamics in porous media, and soil physics in agriculture.

With the increased public awareness of environmental problems, including soil and groundwater pollution and contamination much attention has been directed to remedying the problems of polluted soil and aquifers. The quality of subsurface water thus has become more relevant.

This commemorative publication has been made possible through the efforts of the Local Organizing Committee, the International Symposium 2000 on Groundwater, IAHR (International Association for Hydraulic Engineering and Research), at Omiya Sonic City, Saitama, Japan, May 8-10, 2000.

The members of the LOC played a very active role in the publication of this book. The editiors also thank Dr. S. A. Bories, directeur émérite de recherche, Institut de Mecanique des Fluides de l'Institut National Polytechnique de Toulouse, France, and Dr. Vu Thanh Ca, Associate professor, Marine Hydrometeorological Center, Vietnam for their support as members of the Committee on Groundwater Hydraulics and IAHR.

November 17, 2003
Kuniaki Sato
Yoshiaki Iwasa
Editors

EDITORIAL COMMITTEE

LIST OF CONTRIBUTORS

Chapter 1: Masaru Morita (Professor, Shibaura Institute of Technology)
Kuniaki Sato (Professor, Saitama University)
Chapter 2: Kuniaki Sato (Professor, Saitama University)
Takayuki Ueno, Dr. Eng. (Obayashi Corporation, Japan)
Chapter 3: Satoru Sugio (Professor, Miyazaki University, Japan)
Kenji Jinno (Professor, Kyushu University, Japan)
Chapter 4: Teruyuki Fukuhara (Professor, Fukui University)
Kuniaki Sato (Professor, Saitama University)
Chapter 5: Takeshi Kawatani (Professor, Kobe University)
Kenji Jinno (Professor, Kyushu University)
Chapter 6: Noriharu Miyake, Dr. Sci. (Shimizu Corporation)
Michiji Tsurumaki, Dr. Sci. (Japan Research Institute of Groundwater Physico-chemistry)
Toichiro Maekawa (Kokusai Kogyo Co., Ltd.)
Kuniaki Sato (Professor, Saitama University)
Chapter 7: Masaru Ojima (Professor, Fukuyama University)
Kuniaki Sato (Professor, Saitama University)
Toshiaki Hirayama (Kokusai Kogyo Co., Ltd.)
Exercises: Takashi Kitagawa, Dr. Eng. (Nishimatsu Construction Co., Ltd.)
Masaru Morita (Professor, Shibaura Institute of Technology)

The Editors

KUNIAKI SATO

	Born 1940, Hiroshima, Japan
Education:	Osaka University, Faculty of Engineering; Dr. Eng.
Present Status:	Professor, Geosphere Research Institute, Saitama University, Japan
Area of Specialization:	Groundwater Hydraulics and Underground Space Technology
Publications:	*Underground Space* (Japan Society of Civil Engineers); *Groundwater Updates* (Springer-Verlag); *Hydraulics in the Subsurface* (Maruzen)

YOSHIAKI IWASA

	Born 1928, Kyoto, Japan
Education:	Kyoto University, Faculty of Engineering; Dr. Eng.
Present Status:	President, Institute of Earth Science and Technology; Professor Emeritus, Kyoto University, Japan
Area of Specialization:	Open-Channel Hydraulics and River Engineering
Publications:	*Hydraulics* (Asakura Publishing); *New River Engineering* (Morikita Shuppan); *Numerical Hydraulics of Open-Channel Flows* (Maruzen); *Engineering Aspects of Lakes* (Morikita Shuppan)

Contents

1

Introduction to Groundwater and Aquifer System

Summary

All water below ground is called groundwater or subsurface water. Groundwater lies in both saturated and unsaturated states in strata and soils, and its movement is slow. Groundwater originates from precipitation (e.g., rainfall and snow) as a process of natural recharge in the hydrologic cycle.

In this chapter, first the physical properties of water are reviewed as fundamentals of groundwater hydraulics. Then, the concepts of porous media and flow characteristics of groundwater are introduced as models. The state of the soil moisture, aquifer systems, the system of groundwater in the hydrologic cycle, and the definition of terms in groundwater are reviewd.

1.1 Groundwater

Groundwater generally encompasses liquid and vapor-phase water in voids below the ground surface and namely originates from rainfall infiltration in the hydrologic cycle. Groundwater is distinctive from surface water in the following respects:

1. Groundwater exists in voids in the subsurface and its movement is very slow.
2. Pore geometry, soil or rock fracture, surface tension, and flow resistance fundamentally affect groundwater movement, both in saturated and unsaturated conditions.
3. Topographic and geologic structures strictly govern groundwater flows.
4. Soil, stratum, rock mineral, and geothermal conditions exert a great influence on the chemical properties of groundwater.

The Earth, an aquatic planet, has fresh and salt water in the atmosphere, land, and oceans. Land water, to which groundwater belongs, is distributed in soil, rivers, lakes, and polar ice. Water and solar radiation are the most important factors affecting the Earth's ecosystem. Groundwater is the subject of study in several science and

K. Sato et al. (eds.), *Groundwater Hydraulics*

technology fields, including hydrology, soil science, hydraulics, and soil engineering. Groundwater hydraulics from the dynamics viewpoint, especially fluid dynamics in porous media, is discussed in this book.

1.2 Units

All hydraulic phenomena of groundwater are described by physical quantities such as soil porosity and particle size (geometric structure), gravity and interfacial tension (driving forces in groundwater flow), viscosity and density (fluid properties), and temperature and pressure (the groundwater physical environment).

Table 1.1. SI units in groundwater hydraulics

	Physical quantities	Names	Units	Dimensions (absolute system)
Fundamental units	Length	meter	m	[L]
	Mass	Kilogram	kg	[M]
	Time	Second	s	[T]
	Absolute temperature	Kelvin	K	[Non-dimensional]
	The ampere (A), mole, and candela (cd) are included in the SI (International System of units.)			
Derived units	Force	Newton [N]	1N 1kg m/s^2	[ML T^{-2}]
	Pressure and stress	Pascal (Pa)	1Pa 1N/m^2	[ML^{-1}T^{-2}]
	Work and energy	Joule (J)	1J 1N· m	[ML^{2}T^{-2}]
	Power	Watt (W)	1W 1J/s	[ML^{2}T^{-3}]
Engineering units:	Engineers often use weight kilogram (kgf) in place of the mass kilogram in SI Units. The weight kilogram is defined as the gravitational force acting on a body of 1kilogram mass under the standard gravitational acceleration (g = 9.80665 m/s^2). [1kgf =1kg × 9.81m/s^2 = 9.81N]. The dimension in absolute units can be rewritten as [F]= [MLT^{-2}].			
Multiple symbols in SI units:	G (giga) = 10^9, M (mega) = 10^6, k (kilo) = 10^3, h (hecto) = 10^2, c (centi) = 10^{-2}, m (milli) = 10^{-3}, μ (micro)= 10^{-6}			

The quantities that describe phenomena in mechanics are referred to as physical quantities. These physical quantities are classified into two categories: fundamental quantities and derived quantities. The latter are derived from and expressed in terms of the fundamental quantities: length [L], mass [M], and time [T]. These are measured in the absolute or physical unit system. In the engineering field, the system of length [L], time [T], and force [F] is sometimes convenient to describe phenomena. The system using force [F] instead of mass [M] is termed the gravitational unit

system or the engineering unit system. **Table 1.1** shows physical quantities with dimensions and units.

For the subject of groundwater hydraulics, water originating outside the hydrologic cycle, e.g., fossil water and magma water, is conventionally excluded.

1.3 Physical Properties of Water

Table 1.2. Physical properties of water

	Definition and conventional symbols	Formulation and Properties	Units	
			SI units	Gravitational units
Density	Density (ρ) is defined as mass per unit volume.	(a) ρ and γ vary with temperature and pressure	kg/m^3	$kgf \cdot s^2/m^4$
Unit weight	Unit weight (γ) is the weight of unit volume of fluid.	(b) $\gamma = \rho g$, where g = acceleration due to gravity	N/m^3	kgf/m^3
Specific weight	Specific weight (s) is the ratio of density (ρ) to reference density (ρ_0) at 4°C under standard atmospheric pressure.	(c) $s = \rho/\rho_0 = \gamma/\gamma_0$	Non-dimensional	Non-dimensional
Viscosity	Viscosity (μ) is a fluid property that relates fluid shear stress to spatial rate of change in the velocity field, and is expressed as: $\tau = \mu \times (du/dy)$	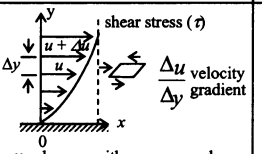 μ : changes with pressure and temperature	$N \cdot m^{-2} \cdot s$ (or $Pa \cdot s$)	$kgf \cdot m^{-2} \cdot s$
Kinematic viscosity	Kinematic viscosity (ν) = μ/ρ		m^2/s	m^2/s
Surface tension	Surface tension (σ) exists in the interface between two fluids as a result of molecular attraction. It is balanced by the internal pressure difference (Δp) as shown by the Laplace equation: $\Delta p = \sigma(1/R_1 + 1/R_2)$	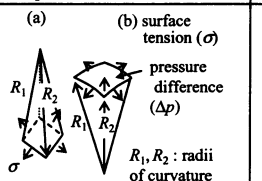 surface tension (σ) depends on temperature and fluid properties	N/m	kgf/m
Capillarity	Capillarity is the result of cohesion between different substances. Capillary rise or height of water (h_c) is given as: $h_c = (4\sigma\cos\theta)/\rho g d$	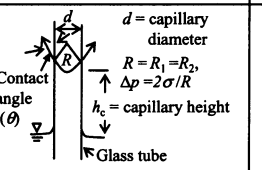	m	m
Compressibility	For a pressure increment (Δp) on an original volume (V), compressibility (β) is defined as: $\beta = -(1/V)\,\Delta V/\Delta p$, and bulk modulus ($E$) = $1/\beta$	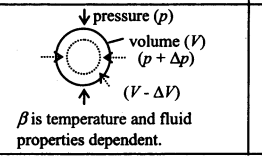 β is temperature and fluid properties dependent.	m^2/N N/m^2	m^2/kgf kgf/m^2

The physical properties of water are quantitatively described by density, viscosity, surface tension (or interfacial tension), and compressibility. Depending on temperature and pressure, water exists in three phases: solid, liquid, and gas. The physical properties of water (G), as shown in **Table 1.2**, are expressed as a function of temperature and pressure:

$$G = G(T, p) \tag{1.1}$$

Density (ρ) is defined as the mass of a substance per unit volume and is measured in kg/m^3 in SI units or in $kgf \cdot s^2/m^4$ in engineering units. The highest water density is 1000.0 kg/m^3 at 4 °C and 1 atmosphere (atm). For a different condition, e.g., 20 °C and 1 atm, the density is 998.2 kg/m^3. Weight per unit volume is a quantity generally called the unit weight and denoted by γ ($\gamma = \rho g$, g: acceleration of gravity). The specific weight of a substance (a non-dimensional quantity) is the ratio of its density (ρ) to that of water at 4 °C and 1 atm (ρ_0).

The surface tension (σ) is defined as the tangential force on a gas–liquid interface or immiscible liquid–liquid interface as a result of molecular attractions. The dimension of the surface tension is F/L (F = force and L = length). The surface tension balances in itself as the interface geometry becomes flat. This force is balanced by the pressure difference (Δp) between the two sides of the curved interface, conforming to Laplace's equation or Plateau's equation given in **Table 1.2**. The pressure balance with surface tension is expressed as $\Delta p = 2\sigma/R$ for a spherical interface, where $R_1 = R_2 = R$.

Consider a vertical standing glass tube in a water tub. In this case, the surface tension between water and air is in equilibrium with the weight of the raised water column in the tube. Thus, the atmospheric pressure equals the water column weight and surface tension components. With mercury in the capillary tube, the interface is convex upwards, indicating a larger mercury pressure than atmospheric pressure. This phenomenon is called capillarity and is explained by Jurin's principle: the equilibrium between the surface tension by curvature and adhesion by molecular attraction of glass (solid) and water (liquid). The contact angle depends on the temperature and pressure of the environment and the properties of the solid and fluids (liquid and gas). In a capillary tube with diameter d, as shown in **Table 1.2**, capillary rise (h_c) is expressed using Laplace's equation as $h_c = (4\sigma/\rho g)(\cos\theta/d)$. Thus, the capillary rise is directly proportional to $\sigma \cos\theta$ and inversely proportional to tube diameter (d).

Consider the compressibility of a liquid with initial pressure (p) and volume (V). If its pressure is increased by Δp at constant temperature, the different pressure and volume will be ($p+\Delta p$) and ($V+\Delta V$), respectively. In this case, compressibility (β) is defined as: $\beta = -(1/V)(\Delta V/\Delta p)$. The reciprocal of compressibility is called the bulk modulus ($E = 1/\beta$). This definition of compressibility is applicable to the gas phase also, but the compressibility of gases is larger than that for liquids. The compressibility for liquid water is 4.5×10^{-10} m^2/N ($E = 2.2 \times 10^9$ N/m^2) at 20 °C and 1 atm pressure. For example, a pressure change of 10 atm for water at the same temperature results in only a 0.046% change in volume. Thus, the compressibility of water is usually negligible for fluid flows in rivers and the ocean; in these cases, water is

assumed to be an incompressible fluid. However, compressibility should be taken into account for groundwater flow in confined aquifers, as will be discussed later.

In addition to the above-mentioned physical properties of water, the viscosity is an important dynamic property. The velocity distribution for water flow along a horizontal plane is shown in **Table 1.2**. Velocity at the wall is zero, increasing with distance from the wall. The distribution is the result of viscous shear stress in the fluid. The viscous shear stress (τ) is proportional to the velocity gradient (du/dy), according to Newton's law of viscosity [$\tau = \mu\, du/dy$, where μ = the dynamic coefficient of viscosity and $u(y)$ = fluid velocity in the x-direction as a function of the normal distance from the wall].

The coefficient of viscosity is strongly dependent on temperature, and decreases with increasing temperature for most liquids. The coefficient of viscosity is expressed in another way as $\nu = \mu/\rho$ which is known as kinematic viscosity (e.g., $\nu = 1.004 \times 10^{-6}\ \mathrm{m^2/s}$ at the ordinary temperature 20 °C and standard atmospheric pressure).

1.4 Porous Media and Groundwater Flow

Groundwater exists within subsurface voids in both saturated and unsaturated conditions. Macroscopically, groundwater is a portion of inland water flowing into the ocean in the hydrologic cycle. In this section, porous media are discussed as the field/vessel of groundwater flow.

1.4.1 Porous Media

1.4.1 (a) Geometric Structure

Aquifers and rock masses are assumed to be porous media with void spaces and solid matrix in the groundwater flow field. **Figure 1.1** shows several types of porous media classified with respect to interstices and porosity. From the viewpoint of void structure, the figure shows media with (a) interconnected pores (interconnected pore system), (b) non-interconnected dispersed pores (non-interconnected pore system), and (c) both interconnected and non-interconnected pores coexisting. These three types of porous media correspond to, for example, sand and gravel aquifers, porous rock masses such as volcanic rocks, and hard rock masses with fractures respectively. Groundwater flow or mass transport generally takes place through porous media with interconnected void systems as in (a) and (c).

A porous medium (PM) is defined in using set theory as shown below.

$$\mathrm{PM}\{S, V\} = S(s_1, s_2, s_3, \ldots) \cup V(v_1, v_2, v_3, \ldots)$$
$$s \in S, \quad v \in V$$

where, S = solid portion, $s_1, s_2, s_3, \ldots$ = solid element, V = void portion, $v_1, v_2, v_3, \ldots$ = void element, $\cup$ and $\in$ = symbols representing "union" and "belongs to" in set theory (Smullyan and Fitting, 1996).

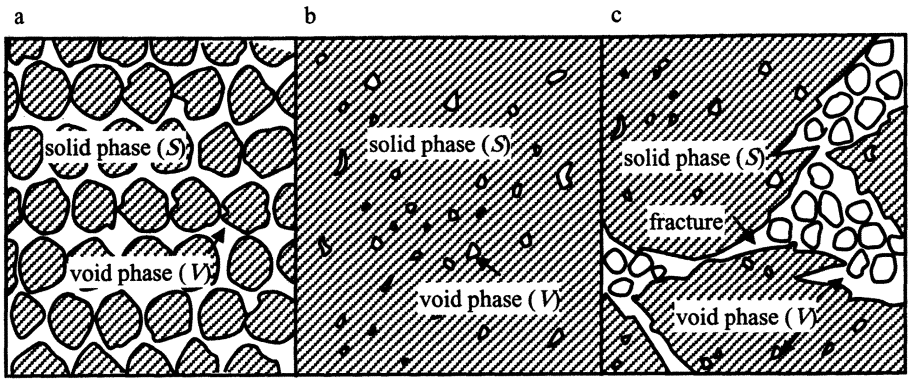

Fig. 1.1 a–c. Pore systems in porous media (A. E. Scheidegger, 1960)

The complementary set (S^c) of the solid portion (S) corresponds to the void portion (V) and (a) the interconnected pore system reversibly changes to (b) the non-interconnected pore system if S and V are interchanged.

1.4.1 (b) Continuum Model and Scaling

Topographic and geologic knowledge are important in the study of groundwater flow. The spatial scale of groundwater flow generally ranges from hundreds of meters for relatively small flow in a local area to several hundreds of kilometers for the flows in topographic units such as plains, alluvial fans, and mountains. Groundwater flow fields, such as geologic formations and rock masses, are considered as porous media from the microscopic viewpoint, although they are essentially anisotropic and inhomogeneous because of their geological history of strata formation. Thus, groundwater hydraulics deals with groundwater flows from the topographic and geologic standpoints, and helps in understanding hydrodynamic mechanics, as stated below.

Consider a spherical soil sample with radius r around a point P with porosity n as a physical characteristic within a porous medium, as shown in **Fig. 1.2**. A volume of porous medium is called *representative elementary volume* (REV). If the radius of the REV is smaller than the diameter of the soil particles (d), then the REV will include a portion of a soil particle. Otherwise, porosity (n) fluctuates with the number of particles in the REV for $r > d$. Furthermore, the porosity statistically approaches a constant value for a large number of particles ($r \gg d$). Thus a porous medium is not microscopically homogeneous for a small number of particles within the REV, but it becomes homogeneous with constant porosity for larger numbers of particles.

The continuum approach to porous media assumes homogeneity in microscopically complicated void structures to simplify its description. This approach makes it easier to mathematically describe porous media phenomena. Porous media with a REV radius $r > r_{max}$ can be treated on the scale of geology.

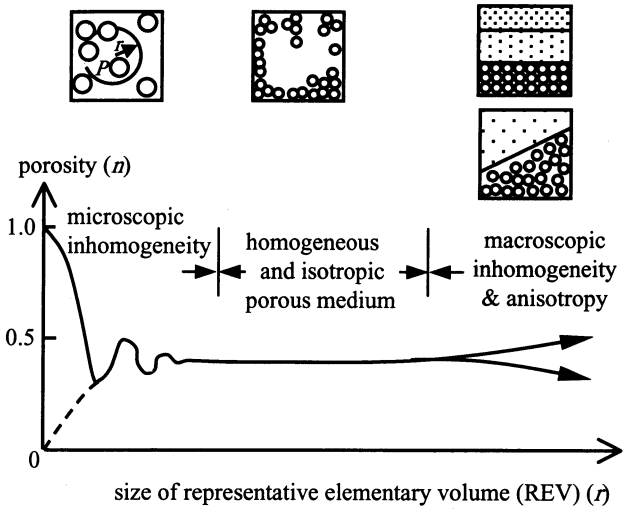

Fig. 1.2. Size of representative elementary volume (REV) and porosity

A continuum model of porous media is defined with porosity $n(r)$, which is one of its physical characteristics (Bear, 1979).

$$\frac{dn(r)}{dr} = 0, \quad r_{\min} < r < r_{\max}$$
$$\frac{dn(r)}{dr} < 0, \quad \frac{dn(r)}{dr} > 0 \quad (0 < r \leq r_{\min} \text{ or } r > r_{\max}) \tag{1.2}$$

Mathematical modeling of groundwater flow is based on the continuum model of porous media.

The REV scale can be extended to macroscopic geologic formations as the groundwater flow field, as depicted on the right hand side of **Fig. 1.2**. Anisotropy and heterogeneity are discussed as macroscopic properties of formations on the geologic scale. The actual stratum is heterogeneous, and porous medium properties such as hydraulic conductivity are direction dependant for a large REV radius. If the properties are direction dependant, then the media or flow fields are called anisotropic. Groundwater flow and transport modeling in porous media are inevitably based on the continuum approach.

1.5 Averaged Properties of Porous Media

Geologic formations and void spaces in soil and rock masses have complicated geometrical structures. Thus, microscopic discussion of pore space geometry and flow mechanism is not always realistic and practical in engineering terms. Consequently, it is advantageous to model groundwater and percolation flows with averaged properties.

Figure 1.3 conceptually shows the definitions of the averaged properties with respect to pore space and the solid, liquid, and gas phases among others. Porosity (n = void volume/ total volume) and void ratio (e = void volume/ solid volume) are principal properties of porous media. In an ideal porous medium packed with spherical particles, porosity ranges from 25.95%–47.6%.

The dry density (ρ_d) is another property of porous media. Because it includes the void space, values are smaller than for solid density. Water content (θ) and saturation degree (S) represent porous medium properties in wet conditions for water and air occupying the void space.

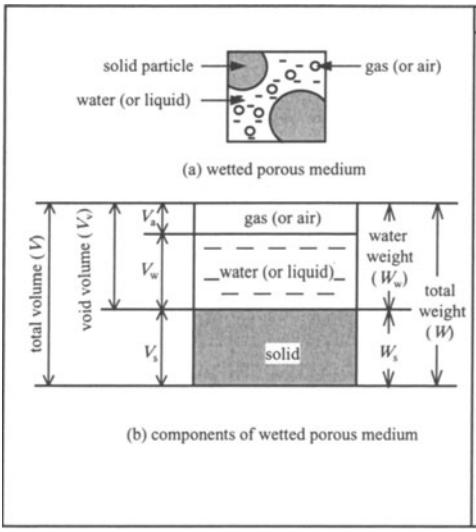

Properties	Definition
porosity (n)	$n = \frac{\text{volume of void}}{\text{total volume}} = \frac{V_v}{V} = \frac{V - V_s}{V} = 1 - \frac{V_s}{V}$ $(0 < n < 1.0)$
void ratio (e)	$e = \frac{\text{volume of void}}{\text{volume of solid}} = \frac{V_v}{V_s}$ $(0 < e)$
volumetric water content (θ)	$\theta = \frac{\text{volume of water (or liquid)}}{\text{total volume}} = \frac{V_w}{V}$ where, $(0 < \theta < 1.0)$
moisture content (w)	$w = \frac{\text{weight of water (or liquid)}}{\text{weight of solid}} = \frac{W_w}{W_s}$
degree of saturation (S)	$S = \frac{\text{volume of water (or liquid)}}{\text{volume of void}} = \frac{V_w}{V_v}$ where, $(0 < V_w < V_v)$
relationship between n and θ	$S = \frac{V_w}{V_v} = \frac{V}{V_v} \cdot \frac{V_w}{V} = \frac{\theta}{n}$
wetted density (ρ_w)	$\rho_w = \frac{W}{V}$
dry density (ρ_d)	$\rho_d = \frac{W_s}{V}$

Fig. 1.3. Properties of porous media

The volumetric water content, often used in groundwater hydraulics, is defined as the ratio of volume of water in the void space to the porous medium volume. Moisture content (w) is the ratio of water weight to the weight of solid.

1.6 Soil Water and Driving Forces for Groundwater Flow

The soil moisture condition (i.e., the moisture content) changes with depth. A typical cross-sectional view of soil moisture distribution and its environment are shown in **Fig. 1.4**.

Groundwater fills the void/pore space in the soil layer and geologic formations in saturated and unsaturated conditions. The soil water zone, usually unsaturated, is the transmission zone or cushion zone between the ground surface and subsurface water and is strongly influenced by the weather and climatic conditions and it brings up

also rootwater supply to vegetation, microbes, and microscopic animals in the soil. The moisture content in the soil water zone increases with rainfall infiltration and decreases with evapotranspiration. This zone plays an important role in rainwater recharge to unconfined aquifers.

An intermediate zone exists between the soil water zone and the capillary fringe. Voids in the intermediate zone are mainly occupied by pendular and funicular typed water. Surface tension balances the gravity force in funicular water. This is a cushion zone through which rainwater in the soil water zone flows down to unconfined groundwater. An unconfined groundwater table with a free surface exists in the saturated zone, and is connected to the atmosphere through the void space in the unsaturated zone. The free surface varies with the water table gradient.

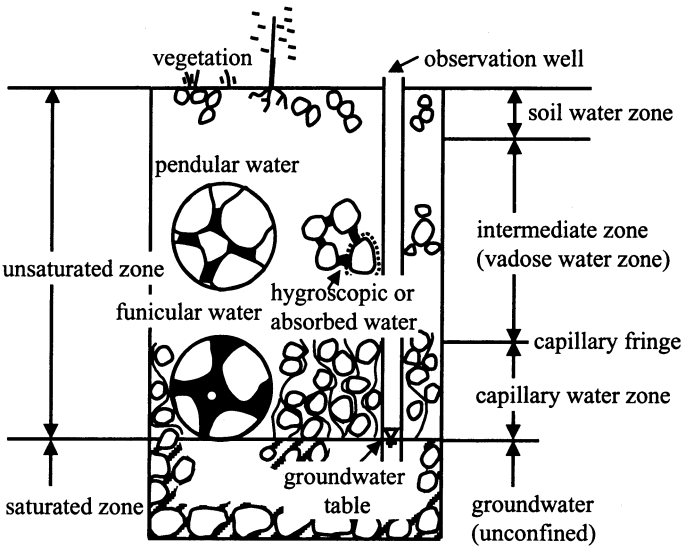

Fig. 1.4. Vertical groundwater profile

The classification of moisture distribution mentioned above is fundamental to groundwater flow and infiltration studies. The soil moisture and its movement are discussed next.

Figure 1.5 shows qualitative relationships between water content (pendular, funicular and saturated cases) and driving forces (surface tension, gravity and pressure head). In areas of low moisture content, pore water is held in contact with soil particles forming liquid islands around the particles. Surface tension plays the dominant role in moisture movement. The liquid islands diminish and air bubbles appear in the pore space as moisture content increases. The influence of surface tension gradually weakens and gravity and pressure head mainly drive water movement. As the water content increases to the saturation value, surface tension has no significant influence on water movement. Thus, surface tension is the major governing force in low

moisture content environments, whereas gravity and pressure head are dominant in saturated conditions. This fact is important to the understanding of groundwater flow modeling and the approach to defining driving forces is important in groundwater flow dynamics. Groundwater hydraulics originated with the study of saturated flow, and as science progressed, the study of unsaturated flow was incorporated.

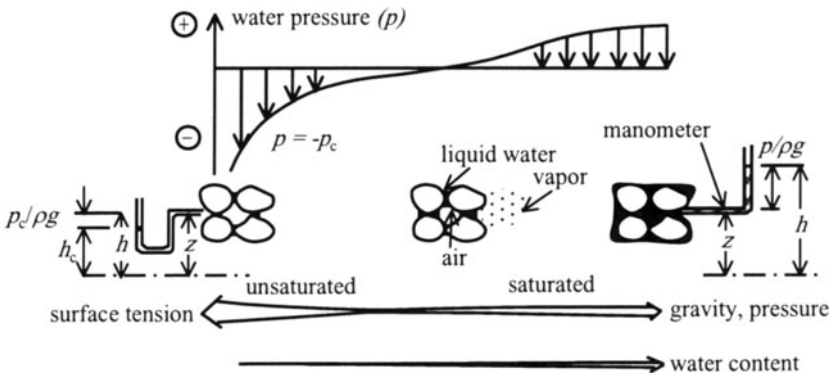

Fig. 1.5. Water content and its driving forces. z, elevation; h, water head; h_c, capillary head; p_c, capillary pressure (negative); $\gamma = \rho g$ = unit weight of water

1.7 Groundwater and Aquifers

Natural topographic and geologic systems control the occurrence of groundwater. Thus, groundwater has various types in flow systems based on the topographic and geologic conditions. **Figure 1.6** shows a typical groundwater system with aquifers and aquicludes maintained by natural recharge. The groundwater flow field mainly consists of rock masses or sediment formations. Most of the sediment formations are heterogeneous. This system consists of alternately overlying permeable layers and less permeable layers and the bottom layer is close to the bedrock, as shown in the figure.

The groundwater table, or the free surface is below the ground surface in the system shown in the figure. The flow field of the unconfined groundwater is called an unconfined aquifer in which the groundwater table forms the upper surface of the saturated zone. The unconfined aquifer is one of the fundamental elements of groundwater systems.

A saturated permeable geologic unit confined between two aquicludes is called a confined aquifer. Confined aquifers without free surface have high permeability and the water levels in the wells are higher than the upper boundary of the aquifers as shown in the figure. Normally, unconfined aquifers having rainwater recharge exist

near the ground surface, whereas confined auifers occur at depth in a groundwater system.

It is important to have information on aquifer pressure to understand groundwater movement. Observation wells with screens give pressure levels in the aquifer. Pressure p dominates groundwater movement and is expressed as the elevation of the water table from a reference level, i.e., piezometric head = $p/\rho g + z$, where, ρ = water density, g = gravitational acceleration.

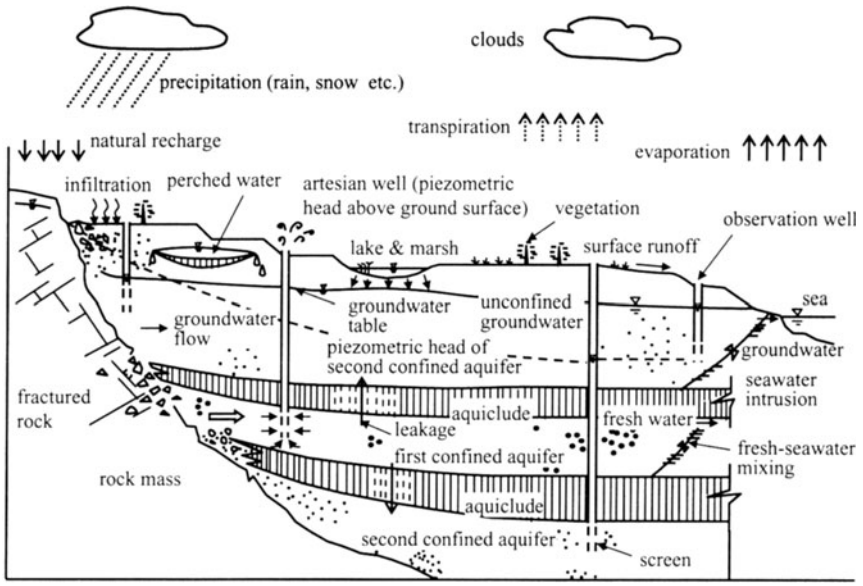

Fig. 1.6. Groundwater classification under the hydrologic cycle

Groundwater flow occurs from an aquifer of higher piezometric head to those with lower heads. Groundwater movement in an aquifer can be easily understood by drawing an envelope line of piezometric heads. In **Fig. 1.6**, the piezometric head of the first confined aquifer is higher than the ground surface. As a result, the observation well is depicted with a fountain and is called an artesian well. Artesian wells and springs are generally explained by this hydraulic mechanism.

There is vertical leakage between adjacent aquifers in **Fig. 1.6** through the aquicludes, which have low and nonuniform permeability as a result of heterogeneous sedimentation processes. The leakage groundwater movement also follows hydraulic potential of piezometric head difference between aquifers.

Water movement in the unsaturated zone above the water table is subject to gravity and surface tension as the driving forces. A small aquifer above low permeable layer in the unsaturated zone results in perched water.

1.8 The Hydrologic Cycle

Groundwater comprises the subsurface water system of the hydrologic cycle. **Figure 1.7** illustrates the processes of the hydrologic cycle, which encompass the surface water system and the subsurface water system. Part of the precipitation infiltrates into the ground and becomes the subsurface water, as shown in the figure.

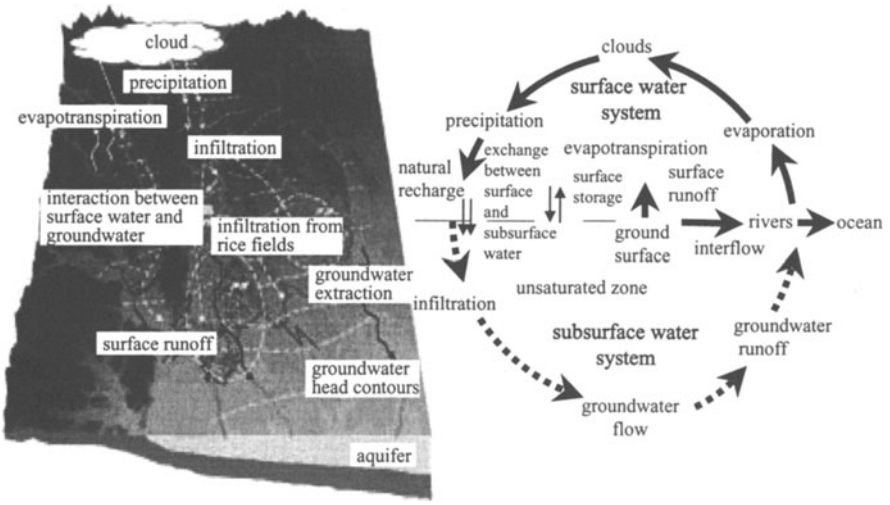

Fig. 1.7. The hydrologic cycle concept

A part of groundwater accretion/surplus resulting from rainfall infiltration eventually reaches rivers or stream channels as groundwater runoff. Both rainfall infiltration and water retained in shallow ditches on the ground surface cultivates soil moisture in the top layer, and ultimately return to the atmosphere by evapotranspiration. Evapotranspiration refers to the simultaneous occurrence of evaporation and transpiration processes. The remaining portion of precipitation rapidly flows into rivers or stream channels as direct runoff (also known as overland flow). Some water infiltrates into shallow soil layers, travels slowly along the soil layer, and eventually joins a river, a process known as interflow. The river water flows downstream and eventually enters the ocean. A relatively small amount of water evaporates from river surfaces, while much more water evaporates from the ocean. Thus, the whole precipitation ultimately returns to the atmosphere and the cycle repeats.

The hydrologic cycle can be quantitatively understood by studying the water balance. The water balance clarifies the characteristics of the hydrologic system and is expressed as follows:

$$\begin{aligned} I(t) \quad &- \quad O(t) \quad = \quad dS/dt \\ \text{(Inflow rate)} &- \text{(Outflow rate)} = \text{(Storage rate)} \end{aligned} \tag{1.3}$$

The way the water balance is quantified is to define a given region of space and time as boundary conditions. Eq. 1.3 states that the difference between water inflow and outflow is the storage rate for a specified period in the system. This is the mass conservation law applied to the hydrologic system.

Exercises

[Ex. 1.1]
The groundwater table is 1 m below the ground surface of a sand layer. The volumetric water content (θ) in the unsaturated zone is 0.10, which increases to 0.15 after rainfall for 2 hr with an intensity of 40 mm/hr. Calculate the rise in groundwater table. The porosity (n) of the sand is 0.4.

[Ex. 1.2]
The groundwater table originating from rainfall on a mountain side is shown in **Fig. E1.1**. Using a tank model, show that the relationship between discharge (Q) and time (t) after the rainfall is exponential.

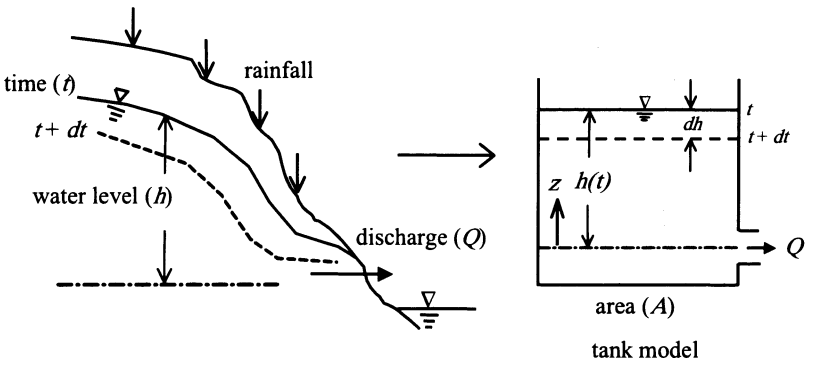

Fig. E1.1 Tank model for discharge

References

Bear J. (1979) Hydraulics of groundwater. McGraw-Hill, New York, p.30

Scheideger A. E. (1960) The physics of flow through porous media. 3rd edn. University of Toronto Press, Tronto, pp 5–8

Smullyan R. M., Fitting M. (1996) Set theory and the continuum problem. Oxford Scientific Publications, Clarendon Press, Oxford, pp 14–25

2

Formulation of the Basic Groundwater Flow Equations

Summary

Groundwater flow in the subsurface is analyzed by introducing transport law (Darcy's law) and mass conservation law (continuity equation) coupled with the specified boundary conditions. Thus, in the so-called deductive method, transport equations for physical quantities such as groundwater, solute matter, and heat are applied to groundwater-related phenomena to obtain the necessary information.

In this chapter, first the methodology for the study of groundwater hydraulics is discussed. Then, basic knowledge such as water velocity, permeability testing, and the equations of motion and the continuity equations are introduced. Finally, the governing equations for groundwater flow in confined and unconfined aquifers and the flow of isothermal unsaturated groundwater are derived.

Groundwater flow in rock masses and gas (air) seepage, which has been not systematically analyzed, will also be introduced. For further explanation and detailed understanding, the application in groundwater flow will be explained by some solved problems.

2.1 Methodology of the Hydraulic Approach

Since groundwater hydraulics deals with the problems of dynamic fluid motion (e.g., water, air, and oil) in porous media, the governing equations in fluid dynamics are introduced for the porous media modeled and solved by incorporating various conditions to obtain the necessary information.

The hydraulic approach to groundwater flow is summarized in **Fig. 2.1**. In general, the approach is classified in two ways: one is used for field applications and the other aims at the modeling and formulation of basic phenomena. In the first approach, the hydraulic conditions must be provided for the basic equations, giving a clear method for solution. The latter approach is used in research when data are insufficient and no established modeling techniques are available.

K. Sato et al. (eds.), *Groundwater Hydraulics*

The hydraulic approach to field application problems is summarized as follows. First the collection and analysis are carried out of all existing and research data on morphology, geology, hydrologic conditions (e.g., vegetation distribution, land and water use, and meteorology), and actual groundwater conditions. Then, solutions are obtained by solving the transport equations (e.g., Darcy's law and Fick's law) and conservation equations (e.g., the continuity equation) for the transport quantities (such as those for water, solutes, and heat) together with the boundary and initial conditions. In general, either analytical or numerical solution methods are applied to the modeled morphology, geology and groundwater to solve the basic equations, which are written by mathematical expression. For this, hydraulic parameters and characteristic formulas (such as the permeability and the coefficient of storage that connect to the actual groundwater flow with the mathematical models) must be determined. Results of the analyses based on the hydraulic approach are applied to understand the present state of the groundwater flow, and to the prediction and evaluation of future scenarios.

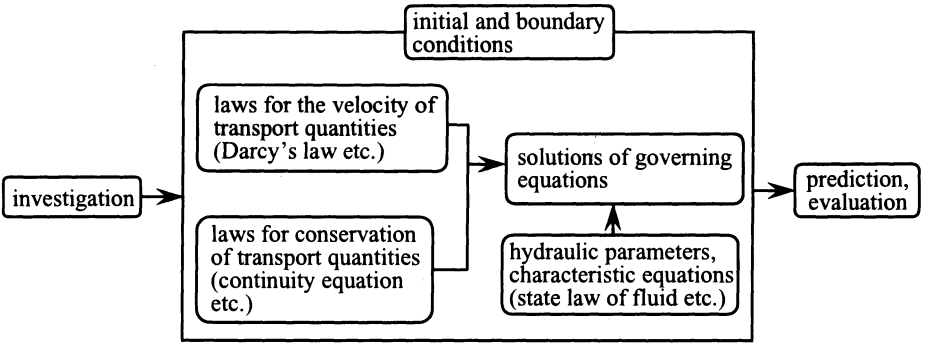

Fig. 2.1. Hydraulic approach to groundwater flow

This is the so-called deductive method. Accordingly, the basic equations, hydraulic parameters, characteristics, and conditions must be determined beforehand. If it is not possible to develop basic equations and obtain solutions by applying the above-mentioned procedure, then further investigation of the problem is required.

2.2 Laws of Velocity for Transport Quantities

2.2.1 Darcy's Law

The basic resistance law for seepage and groundwater flows was made clear in the permeability experiments conducted by Darcy H. (1857). Darcy's experimental equipment is shown in **Fig. 2.2**. It consists of a vertical cylindrical column 2.5 m

in height and 0.35 m in internal diameter filled with the material to be tested. Mercury manometers for pressure measurement are installed at the two ends. Tap water is supplied to the upper end and discharged from the lower end of the column under saturated state. The soil sample is placed above a permeable sheet and a metal net, which covers the entire pipe crosssection at 20 cm from the lower end. Silica sand was used as a test sample with particle diameters of 0.77–2.0 mm and a porosity of about 38%. The sand was collected from a tributary of the Rhone, the Saône river, in France.

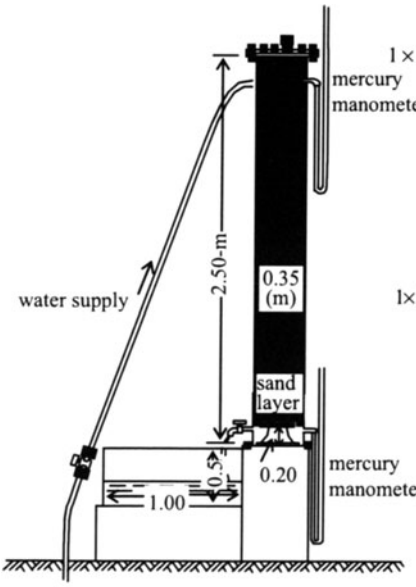

Fig. 2.2. Darcy's experimental setup (after original literature by H. Darcy 1857, France)

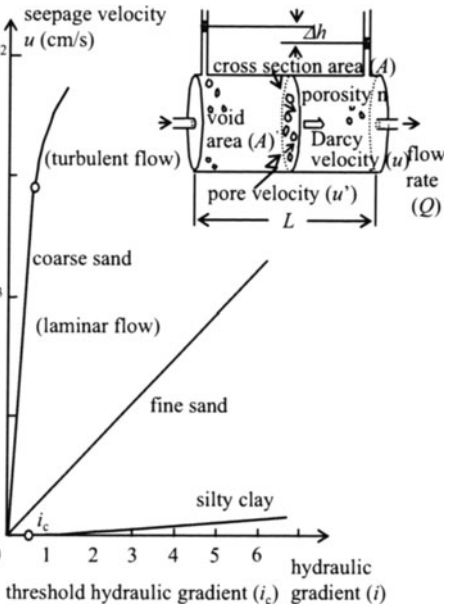

Fig. 2.3. Experimental relationship between flow velocity and hydraulic gradient

The column was first fully filled with water so that no air bubbles remained in the sand layer. During the first experiment, flow discharges were measured for four cases with sand layer thicknesses of 0.58 m, 1.14 m, 1.70 m, and 1.71 m and the hydraulic head difference between upper and lower ends of the column varying in the range of 1.11–13.93 m.

The experimental results showed that the flow discharge (Q) was proportional to the pressure difference between the upper and lower ends of the sand layer, as depicted in Eq. 2.1:

$$Q = Au, \quad u = ki, \quad i = \frac{\Delta h}{L} \tag{2.1}$$

where A = pipe cross-sectional area, k = hydraulic conductivity (or permeability), Δh = difference in hydraulic heads between the upper and lower ends of the sand column, L = sand layer thickness, and i = hydraulic gradient.

Equation 2.1 is known as Darcy's law, in which the discharge velocity or Darcy velocity (u), is proportional to the hydraulic gradient (i). The proportionality coefficient (k) is called the permeability or hydraulic conductivity, having the dimension of velocity.

The experimentally determined relationships between discharge velocity and hydraulic gradient for silty clay, fine sand, and coarse sand by several authors are shown in **Fig. 2.3**.

The relationship for very fine particles (e.g., silt and clay) has three transit characteristics. The first is the critical or threshold hydraulic gradient (i_c). Flow does not take place while the gradient is below its critical value ($i < i_c$). A curvilinear (nonlinear) relationship between flow velocity and hydraulic gradient exists for $i_c \leq i \leq i_0$, and a straight line (linear) relationship exists for $i > i_0$. Usually a fine silty clay, originating from sediments or weathered rocks, has a high porosity and is easily deformed due to external forces. This is one of dynamic characteristics of deformable porous media.

The relationship between u and i for fine sand is linear, and the pore flow velocity is directly proportional to the hydraulic gradient. Thus, Darcy's law expresses a linear resistance law. For coarse sand, the flow follows Darcy's law for low flow velocities. But when the hydraulic gradient grows larger, the flow velocity is directly proportional to $i^{1/2}$ instead of i (the flow velocity is proportional to the one-half power of the hydraulic gradient).

The flow velocity (u) calculated using Darcy's Law, based on the cross-sectional area (A) of the test sample and the flow discharge (Q) as shown in **Fig. 2.3**, is different from the pore velocity (u'). The Darcy velocity ($u = Q/A$), and the pore velocity ($u' = Q/A'$, where A' = void area in the cross-section) are related as shown in Eq. 2.2:

$$u = \frac{A'}{A}u' = nu', \quad n < 1, \; u < u' \tag{2.2}$$

where $n = A'/A$ is called the area porosity. Since the porosity is less than one, the pore velocity is larger than the Darcy velocity.

2.2.2 Dynamic Meaning of Permeability

The permeability, which is defined on the basis of Darcy's Law, is the proportionality coefficient between discharge velocity (or Darcy velocity) and hydraulic gradient (piezometric head gradient: gradient of forces originating from pore pressure and gravity). Its hydraulic meaning will be discussed in the following paragraphs.

Figure 2.4 shows micropipe and parallel pore models for a porous medium and fractures in a rock mass, respectively. These two models (a and b) are simplified as viscous fluid flows in a circular pipe and parallel interstice, respectively. Since Darcy's Law is applicable only for laminar flow, it is possible to explain it using a simplified viscous fluid flow in a circular pipe. According to the law for a viscous

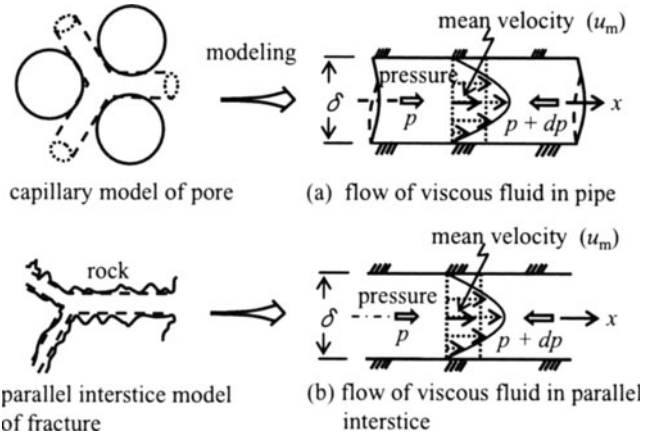

Fig. 2.4. Hydraulic model in seepage flow

fluid flow in a circular pipe (Poiseuille's law), there is a force balance between pressure and shear stress. The average flow velocities (u_m) in circular and parallel pipes are expressed by Eq. 2.3.

$$\begin{aligned} u_m &= -\frac{\delta^2}{32\mu}\frac{dp}{dx} = ki, \quad k = \frac{\delta^2}{32\mu}\rho g, \quad i = -\frac{1}{\rho g}\frac{dp}{dx} \qquad \text{(circular)} \\ u_m &= -\frac{\delta^2}{12\mu}\frac{dp}{dx} = ki, \quad k = \frac{\delta^2}{12\mu}\rho g, \quad i = -\frac{1}{\rho g}\frac{dp}{dx} \qquad \text{(parallel)} \end{aligned} \tag{2.3}$$

where δ = the pipe diameter (corresponds to the pore diameter or width of interstice), μ = fluid viscosity, ρ = fluid density, p = pressure, g = gravitational acceleration, and x = coordinate along the pipe.

If the flow inside the porous medium is laminar, the hydraulic conductivity is proportional to the medium pore size and fluid viscosity, as given in Eq. 2.4:

$$k = f(\delta, \mu, \rho, g), \quad \delta = f(n, d, \varepsilon) \tag{2.4}$$

where $f(\ )$ = a function, n = porosity, d = particle diameter of the porous medium, and ε = particle geometrical coefficient (e.g., the ratio between the lengths of the long and short axes of the particle).

Usually, the pore size, one of the geometrical characteristics of a porous medium, is dependent on particle size, porosity, and particle geometry. Further, viscosity (μ) and fluid density (ρ) are dependent on temperature (T) and pressure (p) [i.e., $\mu(T, p)$ and $\rho(T, p)$]. The gravitational acceleration varies with the elevation, and so it is reasonable to argue that fluid permeability (for water, oil, or gas) is mainly determined by geometrical characteristics, fluid properties, location, and pore size.

$$k = \frac{K}{\mu}\rho g, \quad K = \delta^2 \tag{2.5}$$

Table 2.1. Range of Darcy's permeability

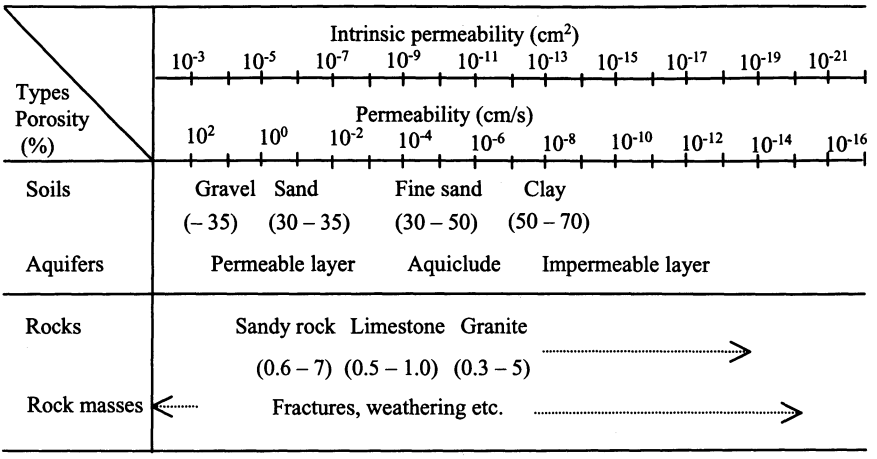

where K = intrinsic permeability. The intrinsic permeability has the dimension of length squared [L^2] and distinguished from the Darcy permeability (see **Table 2.1**).

2.2.3 Relationship Between Resistance Coefficient and Reynolds Number

Saturated flow in a porous medium entails a flow inside the pores. The resistance to flow in a porous medium can be evaluated based on the coefficient of resistance (ζ) and the Reynolds number (R_e), similarly to that for flow in a circular pipe. The relationship between ζ and R_e for flow through a porous medium is defined by Eq. 2.6.

$$i = \frac{\zeta}{d}\frac{u^2}{2g}, \quad R_e = \frac{ud}{\nu} \tag{2.6}$$

where i = hydraulic conductivity, d = particle diameter, u = Darcy velocity, and ν = kinematic viscosity of the fluid.

Figure 2.5 shows the experimentally determined relationships between Reynolds number and coefficient of resistance for microseepage in clay and flow in sand or glass particles (laminar and turbulent flow). It can be observed that the coefficient of resistance becomes larger for smaller Reynolds number, and as R_e increases, ζ decreases. Three distinct regions can be found in the figure with respect to the Reynolds number.

1. The lower Reynolds number region in **Fig. 2.5** is characterized by the increase in resistance coefficient caused by the additional forces at the interface between water molecules and soil particles (e.g., the absorbing effect in clay for $R_e < 10^{-5}$–10^{-6}).
2. The region with laminar flow ($R_{em} < R_e < R_{ec}$), where R_{em} = the lowest Reynolds number of laminar flow, R_{ec} = the Reynolds number when the flow changes from laminar to turbulent, or the critical Reynolds number, R_{ec} = 1–10.

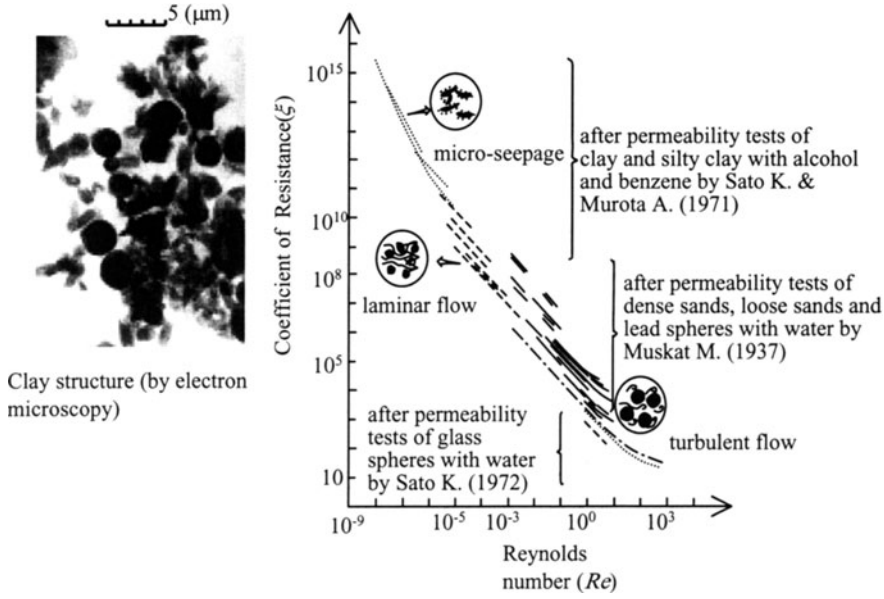

Fig. 2.5. Experimental relationship between Reynolds number (R_e) and coefficient of resistance (ζ)

3. The region with turbulent flow ($R_e > R_{ec}$).

In the region between turbulent and laminar flows, experimental relationships between ζ and R_e can be expressed by the following equation.

$$R_e\zeta = a + bR_e, \tag{2.7}$$

where a and b are constants. The coefficient a, determined from the experiments in **Fig. 2.5**, is in the range 10^3–10^6, whereas b is in the range 10–10^2.

As shown in the figure, the flow velocity is affected by an "additional viscosity," which results from the adhesive forces between soil particles on the microscale (10^{-5} m, refer to **Fig. 2.5** for microscopic clay structure) and water particles (on the scale of 10^{-10} m); flow velocity is also affected by chemical forces between water molecules and organic matter (the treatment of chemical forces is outside the scope of hydraulics).

Flow is laminar for a wide range of Reynolds number, and in this regime, the interaction between water molecules governs the resistance force. As the Reynolds number increases, internal friction and turbulence in the fluid flow consume flow kinetic energy. Pore size restricts the scale of turbulent eddies, the size of which resembles the pore size distribution in the porous medium.

2.2.4 Methods of Permeability Determination

Permeability is one of the basic parameters for groundwater flow and needs to be determined empirically. Generally, there are two methods of determining permeability:

1. Empirical equations and laboratory tests (indoor methods)
2. Field tests (outdoor methods)

In laboratory tests, soil properties (i.e., particle distribution and pore distribution) are analyzed and sampling tests are carried out to determine permeability on the laboratory scale. In contrast outdoor methods (pumping tests or insitu permeability tests) examine the permeability of aquifers or rock masses by recharging water or taking up water from observation wells bored in the field, in which case, an average permeability for groundwater flow is determined. Because details on field methods will be elaborated in Chapter 6, Groundwater Investigation, this chapter will focus on a brief explanation of the laboratory methods.

2.2.4 (a) Permeability Tests in the Laboratory

Table 2.2 shows typical permeability tests carried out in the laboratory. They are (a) the constant head permeability test, (b) the falling head permeability test, and (c) the constant pressure rock permeability test. Corresponding permeability equations for each test method are also given. For low permeability materials such as clay, the falling head permeability test is preferable.

Very low permeability materials such as rocks need high pressure to be applied, and nondeformable samples of the material tend to result in gaps between the rock specimen and the wall of the cylindrical container. Thus, a gum membrane must be wrapped around the test sample first and a circumferential pressure (p_s) applied to make a good contact between the gum membrane and the rock sample. Then, pressures are applied to the upper and lower ends of the sample to obtain a pressure difference (Δp) between them. The permeability test must be carried out under the condition that $p_s > p_1$ (p_1 = pressure at the upper end).

The testing methods are now briefly explained. In the constant head permeability test, both undisturbed samples and disturbed samples (samples in a state different from the insitu state) may be put in the cylindrical test tank above the porous plate. Then, water is supplied from the downstream tank to avoid any entrapment of air in the sample, and the discharge is measured under a fixed hydraulic head difference between the upper and lower ends of the sample. The, permeability is determined following the equation in **Table 2.2a**.

The falling head permeability test is useful for materials with low permeability such as clay. The standpipe and test sample are filled with water and the variation in water level inside the tank is measured with a scale on the transparent wall of the tank. The permeability is then calculated using the equation in **Table 2.2b**.

In laboratory permeability tests for rocks, a high acting pressure (high pressure is required because of the low permeability) is applied at the upper end of the sample.

Table 2.2. Permeability tests and associated formulae

Test methods	Test setup	Permeability
(a) Constant head permeability test	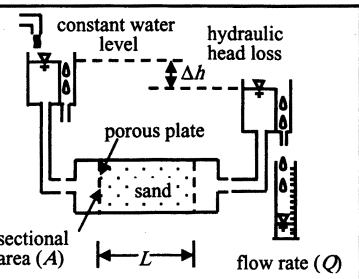	$k = \frac{LQ}{\Delta hA}$ k: permeability Δh: hydraulic head loss A: sectional area L: sample length Q: flow rate
(b) Falling head permeability test	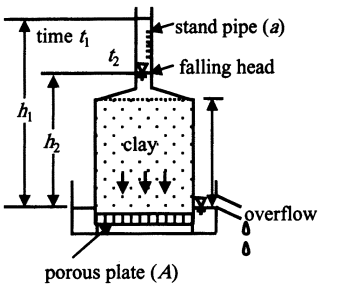	$k = \frac{aL}{A(t_2-t_1)} \log \frac{h_1}{h_2}$ k: permeability a: sectional area of stand pipe L: sample length A: sectional area of the sample h_1, h_2: water level in stand pipe at t_1 and t_2 ($h_1>h_2$, $t_1<t_2$) **Note:** The test is applicable to low permeability materials like clay
(c) Constant pressure rock permeability test	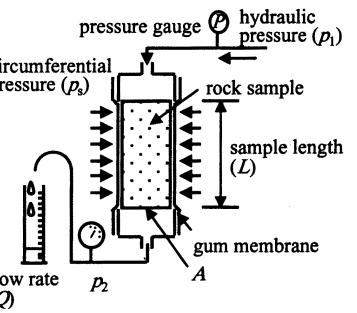	$k = \frac{\rho gLQ}{\Delta pA}$ k: permeability Δp: pressure difference (p_1-p_2) ρ: water density g: acceleration (gravity) L: sample length A: sample sectional area p_s: circumferential pressure on gum membrane ($p_s>p_1$)

With the pressure difference (Δp) between the upper and lower ends of the sample and the measured flow discharge (Q), the permeability is calculated using the equation in **Table 2.2c**.

It is possible to carry out gas permeability tests with the same procedure by replacing water with gas, but the method for gas discharge measurement (Q) at the lower end is different. Gas discharge measurement can be carried out using a gas-capturing tube installed in the water tank as shown in **Table 2.3**. It is not possible to

accurately calculate the air permeability with the equation given in **Table 2.3** because of gas compressibility, the theoretical background to which will be discussed later in Sect. 2.7. However, the equation discussed for water permeability can be used with a small error for small pressure differences.

Table 2.3. Typical test methods for saturated/unsaturated permeability

Test method	Test setup	Permeability
(a) Unsaturated permeability test (for loam and clay)	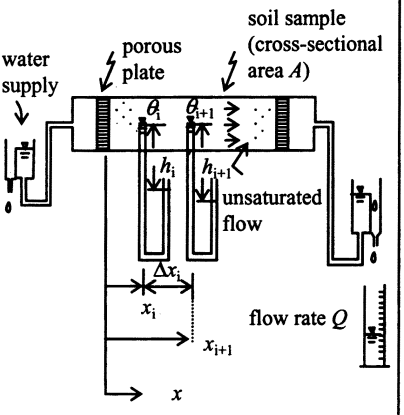	$k(\theta)=u\Big/\left(-\frac{dh_c}{dx}\right)$ $=u\Big/\left(-\frac{\partial h_c}{\partial\theta}\cdot\frac{d\theta}{dx}\right)$ $k(\theta)$: unsaturated permeability θ: volumetric water content h_c: capillary head x: distance, Q: flow rate u: seepage velocity 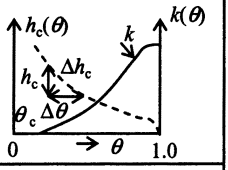
(b) Constant pressure gas permeability test (for permeable soils)	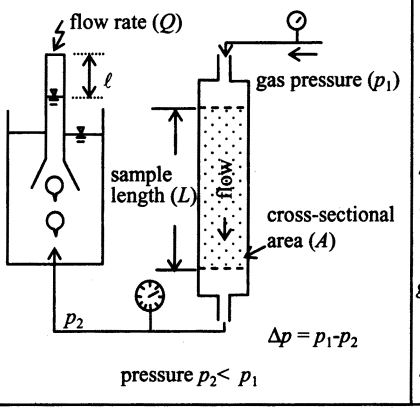	$k=\frac{\rho g Q L}{A\Delta p}$ $K = k\mu/\rho g$ K: intrinsic permeability k: permeability Δp: pressure difference Q: flow rate ρ: fluid density g: acceleration of gravity L: length of sample μ: gas viscosity

Unsaturated permeability [$k(\theta)$, θ = volumetric soil water content] for low permeability soil (such as loam and clay) under the action of surface tension can be determined using the unsaturated permeability test as shown in **Table 2.3**. In this

case, a capillary head difference (Δh_c) between the upstream and downstream ends of the test sample generates unsaturated flow. At least two tensiometers (a manometer fully filled with water and connected to a porous cup at one end) are localted with a known separation (Δx) inside the test sample to measure the capillary head difference and the volumetric water content. The flow discharge (Q) at the downstream end of the sample is noted. Then, using u (= Q/A, A = test sample cross-sectional area), $\Delta\theta/\Delta x$ and $\Delta h_c/\Delta\theta$, unsaturated permeability $k(\theta)$ is calculated from $u/(\Delta h_c/\Delta\theta \times \Delta\theta/\Delta x)$ or $u/(\Delta h_c/\Delta x)$. Practically, the maximum possible number of tensiometers are inserted into the test sample. The number is chosen so that the tensiometers do not significantly disturb or interfere with the flow, thus h_c and θ are measured at many points, which will be discussed later. Based on the measured data, the relationship between h_c and θ (known as the moisture characteristic curve) is plotted, and hence the unsaturated permeability is determined. With the unsaturated permeability [$k(\theta)$] determined, it is then possible to apply it to a host of unsaturated flow analyses.

Table 2.4. Some permeability formulae

Authors	Empirical formulae (unit)	Notations
Hazen (1893)	$k = 116 d_e^2(0.7 + 0.03T)$ (cm/s)	k: Darcy's permeability (cm/s) d_e: 10% effective grain size on cumulative grain size distribution (cm) T: temperature (°C)
Carman-Kozeny (1937)	$k = \frac{g}{5\nu}[n^3/(1-n)^2]/M_s^2$ (cm/s)	k: Darcy's permeability (cm/s) ν: kinematic viscosity (cm^2/s) g: acceleration due to gravity (cm/s^2) n: porosity M_s: specific surface/unit soil volume (For spherical particle, $M_s = 6/d$)
Terzaghi (1924)	$k = (460 - 800)\left(\frac{\mu_0}{\mu_t}\right)\left(\frac{n - 0.13}{\sqrt[3]{1-n}}\right)^2 d^2$ (cm/s)	k: Darcy's permeability (cm/s) μ_0: fluid viscosity at 10 °C temperature μ_t: fluid viscosity at T °C temperature d: 10% effective size (cm) n: porosity (**Note:** the coefficient value for a smooth particle surface is 800 and for an angular particle is 460)

Gas permeability of relatively permeable soils can be measured using a constant pressure gas permeability test, as shown in **Table 2.3**. In such cases, the pressure difference (Δp) between the upper and lower ends of the test sample should be small so that the effect of gas compressibility is not pronounced.

2.2.4 (b) Formulae for Permeability

Permeability is defined simply as the resistance coefficient in Darcy's law for flow discharge. In practice, it is a very important parameter governing infiltration and groundwater flows. Various empirical formulae for the calculation of permeability have been proposed for simplified sand layers, such as filter layers or ion exchange layers at water chemical plants, based on particle size distribution, porosity, and viscosity of the fluid. **Table 2.4** shows some of these formulae (Harzen A., 1893, Bear J., 1972., Terzaghi K., 1924).

2.3 Basic Equations for Saturated Groundwater Flow

This section focuses on the derivation of basic equations, i.e., continuity and transport equations, for saturated groundwater flow. In general, these equations are classified into those for confined and unconfined aquifers.

2.3.1 Continuity Equation

Consider the mass balance for water inside an infinitesimal control volume with dimensions Δx, Δy, Δz and centered at a point $P(x, y, z)$ in the Cartesian coordinate system, as shown in **Fig. 2.6**. Darcy's velocity components at point P in three directions are denoted by u, v, and w, respectively. The net water mass entering the control volume through its surfaces within an infinitesimal time (Δt) can be expressed by the following equation:

$$\begin{aligned}
&\left[\left(\rho u - \frac{\partial \rho u}{\partial x}\frac{\Delta x}{2}\right) - \left(\rho u + \frac{\partial \rho u}{\partial x}\frac{\Delta x}{2}\right)\right]\Delta y\,\Delta z\,\Delta t \\
&+\left[\left(\rho v - \frac{\partial \rho v}{\partial y}\frac{\Delta y}{2}\right) - \left(\rho v + \frac{\partial \rho v}{\partial y}\frac{\Delta y}{2}\right)\right]\Delta z\,\Delta x\,\Delta t \\
&+\left[\left(\rho w - \frac{\partial \rho w}{\partial z}\frac{\Delta z}{2}\right) - \left(\rho w + \frac{\partial \rho w}{\partial z}\frac{\Delta z}{2}\right)\right]\Delta x\,\Delta y\,\Delta t \\
&= -\left[\frac{\partial}{\partial x}(\rho u) + \frac{\partial}{\partial y}(\rho v) + \frac{\partial}{\partial z}(\rho w)\right]\Delta x\,\Delta y\,\Delta z\,\Delta t
\end{aligned}$$

where ρ = water density.

The change in water mass inside the control volume can also be expressed as $\partial/\partial t\,(n\rho\,\Delta x\,\Delta y\,\Delta z)\Delta t$, where n = soil porosity and t = time. Then, the continuity equation can be written in the following form:

$$-\nabla \rho \mathbf{q} = -\left[\frac{\partial}{\partial x}(\rho u) + \frac{\partial}{\partial y}(\rho v) + \frac{\partial}{\partial z}(\rho w)\right] = \frac{\partial(\rho n)}{\partial t} \tag{2.8}$$

where $\mathbf{q}(u, v, w)$ = the flow velocity vector, and $\nabla = (\partial/\partial x, \partial/\partial y, \partial/\partial z)$.

Equation 2.8 expresses the water mass conservation law for a unit volume. Different forms of the equation are in use depending on whether water density and porosity are constant and whether the aquifers under consideration are confined or unconfined. For a steady flow ($\partial/\partial t = 0$) and constant values for ρ and n, Eq. 2.8 is expressed in the following form:

$$\frac{\partial u}{\partial x} + \frac{\partial v}{\partial y} + \frac{\partial w}{\partial z} = 0 \tag{2.9}$$

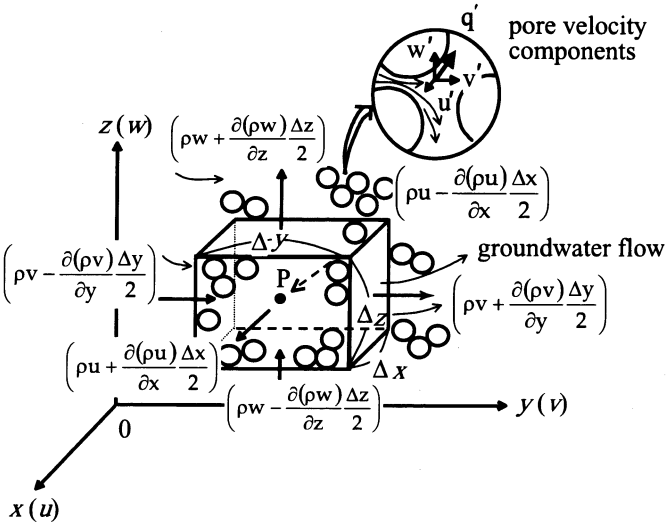

Fig. 2.6. Control volume in groundwater flow

2.3.2 Equation of Motion

The pore velocity in **Fig. 2.6** is denoted by $\mathbf{q}'(u', v', w')$, and the Navier–Stokes equation for viscous fluid flow inside pores can be expressed in the following equations:

$$\left.\begin{aligned} \frac{du'}{dt} &= -\frac{1}{\rho}\frac{\partial p}{\partial x} + \frac{\mu}{\rho}\nabla^2 u', \qquad \frac{d}{dt} = \frac{\partial}{\partial t} + u'\frac{\partial}{\partial x} + v'\frac{\partial}{\partial y} + w'\frac{\partial}{\partial z} \\ \frac{dv'}{dt} &= -\frac{1}{\rho}\frac{\partial p}{\partial y} + \frac{\mu}{\rho}\nabla^2 v', \qquad \nabla^2 = \frac{\partial^2}{\partial x^2} + \frac{\partial^2}{\partial y^2} + \frac{\partial^2}{\partial z^2} \\ \frac{dw'}{dt} &= -\frac{1}{\rho}\frac{\partial p}{\partial z} - g + \frac{\mu}{\rho}\nabla^2 w' \end{aligned}\right\} \tag{2.10}$$

where u', v', and w' are components of pore velocity vector in the x-, y- and z-directions, respectively; p = pressure; and g = gravitational acceleration.

Generally, the pore velocity ($\mathbf{q}'$) is very small and the nonlinear terms in Eq. 2.10 can be neglected. Noting the relationship between the Darcy and pore velocities [$\mathbf{q}(u, v, w) = n\mathbf{q}'(u', v', w')$], the following equations can be written:

$$\left.\begin{aligned} \frac{1}{n}\frac{\partial u}{\partial t} &= -\frac{1}{\rho}\frac{\partial p}{\partial x} + \frac{\mu}{n\rho}\nabla^2 u \\ \frac{1}{n}\frac{\partial v}{\partial t} &= -\frac{1}{\rho}\frac{\partial p}{\partial y} + \frac{\mu}{n\rho}\nabla^2 v \\ \frac{1}{n}\frac{\partial w}{\partial t} &= -\frac{1}{\rho}\frac{\partial p}{\partial z} - g + \frac{\mu}{n\rho}\nabla^2 w \end{aligned}\right\} \tag{2.11}$$

The following equations are obtained by substituting the coefficients in the viscous terms on the right hand side of Eq. 2.11 with the Darcy permeability $k = (n\rho g/\mu)K$, where K = intrinsic permeability [L^2]:

$$\frac{\mu}{n\rho}\nabla^2 u,\ \frac{\mu}{n\rho}\nabla^2 v,\ \frac{\mu}{n\rho}\nabla^2 w \approx -g\frac{u}{k},\ -g\frac{v}{k},\ -g\frac{w}{k} \tag{2.12}$$

The Darcy flow velocity ($\mathbf{q}$) can be expressed in terms of the velocity potential (ϕ) as shown in Eq. 2.13.

$$u = -\frac{\partial \phi}{\partial x},\quad v = -\frac{\partial \phi}{\partial y},\quad w = -\frac{\partial \phi}{\partial z} \tag{2.13}$$

Equation 2.11 can be written in the following form by substituting Eq. 2.13 into it:

$$\left.\begin{aligned} -\frac{1}{ng}\frac{\partial}{\partial t}\left(\frac{\partial \phi}{\partial x}\right) &= -\frac{1}{\rho g}\frac{\partial p}{\partial x} + \frac{1}{k}\left(\frac{\partial \phi}{\partial x}\right) \\ -\frac{1}{ng}\frac{\partial}{\partial t}\left(\frac{\partial \phi}{\partial y}\right) &= -\frac{1}{\rho g}\frac{\partial p}{\partial y} + \frac{1}{k}\left(\frac{\partial \phi}{\partial y}\right) \\ -\frac{1}{ng}\frac{\partial}{\partial t}\left(\frac{\partial \phi}{\partial z}\right) &= -\frac{1}{\rho g}\frac{\partial p}{\partial z} - 1 + \frac{1}{k}\left(\frac{\partial \phi}{\partial z}\right) \end{aligned}\right\} \tag{2.14}$$

Multiplying each component equation in Eq. 2.14 by dx, dy, and dz, respectively, and then taking summation and changing the order of differentiation gives:

$$\begin{aligned} &-\frac{1}{ng}\left[\frac{\partial}{\partial x}\left(\frac{\partial \phi}{\partial t}\right)dx + \frac{\partial}{\partial y}\left(\frac{\partial \phi}{\partial t}\right)dy + \frac{\partial}{\partial z}\left(\frac{\partial \phi}{\partial t}\right)dz\right] \\ &= -\frac{1}{\rho g}\left(\frac{\partial p}{\partial x}dx + \frac{\partial p}{\partial y}dy + \frac{\partial p}{\partial z}dz\right) + \frac{1}{k}\left(\frac{\partial \phi}{\partial x}dx + \frac{\partial \phi}{\partial y}dy + \frac{\partial \phi}{\partial z}dz\right) - dz \end{aligned}$$

The definition of the total differential with respect to x, y, and z gives:

$$-\frac{1}{ng}d\left(\frac{\partial \phi}{\partial t}\right) = -\frac{1}{\rho g}dp + \frac{1}{k}d\phi - dz$$

Integrating the above equation with respect to spatial variables, the following equation is obtained:

$$-\frac{1}{ng}\frac{\partial \phi}{\partial t} + \frac{p}{\rho g} - \frac{\phi}{k} + z = C(t) \tag{2.15}$$

where $C(t)$ is the integration constant, which is a function of time only.

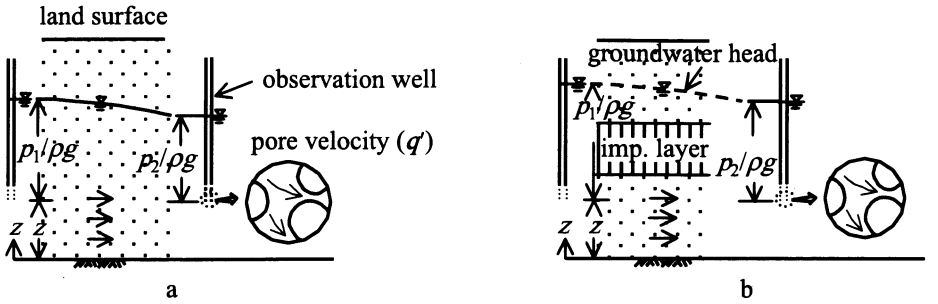

Fig. 2.7. Definition of piezometric head in an unconfined aquifer (**a**) and a confined aquifer (**b**)

Equation 2.15 is known as the equation of motion for groundwater flow. In general, groundwater flow is slow, and hence it is reasonable to assume that $\partial/\partial t \approx 0$. Thus, the equation can be written in the following form by taking $C(t) = 0$:

$$\phi = k\left(\frac{p}{\rho g} + z\right) = kh,\ h = \left(\frac{p}{\rho g} + z\right) \tag{2.16}$$

$$\left.\begin{aligned} u &= -\frac{\partial \phi}{\partial x} = -k\frac{\partial h}{\partial x} = -\frac{k}{\rho g}\frac{\partial p}{\partial x} \\ v &= -\frac{\partial \phi}{\partial y} = -k\frac{\partial h}{\partial y} = -\frac{k}{\rho g}\frac{\partial p}{\partial y} \\ w &= -\frac{\partial \phi}{\partial z} = -k\frac{\partial h}{\partial z} = -\frac{k}{\rho g}\left(\frac{\partial p}{\partial z} + \rho g\right) \end{aligned}\right\} \tag{2.17}$$

The equation of motion for groundwater flow expresses Darcy's law in terms of velocity potential (ϕ) and piezometric head (h). From these discussions, it can be seen that the basic groundwater flow equation can be derived by combining the continuity equation with Darcy's formula. Darcy's formula is introduced only for a steady flow, whereas the unsteady nature of the basic equation is obtained from the continuity equation.

Groundwater in pore spaces and fractures in soils and rock masses in both saturated and unsaturated conditions is either at rest or in motion. In this section, the basic equations are derived for isothermal (i.e., groundwater moving without changing its temperature) saturated groundwater flows. **Figure 2.7** shows groundwater flow and piezometric heads in unconfined and confined aquifers. Hydrodynamically, these two situations can be expressed by considering hydraulic quantities originating in the

forces (gravity and pressure for saturated groundwater flow) acting on the groundwater.

As shown in the figure, an observation well or a borehole in the groundwater aquifer is required to measure the pressure at an elevation (z) from the impervious bottom. In this case, if there is no groundwater flow, for both confined and unconfined aquifers, the pressure inside the observation well represents the hydrostatic pressure (p_s). Strictly speaking, this well pressure measured as the average pressure around the screen pipe (a porous pipe) at the well bottom is different from the pore pressure (or void pressure, p'); however, this difference is not significant in practice. Similarly, for flowing groundwater, the pressure (p) is measured in a well, but there is a difference between pressures p_1 and p_2 measured upstream and downstream of the groundwater aquifer, respectively. In general, if the groundwater is flowing, the water pressure decreases because of the influence of flow velocity and flow resistance.

The piezometric head (h), the most useful hydraulic quantity, is introduced for a groundwater flow as follows:

$$h = \frac{p}{\rho g} + z \tag{2.18}$$

where p = water pressure, ρ = water density, g = gravitational acceleration, and z = elevation.

The basic equations for steady groundwater flow both in confined and unconfined aquifers are derived in the following section.

2.3.3 Basic Equations for Steady Groundwater Flow

The basic equation for steady groundwater flow can be derived by substituting Eq. 2.13 into continuity equation Eq. 2.9, and is expressed as follows:

$$\nabla^2\phi = \frac{\partial^2\phi}{\partial x^2} + \frac{\partial^2\phi}{\partial y^2} + \frac{\partial^2\phi}{\partial z^2} = 0 \tag{2.19}$$

where the Laplacian operator $\nabla^2 = \partial^2/\partial x^2 + \partial^2/\partial y^2 + \partial^2/\partial z^2$.

This equation is known as Laplace's equation, which is an elliptic type of partial differential equation. When this equation is solved under boundary conditions, it is called the boundary value problem, and is used in potential theory. Laplace's equation has been used as a core equation in fluid mechanics, and tools to solve it have been based on conformal mapping and the use of of complex functions and, among others.

2.3.4 Basic Groundwater Flow Equations in Confined Aquifers

The basic groundwater flow equation for an aquifer with thickness b between an impervious basement and a confining layer (a confining stratum) can be derived using Eq. 2.8 (De Wiest R. J. M., 1969):

$$-\nabla\rho\mathbf{q} = \frac{\partial(n\rho)}{\partial t} = \rho\frac{\partial n}{\partial t} + n\frac{\partial \rho}{\partial t} \tag{2.20}$$

The piezometric head inside the confined aquifer $h(x, y)$ is dependent on horizontal coordinate (x, y) and time (t). It is assumed that the confined aquifer has elastic deformation resulting from changes in hydraulic head in the vertical direction (z) only, and the pore water is considered compressible.

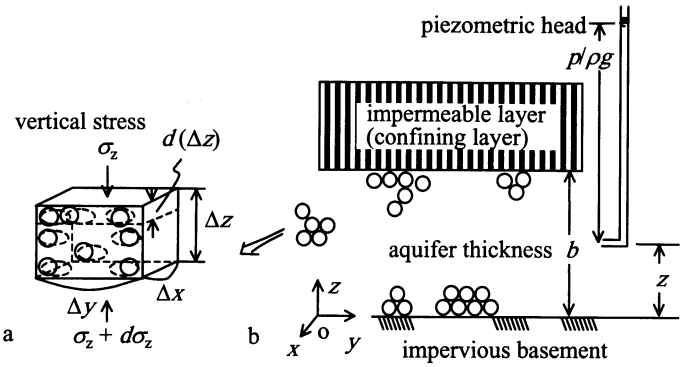

Fig. 2.8. Control volume (**a**) for flow in a confined aquifer (**b**)

Taking an infinitesimal volume ($\Delta V = \Delta x\,\Delta y\,\Delta z$) of the aquifer as shown in **Fig. 2.8a**, let us investigate the $\partial(n\rho\Delta x\,\Delta y\,\Delta z)/\partial t$ term on the right hand side of Eq. 2.20. Because the aquifer is deformable in the z-direction only, $\Delta x = \Delta y =$ constant, and $\rho n\,\partial(\Delta x)/\partial t = \rho n\,\partial(\Delta y)/\partial t = 0$, then the equation can be written in the following form:

$$\frac{\partial}{\partial t}(\rho n\,\Delta x\,\Delta y)\Delta z = \left(n\frac{\partial \rho}{\partial t}\Delta z + \rho\frac{\partial n}{\partial t}\Delta z + \rho n\frac{\partial(\Delta z)}{\partial t}\right)\Delta x\,\Delta y \tag{2.21}$$

From the definition of the compression coefficient for water (β, where $\beta\rho = \partial\rho/\partial p$), the first term in the right hand side of Eq. 2.21 can be written as $\partial\rho/\partial t = \rho\beta\,\partial p/\partial t$. Assuming that the solid volume in an confined aquifer $[(1 - n)\Delta x\,\Delta y\,\Delta z]$ is constant, and since $(1 - n)d(\Delta z) - \Delta z\,dn = 0$, the time derivative can be written as $\Delta z(\partial n/\partial t) = (1 - n)\partial(\Delta z)\partial t$. Denoting the compressibility of the infinitesimal aquifer by α, $\alpha(1 - n) = \partial n/\partial\sigma_z$, where σ_z = vertical stress, one can write $\partial n/\partial t = -\alpha(1 - n)\partial\sigma_z/\partial t$. Also, the relationship between pore pressure (p) and effective soil stress (σ_z) in the vertical direction can be determined based on the consolidation theory using Terzaghi's effective stress concept ($p + \sigma =$ constant, i.e., the sum of the pore water pressure and the effective stress acting on the soil particle frame is constant). Then, $\partial\sigma_z/\partial t = -\partial p/\partial t$, and the relationship between piezometric hydraulic head (h) and pressure (p) can be expressed as $\partial p/\partial t = \rho g\,\partial h/\partial t$.

Substitution of these expressions into Eq. 2.21 gives:

$$\frac{\partial}{\partial t}(\rho n) = \rho[\alpha(1 - n) + \beta n]\frac{\partial p}{\partial t} \tag{2.22}$$

The left hand side $(-\nabla\rho\mathbf{q})$ in Eq. 2.20 is rewritten using Darcy's law as:

$$-\nabla\rho\mathbf{q} = -\rho\left(\frac{\partial u}{\partial x} + \frac{\partial v}{\partial y} + \frac{\partial w}{\partial z}\right) - \left(u\frac{\partial \rho}{\partial x} + v\frac{\partial \rho}{\partial y} + w\frac{\partial \rho}{\partial z}\right)$$

Compressibility (β) and piezometric head (h) are defined as:

$$\mathbf{q} = -\frac{K}{\mu}(\rho g\nabla z + \nabla p),\ \nabla\rho = \rho\beta\nabla p,\ \nabla p = \rho g\nabla(h - z) \quad \text{and}$$

$$\left(\frac{\partial h}{\partial x}\right)^2 = \left(\frac{\partial h}{\partial y}\right)^2 = \left(\frac{\partial h}{\partial z}\right)^2 \approx 0$$

$$-\nabla\rho\mathbf{q} = \frac{\rho^2 Kg}{\mu}\left(\nabla^2 h - 2\rho\beta g\frac{\partial h}{\partial z}\right) \tag{2.23}$$

Integration of Eq. 2.20 from $z = 0$ to $z = b$ in the z-direction is realized:

$$-\int_0^b \nabla\rho\mathbf{q}\, dz = \int_0^b \frac{\partial(n\rho)}{\partial z} dz \tag{2.24}$$

and

$$\frac{\partial p}{\partial t} = \rho g\frac{\partial h}{\partial t}$$

Because the average velocity ($\overline{w} = -k\partial\overline{h}/\partial z$) in the z-direction must be zero at $z = 0$ and b, the basic equation of confined groundwater flow becomes:

$$\nabla^2\overline{h} = \frac{\partial^2\overline{h}}{\partial x^2} + \frac{\partial^2\overline{h}}{\partial y^2} = \frac{S}{T}\frac{\partial\overline{h}}{\partial t} \tag{2.25}$$

$$\overline{h} = \frac{1}{b}\int_0^b h\, dz \tag{2.26}$$

$$S = S_s b = \rho g(\alpha + n\beta)b \tag{2.27}$$

$$T = kb, \quad D_h = \frac{T}{S}, \quad k = \frac{K\rho g}{\mu} \tag{2.28}$$

in which S = coefficient of storage, T = transmissivity, D_h = head diffusivity and S_s = specific storage (L^{-1}).

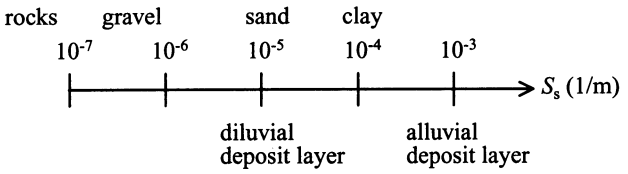

Fig. 2.9. General values of specific storage (S_s)

Equation 2.25 is the basic equation of groundwater flow in a confined aquifer. The equation is derived from the Darcy equation and the continuity equation under the assumption that the aquifer is deformable and pore water is compressible. This equation is a linear partial differential equation of the parabolic type (as is found in the heat conduction equation or diffusion equation). In many cases, for convenience, h is written instead of h.

Denoting discharge flow into or out of the aquifer through a unit area in a unit time by N_i, the following equation is obtained:

$$\frac{\partial^2 h}{\partial x^2} + \frac{\partial^2 h}{\partial y^2} + \frac{\sum_i N_i}{T} = \frac{S}{T}\frac{\partial h}{\partial t} \tag{2.29}$$

where N_i ($i = 1, 2, 3, \ldots$). As an example, $i = 1$ represents uptake or discharge per unit time per unit area and $i = 2$ is for vertical leakage in a compressed layer.

Hydraulic parameters such as S and k must be determined to find the hydraulic head (h) by solving Eq. 2.29. A practical approach for this purpose is to rewrite Eq. 2.29 in the cylindrical coordinate system, solve it using well theory, and then compare the solutions with field pumping test results. In some cases, Eq. 2.29 is invalid and the hydraulic parameters are determined based on numerical simulation results and hydraulic heads measured in numerous neighboring wells. This is known as the inverse identification method. In either case, the hydraulic parameters can be obtained.

Figure 2.9 shows storativity values used in general practice. In general, storativity values (defined for unit thickness and length, and denoted by S_s) for rocks are very small and for gravel and sand are relatively small. The values for clay and silt are slightly larger, whereas alluvial deposits have smaller values than that for diluvium.

2.3.5 Basic Groundwater Flow Equation in an Unconfined Aquifer

2.3.5 (a) Dupuit's Uniform Flow Approximation

Dupuit's uniform flow approximation for an unconfined aquifer states that the slope of the phreatic surface is very small ($\beta < 10$ degrees), as shown in **Fig. 2.10**. Thus, it is permissible to neglect vertical velocity (w) and consider horizontal groundwater flow using Dupuit's approximation. In this case, as depicted in **Fig. 2.10**, we can choose a coordinate system with the x-axis along the main flow direction and neglect the flow component in the transverse direction. The flow velocity near the free surface can be expressed as: $q_s = -k\,dz/ds = -k\sin\beta$, where k = hydraulic conductivity and β = free groundwater surface slope. For small values of β, $\sin\beta \approx \tan\beta\, dh/dx$, $q_s \to u$, $w \to 0$, and u is expressed by the following equation:

$$u = -k\frac{dh}{dx} \tag{2.30}$$

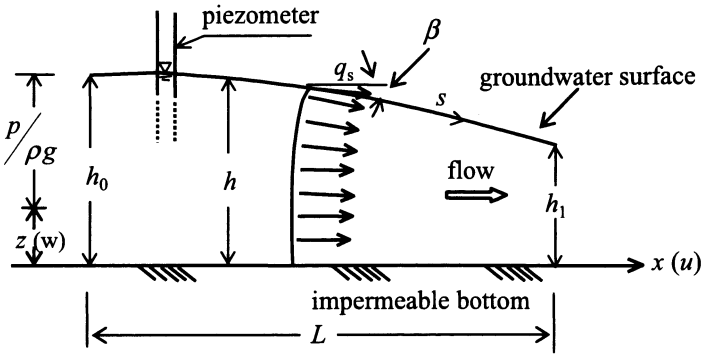

Fig. 2.10. Dupuit's uniform flow in an unconfined aquifer

Equation 2.30 is known as Dupuit's approximation in unconfined groundwater flow (Dupuit J., 1863). Dupuit's approximation is applicable not only for general groundwater flow with a free surface, but it is very useful for flows with an interface (such as the fresh water–sea water interface in coastal aquifers, cf. Fig. 3.11) to approximate two-dimensional flows by one-dimensional flows.

2.3.5 (b) Basic Equation

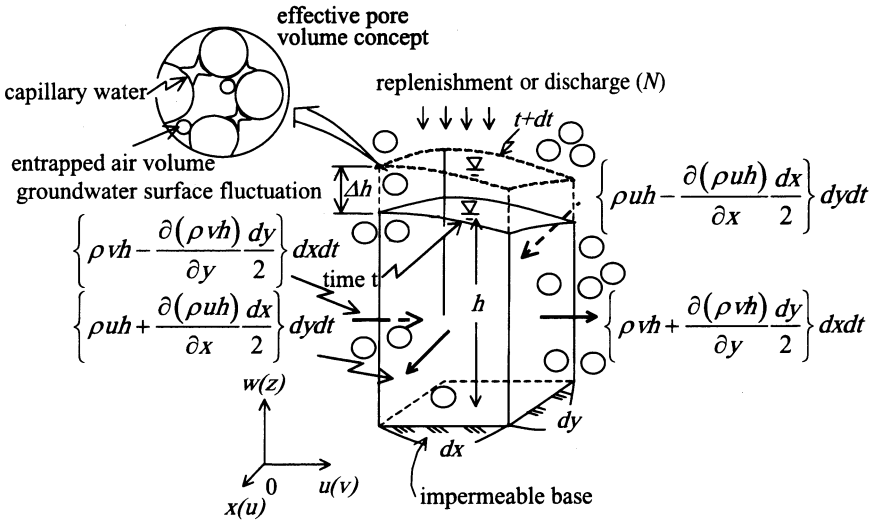

Fig. 2.11. Mass balance for an unconfined aquifer

Consider the mass balance in an infinitesimal control volume dx, dy, and height h, as shown in **Fig. 2.11**. During a short time interval (dt), the difference in water inflow

and outflow can be expressed by the following equation:

$$\left[\rho uh - \frac{\partial(\rho uh)}{\partial x}\frac{dx}{2}\right]dy\,dt - \left[\rho uh + \frac{\partial(\rho uh)}{\partial x}\frac{dx}{2}\right]dy\,dt + \left[\rho vh - \frac{\partial(\rho vh)}{\partial y}\frac{dy}{2}\right]dx\,dt - \left[\rho vh + \frac{\partial(\rho vh)}{\partial y}\frac{dy}{2}\right]dx\,dt + \rho N\,dx\,dy\,dt = -\left[\frac{\partial(\rho uh)}{\partial x} + \frac{\partial(\rho vh)}{\partial y} - \rho N\right]dx\,dy\,dt$$

where ρ = water density; u and v = Dupuit's uniform flow velocities in the x- and y-directions, respectively; and N = replenishment rate into the control volume in the vertical direction (for unit ground surface area in unit time [LT^{-1}]).

The rate of change of mass in the control volume ($\rho n_e h\,dx\,dy$) can also be written as $\rho n_e(\partial h/\partial t)dx\,dy\,dt$. Then, the following equation is obtained using Dupuit's uniform flow approximation (i.e. $u = -k\,\partial h/\partial x$, $v = -k\,\partial h/\partial y$):

$$\frac{\partial}{\partial x}\left(h\frac{\partial h}{\partial x}\right) + \frac{\partial}{\partial y}\left(h\frac{\partial h}{\partial y}\right) + \frac{N}{k} = \frac{n_e}{k}\frac{\partial h}{\partial t} \tag{2.31}$$

where n_e = effective porosity.

Equation 2.31 is known as Boussinesq's approximation equation. Because this is a nonlinear equation, it is not possible to obtain an analytical solution in general. Therefore, many efforts have been made to find solutions under different initial and boundary conditions. In groundwater terminology, this is called Boussinesq's problem. Two techniques are commonly applied to allow anallytical solutions of Eq. 2.31: (a) applying methods to particular solutions and (b) the linearization method (see examples for analytical solutions). Because groundwater flow is slow, it is weakly unsteady, and hence it can be considered as a time-dependent steady flow in many cases. Thus, it can be treated as successive steady state flows.

(Example 2.1)
Prove that the Boussinesq's approximation Eq. 2.31 can be derived directly from the basic groundwater flow equation ($-\nabla\rho\mathbf{q} = \partial(n\rho)/\partial t$).

(Answer)
Integrating the basic groundwater flow equation from the bottom of an impermeable base ($h = 0$) to the free groundwater surface (h), and using effective porosity (n_e), the following equation is obtained.

$$-\left[\int_0^h \frac{\partial}{\partial x}(\rho u)dz + \int_0^h \frac{\partial}{\partial y}(\rho v)dz + \int_0^h \frac{\partial}{\partial z}(\rho w)dz\right] = \int_0^h \frac{\partial}{\partial t}(\rho n_e)dz \tag{2.32}$$

Applying Leibnitz' rule to evaluate differentiation of an integral with variable limits, and for constant water density in an unconfined aquifer (ρ = constant), the left hand

side of Eq. 2.32 is expressed as follows[1]:

$$\begin{aligned}\int_0^h \frac{\partial}{\partial x}(\rho u)dz &= \rho\left[\frac{\partial}{\partial x}\int_0^h u\,dz - [u]_h\frac{\partial h}{\partial x}\right]\\ \int_0^h \frac{\partial}{\partial y}(\rho v)dz &= \rho\left[\frac{\partial}{\partial y}\int_0^h v\,dz - [v]_h\frac{\partial h}{\partial y}\right]\\ \int_0^h \frac{\partial}{\partial z}(\rho w)dz &= \rho[w]_h\end{aligned} \tag{2.33}$$

where $[\ ]_h$ denotes the value at the groundwater surface (h). Also, $\partial(\rho n_e)/\partial t = 0$ for ρn = constant.

Next, let the variable boundary conditions at the free groundwater surface be denoted by a function $F(x, y, z, t) = z - h(x, y, t)$. Then, the boundary condition at the surface ($dF/dt = 0$) can be expressed by the following equation[2]:

$$\frac{dF}{dt} = \frac{\partial F}{\partial t} + \frac{\partial F}{\partial x}\frac{dx}{dt} + \frac{\partial F}{\partial y}\frac{dy}{dt} + \frac{\partial F}{\partial z}\frac{dz}{dt} = 0$$

Since $\partial F/\partial z = 1$, $\partial F/\partial t = -\partial h/\partial t$, $\partial F/\partial x = -\partial h/\partial x$, $\partial F/\partial y = -\partial h/\partial y$, and the pore velocity component ($u' n_e = n_e\,dx/dt = u_s$, i.e., the Darcy velocity) is $n_e\,dy/dt = v_s$, $n_e\,dz/dt = w_s$, the following equation can be obtained.

$$n_e\frac{\partial h}{\partial t} + u_s\frac{\partial h}{\partial x} + v_s\frac{\partial h}{\partial y} = w_s \tag{2.34}$$

where the subscript (s) denotes values at the water surface.

Now, substituting Eqs. 2.33 and 2.34 into Eq. 2.32 near the ground surface, and with the flow velocities satisfying the conditions: $u_s = [u]_h$, $v_s = [v]_h$, and $w_s = [w]_h$, the following equation is obtained:

$$\frac{\partial}{\partial x}\int_0^h u\,dz - [u]_h\frac{\partial h}{\partial x} + \frac{\partial}{\partial y}\int_0^h v\,dz - [v]_h\frac{\partial h}{\partial y} + [w]_h = \frac{\partial(h\bar{u})}{\partial x} + \frac{\partial(h\bar{v})}{\partial y} + n_e\frac{\partial h}{\partial t} = 0$$

where $\bar{u} = \frac{1}{h}\int_0^h u\,dz$, $\bar{v} = \frac{1}{h}\int_0^h v\,dz$.

---

[1] **Leibnitz' Rule:**
Integration of a function $\partial f(x, y, z, t)/\partial t$ with respect to z over the range a_1, a_2 is given, for example,

$$\int_{a_1(x,y,t)}^{a_2(x,y,t)}\frac{\partial f}{\partial t}dz = \frac{\partial}{\partial t}\int_{a_1}^{a_2} f\,dz - [f]_{a_2}\frac{\partial a_2}{\partial t} + [f]_{a_1}\frac{\partial a_1}{\partial t}$$

[2] **Total differential formula:**
Total differential df of a function $f(x, y, z, t)$ is defined as,

$$df = \frac{\partial f}{\partial x}dx + \frac{\partial f}{\partial y}dy + \frac{\partial f}{\partial z}dz + \frac{\partial f}{\partial t}dt$$

Following the Dupuit uniform flow approximation, $\overline{u} = -k\,\partial h/\partial x$, $\overline{v} = -k\,\partial h/\partial y$, then Eq. 2.31 is obtained:

$$\frac{\partial}{\partial x}\left(h\frac{\partial h}{\partial x}\right) + \frac{\partial}{\partial y}\left(h\frac{\partial h}{\partial y}\right) = \frac{n_e}{k}\frac{\partial h}{\partial t}$$

2.3.5 (c) Dupuit's Formula

An unconfined steady groundwater flow in the x-direction, as shown in **Fig. 2.10**, will now be investigated. Because $\partial h/\partial t = 0$ and $\partial h/\partial y = 0$, Eq. 2.31 becomes $\partial(h\,\partial h/\partial x)/\partial x = 0$, where h is a function of x only. Integration of this equation with respect to x results in $h\,dh/dx = C_0$ (C_0 = the integration constant). Multiplying both sides of this equation by k and integrating it, one obtains: $kh \times dh/dx = kC_0$ ($= -Q$, where Q = flow discharge). Now, integrating the above equation results in the following:

$$k\int h\,dh = -\int Q\,dx, \quad \frac{k}{2}h^2 = -Qx + C$$

where C = the integration constant.

Using the boundary conditions: $x = 0$ and $h = h_0$, $C = kh_0^2/2$, the above equation can be expressed as follows:

$$\frac{k}{2}(h_0^2 - h^2) = Qx, \quad h_0 > h \tag{2.35}$$

where h_0 is the groundwater level at $x = 0$. This equation expresses the ground water surface. If $x = 0$, $h = h_0$, $x = L$ (distance), $h = h_1$, then

$$Q = \frac{k}{2L}(h_0^2 - h_1^2), \quad h_0 > h_1 \tag{2.36}$$

Equation 2.36 is known as Dupuit's formula.

2.4 Typical Analytical Solutions of the Basic Equations

Analytical solutions for the basic groundwater flow Eq. 2.25 and Eq. 2.31 in confined and unconfined aquifers are very important in understanding flow behavior. This section will introduce unsteady flows resulting from pumping from wells, variations in water level and hydraulic head in an aquifer as a result of tidal fluctuations, and Boussinesq's approximation problems.

2.4.1 Groundwater Flow around a Pumping Well

2.4.1 (a) Unsteady Flow

Figure 2.12 shows groundwater flow around single well in unconfined and confined aquifers. The flow converges toward the well in the horizontal direction and is called converging radial flow.

The basic groundwater flow equation in an unconfined aquifer (Eq. 2.31) can be generalized by assuming the decrease in hydraulic head ($s = H - h$) to be small and the infiltration rate to be zero ($N = 0$). In the case of a confined aquifer, N_i is zero in Eq. 2.29. Using the cylindrical coordinate system to represent the Laplace operator on the left hand sides of Eqs. 2.29 and 2.31, the following equations are obtained[3]:

$$\text{For unconfined aquifers:} \qquad \nabla^2 h = \frac{\partial^2 h}{\partial r^2} + \frac{1}{r}\frac{\partial h}{\partial r} \approx \frac{n_e}{kh}\frac{\partial h}{\partial t} \tag{2.37}$$

$$\text{For confined aquifers:} \qquad \nabla^2 h = \frac{\partial^2 h}{\partial r^2} + \frac{1}{r}\frac{\partial h}{\partial r} \approx \frac{S}{kb}\frac{\partial h}{\partial t} \tag{2.38}$$

where $T = kb \approx kh$, and h is the average water depth.

The above two equations are linear partial differential equations of the same category as heat conduction or diffusion equations. By using a decreasing hydraulic head ($s = H - h$), the following equation is obtained:

$$\frac{\partial^2 s}{\partial r^2} + \frac{1}{r}\frac{\partial s}{\partial r} = \kappa \frac{\partial s}{\partial t} \tag{2.39}$$

where $\kappa = n_e/T = S/T$ and $D_h = 1/\kappa$ are respectively the diffusion coefficients for the water level (unconfined aquifers) and for the hydraulic head (confined aquifers).

It is possible to understand groundwater flows in confined and unconfined aquifers by solving Eq. 2.39 with initial and boundary conditions. The initial and boundary conditions are expressed as follows:

$$\left.\begin{array}{l} \text{At time } t = 0,\ s = 0 \text{ (initial water level, hydraulic head)} \\ \text{At very far from the well, } r = \infty,\ s = 0,\ t > 0 \\ r = r_0 \text{ (well wall)} \approx 0, \text{ pumping} = Q = (2\pi r T)\partial s/\partial r = \text{constant} \end{array}\right\} \tag{2.40}$$

Several methods are available for solving Eq. 2.39; however, only the most common method is briefly described here. By substituting for variable $\zeta = \sqrt{\kappa}\, r/2\sqrt{t}$, the partial differential equation is converted into an ordinary differential equation, as shown below, and can be solved.

$$\frac{\partial \zeta}{\partial t} = -\frac{\sqrt{\kappa}\, r}{4t^{3/2}} = -\frac{\zeta}{2t},\quad \frac{\partial \zeta}{\partial r} = \frac{\sqrt{\kappa}}{2\sqrt{t}} = \frac{\zeta}{r},\quad \frac{\partial s}{\partial t} = \frac{\partial \zeta}{\partial t}\frac{ds}{d\zeta} = -\frac{\zeta}{2t}\frac{ds}{d\zeta}$$

$$\frac{1}{r}\frac{\partial s}{\partial r} = \frac{1}{r}\frac{\partial \zeta}{\partial r}\frac{ds}{d\zeta} = \frac{\zeta}{r^2}\frac{ds}{d\zeta},\quad \frac{\partial \zeta}{\partial r} = \frac{\sqrt{\kappa}}{2\sqrt{t}}$$

$$\frac{\partial^2 s}{\partial r^2} = \frac{\partial}{\partial r}\left(\frac{\partial s}{\partial r}\right) = \frac{\partial}{\partial \zeta}\left(\frac{\kappa}{4t}\frac{\partial s}{\partial \zeta}\right) = \frac{\zeta^2}{r^2}\frac{d^2 s}{d\zeta^2}$$

[3] **Laplace operator:**
Transformation of Laplace operator ∇^2 in Cartesian coordinates (x, y, z) into cylindrical coordinates (r, θ, z) is written by

$$\nabla^2 = \frac{\partial}{\partial x^2} + \frac{\partial}{\partial y^2} + \frac{\partial}{\partial z^2} = \frac{\partial}{\partial r^2} + \frac{1}{r}\frac{\partial}{\partial r} + \frac{1}{r^2}\frac{\partial^2}{\partial \theta^2} + \frac{\partial^2}{\partial z^2}$$

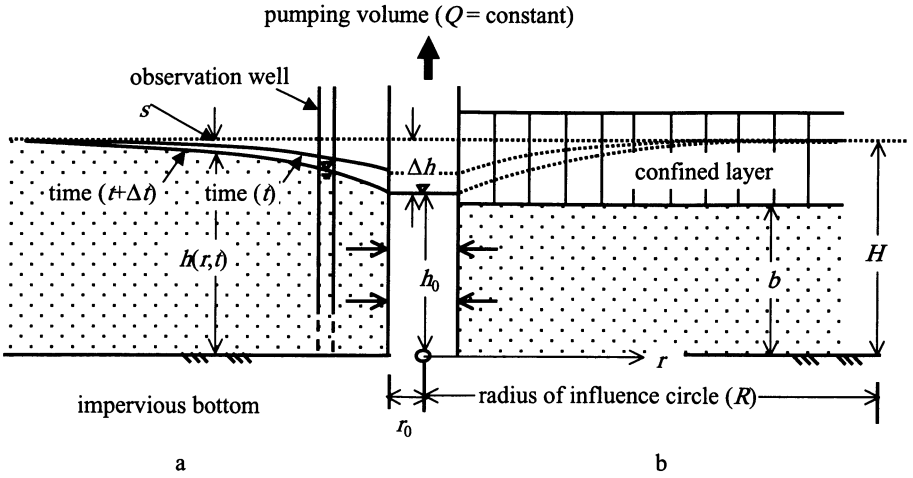

Fig. 2.12. Unsteady flow around a pumping well for **a** unconfined aquifers and **b** confined aquifers

The following equation is obtained:

$$\frac{d^2s}{d\zeta^2} + \left(\frac{1}{\zeta} + 2\zeta\right)\frac{ds}{d\zeta} = 0 \tag{2.41}$$

Arranging the ordinary differential equation and integrating it with respect to ζ, the following equation is obtained:

$$-\int \frac{\frac{d}{d\zeta}\left(\frac{ds}{d\zeta}\right)}{\frac{ds}{d\zeta}} d\zeta = \int \left(2\zeta + \frac{1}{\zeta}\right) d\zeta + C_0, \quad -\log\left(\frac{ds}{d\zeta}\right) = \zeta^2 + \log\zeta + C_0$$

$$\log\zeta\frac{ds}{d\zeta} = -\zeta^2 + C_0, \quad \frac{ds}{d\zeta} = C\frac{e^{-\zeta^2}}{\zeta} \tag{2.42}$$

where C_0 and C are integration constants.

Furthermore, according to the conditions expressed in Eq. 2.40, $t = 0$, $s = 0$ and $\zeta = \infty$, $s = 0$, then s is expressed in the following form:

$$s = C\int_{\zeta}^{\infty} \frac{e^{-\zeta^2}}{\zeta} d\zeta = \frac{Q}{2\pi T}\int_{\zeta}^{\infty} \frac{e^{-\zeta^2}}{\zeta} d\zeta$$

The constant C in Eq. 2.42 is determined as follows:

$$Q = \lim_{r\to 0} 2\pi r T\frac{\partial s}{\partial r} = \lim_{r\to 0} 2\pi r T\frac{\partial \zeta}{\partial r}\frac{ds}{d\zeta} = \lim_{r\to 0} 2\pi r T\frac{\zeta}{r}\frac{ds}{d\zeta} = \lim_{\zeta\to 0} 2\pi C T e^{-\zeta^2}$$

and $C = Q/2\pi T$.

Then, the decrease of hydraulic head (s) is expressed by a new variable, $u = \zeta^2 = \kappa r^2/4t$, $d\zeta = du/2\zeta$ as follows.

$$s = H - h = \frac{Q}{4\pi T}\int_u^\infty \frac{e^{-u}}{u}du = \frac{Q}{4\pi T}W(u) \tag{2.43}$$

$$u = \frac{\kappa r^2}{4t}, \quad W(u) = \int_u^\infty \frac{e^{-u}}{u}du \tag{2.44}$$

where $W(u)$ is called the well function and can be evaluated by using a power series expansion as follows[4]:

$$\begin{aligned} W(u) &= -0.5772 - \log u + u + \frac{u^2}{2\cdot 2!} + \frac{u^3}{3\cdot 3!} + \cdots \\ &\approx \log\frac{1}{u} - 0.5772, \quad (u \ll 1). \end{aligned} \tag{2.45}$$

2.4.1 (b) Steady Flow

If a constant discharge is pumped from a well in an aquifer (confined or unconfined) over a long period, the radial flow discharge will be equal to the pumping discharge, and a steady state is reached. Theories for steady flow under these conditions are fundamental in hydraulics and several such examples are shown below.

Wells in a Confined Aquifer

Putting $\partial/\partial t = 0$ into Eq. 2.38 and integrating with respect to r, the following equations are obtained:

$$r\frac{dh^2}{dr^2} + \frac{dh}{dr} = \frac{d}{dr}\left(r\frac{dh}{dr}\right) = 0 \tag{2.46}$$

$$r\frac{dh}{dr} = C_1, \quad h = C_1 \log r + C_2 \tag{2.47}$$

where C_1 and C_2 are integration constants.

The radial flow velocity (v_r) is expressed by the following equation:

$$v_r = -k\frac{dh}{dr} = -k\frac{C_1}{r} \quad \begin{matrix} (C_1 > 0\text{: Pumping}) \\ (C_1 < 0\text{: Recharge}) \end{matrix}$$

Given that $Q_r = 2\pi br|v_r|$, then $C_1 = Q_r/2\pi kb$. The boundary condition at the well surface requires the groundwater level to be equal to the water level inside the well

[4] **Integration formula of exponential function:**

$$\int_x^\infty \frac{e^{-x}}{x}dx = -\log x - \gamma + x - \frac{x^2}{2\cdot 2!} + \cdots + \frac{(-x)^n}{n\cdot n!} - \cdots$$

$x > 0$, $\gamma = 0.5772$ (Euler's constant) (Mathematics Formula-I, S. Moriguchi et al., Iwanami. p. 154 in Japanese).

($h = h_0$) at $r = r_0$. Then, $C_2 = -(Q_r \log r_0)/2\pi kb + h_0$ and Eq. 2.47 is expressed as follows:

$$h - h_0 = \frac{Q_r}{2\pi kb} \log\left(\frac{r}{r_0}\right) \tag{2.48}$$

Putting $h = H$ (initial hydraulic head) at $r = R$ (R = radius of influence of the well), the following equation is obtained:

$$Q_r = \frac{2\pi kb(H - h_0)}{\log\left(\frac{R}{r_0}\right)} = \frac{2\pi kb(H - h_0)}{2.30 \log_{10}\left(\frac{R}{r_0}\right)} \tag{2.49}$$

Wells in an Unconfined Aquifer

The same procedure can be applied to wells in an unconfined aquifer. However, in this case the aquifer thickness (b) in Eqs. 2.48 and 2.49 should be replaced by $(h + h_0)/2$. Using the conditions at $r = R$ and $h = H$, the following equations are obtained:

$$h^2 - h_0^2 = \frac{Q_r}{\pi k} \log \frac{r}{r_0} \tag{2.50}$$

$$Q_r = \frac{\pi k(H^2 - h_0^2)}{\log\left(\frac{R}{r_0}\right)} = \frac{\pi k(H^2 - h_0^2)}{2.30 \log_{10}\left(\frac{R}{r_0}\right)} \tag{2.51}$$

2.4.2 Water Level Fluctuation in a Coastal Aquifer as a Result of Tides

Figure 2.13 simultaneously shows changes in water level or hydraulic head (h) in a confined and an unconfined coastal aquifer as a result of tide propagation (Jacob C. E., 1951). Substituting $N = 0$ and denoting $s = (h_0 - h)$ as the change in hydraulic head, the basic equation (Eqs. 2.29 and 2.31) can be expressed in the following form:

$$\frac{\partial^2 s}{\partial x^2} = \kappa \frac{\partial s}{\partial t}, \quad \kappa = \frac{S}{T} \approx \frac{n_e}{kh_0} \tag{2.52}$$

where h_0 = average tidal height.

The boundary conditions are as follows:

$$\left.\begin{array}{ll} x = 0, & s = a\cos\sigma t, \quad t > 0 \\ x \to \infty, & s = 0, \quad t > 0 \end{array}\right\} \tag{2.53}$$

where a = tidal amplitude and σ = angular frequency of the tide.

Euler's formula ($e^{i\sigma t} = \cos\sigma t + i \sin\sigma t$) is used to obtain a solution of the equation:

$$s = \cos\sigma t f(x) = R[e^{i\sigma t} f(x)] \tag{2.54}$$

Substituting Eq. 2.54 into Eq. 2.52, the following is obtained:

$$\frac{d^2 f}{dx^2} - i\sigma\kappa f(x) = 0 \tag{2.55}$$

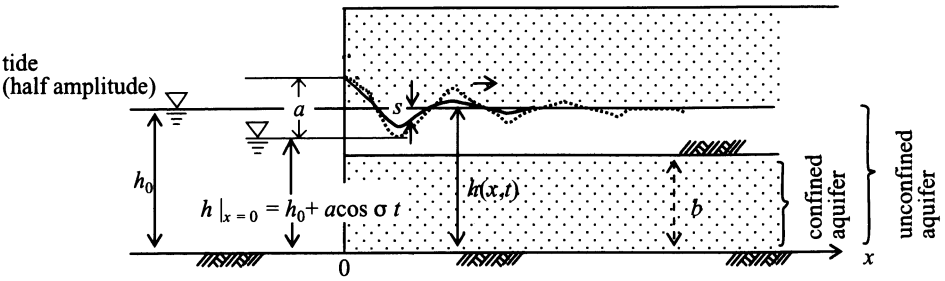

Fig. 2.13. Variation in groundwater level as a result of tides in a coastal aquifer. Solid line, free water surface; dashed line, hydraulic head in a confined aquifer

where $R[\ ]$ denotes the real part and $i = \sqrt{-1}$ = the imaginary unit.

Noting that $\sqrt{i} = (1 + i)/\sqrt{2}$ and that $(\cos\theta + i\sin\theta)^n = \cos n\theta + i\sin n\theta$, the solution of Eq. 2.55 can be obtained as follows:

$$\begin{aligned} f(x) &= Ae^{\sqrt{i\sigma\kappa}x} + Be^{-\sqrt{i\sigma\kappa}x} \\ &= Ae^{\sqrt{\frac{\sigma\kappa}{2}}(1+i)x} + Be^{-\sqrt{\frac{\sigma\kappa}{2}}(1+i)x} \end{aligned} \tag{2.56}$$

where A and B are constants.

As $x \to \infty$ and $s = f(x) = 0$, then $A = 0$, and as $x = 0$ and $f(x) = a$, then $B = a$. Therefore, the final solution is expressed as follows:

$$s = ae^{-\sqrt{\frac{\sigma\kappa}{2}}x}\cos\left(\sigma t - \sqrt{\frac{\sigma\kappa}{2}}x\right) \tag{2.57}$$

It is clear from Eq. 2.57 that time variations in water level or hydraulic head as a result of tide propagation in the x-direction decrease exponentially. As an example, assume that $h_0 = b = 10\,\text{m}$, $k = 10^{-4}\,\text{m/s}$, and $n_e = 10^{-1}$. Then, $\kappa = n_e/kh_0 = 10^2\,\text{s/m}^2$ for an unconfined aquifer. The specific storage ($S_s = S/b$) is of the order of $10^{-5}/\text{m}$ (from **Fig. 2.9**) and $\kappa = S/(kb) = 10^{-1}\,\text{s/m}^2$ for a confined aquifer. Thus, the tidal amplitude dissipation ($\sqrt{\sigma\kappa/2}$) for a confined aquifer is larger than that for an unconfined aquifer, and hence the tidal wave cannot propagate a great distance. On the other hand, waves can propagate far enough for small wave amplitude dissipation in confined aquifer. Also, the wave celerity (c) is small for an unconfined aquifer and large for a confined aquifer because $c = \sigma/\sqrt{\sigma\kappa/2} = \sqrt{2\sigma/\kappa}$.

2.5 Steady Two-Dimensional Potential Flow

This section deals with the application of potential theory for formulating time-independent steady groundwater flow, which reduces to the geometrical analysis of flow patterns.

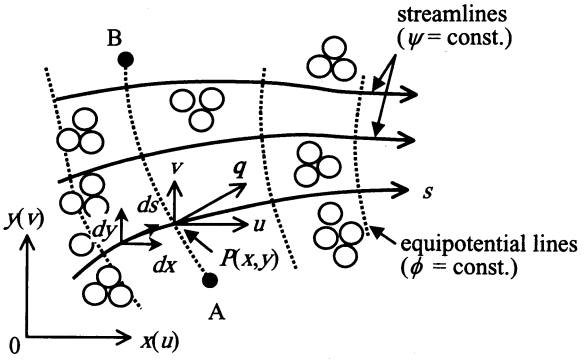

Fig. 2.14. Relationship between streamlines and velocity components

2.5.1 Relationship Between Stream Function and Velocity Potential

It is possible to visualize groundwater flow (along s) by tracing some marked particles in a two-dimensional steady flow as shown in **Fig. 2.14**. If the flow direction of velocity vector $\mathbf{q}(u, v)$ at a point $P(x, y)$ coincides with that of the infinitesimal element ds (dx, dy), the equation of the streamline is formulated by:

$$\frac{dx}{u} = \frac{dy}{v}, \quad \text{or} \quad v\,dx - u\,dy = 0 \tag{2.58}$$

If Eq. 2.58 is compared with the total differential $(d\psi)$ of a function ψ, then u and v can be written as follows:

$$d\psi = v\,dx - u\,dy = \frac{\partial \psi}{\partial x}dx + \frac{\partial \psi}{\partial y}dy = 0$$

$$u = -\frac{\partial \psi}{\partial y}, \quad v = \frac{\partial \psi}{\partial x} \tag{2.59}$$

The function (ψ) is called the stream function, and ψ = constant indicates a streamline, according to its definition.

Physically, $d\psi = u\,dx - v\,dy$ expresses the flow discharge in unit tube along the s-direction. For example, noting a finite section connecting points A and B in **Fig. 2.14**, the flow discharge between these two points can be expressed by the following equation:

$$\int_A^B d\psi = \psi_B - \psi_A \tag{2.60}$$

On the other hand, the zero vorticity for irrotational flow is written by $\partial v/\partial x - \partial u/\partial y = 0$, and $u\,dx + v\,dy$ is necessary and sufficient condition for the existence of total differential, and the total differential of a function (ϕ) is expressed as follows:

$$-d\phi = u\,dx + v\,dy = -\left(\frac{\partial \phi}{\partial x}dx + \frac{\partial \phi}{\partial y}dy\right)$$

Then, the flow velocity components u and v in the x- and y-directions can be expressed in the following form:

$$u = -\frac{\partial \phi}{\partial x}, \quad v = -\frac{\partial \phi}{\partial y} \tag{2.61}$$

Because the velocity components in Eq. 2.61 are defined in terms of the total differential of function (ϕ), the function is called the velocity potential. A line with ϕ = constant (i.e., $d\phi = 0$) is called an equipotential line.

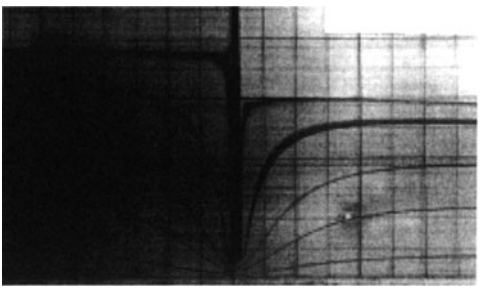

Fig. 2.15. Groundwater flow around a cut-off wall (after the Hele-Shaw model)

The total velocity vector can be expressed as: $\mathbf{q}_s = -\partial\phi/\partial x$. An example of groundwater flow streamlines around a cut-off wall is shown in **Fig. 2.15**.

2.5.2 Complex Potential Theory for Solving Steady State Flow

The velocity components in two-dimensional flow (u and v) can be defined in terms of velocity potential (ϕ) and stream function (ψ) as follows:

$$u = -\frac{\partial \phi}{\partial x} = -\frac{\partial \psi}{\partial y}, \quad v = -\frac{\partial \phi}{\partial y} = \frac{\partial \psi}{\partial x} \tag{2.62}$$

The velocity components (u and v) can be expressed in the following form by changing them from the Cartesian coordinate system (x, y) to polar coordinates (r, θ) and denoting velocity in the radial (r) and angular (θ) directions by v_r and v_θ, respectively:

$$v_r = u\cos\theta + v\sin\theta, \quad v_\theta = -u\sin\theta + v\cos\theta,$$
$$\cos\theta = \partial x/\partial r = \partial y/r\,\partial\theta, \quad \sin\theta = \partial y/\partial r = -\partial x/r\,\partial\theta$$

or

$$v_r = -\frac{\partial \phi}{\partial r} = -\frac{\partial \psi}{r\,\partial \theta}, \quad v_\theta = -\frac{\partial \phi}{r\,\partial \theta} = \frac{\partial \psi}{\partial r} \tag{2.63}$$

The equation of continuity under irrotational conditions for an incompressible fluid can be expressed by the following equations:

$$\frac{\partial u}{\partial x} + \frac{\partial v}{\partial y} = 0, \qquad \nabla^2\phi = \frac{\partial^2\phi}{\partial x^2} + \frac{\partial^2\phi}{\partial y^2} = 0 \tag{2.64}$$

$$\frac{\partial v}{\partial x} - \frac{\partial u}{\partial y} = 0, \qquad \nabla^2\psi = \frac{\partial^2\psi}{\partial x^2} + \frac{\partial^2\psi}{\partial y^2} = 0 \tag{2.65}$$

Thus, both velocity potential and stream functions satisfy Laplace's equation.

Equations 2.62 are called the Cauchy–Riemann differential equations. They express necessary and sufficient conditions for the existence of a regular complex function as shown in Eq. 2.66:

$$w(z) = \phi + i\psi \tag{2.66}$$

Similarly, Eq. 2.62 can be written in the following form by expressing the differential dw/dz with respect to x and y:

$$\frac{dw}{dz} : \frac{\partial\phi}{\partial x} + i\frac{\partial\psi}{\partial x} = -u + iv = \frac{1}{i}\left(\frac{\partial\phi}{\partial y} + i\frac{\partial\psi}{\partial y}\right) \tag{2.67}$$

Because the real and imaginary parts of the differential Eq. 2.67 for w are velocity components, the function $w(z)$ is called the complex potential.

2.5.3 Conformal Mapping

The Laplace equation ($\nabla^2\phi = 0$ and $\nabla^2\psi = 0$) for steady groundwater flow (discussed later) can be solved under field boundary conditions. One of the solution methods is known as conformal mapping.

The complex function $w = f(z)$, $w(z) = \phi + i\psi$, $\phi = \phi(x, y)$, $\psi = \psi(x, y)$ is a single value function (a function which takes only one dependent value w for an independent variable z). Thus, a figure A drawn from a point (z) in the z-plane is reflected on another figure B drawn from point w in the w-plane. This is called the mapping of figure A in the z-plane onto figure B in the w-plane through a function $w = f(z)$. If the function $w = f(z)$ is a regular function (differentiable function), and $f'(a) \neq 0$, an intersecting angle of two curves at a point (a) in the z-plane is mapped onto an equal angle in the w-plane, the mapping is called conformal mapping.

The conformal mapping technique can be applied to solve boundary value problems of Laplace's equation, such as in the fields of fluid flow, heat conduction, and stress analysis. To attein solutions, the reflected image of Schwarz (if two points are symmetric, then one point is called the reflected image of the other) and the Schwarz–Christoffel transformation (which transforms the inner portion of a polygon into the upper half plane by conformal mapping) are usually used.

These days, numerical methods are commonly used for the analysis of groundwater problems; however, the conformal mapping technique is still useful in analytical methods, and can improve understanding of the basic phenomena.

2.5.4 Boundary Conditions

In general, the boundary conditions for groundwater flow analyses are shown in **Fig. 2.16**, and classified as follows.

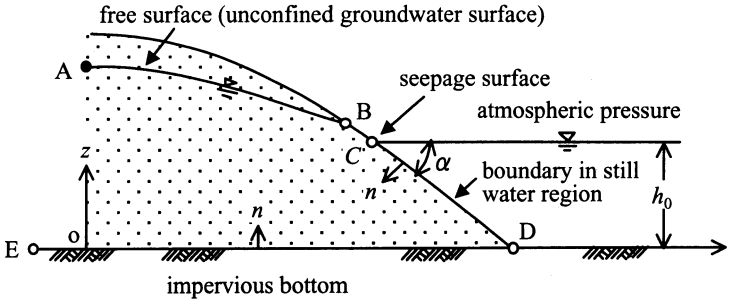

Fig. 2.16. Boundary conditions

1. Free Surface *AB*

The surface of the ground water table in unconfined aquifers is in direct contact with the atmosphere. Thus, the pressure at the surface equals atmospheric pressure (p_0, also known as gauge pressure = 0). Sometimes the interface between the water table and the atmosphere is treated as nonmixing, similar to the interface between two immiscible fluids. At the interface, pressure $p = p_0$, velocity potential $\phi = kz$ + constant, and stream function ψ = constant (the boundary streamline).

2. Seepage Surface *BC*

Because seeping water is in direct contact with the atmosphere and flows down along slope *BC* within a thin layer, then $p = p_0$, $\phi = kz$ + constant, and $-\partial\phi/\partial n = -k\,\partial z/\partial n = -k\cos\alpha$, where $n(x, y)$ = the normal distance to the boundary and α = angle of the slope.

3. Boundary in the Still Water Region *CD*

The equipotential lines and streamlines for the sloping surface *CD* in a still water region are given by: $\phi = k(z + p/\rho g)$ = constant and $\partial\phi/\partial n = 0$, respectively ($\rho$ = water density and g = gravitational acceleration).

4. Impermeable Surface *DE*

Groundwater flows along any impermeable surface such as the rock basement *DE* in **Fig. 2.16**. The surface itself becomes a streamline in such a case. Because there is no flow in the normal direction to the surface, ψ = constant, and $\partial\phi/\partial n = 0$.

The above-mentioned four boundary conditions appear in various geometries of the flow domain. Problems solving Laplace's equations ($\nabla^2\phi = 0$ and $\nabla^2\psi = 0$) satisfying these conditions are known as boundary value problems.

2.5.5 Examples of Two-Dimensional Steady State Flow

Worked examples on basic groundwater flow and two-dimensional flows based on complex potential theory, reflected images, and conformal mapping are presented in this section.

2.5.5 (a) Radial Flow

A uniform radial flow is depicted in **Fig. 2.17a**. Assuming the complex potential $w(z)$ in a logarithmic form, the following equation can be written:

$$w(z) = -\frac{q_r}{2\pi}\log z, \quad q_r = \text{constant} \tag{2.68}$$

Using Euler's formula [$z = r(\cos\theta + i\sin\theta) = re^{i\theta}$], the following equation is obtained:

$$w = -\frac{q_r}{2\pi}\log r - i\frac{q_r}{2\pi}\theta = \phi + i\psi \tag{2.69}$$

where $\phi = -(q_r/2\pi)\log r$ = constant, r = constant, and $\psi = -(q_r/2\pi)\theta$ = constant.

This flow has circular equipotential lines for $\log r$ = constant, and streamlines radiate from the flow source. The radiating velocity (v_r) is given by the following equation:

$$v_r = -\frac{\partial\phi}{\partial r} = \frac{q_r}{2\pi r}$$

As $r \to 0$, $v_r \to \infty$, and as $r \to \infty$, $v_r \to 0$. For $q_r > 0$, the flow is known as diverging flow (a source) and for $q_r < 0$, it is known as converging flow (a sink), where q_r = flow discharge per unit width per unit time, and is called the source or sink intensity (for a thickness b, flow discharge = $Q_r = bq_r$). If a source ($q_r > 0$) is located at $x = a$ on the x-axis, then the complex potential can be written as $w = -(q_r/2\pi)\log(z - a)$.

2.5.5 (b) Flow to a Drainage Pipe or Undersea Tunnel

A source ($q_r > 0$) at $x = -x_0$ on the vertical x-axis is symmetrical to a sink ($q_r < 0$) at $x = x_0$ through the x-axis on the water bottom basement, as shown in **Fig. 2.17b**.

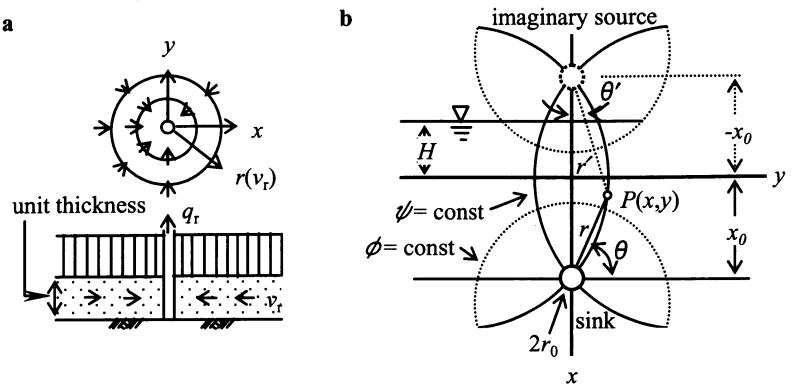

Fig. 2.17 a, b. Two-dimensional groundwater flow. **a** Radial flow and **b** flow to a drain or an undersea tunnel

These two points are mirror images. In this case, the complex potential is the sum of the potentials at corresponding points, and is expressed as follows:

$$w(z) = -\frac{q_r}{2\pi}\log(z - x_0) + \frac{q_r}{2\pi}\log(z + x_0)$$
$$= -\frac{q_r}{2\pi}\log\left(\frac{z - x_0}{z + x_0}\right) \tag{2.70}$$

Equation 2.70 can be expressed in the following form assuming that the distances of a point $P(x, y)$ from the sink and source are r and r', respectively, and that θ and θ' are the angles of the respective lines. Using the Euler's equations ($z + x_0 = re^{i\theta}$, $z - x_0 = r'e^{i\theta'}$) gives:

$$w(z) = -\frac{q_r}{2\pi}\log\frac{r}{r'} - i\frac{q_r}{2\pi}(\theta - \theta') = \phi + i\psi \tag{2.71}$$
$$\phi = -\frac{q_r}{2\pi}\log\frac{r}{r'} = \frac{q_r}{2\pi}\log\frac{r'}{r}, \quad \psi = -\frac{q_r}{2\pi}(\theta - \theta')$$

Therefore, the streamlines that satisfy the condition ($\theta - \theta'$ = constant) are a group of circles centered on the y-axis, and the equipotential lines satisfying the condition (r'/r = constant) are a group of circular lines centered on the x-axis.

The velocity potential (ϕ) can be generalized as shown below:

$$\phi = \phi_0 + \frac{q_r}{2\pi}\log\frac{r'}{r} = kH + \frac{q_r}{4\pi}\log\frac{(x - x_0)^2 + y^2}{(x + x_0)^2 + y^2} \tag{2.72}$$

where ϕ_0 = a reference potential with $\phi_0 = kH$ = constant at $x = 0$, k = permeability, and H = water depth.

The velocity potential (ϕ_{x_0}) at the vicinity of a drainage pipe with the radius r_0 and $x \approx x_0$, $y \approx y_0$, ($r' = \sqrt{(x - x_0)^2 + y^2} \approx r_0$, $r = 2x_0$) is expressed as follows:

$$\phi_{x_0} = kH + \frac{q_r}{2\pi}\log\frac{r_0}{2x_0} = kh_{x_0}$$

$$q_r = \frac{2\pi k(h_{x_0} - H)}{\log\left(\frac{r_0}{2x_0}\right)} = 2\pi k(H - h_{x_0}) \log\left(\frac{2x_0}{r_0}\right), \quad \frac{2x_0}{r_0} > 1 \tag{2.73}$$

$$= 4.6\pi k(H - h_{x_0}) \log_{10}\left(\frac{2x_0}{r_0}\right)$$

where h_{x_0} = piezometric head inside the drain pipe (if the inside pressure of the drain pipe is atmospheric, then $p_0/\rho g = 0$ and $h_{x_0} = -x_0$).

This flow is the combination of two flows: that resulting from the sink ($q_r < 0$) at $x = x_0$ and that from the source ($q_r > 0$) at $x = -x_0$. Since each flow satisfies Laplace's equation, the combined flow also satisfies this condition. Laplace's equation is a linear partial differencial equation and it is therefore possible to obtain a solution for the combined flow by summing the individual solutions for each flow. This is called the principle of superposition.

2.6 Isothermal Unsaturated Flow

Groundwater is classified as either saturated or unsaturated. Surface tension and gravity are the driving forces for unsaturated groundwater flow. Knowledge of unsaturated groundwater flow is very important in various aspects of groundwater hydrology. Soil water movement in the upper unsaturated zone above the groundwater table, evaporation at the land surface and rainfall, and infiltration within soil structures such as dikes are a few examples that will be considered.

Unsaturated flow is classified mainly into two categories depending on whether heat transport significantly influences the soil moisture movement (thermally induced flow) or whether the thermal effect is negligibly small. The latter type of flow is known as isothermal flow.

This section deals with the characteristics and application of isothermal unsaturated groundwater flow, the physical relationships among various parameters, and methods for analyzing the transport and mass conservation equations. In addition, some examples of field application are introduced to help understanding of the problems.

2.6.1 Characteristics of the Unsaturated Flow Field

(a) Unsaturated Flow Fields

As stated in Chap. 1, the dynamic balance between surface tension and gravity forces governs unsaturated groundwater flow. The participating quantities and flow mechanism for an isothermal groundwater flow are depicted in **Fig. 2.18** (see Chap. 4 for thermal unsaturated groundwater flow). In general, an unsaturated groundwater flow field comprises the following elements:

1. A porous medium (soil or rock mass consisting of solid particles)
2. Gas in a part of the porous space (air or gas)

3. Unsaturated flow with liquid water and water vapor
4. Air (or gas) bubbles trapped by liquid water
5. Phase change between liquid water and water vapor (i.e., the vapor pressure relationship between liquid water and water vapor)

External forces (e.g., surface tension, gravity, and pressure gradient) acting on liquid- and vapor-phase water drive unsaturated groundwater flow. Denoting two points on the upstream and downstream sides of the x-axis by x_1 and x_2, respectively, these driving forces are capillary pressure (p_{c1} and p_{c2}) and vapor pressure (p_{v1} and p_{v2}) at these points. Assuming $\theta_1 > \theta_2$ (water content), $p_{c1} < p_{c2}$ (negative pressure) and $p_{v1} > p_{v2}$ (vapor pressure), the unsaturated groundwater flow is in the direction of the x-axis. For high water content values, the downward movement resulting from gravity increases, and movement caused by the difference in capillary pressure along the x-axis decreases. Surface tension plays a dominant role for low water content environments, and hence movement due to capillary pressure increases. Thus, spatial variation in capillary pressure drives unsaturated groundwater flow.

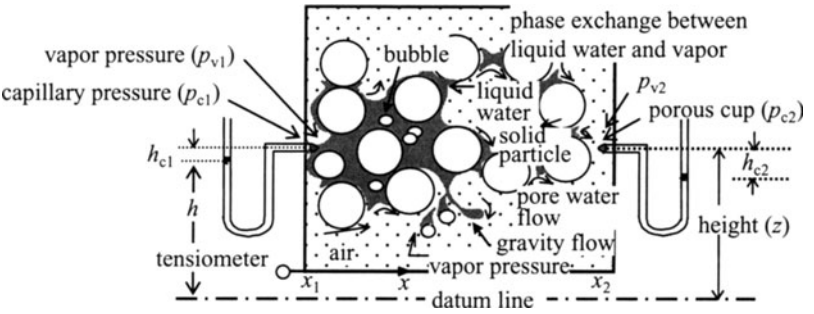

Fig. 2.18. Unsaturated flow with various parameters

The suction pressure (negative) in unsaturated groundwater flow conditions is measured using a tensiometer (which corresponds to manometer as used in saturated groundwater flow with a porous cup at one end). The measured pressure is a result of the vapor pressure and capillary pressure in the matrix of the pores. Because vapor pressure is very small in unsaturated groundwater flow at normal temperatures, the capillary pressure, which depends on pore size and geometry, mainly determines the measure pressure.

(b) Darcy's Formula for Unsaturated Flow

The transport equation in unsaturated flow is also Darcy's law. However, the flow velocity (u) depends on the volumetric water content (θ) and capillary head ($h = z - h_c$, $h_c = p_c/\rho g$) as follows:

$$u(\theta, h_c) = -k(\theta)\frac{dh_c(\theta)}{dx} = D(\theta)\frac{\partial\theta}{\partial x} \tag{2.74}$$

$$D(\theta) = -k(\theta)\frac{dh_c}{d\theta} = \frac{k(\theta)}{C_w}, \quad C_w = -\frac{d\theta}{dh_c} \tag{2.75}$$

or

$$u(\theta, h_c) = -k_0 k_r \frac{dh_c(\theta)}{dx}, \quad k_r(\theta) = \frac{k(\theta)}{k_0} \tag{2.76}$$

where $k(\theta)$ = unsaturated permeability, $D(\theta)$ = unsaturated water diffusivity, $k_r(\theta)$ = relative unsaturated permeability [$k_r(\theta) = k(\theta)/k_0$ and $0 \le k_r(\theta) \le 1.0$], k_0 = saturated permeability coefficient, and C_w = specific moisture capacity.

Darcy's formula states that the unsaturated flow velocity is proportional to the capillary head gradient (matrix head gradient), and is the transport equation for unsaturated flow.

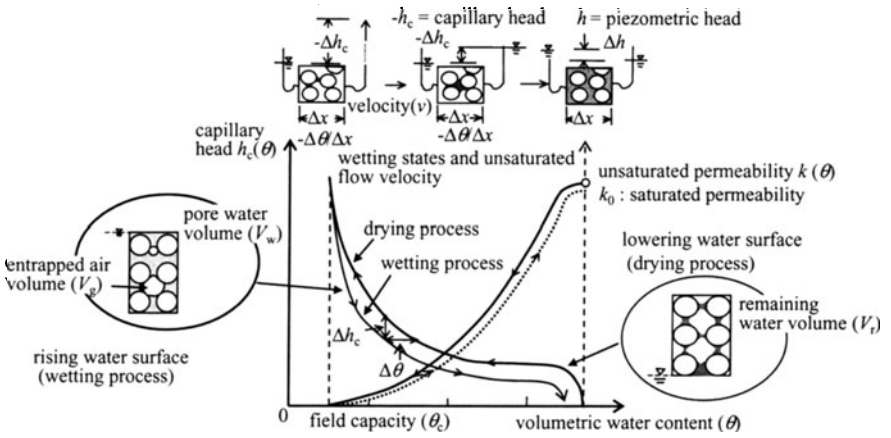

Fig. 2.19. Hysteresis in wetting and drying processes for the relationship between $h_c(\theta)$ and $k(\theta)$

Therefore, to determine the unsaturated flow velocity (u), it is necessary to find functional relationships among water content (θ), capillary head (h_c), and permeability (k). Since $k(\theta)$ and $h_c(\theta)$ vary with soil type and water content, these parameters have to be determined experimentally. There are several methods for experimental determination of these relationships. For example, $k(\theta)$ and $h_c(\theta)$ are functions of volumetric water content, as shown in **Fig. 2.19**. The volumetric water content changes between the lowest value θ_c (which is called the field capacity and is a balance between water retention and gravity) to its saturated value $\theta_s = 1$ ($\theta_c < \theta < \theta_s$). Capillary head ($h_c$) decreases with the increase in θ, and becomes zero at saturation. On the other hand, $k(\theta)$ increases with an increase in θ, and becomes a maximum value at saturation. These relationships among h_c, k, and θ are sometimes called the unsaturated characteristics.

In reality, the variation in $h_c(\theta)$ and $k(\theta)$ with water content does not have unique values because of hysteresis. Hysteresis can be determined by measuring variations of these quantities during water content change for both wetting and drainage processes. Hysteresis in $h(\theta)$ and $k(\theta)$ can be explained with the help of microphenomena inside soil pores in drainage and wetting processes (e.g., the ink bottle effect and pore size and its distribution).

2.6.2 Basic Equations for Unsaturated Flow

The basic equations for unsaturated flow are derived from the mass conservation law for pore water and from the extended Darcy's law.

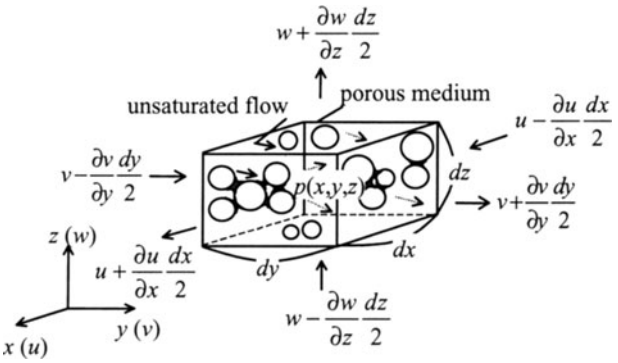

Fig. 2.20. Control volume for an unsaturated flow field

An infinitesimal control volume dV ($dV = dxdydz$) centered at point $P(x, y, z)$ in a uniform unsaturated flow in the Cartesian coordinate system is shown in **Fig. 2.20**. Consider the difference in water mass between inflow and outflow in dV during a small time interval (dt). For example, the difference in the x-direction is as follows.

$$\rho\left(u-\frac{\partial u}{\partial x}\frac{dx}{2}\right)dy\,dz\,dt-\rho\left(u+\frac{\partial u}{\partial x}\frac{dx}{2}\right)dy\,dz\,dt=-\frac{\partial u}{\partial x}\rho\,dx\,dy\,dz\,dt$$

Similar expressions can be written in the y- and z-directions. Summation of these differences in water mass between inflow and outflow in the control volume are expressed as:

$$-\rho\left(\frac{\partial u}{\partial x}+\frac{\partial v}{\partial y}+\frac{\partial w}{\partial z}\right)dx\,dy\,dz\,dt$$

where u, v, and w = velocity (Darcy) components in the x-, y-, and z-directions, respectively and ρ = water density.

The net inflow/outflow of water mass must be equal to its rate of change $[(\partial\rho\theta/\partial t)dt\,dx\,dy\,dz]$ in the control volume ($\rho\theta\,dx\,dy\,dz$). Because water density is considered constant, mass conservation for pore water can be written as follows:

$$\frac{\partial \theta}{\partial t} = -\left(\frac{\partial u}{\partial x} + \frac{\partial v}{\partial y} + \frac{\partial w}{\partial z}\right) = -\nabla \mathbf{q} \tag{2.77}$$

where $\mathbf{q}(u, v, w)$ is the velocity vector, and $\nabla = (\partial/\partial x, \partial/\partial y, \partial/\partial z)$.

The velocity components in Eq. 2.77 can also be written in terms of Darcy's law as:

$$u = -k\frac{\partial h}{\partial x}, \quad v = -k\frac{\partial h}{\partial y}, \quad w = -k\frac{\partial h}{\partial z} \tag{2.78}$$

where $h = z - p_c/\rho g$ is the tensiometer head.

The basic equation for unsaturated flow in a uniform porous medium is derived from Darcy's equation and mass conservation equation, and can be expressed in several different forms. One of these expressions is given below:

$$-\nabla \mathbf{q} = -\frac{\partial}{\partial x}\left(k\frac{\partial h_c}{\partial x}\right) - \frac{\partial}{\partial y}\left(k\frac{\partial h_c}{\partial y}\right) - \frac{\partial}{\partial z}\left(k\frac{\partial h_c}{\partial z}\right) + \frac{\partial k}{\partial z} = \frac{d\theta}{dh_c}\frac{\partial h_c}{\partial t} \tag{2.79}$$

Equation 2.79 is called Richards' equation. It is not possible to solve this equation in its present form because the unsaturated permeability $k(\theta)$ and tensiometer head $h_c(\theta)$ are dependent on water content (θ). Therefore, $h_c(\theta)$ and $k(\theta)$ have to be given beforehand. By analogy with the diffusion equation, the following equation is obtained:

$$\frac{\partial \theta}{\partial t} = \frac{\partial}{\partial x}\left(D\frac{\partial \theta}{\partial x}\right) + \frac{\partial}{\partial y}\left(D\frac{\partial \theta}{\partial y}\right) + \frac{\partial}{\partial z}\left(D\frac{\partial \theta}{\partial z}\right) + \frac{\partial k}{\partial z} = -\nabla \mathbf{q} \tag{2.80}$$

$$D(\theta) = \frac{k(\theta)}{C_w}, \quad C_w = -\frac{\partial \theta}{\partial h_c}$$

The above equation is called the Klute equation. Basically, Richards' equation and the Klute equation are the same, but, Richards' equation uses h_c as the independent variable and Klute uses θ as the independent variable.

The above equations can be solved by adding the $k(\theta)$ and $h_c(\theta)$ relationships into the mass conservation equation and Darcy's equation under initial and boundary conditions.

2.6.3 Examples of Basic Unsaturated Flow

Unsaturated flows are classified as either horizontal unsaturated flows, in which the water content gradient is dominant or vertical unsaturated flows, in which gravity and the water content gradient act on pore water as the driving force. Analytical solution methods are presented for limited number problems in the following sections (Swartzendruber D., 1969, De Wiest R. J. M., 1969). If solutions to boundary condition are required, numerical computation techniques might be applicable.

2.6.3 (a) Horizontal Unsaturated Flow

Equation 2.80 with $\partial k/\partial z = 0$ and $\partial \theta/\partial y = \partial \theta/\partial z = 0$ and initial and boundary conditions can be written as:

$$\frac{\partial \theta}{\partial t} = \frac{\partial}{\partial x}\left(D\frac{\partial \theta}{\partial x}\right) \tag{2.81}$$

$$\left.\begin{aligned} \theta(x,0) &= \theta_0 \\ \theta(0,t) &= \theta_1 \end{aligned}\right\} \quad \text{constant} \tag{2.82}$$

where θ_0 = initial water content, θ_1 = water content at boundaries, and $D = D(\theta)$.

This is a problem for determining water content of an unsaturated flow in fine-grained soil (such as silt or clay) when the initial constant value θ_0 at $x = 0$ suddenly changes to another constant value $\theta_1 (\theta_0 \neq \theta_1)$ at time $t = 0$. This type of problem was intensively studied over the two decades from 1940 to 1960. The problem was solved as follows.

Applying the Boltzmann transformation ($\eta = x/t^{1/2}$) to Eq. 2.81, the following equations are obtained:

$$\frac{\partial \theta}{\partial t} = \frac{\partial \eta}{\partial t}\frac{d\theta}{d\eta} = -\frac{1}{2}\eta t^{-1}\frac{d\theta}{d\eta}, \quad \frac{\partial \theta}{\partial x} = \frac{\partial \eta}{\partial x}\frac{d\theta}{d\eta} = t^{-\frac{1}{2}}\frac{d\theta}{d\eta},$$

$$\frac{\partial}{\partial x}\left(D\frac{\partial \theta}{\partial x}\right) = \frac{\partial \eta}{\partial x}\frac{d}{d\eta}\left(D\frac{\partial \theta}{\partial x}\right) = t^{-1}\frac{d}{d\eta}\left(D\frac{d\theta}{d\eta}\right)$$

or

$$\eta\frac{d\theta}{d\eta} + 2\frac{d}{d\eta}\left(D\frac{d\theta}{d\eta}\right) = 0 \tag{2.83}$$

Equation 2.83 is an ordinary differential equation.

Furthermore, the following equation is obtained by integrating the transformed variable from θ_0 to θ:

$$\eta = -2\frac{d}{d\theta}\left(D\frac{d\theta}{d\eta}\right)$$

$$\int_{\theta_0}^{\theta} \eta\, d\theta = -2\int_{\theta_0}^{\theta} d\left(D\frac{d\theta}{d\eta}\right) = -2D\frac{d\theta}{d\eta} \tag{2.84}$$

where $d\theta/d\eta = 0$ and $2D\, d\theta/d\eta|_{\theta_0} = 0$ at θ_0.

Thus, the basic unsaturated flow is changed into Eq. 2.84 by applying the Boltzmann transformation, and correspondingly, the boundary conditions must also be transformed. Because $\theta(x,0) = \theta_0$ at $\eta = x^{-1/2}$ and $\theta(0,t) = \theta_1$, the boundary conditions can be written as:

$$\eta(\theta_1) = 0, \quad \eta(\theta_0) \to \infty \tag{2.85}$$

In conclusion, knowledge of the diffusion coefficient $D(\theta)$ is necessary to solve horizontal unsaturated flow Eq. 2.84 coupled with the conditions of Eq. 2.85; however, it is not possible to obtain an analytical solution $\theta(\eta)$ even if $D(\theta)$ is known. The easiest way to obtain solutions of the problem is to apply numerical techniques.

Figure 2.21 shows the setup for an experiment on horizontal unsaturated groundwater flow. In the experiment, a horizontal soil column (with initial water content θ_0)

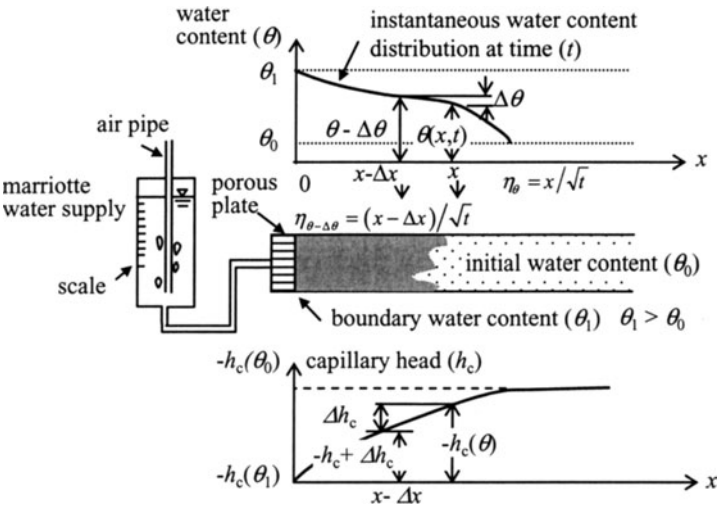

Fig. 2.21. Experimental setup for horizontal unsaturated flow

is connected to a porous plate and a Marriotte water supply (boundary water content $\theta_1 > \theta_0$) at $x = 0$. The water content distribution $\theta(x, t)$ changes with time. If the water content distribution is measured at time t, then the diffusivity (D) in Eq. 2.81 and the functional relationship between D and θ can be determined by inverse analysis. Similarly, if we can obtain $D(\theta)$ for different soils, then the water content distribution $\theta(x, t)$ can be computed. Also, the finite difference solution of $\theta(x, t)$ using Eq. 2.84 can be explained, for instance, according to Childs E. C. (1969). Given that the values of η at x and $x - \Delta x$ are, respectively, $\eta_\theta = x/\sqrt{t}$ and $\eta_{\theta-\Delta\theta} = (x - \Delta x)/\sqrt{t}$, it is possible to write:

$$-\frac{(\eta_{\theta-\Delta\theta} - \eta_\theta)}{\Delta\theta} = \frac{2D_{(\theta-\Delta\theta/2)}}{\int_{\theta_0}^{(\theta-\Delta\theta/2)} \eta \, d\theta} \tag{2.86}$$

If it is possible to measure θ at t, $t + \Delta t$, $t + 2\Delta t$ and so on, then the unsaturated permeability $k(\theta) = D\,d\theta/dh_c$ ($= D\,\Delta\theta/\Delta h_c$) can be determined. Nonetheless, the functional relationships $h_c(\theta)$ and $k(\theta)$ [or $k(h_c)$], which are known as moisture characteristic curves, are needed in any case.

2.6.3 (b) Formulation of $h_c(\theta)$ and $k(\theta)$

Basically, the suction head $h_c(\theta)$ and the unsaturated permeability $k(\theta)$ are determined experimentally for different soil types; however, their functional relationships for unsaturated flow are formulated for the sake of convenience. The functions $h_c(\theta)$ and $k(\theta)$, as shown in **Fig. 2.19**, can be approximated by algebraic expressions and several formulae have been introduced. **Table 2.5** shows several functional relationships between $h_c(\theta)$ and $k(\theta)$. The constants and exponents in these expressions vary greatly depending on soil type. It must be noted that the values of $k(\theta)$ at $\theta \approx 1$

Table 2.5. Typical $h_c(\theta)$ and $k(\theta)$ or $k(h_c)$ relationships

Functions	$h_c(\theta)$	$k(\theta)$
Type-I		$k = k_0 \left(\frac{\theta-\theta_c}{\theta_s-\theta_c}\right)^n$ (Irmay, 1954)
Type-II	$\left(\frac{\theta-\theta_c}{\theta_s-\theta_c}\right) = \exp[\alpha(h_c - h_{cr})]$ (Kroszynski, 1975)	$k = k_0 \exp(-\alpha h_c)$, $k = \frac{a}{\lvert h_c\rvert^m + b}$ $(a \neq 0)$ (Gardner, 1958)
Type-III (Brooks & Cory, 1964)	$\left(\frac{\theta-\theta_c}{\theta_s-\theta_c}\right) = \left(\frac{h_{cr}}{h_c}\right)^n$	$k = K_0$ $(h_{cr} \leq h_c)$; $k = K_0(h_{cr}/h_c)^n$ $(h_{cr} \geq h_c)$
Type-IV (Mualem, 1976; van Genuchten, 1980)	$\left(\frac{\theta-\theta_c}{\theta_s-\theta_c}\right) = \left(\frac{1}{1+(\alpha h_c)^n}\right)^m$	$k = \left(\frac{\theta-\theta_c}{\theta_s-\theta_c}\right)^{1/2} \left[1 - \left\{1 - \left(\frac{\theta-\theta_c}{\theta_s-\theta_c}\right)^{1/m}\right\}^m\right]^2$

θ, soil water content; θ_s and θ_c, saturated and residual water content, respectively; a, b, m, n, α, empirical parameters; k and k_0, unsaturated and saturated permeability (hydraulic conductivity), respectively; K and K_0, unsaturated and saturated intrinsic permeability; h_c, capillary pressure head; h_{cr}, threshold capillary pressure head.

(permeability near the saturated state, where $dh_c/d\theta$ becomes very large) are very sensitive in analysis.

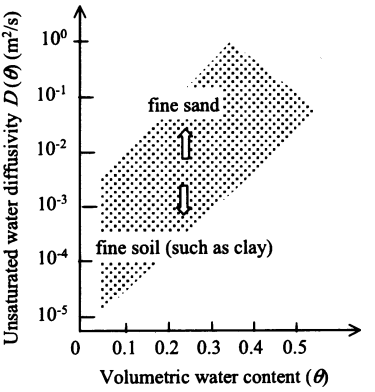

Fig. 2.22. Range of water diffusivity

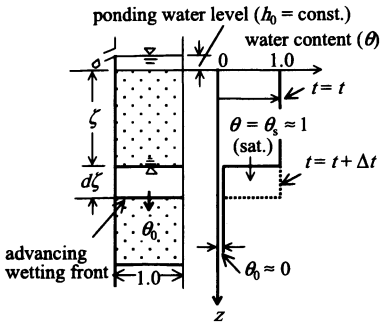

Fig. 2.23. Vertically moving front

Figure 2.22 shows the range of water diffusivity $D(\theta)$ for different soil types. $D(\theta)$ is small for fine-grained soils, such as clay, and larger for fine sand. The functional relationships between $D(\theta)$ and θ on semilogarithmic paper are straight lines with different slopes. Gardner W. R. and Mayhuge M. S. (1958) assumed that

$D(\theta) = D_1 \exp[\beta(\theta - \theta_1)]$ with $D_1(\theta_1)$ as the value of D at θ_1, and β as a constant (dependent on the slope of the straight line).

(Example 2.2)
Determine the transient depth $\zeta(t)$ of the wetting front when water with a small hydraulic head h_0 (= constant) is ponded at the upper end of a soil column with initial water content θ_0 (≈ 0), as shown in **Fig. 2.23.**

(Answer)
The motion and continuity relation for a vertical water column with a unit cross-section with $\theta_s \approx 1.0$ (approximately equal to the effective porosity, n_e) are as follows:

$$w = k\frac{\zeta + \zeta_c + h_0}{\zeta}, \quad w = n_e\frac{d\zeta}{dt} \tag{2.87}$$

where ζ_c = capillary head, k = saturated permeability, and w = flow velocity in the vertical direction.

Integration of these equations with conditions $t = 0$ and $\zeta = 0$ gives:

$$\int\left(\frac{\zeta}{\zeta + \zeta_c + h_0}\right)d\zeta = \int\frac{k}{n_e}dt + C$$

Because the integration constant $C = -(\zeta_c + h_0)\log(\zeta_c + h_0)$, then:

$$\zeta - (\zeta_c + h_0)\log\left[1 + \frac{\zeta}{\zeta_c + h_0}\right] = \frac{k}{n_e}t \tag{2.88}$$

Consider the power series expansion with terms up to the second order retained. Then the moving wetting front can be approximated by:

$$\zeta \approx \eta_0 t^{1/2}, \quad \eta_0 = \left[\frac{2k(\zeta_c + h_0)}{n_e}\right]^{1/2} \tag{2.89}$$

Since η_0 is constant, the moving front is almost proportional to $t^{1/2}$. This relationship is valid only for fine sand, where diffusion (microscopic) is predominant. For other soils, the fingering effect (macroscopic diffusion) will be observed (see **Fig. 2.24**).

2.6.3 (c) Saturated–Unsaturated Groundwater Flow

The existence of a saturated–unsaturated groundwater zone is shown in **Fig. 2.25**. There is a capillary zone above the groundwater table, where capillary and gravity forces balance each other. Saturated and unsaturated flows take place below and above the zone, respectively. Gravity governs saturated flow in an unconfined aquifer, while Dupuit's uniform flow assumption drives flow in the horizontal direction. These flows possess the following characteristics:

1. Saturated zone: water level $h > 0$, water content $\theta = n$ (porosity), and permeability $k(\theta) = k_0$ = constant

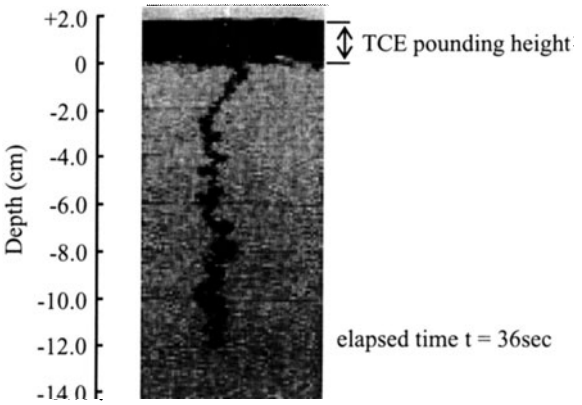

Fig. 2.24. A typical TCE finger in a water-saturated glass bead porous medium

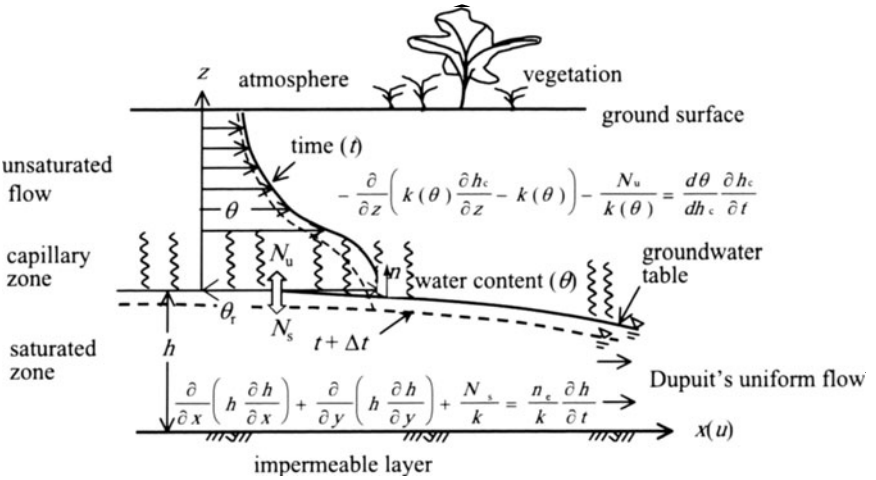

Fig. 2.25. Unsaturated vertical flow

2. Unsaturated zone: $h = h_c$ (negative capillary head), θ_r (field capacity) $< \theta < n$, $k(\theta) \neq$ constant

At times t and $(t + \Delta t)$, moisture profiles above the groundwater table are $\theta(z, t)$ and $\theta(z, t+\Delta t)$, respectively. Moisture content at the ground surface $\theta(z, t)$ depends on meteorological conditions (e.g., precipitation, air temperature, humidity, solar radiation, wind, and plant conditions). For a deep groundwater surface, the influence of meteorology is very weak or not present at all.

Exchange rates N_s and N_u exist between saturated and unsaturated zones, respectively, per unit area in unit time and $N_s = N_u$ for natural conditions. If there is

pumping source from the saturated zone, then $N_u < N_s$. For a numerical model, the two equations in **Fig. 2.25** are coupled, and solved simultaneously.

2.6.3 (d) Measurement of Unsaturated Flow

The necessary hydraulic quantities in the basic unsaturated flow equations are $h_c(\theta)$ and $k(\theta)$. In general, the measurement techniques for these quantities can be classified as laboratory experimentation and field observation. In laboratory experiments, it is necessary to measure capillary head or pressure head (h_c), volumetric moisture distribution (θ), saturated permeability (k_s), and physical properties of the soil (such as porosity, density, and particle size distribution). The quantities to be measured are the same for field observations, but the measurement methods for these two cases are different and are summarized in **Table 2.6**.

Table 2.6. Measurement of unsaturated flow

Test type	Test setup	Measured quantities
Laboratory experiment	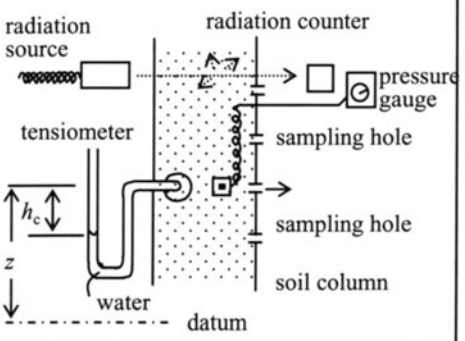	Capillary head (pressure) Water content distribution Unsaturated permeability Soil physical properties
Field measurement	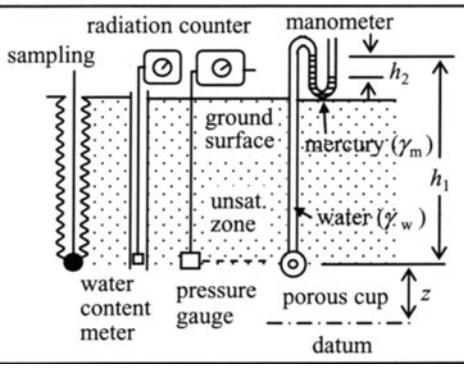	γ_w and γ_m are, respectively, the densities for water and mercury

Measurement of moisture content is usually carried out using the relationship between radiation from a source and moisture content in the soil column (indi-

rect method) or by sampling techniques (direct method). Furthermore, the capillary head (h_c) is measured with a tensiometer or by direct measurement of negative pressure. Quantities measured in laboratory experiments as well as field measurements are used for analyzing unsaturated flow under given conditions.

2.7 Gas Seepage Flow

In fluid dynamics, the treatment of gas seepage flow is similar to that of groundwater, except that fluid compressibility and thermal effects need to be considered. Compressibility characterizes gas seepage under normal temperatures. Gas seepage flow was not a commonly studied aspect of groundwater hydraulics until comparatively recently. However, recent problems such as the remediation of contaminated soils and the escape of gas from fuel storage caverns in rock masses, have stimulated research in the field of gas seepage flow. The basic theory for gas seepage flow and its features are discussed here (according to V. I. Aravin and S. N. Numerov, 1965).

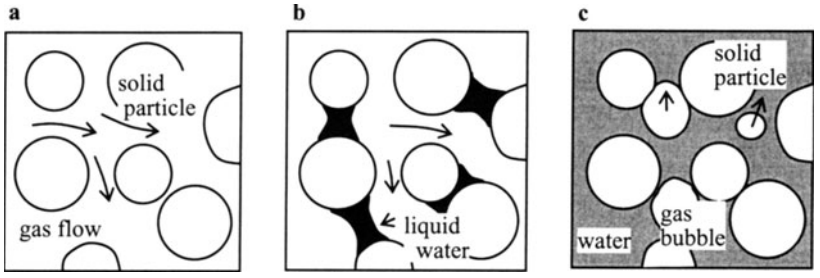

Fig. 2.26 a–c. Models of gas seepage flow. **a** Gas flow in a dry porous medium, **b** gas flow in a wetted porous medium, **c** gas flow (bubble) in a saturated porous medium

Figure 2.26 shows typical patterns of gas seepage flow with different degrees of water saturation in a porous medium. Gas seepage flow in a dry porous medium, a wetted porous medium, and a saturated medium are indicative of different mechanisms. From a dynamic point of view, the gas movement is continuous within the pores in the dry and wetted stages, even though these stages have different saturation levels. In a saturated pore space, however, gas bubbles move under the combined action of gravity and surface tension. Only gas seepage flow in a dry medium as the basic case will be considered here.

Gas is considered to be compressible and to follow Darcy's law. The inertial force acting on the gas is neglected in the following mathematical formulation. Usually, there is no free surface in gas seepage flow.

Putting the velocity components u, v, w in the Cartesian coordinate system, Darcy's law is written as:

$$u = -\frac{K}{\mu}\frac{\partial p}{\partial x}, \quad v = -\frac{K}{\mu}\frac{\partial p}{\partial y}, \quad w = -\frac{K}{\mu}\frac{\partial p}{\partial z} \tag{2.90}$$

where μ = gas viscosity, K = intrinsic permeability (L^2), and p = gas pressure.

The continuity equation for porous media with constant porosity is given as:

$$\frac{\partial(\rho u)}{\partial x} + \frac{\partial(\rho v)}{\partial y} + \frac{\partial(\rho w)}{\partial z} + n\frac{\partial \rho}{\partial t} = 0 \tag{2.91}$$

where n = porosity and ρ = gas density.

For a constant temperature, gas density is assumed to be a function of pressure only (equation of state):

$$\rho = \frac{1}{\beta} p^{\frac{1}{m}} \begin{Bmatrix} \text{(isothermal change) } m = 1 \\ \text{(adiabatic change) } m = c_p/c_v \end{Bmatrix} \tag{2.92}$$

where β = constant, c_p = specific heat under constant pressure, and c_v = specific heat under constant volume (for air, $1 < m < c_p/c_v$ and $m = 1.405$).

The mass flux (ρu) in the x-direction is evaluated from Eq. 2.90 using Eq. 2.92 as follows:

$$\rho u = -\frac{K}{\mu}\rho\frac{\partial p}{\partial x} = -\frac{K}{\mu}\frac{1}{\beta}p^{\frac{1}{m}}\frac{\partial p}{\partial x} = -\frac{K}{\mu\beta\left(1+\frac{1}{m}\right)}\frac{\partial}{\partial x}\left(p^{1+\frac{1}{m}}\right) \tag{2.93}$$

and

$$\rho u = -\frac{K}{\mu}\frac{\partial P}{\partial x}, \quad P = \frac{m}{\beta(1+m)}p^{1+\frac{1}{m}} \tag{2.94}$$

Accordingly, Eq. 2.90 becomes:

$$\rho u = -\frac{K}{\mu}\frac{\partial P}{\partial x}, \quad \rho v = -\frac{K}{\mu}\frac{\partial P}{\partial y}, \quad \rho w = -\frac{K}{\mu}\frac{\partial P}{\partial z} \tag{2.95}$$

p and ρ in Eq. 2.94 can be expressed in term of P as follows:

$$p = \left\{\frac{\beta(1+m)}{m}\right\}^{\frac{m}{1+m}} P^{\frac{m}{1+m}}, \quad \rho = \frac{1}{\beta}\left\{\frac{\beta(1+m)}{m}\right\}^{\frac{1}{1+m}} P^{\frac{1}{1+m}} \tag{2.96}$$

On the other hand, $\partial\rho/\partial t$ can be evaluated from Eq. 2.96 as:

$$\frac{\partial \rho}{\partial t} = \frac{1}{\beta(1+m)}\left\{\frac{\beta(1+m)}{m}\right\}^{\frac{1}{1+m}} P^{-\left(\frac{m}{1+m}\right)}\frac{\partial P}{\partial t} \tag{2.97}$$

Then, the continuity equation (Eq. 2.91) can be written in the following form using Eqs. 2.95 and 2.97:

$$\frac{\partial^2 P}{\partial x^2} + \frac{\partial^2 P}{\partial y^2} + \frac{\partial^2 P}{\partial z^2} - \frac{n\mu}{K\beta(1+m)}\left\{\frac{\beta(1+m)}{m}\right\}^{\frac{1}{1+m}} P^{-\frac{m}{1+m}}\frac{\partial P}{\partial t} = 0 \tag{2.98}$$

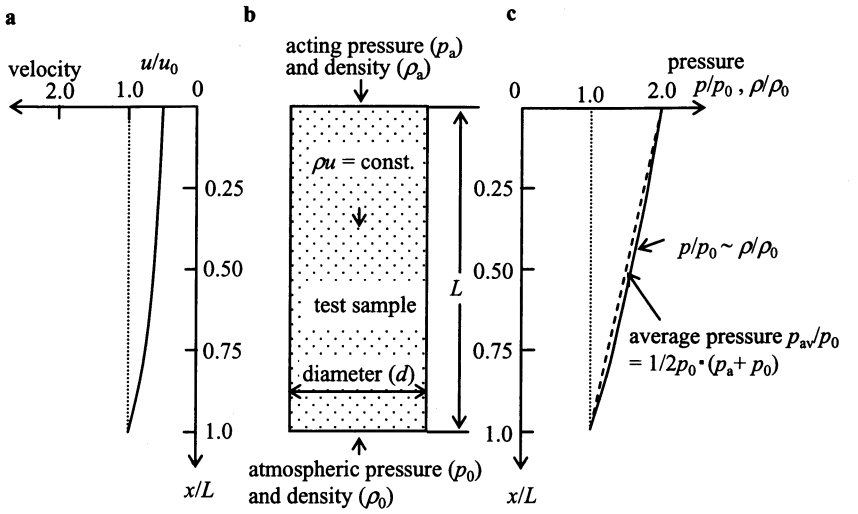

Fig. 2.27 a–c. Isothermal steady air seepage flow. **a** Velocity profile, **b** test sample, **c** pressure profile

Equation 2.98 is the basic equation for a compressible gas and is called the Leibenzon's equation for gas seepage flow.

For the steady state condition, Eq. 2.98 becomes Laplace's equation:

$$\frac{\partial^2 P}{\partial x^2} + \frac{\partial^2 P}{\partial y^2} + \frac{\partial^2 P}{\partial z^2} = 0 \tag{2.99}$$

(Example 2.3)

As shown in **Fig. 2.27**, a pressure ($p_a = 2p_0$) is applied at the upper end ($x/L = 0$, x: coordinate along test sample), and a constant atmospheric pressure (p_0) is maintained at the lower end ($x/L = 1.0$) of a porous test sample with length L and diameter d in an isothermal steady air seepage flow experiment. Determine pressure distributions (p/p_0) and flow velocity (u/u_0, u_0 = flow velocity at the lower end of the sample) inside the test sample and its intrinsic permeability.

(Answer)

The flow is steady and one-dimensional (along the x-direction). Therefore, in Eq. 2.98:

$$\partial^2/\partial y^2 = \partial^2/\partial z^2 = \partial/\partial t = 0$$

The equation for isothermal steady air seepage flow as shown in **Fig. 2.27** becomes:

$$\frac{\partial^2 P}{\partial x^2} = 0, \quad P = C_1 x + C_2 \tag{2.100}$$

The integration constants C_1 and C_2 can be determined using the boundary conditions:

$$x = 0, \qquad p = p_a, \qquad P_a = \frac{m}{\beta(m+1)} p_a^{\frac{m+1}{m}}$$

$$x = L, \qquad p = p_0, \qquad P_0 = \frac{m}{\beta(m+1)} p_0^{\frac{m+1}{m}}$$

In Eq. 2.100, $P = P_a$ at $x = 0$, then $C_2 = P_a$, and $P = P_0$ at $x = L$. Then,

$$C_1 = \frac{P_0 - P_a}{L} = \frac{m}{\beta(m+1)L}\left(p_0^{\frac{m+1}{m}} - p_a^{\frac{m+1}{m}}\right)$$

Accordingly, Eq. 2.100 becomes:

$$P = P_a - \frac{x}{L}(P_a - P_0) \tag{2.101}$$

or

$$p^{\frac{m+1}{m}} = p_a^{\frac{m+1}{m}} - \frac{x}{L}\left(p_a^{\frac{m+1}{m}} - p_0^{\frac{m+1}{m}}\right) \tag{2.102}$$

Because this is isothermal air seepage flow, $m = 1$, and from Eq. 2.102, the pressure distribution (p/p_0) inside the test sample is written as:

$$\left(\frac{p}{p_0}\right)^2 = \left(\frac{p_a}{p_0}\right)^2 - \frac{x}{L}\left[\left(\frac{p_a}{p_0}\right)^2 - 1\right] \tag{2.103}$$

The pressure applied at the upper end of the test sample is $p_a = 2p_0$, and so $p/p_0 = \sqrt{(4 - 3x/L)}$ (see the pressure distribution in **Fig. 2.27**).

Next, the mass flux (ρu) is determined from Eq. 2.103 as:

$$\rho u = \frac{K}{2\beta\mu L}(p_a^2 - p_0^2) = \text{constant} \tag{2.104}$$

The pressure (air density $\rho = p/\beta$) decreases, and the flow velocity, which is inversely proportional to density ($u/u_0 = \rho_0/\rho$, where u_0 and ρ_0 are flow velocity and air density, respectively, at the lower end of the test sample), increases from the upper end of the test sample toward the lower end (see the distribution in **Fig. 2.27**).

Furthermore, the intrinsic permeability is determined as follows. The average pressure in Eq. 2.104 is: $\overline{p} = (p_a + p_0)/2$ and $\beta\overline{p} = \overline{p}$ (for isothermal conditions, $\overline{\rho} = (\rho_a - \rho_0)/2$, where ρ_a = density at pressure p_a at lower end of the test sample). Then,

$$\overline{Q} = \frac{K}{\mu} A \frac{p_a - p_0}{L}, \quad K = \frac{\mu \overline{Q} L}{A(p_a - p_0)} \tag{2.105}$$

where $\overline{Q}$ = average seepage discharge and A = cross-sectional area of the test sample.

If the pressure difference $(p_a - p_0)$ between the two ends of the test sample is large, it is not possible to assume a linear pressure distribution inside the test sample. At the same time, a large amount of heat will be generated as a result of the compressibility. Therefore, an isothermal state no longer exists and an adiabatic change $(\rho = p^{1/m}/\beta)$ takes place. Thus, it is unadvisable to determine intrinsic permeability (K) from Eq. 2.105 for large pressure differences.

2.8 Groundwater Flow in Rock Masses

2.8.1 Groundwater in Rock Masses

A rock mass is defined as a natural aggregate of rocks with reasonable dimensions. As shown in **Fig. 2.28a**, a rock mass consists of two parts: solid rock and fractures. Groundwater is either at rest or flowing. Groundwater flow velocities are different within the rock part and the fractures within the rock mass and thus phenomenon is known as the double porosity system. The groundwater flow velocity in rock is usually small, although it depends on the type of rock. Groundwater flow is heavily influenced by the continuity of fractures and the permeability of the rock mass.

Modeling and formulation of groundwater flow in rock masses reflect the following characteristics:

1. Rock mass porosity (n) is the sum of porosity n_1 of the rock and n_2 of the fracture, i.e., $n = n_1 + n_2$.
2. Flow velocity ($\mathbf{q}$) comprises two components: the velocity inside the rock and the velocity in the fractures.
3. Permeability (k) consists of two parts: k_1 and k_2 for the rock and the fractures, respectively.
4. Groundwater flow in a rock mass follows the geometry of channeling fractures with spatial shape and direction (i.e., the anisotropy of fracture geometry).

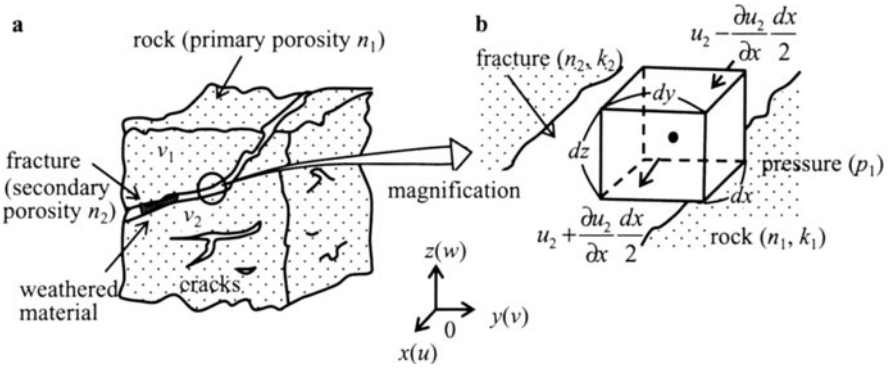

Fig. 2.28. Groundwater flow model in a rock mass. **a** Rock mass model, **b** control volume

The concept of the above-mentioned rock seepage model follows from Barenblatt G. I. et al. (1960, 1990). Undoubtedly, if the permeability of the rock itself is ignored in the double porosity system ($k_1 = n_1 = \mathbf{q}_1 = 0$), the flow through an ordinary porous medium will result.

Two important points should be kept in mind while studying flow through rock masses. One is that water pressure dominates gravity as the driving force for flows in

rock masses because pore size and permeability are very small. The other is that there is no defined impermeable basement as there is with groundwater flow in ordinary porous media. Therefore, the hydraulic concept of piezometric head ($h = p/\rho g + z$) becomes ambiguous, and sometimes ineffective.

2.8.2 Basic Equations for Groundwater Flow in Rock Masses

The basic equations for groundwater flow in rock masses are derived from mass conservation and transport equations (Darcy's equation) based on the double porosity system.

2.8.2 (a) Predominant Seepage in the Rock ($k_1 > k_2$)

The basic equations for this case are derived from mass conservation and Darcy's equations by focusing on the flow inside the rock mass:

$$-\nabla\rho\mathbf{q}_1 = \frac{\partial(n_1\rho)}{\partial t} \tag{2.106}$$

$$\mathbf{q}_1 = -\frac{K}{\mu}\nabla p_1, \quad \text{or} \quad -\frac{K}{\mu}\,\text{grad}\,p_1 \tag{2.107}$$

where ρ = water density, n_1 = porosity of the rock mass, μ = viscosity of water, g = gravitational acceleration, K = intrinsic permeability [L^2], p_1 = pressure inside the rock mass, $\mathbf{q}_1(u_1, v_1, w_1)$ = flow velocity vector, and ∇p_1, or grad p_1, is defined as $(\partial p_1/\partial x, \partial p_1/\partial y, \partial p_1/\partial z)$.

This equation is the same as the ordinary equations in porous media ($n_z = k_z = 0$), but permeability greatly varies for different kinds of rocks and piezometric head replaces pressure (p_1) for smaller p_1. Both Eqs. 2.106 and 2.107 are valid only when a number of fractures/weathered materials (like weathered clay) or open fractures are present as a result of high rock pressure in permeable rock masses.

2.8.2 (b) Dominant Flow in the Fractures ($k_1 \ll k_2$)

The governing equation in this case is derived by considering that groundwater flow in fractures will be dominant, but will interact with rock permeability. As shown in **Fig. 2.28b**, an infinitesimal control volume ($dV = dx\,dy\,dz$) is placed within a fracture of the rock model. The mass balance equation then is obtained considering the difference of inflow and outflow in the control volume. The equation in the x-direction for unit time is given by:

$$[\rho u_2 - \partial\rho u_2/\partial x(dx/2)]dy\,dz - [\rho u_2 + \partial\rho u_2/\partial x(dx/2)]dy\,dz$$
$$= -(\partial\rho u_2/\partial x)dx\,dy\,dz$$

The equations in the y- and z-directions, respectively, are as follows:

$$-(\partial\rho v_2/\partial y)dx\,dy\,dz, \quad -(\partial\rho w_2/\partial z)dx\,dy\,dz$$

The net groundwater flow into the control volume in unit time, by taking account of an interaction rate ε between the fracture and the rock in control volume ΔV, becomes:

$$-\left[\frac{\partial(\rho u_2)}{\partial x}+\frac{\partial(\rho v_2)}{\partial y}+\frac{\partial(\rho w_2)}{\partial z}\right]dx\,dy\,dz+\varepsilon\,dx\,dy\,dz$$

According to the principle of mass conservation, the difference in inflow and outflow in unit time must equal the rate of mass change in the control volume. Thus, the mass balance equation can be written as:

$$-\nabla\rho\mathbf{q}_2+\varepsilon=\frac{\partial(\rho n_2)}{\partial t} \tag{2.108}$$

This is the mass conservation equation inside the fracture. It is necessary also to consider the mass balance inside the rock, which can be derived in a similar manner and expressed as:

$$-\nabla\rho\mathbf{q}_1-\varepsilon=\frac{\partial(\rho n_1)}{\partial t} \tag{2.109}$$

The groundwater mass balance equation can now be obtained by summing Eqs. 2.108 and 2.109, i.e., $-\nabla\rho\mathbf{q}=\partial(\rho n)/\partial t$. Here, porosity $(n)=n_1+n_2$ and flow velocity $(\mathbf{q})=\mathbf{q}_1+\mathbf{q}_2$. The basic equation is obtained by combining with Darcy's equation $(\mathbf{q}_i=-(K_i\rho g/\mu)\nabla p_i, i=1,2)$. Barenblatt G. I. et al. (1960) considered that if groundwater flow within the rock is negligible (i.e. $\mathbf{q}_1\approx 0$) in Eq. 2.109, the inflow ratio (ε) is defined as follows:

$$\frac{\partial(n_1\rho)}{\partial t}+\varepsilon=0 \tag{2.110}$$

$$\varepsilon\propto\frac{K_1}{\mu}\rho\frac{(p_1-p_2)}{\ell}\cdot\frac{S_r}{\ell} \tag{2.111}$$

where p_1 and p_2 are, respectively, the pressure inside the rock and the fracture, ℓ = a representative size of rock mass, and S_r = constant.

If the fracture porosity (n_2) in Eq. 2.108 is extremely small $(n_1\gg n_2)$, then it can be considered that $\partial(\rho n_2)/\partial t=0$. Thus, the basic groundwater flow equation in the rock mass can be derived from mass balance Eqs. 2.110 and 2.111 as:

$$\nabla^2 p_2+K_r(p_1-p_2)=0 \tag{2.112}$$

$$\frac{\partial p_1}{\partial t}+K(p_1-p_2)=0 \tag{2.113}$$

where $K_r=(K_1/K_2)(S_r/\ell^2)$, $\nabla^2=\partial^2/\partial x^2+\partial^2/\partial y^2+\partial^2/\partial z^2$, $K=(S_r/S_s)(K_1\rho/\mu\ell^2)$, and S_r = relative storativity of the rock mass (dependent on water compressibility in the rock and fractures, as will be seen in Example 2.4).

Thus, it can be concluded that in the double porosity model, groundwater flow takes place in the fractures and storage takes place in the rock.

(Example 2.4)

Express and state the physical meaning of the term $\partial/\partial t$ in the mass conservation equation derived in the double porosity model.

(Answer)
The right-hand-side term in Eqs. 2.108 and 2.109 is expressed as:

$$\frac{\partial(\rho n)}{\partial t} = \rho\frac{\partial n}{\partial t} + n\frac{\partial \rho}{\partial t} \tag{2.114}$$

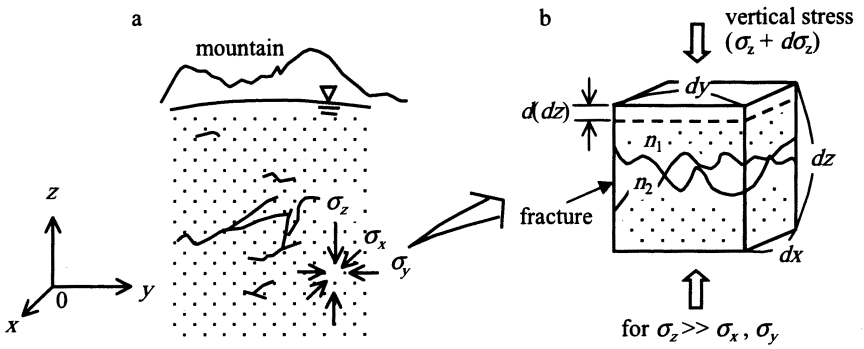

Fig. 2.29 a, b. Rock mass beneath a mountain. **a** Stresses beneath a mountain, **b** microscopic rock element

Consider an infinitesimal rock mass volume ($dV = dx\,dy\,dz$) under a mountain with the stresses acting as shown in **Fig. 2.29a** (the vertical stress is much larger than the horizontal stresses, i.e., $\sigma_z \gg \sigma_x, \sigma_y$). The infinitesimal volume (dV) is made up of the sum of the solid volume [$dV_s = (1 - n)\,dx\,dy\,dz$] and the pore volume ($dV_p = n\,dx\,dy\,dz$). If elastic deformation is assumed in the rock mass, then $d[dV_s] = 0$ and $dn = [(1 - n)d(dz)/dz] = -(1 - n)\alpha\,d\sigma_z$, i.e., the rock mass compressibility $= -(1/dz)[d(dz)/d\sigma_z]$. Then,

$$\rho\frac{\partial n}{\partial t} = -\rho\alpha(1 - n)\frac{\partial \sigma_z}{\partial t} \tag{2.115}$$

Similarly, if the water mass in the pores is conserved, then $d(\rho n\,dV_p) = d\rho n\,dV_p + \rho d(n\,dV_p) = 0$, and $d\rho = \beta\rho\,dp$, where β = water compressibility $= -(1/n\,dV_p)d(n\,dV_p)/dp$. Then,

$$n\frac{\partial \rho}{\partial t} = n\rho\beta\frac{\partial p}{\partial t} \tag{2.116}$$

On the other hand, if the sum of pore water pressure and vertical stress is kept constant (i.e., $p + \sigma_z$ = constant), then $d\sigma_z = -dp$. Therefore,

$$\frac{\partial \sigma_z}{\partial t} = -\frac{\partial p}{\partial t} \tag{2.117}$$

Now, using Eqs. 2.115, 2.116, and 2.117, Eq. 2.114 can be written as:

$$\frac{\partial(\rho n)}{\partial t} = \rho\left[\alpha(1-n)+\beta n\right]\frac{\partial p}{\partial t} = S_s\frac{\partial p}{\partial t},$$
$$S_s = \rho[\alpha(1-n)+\beta n] \tag{2.118}$$

Because the porosity of the rock mass $= n_1 + n_2$, $\partial(\rho n)/\partial t = \partial(\rho n_1)/\partial t + \partial(\rho n_2)/\partial t$. If the fracture porosity (n_2) is extremely small (i.e., $n_1 \gg n_2$), then $\partial(\rho n)/\partial t \approx \partial(\rho n_1)/\partial t$, $\partial p/\partial t \approx \partial p_1/\partial t$, and $S_s \approx \rho[\alpha(1-n)+\beta n_1]$, where S_s = specific storage and represents the compressibility of the rock mass and the pore water.

In the discussion of rock masses with predominant flow in fractures, pores within the fracture and rock are sometimes called channeling pores and storage pores, respectively.

2.8.3 Permeability Tensor for Discontinuous Rock Masses

As stated above, groundwater flow in permeable and homogeneous fractured rock can be treated in a similar way to that in ordinary porous media. However, groundwater movement is subject to the discontinuity and heterogeneity of fractures and hence the flow direction is strongly dependent on the geometry of fractures.

In general, flow velocity $\mathbf{q}(u, v, w)$ in an anisotropic porous medium is given by:

$$\mathbf{q} = \mathbf{ki} = -k_{ij}\nabla h \tag{2.119}$$

where $\mathbf{k}$ = permeability (with components k_{ij}), $\mathbf{i}$ = hydraulic gradient (with components i_j), h = piezometric head, $\nabla = (\partial/\partial x, \partial/\partial y, \partial/\partial z)$, and

$$\left.\begin{aligned} u &= k_{11}i_1 + k_{12}i_2 + k_{13}i_3 \\ v &= k_{21}i_1 + k_{22}i_2 + k_{23}i_3 \\ w &= k_{31}i_1 + k_{32}i_2 + k_{33}i_3 \end{aligned}\right\} \tag{2.120}$$

The subscripts i and j are defined as: $x_1 = x$, $x_2 = y$ and $x_3 = z$.

Permeability within an anisotropic porous medium, which is characterized by changes in density, porosity, and permeability with direction, is a tensor (called the permeability tensor or hydraulic conductivity tensor). For $i \neq j$, $k_{ij} = 0$, and for $i = j$, $k_{ij} \neq 0$ (x-, y-, and z-directions), and so the permeability tensor of an anisotropic porous medium in the principal axes can be written as:

$$\mathbf{k} = \begin{pmatrix} k_{11} & 0 & 0 \\ 0 & k_{22} & 0 \\ 0 & 0 & k_{33} \end{pmatrix}, \quad \mathbf{T} = \begin{pmatrix} T_{11} & 0 & 0 \\ 0 & T_{22} & 0 \\ 0 & 0 & T_{33} \end{pmatrix}, \tag{2.121}$$

where $\mathbf{T}$ = permeability tensor ($k_{ij} \times b_{ij}$, with b_{ij} as thickness).

2.8.4 Better Understanding of Groundwater Flow in Rock Masses

2.8.4 (a) Geometrical Characteristics of Fractures

Percolation theory provides the basic concepts for (a) fracture modeling, (b) fracture continuity, and (c) the quantitative formulations of (a) and (b) (Berkowitz B. and

Balberg I., 1993). With regard to fracture modeling, assume that N fractural elements are randomly distributed in different directions, as shown in **Fig. 2.30**. If the length of a fractural element (ℓ) is much longer than the length of the rock mass (L), i.e., $\ell/L \gg 1$, then the structure is called a tectonic line or linearment in geology. The structure is known as a fractured joint or fracture (or fractured zone) for $\ell/L \approx 1$. Similarly, it is called a fracture or crack for $\ell/L \ll 1$. In percolation theory, it is assumed that $\ell/L < 1$ or $\ell/L \ll 1$.

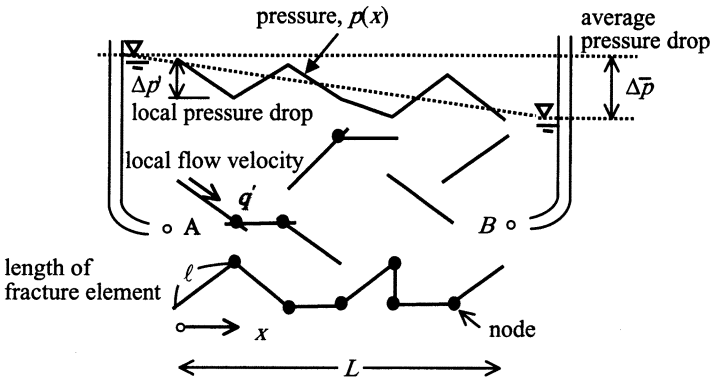

Fig. 2.30. Fractures and hydraulic pressure in the rock mass

For cases in which $\ell/L \gg 1$, $\ell/L > 1$, or $\ell/L \approx 1$, discontinuous lines are structurally formed by geological forces. If fracture distributions are random, then each element can be independent and separate or some fractures can be connected.

The continuity indicator (percolating quantity) Q of N fractures is empirically expressed as:

$$Q \propto (N - N_c)^{\kappa} \quad \text{or} \quad Q \propto (p - p_c)^{\kappa} \tag{2.122}$$

where N_c = total number of connected fractures (fractures with transmission), κ = an exponent, p (= N/N_c) = probability for connected fracture numbers, p_c (= N_c/N_0), and N_0 = total number of fractures (e.g., $N_0 > 100$).

In other words, Eq. 2.122 states that the numbers of seepage fractures ($N - N_c$) and κ determine seepage discharge. Here, N_c and κ are values characterizing fracture geometry and are the most important parameters governing fracture flows.

2.8.4 (b) Characteristics of Flow in Fractures

As discussed earlier, fracture seepage depends on the geometrical characteristics of fractures. As shown in **Fig. 2.30**, if points A and B are separated by a rock mass (size L), and the average pressure difference between them is $\Delta\bar{p}$, then the pressure

distributions along the x-axis [$p(x)$] vary with the connectivity of the fractures. The average flow velocity (Darcy's flow velocity, u) across A and B, and the local flow velocity inside the fracture (u') are given as:

$$u \propto \overline{k}\,\Delta\overline{p}, \quad u' \propto k'\Delta p' \tag{2.123}$$

where $\overline{k}$ = Darcy's permeability, k' = local permeability, and Δp = local water pressure difference.

Darcy's permeability (k) is given by:

$$k \propto (p - p_c)^{\kappa} \tag{2.124}$$

Exercises

[Ex. 2.1]
Examine whether Bernoulli's theorem is applicable or not to seepage flow.

[Ex. 2.2]
$\psi(x, y)$ = constant is a general solution of the total differential equation $d\psi(x, y) = u(x, y)dx + v(x, y)dy = 0$. Show that $(u\,dx + v\,dy) = 0$ is an exact differential equation.

[Ex. 2.3]
Show that the velocity potential $\phi(x, y)$ = constant and the stream function $\psi(x, y)$ = constant cross at right angle.

[Ex. 2.4]
Discuss the static stability of the dam shown in **Fig. E2.1**.

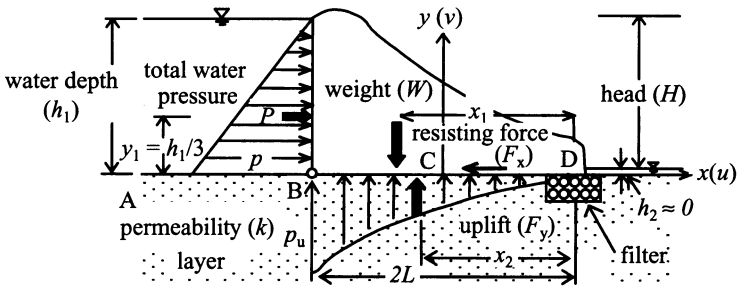

Fig. E2.1 Static forces acting on a dam

[Ex. 2.5]
Derive the relationship between pumping discharge (Q_i) and well water level (h_i) for a group of wells as shown in **Fig. E2.2**, where $i = 1, 2, 3, \ldots, n$.

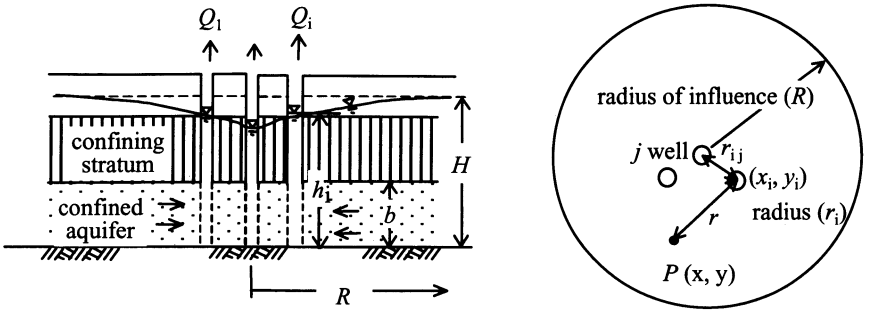

Fig. E2.2 Group of wells in a confined aquifer

[Ex. 2.6]

As shown in **Fig. E2.3**, two faults AB and BC cross at point B. There is a spout at point C with precipitation (N) at point A. Calculate the piezometric head at B (h_B), and show the condition for the persistence of the spout.

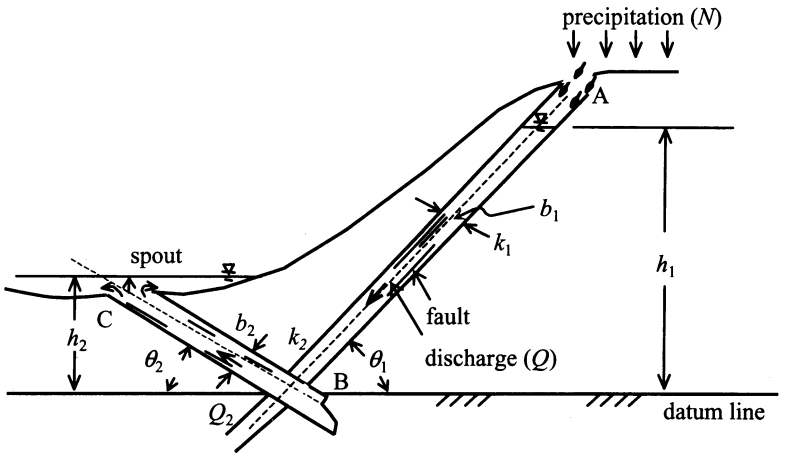

Fig. E2.3 Mechanism of faults and spouts

References

Aravin VI, Numerov SN (1965) Theory of fluid flow in undeformable porous media (translated from Russian). Israel Program for Scientific Translations, Jerusalem, pp 54–56, 300–308

Barenblatt GI, Zheltov IP, Kochina IN (1960) Basic concept in the theory of seepage of homogeneous liquids in fissured rock. Soviet Appl Math Mech (PMM) 24: 852–864

Barenblatt GI, Entov VM, Ryzhik VM (1990) Theory of fluid flows through natural rocks. Kluwer, Dordrecht, pp 34–46

Bear J (1972) Dynamics of fluids in porous media. American Elsevier, New York, pp 165–167

Berkowitz B, Balberg I (1993) Percolation theory and its application to groundwater hydrology. Water Resources Res 29(4): 775–794

Brook R H and Corey A T (1964) Hydraulic properties of porous media. Hydrology paper No 3, Colorado State University

Carman PC (1937) Fluid through a granular bead. Trans Inst Chem Eng, London 15: 150–156

Childs EC (1969) Introduction to the physical basis of soil water phenomena. Wiley-Interscience, London, pp 223–240

Darcy H (1857) Les fontaines publiques de la ville de Dijon. Victor Dalmont, Paris, pp 590–594

De Wiest RJM (1969) Flow through porous media. Academic, New York, pp 16–17, 215–236

Dupuit J (1863) Études theoriques et practiques sur le mouvement des eaux dans les canaus découverts et á travers les terrains permeables. Dunod, Paris, pp 229–239

Gardner W R (1958) Some steady state solution of the unsaturated flow equation with application to evaporation from a water table. Soil Sci, Vol 85: 228–232

Gardnar WR, Mayhugh MS (1958) Solution and tests of diffusion equation for the movement of water in soil. Soil Sci Soc Am Proc 22: 197–201

Hazen A (1893) Some physical properties of sand and gravel with special reference to the use in filtration. The 24th Annual Report, State Board of Health, Boston

Irmay S (1954) On the hydraulic conductivity of unsaturated soil. Trans Amer Geophys Union, Vol 35: 463–153

Jacob CE (1951) Flow of groundwater. ln: Rouse H (ed) Engineering hydraulics, Wiley, New York, pp 321

Kroszynski U (1975) Flow in a vertical porous column drained at its bottom at constant flux. J Hydro, Vol 24: 135–153

Mualem Y (1976) A model for predicting the hydraulic conductivity of unsaturated porous media. Water Resource Res 12(3): 513–522

Muskat M (1937) The flow of homogeneous fluids through porous media, 1st edn. McGraw-Hill, New York, p60

Sato K, Murota A (1971) Experimental study of the absorbed water for microseepage (in Japanese). Jpn Soc Civil Eng 195: 67–75

Sato K (1972) Fundamental study on groundwater flow mechanism. Doctoral thesis, Osaka Univ (in Japanese): p195

Swartzendruber D (1969) Flow through porous media. Edited by Rojer JM De Wiest, Academic, New York, pp215–292

Terzaghi K (1924) Erdbaumechanik auf bodenphysikalischer grundlage. Deuticke, Vienna, pp 119–120

Van Genuchten MT (1980) A closed form equation for predicting the hydraulic conductivity of unsaturated soils. Soil Sci Am J 44: 892–898

3

Dispersion Process and Saltwater Intrusion in Groundwater

Summary

Dispersion phenomena of solutes and pollutants (contaminants/tracers) in subsurface water and porous media have caught the interest of researchers since the 1960s. The mathematical formulation of problems in terms of hydraulics has been realized by applying mass conservation (including source or sink terms for dispersed matter), Fick's law and empirical correlations on the parameters for linking practice and mathematical models.

Simultaneous two-phase-flow of seawater and freshwater in coastal aquifer with a sharp interface is one of the themes.

In this chapter, mathematical modeling for convective and hydraulic equations, their typical analytical solutions, and the methods to determine dispersion coefficients are discussed in addition to formulation of the saltwater–freshwater interface in coastal aquifers.

3.1 Dispersion Processes in Aquifers

3.1.1 Hydraulic Dispersion

Hydraulic dispersion is defined as a transport phenomenon of dispersive matter (e.g., solutes and tracers), which appears in fluid flow through porous media. Knowledge of hydraulic dispersion problems is indispensable for studying groundwater quality and pollution/contamination. The physical and biochemical processes within aquifer matrices affect fluid flow and transport of dissolved chemical compounds in groundwater. The velocity and its spatial distribution are governing factors for mass transport in porous media. **Fig. 3.1** illustrates a vertical sectional view of an unconsolidated groundwater aquifer consisting of several layers with different permeabilities in the x and z-directions. As shown in the figure, molecular diffusion, hydraulic dispersion and macroscopic dispersion influence tracer transport as a result of convection. As time elapses from t_1 to t_2, the tracer slug stretches under the

K. Sato et al. (eds.), *Groundwater Hydraulics*

effect of local velocity variations and molecular diffusion, both on the microscopic and macroscopic scales. Microscopic dispersion processes occur at the size scale of grains, whereas macroscopic dispersion occurs on the same spatial scale as variations in permeability. Microscopic observation at the size scale of grains reveals that local flow with molecular diffusion is responsible for tracer transport.

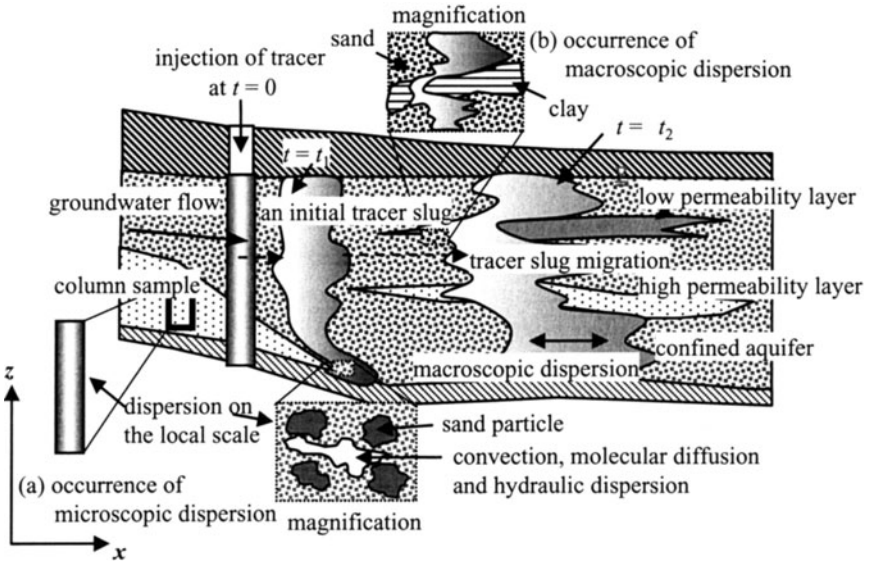

Fig. 3.1. Mass transport and dispersion processes in an aquifer

Macroscopic dispersion dominates transport in a large-scale aquifer, where spatial variation in permeability causes velocity gradients in a whole basin.

A model of dispersion processes in a grain-sized channel is shown in **Fig. 3.2**, where the upper and lower surfaces are bounded by solid particles. Fluid velocities at the solid boundaries are assumed to be zero by the nonslip boundary condition. Clearly, maximum velocity occurs at the center of the crosssection. Transport of a chemically inert contaminant with an instantaneous slug injection at $x = 0$ is considered, as shown in **Fig. 3.2**. If convection in the transverse direction is negligible, compared to that in the longitudinal direction (average flow direction), the driving force for contaminant transport in the transverse direction is limited to molecular diffusion. Except for microscopic interactions in the vicinity of the solid surface, contaminant transport as a result of convection mainly takes place in the longitudinal direction.

$C(x, z, t)$ denotes the contaminant concentration distribution, and two concentration profiles at times t_1 and t_2 are illustrated in **Fig. 3.2**. The profiles are increasingly stretched in the x-direction as time elapses. It is clear that irregular stretching is the result of local velocity variation in the z-direction.

Consider the cross-sectional concentration variation in the z-direction at t_2 at a downstream point on the x-axis. The concentration increases gradually in the upper and lower parts close to the top and bottom solid surfaces.

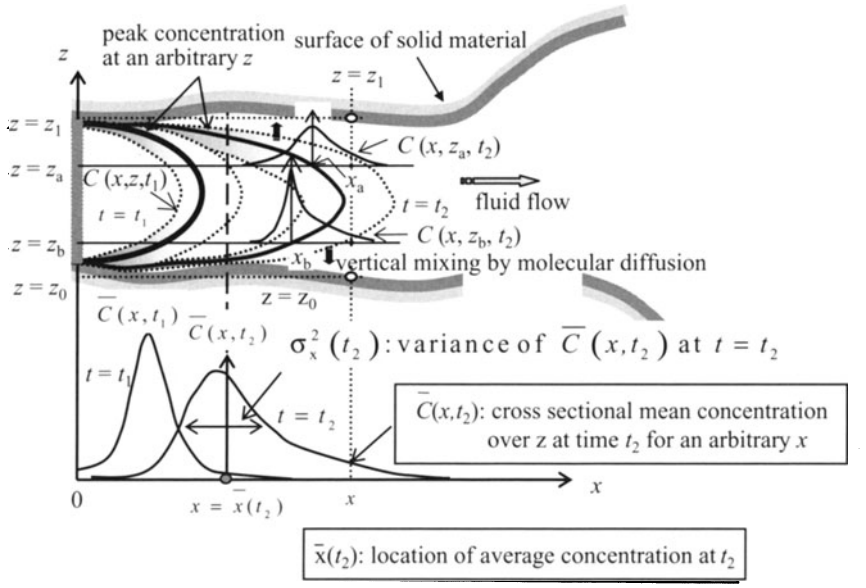

Fig. 3.2. Hydraulic dispersion mechanism for pore-scale fluid flow

The thick line in the center of the figure demonstrates the travel path of peak concentration for a specified value of z. For example, the concentration profile at t_2 in the x-direction for z_a denoted by $C(x, z_a, t_2)$, has peak concentration on the thick line at x_a. Similarly, $C(x, z_b, t_2)$ has peak concentration on the thick line at x_b. $C(x_a, z_a, t_2)$ is not necessarily equal to $C(x_b, z_b, t_2)$, and the difference in these two peaks increases with time.

The term "hydraulic dispersion" can be used to define such a tracer spreading in the flow direction as a result of differences in local flow velocity in the transverse direction. Detailed approaches to this dispersion process in a capillary tube and in interconnected capillary tubes, as well as in models of three-dimensional porous media, have been studied by, for example, Taylor (1952), Aris (1956), Josselin (1959), and Saffman (1956).

3.1.2 Determination of the Microscopic Dispersion Coefficient Using Column Test

The mathematical formulation and statistical meaning of concentration distribution along the x-axis are discussed here. The average concentration between ranges z_0

and z_1 in the z-direction perpendicular to the x-axis at time t_2 for an arbitrary section of x within $-\infty$ to ∞, is defined by Eq. 3.1:

$$\overline{C}(x, t_2) = \frac{\int_{z_0}^{z_1} C(x, z, t_2) dz}{z_1 - z_0} \tag{3.1}$$

The quantity $\overline{C}(x, t_2)$ represents one-dimensional concentration distribution in the x-direction at time t_2. The first-order moment of x using the weighted concentration distribution at time t_2 is represented by Eq. 3.2 as:

$$\overline{x}(t_2) = \frac{\int_{-\infty}^{\infty} x \cdot \overline{C}(x, t_2) dx}{\int_{-\infty}^{\infty} \overline{C}(x, t_2) dx} \tag{3.2}$$

In other words, Eq. 3.2 defines the mean travel distance on the x-axis of the concentration distribution.

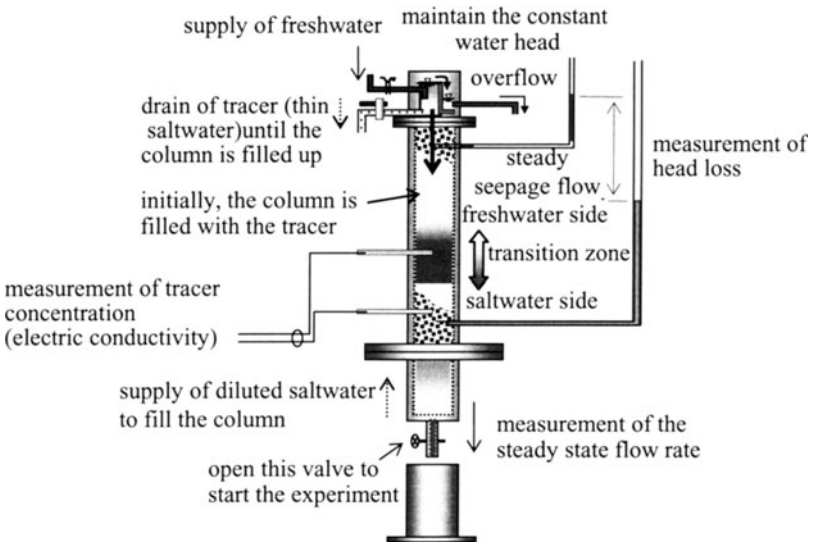

Fig. 3.3. Determination of the longitudinal dispersion coefficient in a column experiment using two different tracers

Similarly, the second-order moment of the deviation of x from $\overline{x}$ at time t_2 is calculated as:

$$\sigma_x^2(t_2) = \frac{\int_{-\infty}^{\infty} (x - \overline{x})^2 \cdot \overline{C}(x, t_2) dx}{\int_{-\infty}^{\infty} \overline{C}(x, t_2) dx} \tag{3.3}$$

Higher order moments of $\overline{C}(x, t_2)$ can be also calculated if more statistical variables are necessary for characterizing concentration distribution.

The microscopic dispersion coefficient $D_{h,x}$, which is usually called "the hydraulic dispersion coefficient" or "the mechanical dispersion coefficient" can be defined as half of the time derivative of $\sigma_x^2(t)$ as follows:

$$D_{h,x}(t_2) = \frac{1}{2}\frac{d\sigma_x^2(t_2)}{dt} \tag{3.4}$$

It is empirically proved that the microscopic dispersion coefficient ($D_{h,x}$) converges for a sufficiently long elapsed time.

Thus, such quantities as $\overline{C}(x,t)$, $\overline{x}(t)$, $\sigma_x^2(t)$, and $D_{h,x}(t)$ can characterize two-dimensional tracer distribution in the vertical crosssection in the x- and z-axes for arbitrary x and t, if fluid flow in the x-direction is dominant and the point of interest is only in that direction.

Figure 3.3 shows an experimental setup to determine the one-dimensional microscopic dispersion coefficient for a homogeneous porous medium.

Initially, the column is saturated with either low-concentration saltwater or freshwater. Then, freshawter or saltwater is supplied to the bottom and top of the column, respectively, as shown in the figure, so that a clear interface between two phases can be maintained at the top of the column. One should be careful not to use high concentration saltwater, because it may induce a significant gravitational effect. The experiment should be started after piezometric heads at two different depths become equal. Freshwater should be supplied instantly once the outlet valve of the column is opened if the column is initially saturated with low concentration saltwater. Sensors along the column will exhibit gradual changes in electric conductivity during the experiment. The flow rate should be measured several times to ascertain consistent conditions in the experiment. The fluid temperature should also be measured to evaluate fluid density, viscosity, Reynolds number, and permeability. Several series of the experiment with different flow rates are needed to establish a correlation between Reynolds number and normalized hydraulic dispersion coefficient.

(Example 3.1)
Explain the determination of the longitudinal dispersion coefficient using the recorded breakthrough curve for the one-dimensional column test shown in **Fig. 3.4**.

(Answer)
The following one-dimensional convection dispersion equation is applicable to describe temporal and spatial concentration distributions (see Sect. 3.2).

$$\frac{\partial C}{\partial t} + u'\frac{\partial C}{\partial x} = D_{h,x}\frac{\partial^2 C}{\partial x^2} \tag{3.5}$$

where $C(x,t)$ = saltwater concentration and u' = real pore velocity obtained from the relationship $u' = u/n$ with u and n as Darcy's velocity and porosity, respectively. The initial and boundary conditions necessary for solving Eq. 3.5 are given below.

When the column is initially saturated with low concentration solute, e.g., saltwater:

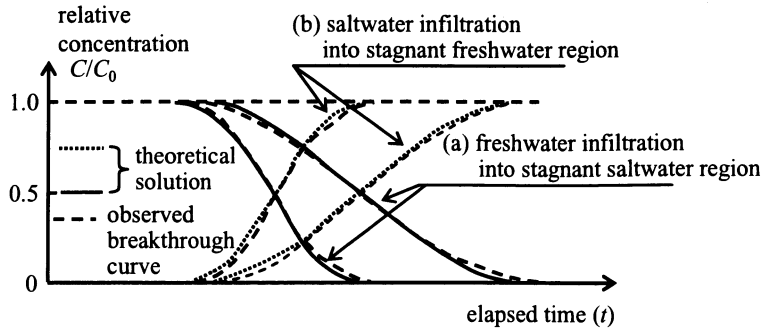

Fig. 3.4. Theoretical and measured breakthrough curves for different tracers

$$\left.\begin{array}{l} C(x,0) = C_0 : \text{initial condition} \\ \left.\begin{array}{l} C(0,t) = 0 \\ C(\infty,t) = C_0 \end{array}\right\} : \text{boundary conditions} \end{array}\right\} \tag{3.6a}$$

When the column is initially saturated with freshwater:

$$\left.\begin{array}{l} C(x,0) = 0 : \text{initial condition} \\ \left.\begin{array}{l} C(0,t) = C_0 \\ C(\infty,t) = 0 \end{array}\right\} : \text{boundary conditions} \end{array}\right\} \tag{3.6b}$$

The analytical solution of the equation for initial and boundary conditions given by Eq. 3.6b is expressed by Eq. 3.7 as (cf. Example 3.2):

$$\frac{C(x,t)}{C_0} = \frac{1}{2}\operatorname{erfc}\left\{\frac{x-u't}{2\sqrt{D_{h,x}t}}\right\} + \frac{1}{2}\exp\left(\frac{u'x}{D_{h,x}}\right)\operatorname{erfc}\left\{\frac{x+u't}{2\sqrt{D_{h,x}t}}\right\} \tag{3.7}$$

where erfc(η): the complementary error function. Relation between error function and its complement is expressed by erfc(η) = 1 − erf(η), and the error function is defined as:

$$\operatorname{erf}(\eta) = \frac{2}{\sqrt{\pi}}\int_0^{\eta} e^{-\xi^2} d\xi \tag{3.8}$$

The observed breakthrough curve can then be compared with the analytical solution given by Eq. 3.7, as shown in **Fig. 3.4**.

Darcy's velocity (u) is calculated using the measured flow rate (Q) and cross sectional area of the column (A) as: $u = Q/A$. Then, u' is obtained from $u' = u/n$. It is also possible to experimentally evaluate u' and determine $D_{h,x}$ after best fit of the observed breakthrough curve with the analytical solution. These dispersion coefficient data for different flow rates can be identified universally using nonlinear least-squares estimation, which can fit the analytical solution for the observed breakthrough curve, as indicated by the broken line in **Fig. 3.4**.

3.1.3 Relationship between Microscopic Hydraulic Dispersion Coefficient and Real Pore Velocity

Many authors have used laboratory experiments to determine the hydraulic dispersion coefficient. For example, Harleman D.R.F. and Rumer R.R. (1963) conducted laboratory experiments to determine the relationships between Reynolds number and longitudinal as well as lateral hydraulic dispersion coefficients. They proposed the following relationship for Reynolds numbers ranging from 10^{-4}–10^{0}.

$$\frac{D_{h,x}}{\nu} = \alpha(R_e)^{\beta} + \frac{\tau}{S_c}, \quad R_e = \frac{d_m u'}{\nu} = \frac{d_m u}{n\nu}, \quad S_c = \frac{\nu}{D_M} \tag{3.9}$$

where ν: kinematic viscosity of fluid, S_c: Schmit number, which characterizes dynamic resistance to molecular diffusion, α = a constant, β =an exponent, which is nearly equal to 1, τ =tortuosity that accounts for twisted flow paths of porous media, d_m = mean particle diameter. A similar expression to Eq. 3.9 is obtained when the Peclet number (P_e) is used.

$$\frac{D_{h,x}}{D_M} = a(P_e)^{b} + \tau, \quad P_e = \frac{d_m u'}{D_M} \tag{3.10}$$

where a: a constant and b: exponent.

Again, the parameters in Eq. 3.10 need to be determined in a laboratory column test. Details on these nondimensional quantities are given by Bear J. and Verruijt A. (1987).

Experimental correlations between R_e and D_M/ν obtained from column tests packed with glass spheres of different diameters are shown in **Fig. 3.5**. The solid line represents the best fitting curve using Eq. 3.9 with $\tau = 1$ (Nakagawa et al., 1998). As seen in the figure, the second term in Eq. 3.9 is negligibly small for Reynolds number ranging from 0.10 to 0.7, because the molecular diffusion coefficient (D_M) is approximately equal to $1.0\times10^{-9}\,m^2s^{-1}$ and kinematic viscosity is $1.0\times10^{-6}\,m^2s^{-1}$. However, the second term becomes dominant for Reynolds number lower than 10^{-3}.

Now, let us assume that Eq. 3.9 is linear, as expressed by Eq. 3.11 (Huyakorn PS & Pinder GF, 1983).

$$D_{h,x} = D_L = \alpha_L|u'| + \tau D_M = \frac{\alpha_L u'^2}{\sqrt{u'^2}} + \tau D_M \tag{3.11}$$

where $D_L = D_{h,x}$: longitudinal dispersion coefficient when the x-axis is taken parallel to the flow direction and, α_L is the longitudinal dispersivity.

This formula can be extended to the three-dimensional flow field in Cartesian coordinates system as follows (Bear and Verruijt 1987). If general expression of dispersion coefficient $D_{h,ij}$ in tensor form is $D_{h,ji} = a_{ijkm}(V_k V_m/V)$, $a_{ijkm} = \alpha_T\delta_{ij}\delta_{km} + (\alpha_L - \alpha_T)(\delta_{ik}\delta_{jm} + \delta_{im}\delta_{jk})/2$ (δ_{ij}: Kronecker delta with $\delta_{ij} = 0$ for $i \neq j$, and $\delta_{ij} = 1$ for $i = j$) for isotropic porous media, it can be written by using the summation convention rule (Einstein's convention: for example a summation $A_1B_1 + A_2B_2 + A_3B_3 = \sum_{i=1}^{3} A_iB_i$ is defined by $A_iB_i = \sum_{i=1}^{3} A_iB_i$ to simplify its expression.

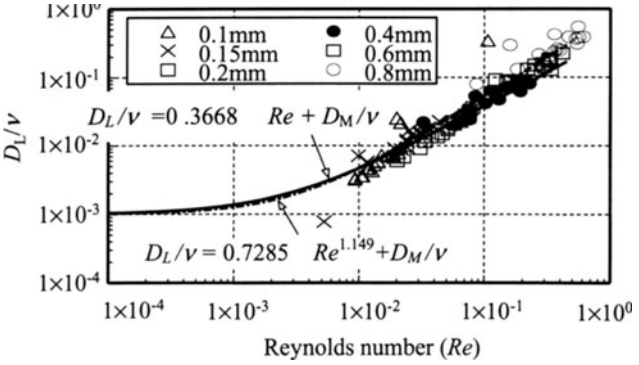

Fig. 3.5. Relation between Reynolds number and normalized microscopic longitudinal dispersion coefficient (Nakagawa et al, 1998)

$$
\begin{aligned}
D_{\mathrm{h},ij} &= a_{ijkm}\frac{V_kV_m}{V} = \sum_{k=1}^{3}\sum_{m=1}^{3} a_{ijkm}\frac{V_kV_m}{V} \\
&= \sum_{k=1}^{3}\sum_{m=1}^{3}\left\{\alpha_{\mathrm{T}}\delta_{ij}\delta_{km} + \frac{\alpha_{\mathrm{L}}-\alpha_{\mathrm{T}}}{2}(\delta_{ik}\delta_{jm}+\delta_{im}\delta_{jk})\right\}\frac{V_kV_m}{V} \\
&= \alpha_{\mathrm{T}}\sum_{k=1}^{3}\sum_{m=1}^{3}\delta_{ij}\delta_{km}\frac{V_kV_m}{V} + \frac{\alpha_{\mathrm{L}}-\alpha_{\mathrm{T}}}{2}\sum_{k=1}^{3}\sum_{m=1}^{3}\delta_{ik}\delta_{jm}\frac{V_kV_m}{V} \\
&\quad + \frac{\alpha_{\mathrm{L}}-\alpha_{\mathrm{T}}}{2}\cdot\sum_{k=1}^{3}\sum_{m=1}^{3}\delta_{im}\delta_{jk}\frac{V_kV_m}{V} \\
&= \alpha_{\mathrm{T}}\sum_{k=1}^{3}\sum_{m=1}^{3}\delta_{ij}\delta_{km}\frac{V_kV_m}{V} + \frac{\alpha_{\mathrm{L}}-\alpha_{\mathrm{T}}}{2}\cdot\sum_{i=k}^{3}\sum_{j=m}^{3}\delta_{ik}\delta_{jm}\frac{V_kV_m}{V} \\
&\quad + \frac{\alpha_{\mathrm{L}}-\alpha_{\mathrm{T}}}{2}\cdot\sum_{i=m}^{3}\sum_{j=k}^{3}\delta_{im}\delta_{jk}\frac{V_kV_m}{V} \\
&= \alpha_{\mathrm{T}}\sum_{k=1}^{3}\delta_{ij}\frac{V_k^2}{V} + \frac{(\alpha_{\mathrm{L}}-\alpha_{\mathrm{T}})}{2}\delta_{ii}\delta_{jj}\frac{V_iV_j}{V} + \frac{(\alpha_{\mathrm{L}}-\alpha_{\mathrm{T}})}{2}\delta_{ii}\delta_{jj}\frac{V_jV_i}{V} \\
&= \alpha_{\mathrm{T}}\delta_{ij}V + (\alpha_{\mathrm{L}}-\alpha_{\mathrm{T}})\frac{V_jV_i}{V}
\end{aligned}
$$

in which, α_{L} (dim. L): longitudinal dispersivity, α_{T} (dim. L): transversal dispersivity, V_k, V_m: velocity components, $V = |V|$, and the last equation holds for each term in the cases of $k = m = 1 \sim 3$, $i = k$, $j = m$ and $i = m$, $j = k$, respectively.

Thus, the following Eq. 3.12 will be given if $V = q'$, $V_1 = u'$, $V_2 = v'$, $V_3 = w'$ by taking molecular diffusion D_{M} and tortuosity τ.

$$\left.\begin{aligned} D_{h,xx} &= \frac{\alpha_L u'^2 + \alpha_T(v'^2 + w'^2)}{q'} + \tau \cdot D_M, & D_{h,xy} &= \frac{(\alpha_L - \alpha_T)u'v'}{q'} = D_{h,yx} \\ D_{h,xz} &= \frac{(\alpha_L - \alpha_T)u'w'}{q'} = D_{h,zx}, & D_{h,yy} &= \frac{\alpha_L v'^2 + \alpha_T(u'^2 + w'^2)}{q'} + \tau \cdot D_M \\ D_{h,yz} &= \frac{(\alpha_L - \alpha_T)v'w'}{q'} = D_{h,zy}, & D_{h,zz} &= \frac{\alpha_L w'^2 + \alpha_T(u'^2 + v'^2)}{q'} + \tau \cdot D_M \end{aligned}\right\} \quad (3.12)$$

where $(q') = \sqrt{(u')^2 + (v')^2 + (w')^2}$, and v' and w' are the real pore velocities in the y- and z-direction, respectively. These nine constitutes compose of the dispersion matrix tensor, which can be simply expressed as $[D_{h,ij}]$. The transverse dispersivity (α_T) is usually assumed to be as: $\alpha_T = (1/10)\alpha_L$. Equation 3.12 can be reduced to a matrix expression with zero values for off-diagonal components if the x-axis is taken to be along the direction of flow and the other two axes perpendicular to the flow, as follows:

$$[D_{h,ij}] = \begin{bmatrix} \alpha_L q' + \tau D_M & 0 & 0 \\ 0 & \alpha_T q' + \tau D_M & 0 \\ 0 & 0 & \alpha_T q' + \tau D_M \end{bmatrix} \quad (3.13)$$

3.1.4 Macroscopic Dispersion in Groundwater Aquifer

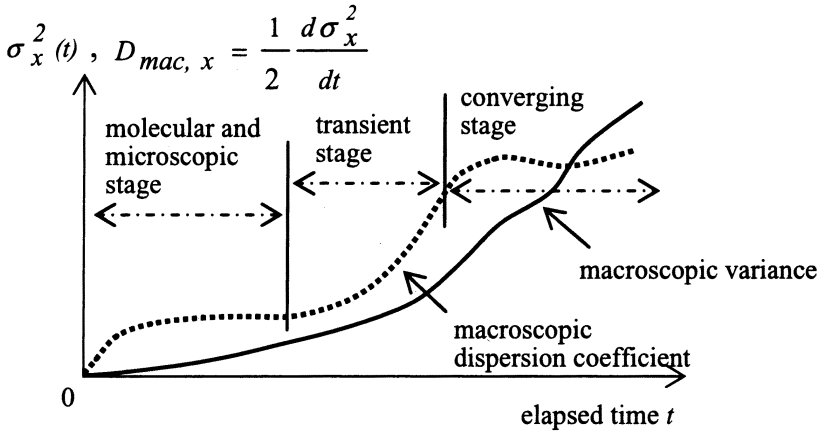

Fig. 3.6. Multistage dispersion processes

As illustrated in **Fig. 3.1**, natural groundwater flow in a heterogeneous aquifer is not uniform. Although molecular diffusion and microscopic dispersion play important roles on the local scale, large-scale dispersion (over several hundreds of meters) is involved in groundwater pollution problems in the field. Macroscopic dispersion gradually develops from microscopic dispersion to more extensive scales with tracer progression to the downstream. The macroscopic dispersion process can be understood

by the existence of a less permeable layer with higher permeability near the center of the flow region in **Fig. 3.1**. **Figure 3.6** conceptually illustrates two transition processes with elapsed time by statistical variance of tracing particles, which can define the dispersion coefficient from both the microscopic and macroscopic view points. Through these transition processes, the cross-sectional mean concentration, mean travel distance, the macroscopic variance, and the macroscopic dispersion coefficient in the pore space shown in **Fig. 3.2** for fixed x at time t can be extended over the aquifer thickness.

The development of macroscopic dispersion structures through three distinct stages, i.e. the molecular and microscopic stage, the transient stage and the converging stage depend on the heterogeneity of permeabilities, and geometry of the strata. Macroscopic dispersion coefficients in the longitudinal and transverse directions can be similarly defined using dispersion lengths α_L and α_T, respectively, and the mean pore velocities u' and w' in the x- and z-direction, respectively, as:

$$D_{mac,x}(t) = \alpha_L \cdot u', \quad D_{mac,z}(t) = \alpha_T \cdot w' \tag{3.14}$$

Generally, theoretical relationships between macroscopic dispersion lengths and the spatial structure of permeability are rarely obtained except for simple aquifer formations. The transient stage from local scale dispersion to the converging macroscopic stage is most important for determining the macroscopic dispersion coefficient if groundwater pollution spreads downstream, where hydrogeological structure changes.

The following empirical relationship between longitudinal and transverse dispersion lengths (α_L and α_T) is assumed.

$$\alpha_T = \frac{1}{10}\alpha_L \tag{3.15}$$

A commonly used diagram for estimating the macroscopic longitudinal dispersion length (α_L) is shown in **Fig. 3.7**. Readers can also refer to textbooks, e.g., these written by Kinzelbach W. (1986) and Appelo C.A.J. and Postma D. (1996). For practical applications, it has to be stressed that macroscopic dispersion processes depends strongly on hydrogeological structure and downstream distance from the pollution source (Nakagawa and Jinno, 2000).

3.2 Mass Transport Resulting from Convection-Dispersion

3.2.1 Continuity Equation

As mentioned in the preceding section, various processes such as convection, molecular diffusion, and dispersion (microscopic and macroscopic) affect mass transport in an aquifer. The mass transport equation describes temporal and spatial concentration variation of a tracer or any chemical species. **Figure 3.8** illustrates the two-dimensional cross-section of an unsaturated microscopic pore space. Although there

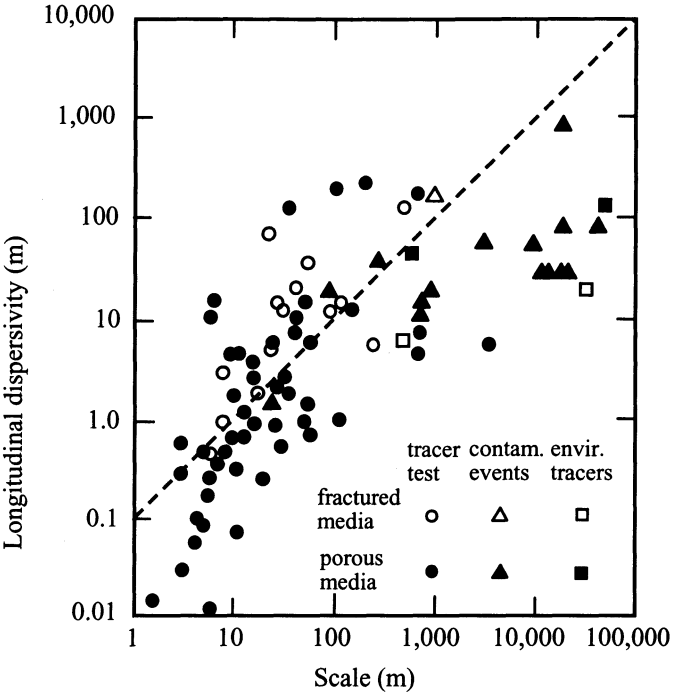

Fig. 3.7. Dependence of longitudinal dispersivity on longitudinal scale (after Appelo and Postma, 1996)

is a component of mass flux in the gaseous phase when the pore space is not completely saturated, only the fundamental equation for mass transport in the liquid phase is introduced here. In this case, the fundamental equation of the water mass balance, which is also called the continuity equation, is written as:

$$\frac{\partial \theta}{\partial t} = -\left(\frac{\partial u}{\partial x} + \frac{\partial w}{\partial z}\right) \tag{3.16}$$

where $\theta(x, z, t)$ is the volumetric water content in a unit soil volume. This equation is identical to the continuity equation in saturated conditions. Denoting $h(x, z, t)$ as the pore water pressure head, Eq. 3.16 is transformed by changing the variable as follows:

$$\frac{\partial \theta}{\partial t} = \frac{d\theta}{dh}\frac{\partial h}{\partial t} = C_w \frac{\partial h}{\partial t}, \quad C_w = \frac{d\theta}{dh} \tag{3.17}$$

Using Eq. 3.17, Eq. 3.16 becomes

$$C_w \frac{\partial h}{\partial t} = -\left(\frac{\partial u}{\partial x} + \frac{\partial w}{\partial z}\right) \tag{3.18}$$

where $C_w(h)$ is called specific water content, which implies a change in water content in response to a change in pressure head.

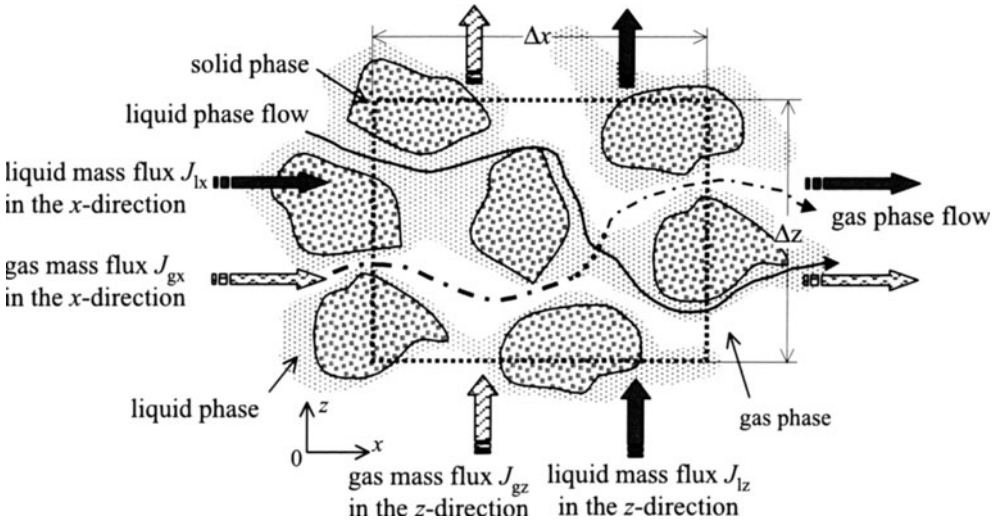

Fig. 3.8. Mass transport in unsaturated porous media

Darcy's law is extended to the unsaturated flow region as follows:

$$u = -k\frac{\partial h}{\partial x}, \quad w = -k\left(\frac{\partial h}{\partial z} + \frac{\rho}{\rho_f}\right) \tag{3.19}$$

where $k(x, z, t)$: permeability applicable for both saturated and unsaturated flow, ρ: fluid density that may vary with temperature (T) or concentration of dissolved contaminant (C), and ρ_f: reference fluid density, which is usually taken as 1000.0 kg m^{-3} at 4 degrees. The pressure head (h) and pressure (p) are correlated as: $h = p/\rho_f g$. The second term in Eq. 3.19 includes the gravitational effect resulting from changes in fluid density. The continuity equation needs to be modified for a sudden change in fluid density, as follows:

$$\frac{\partial(\theta\rho)}{\partial t} = \rho\frac{\partial\theta}{\partial t} + \theta\frac{\partial\rho}{\partial t} = \rho\frac{\partial\theta}{\partial t} + \theta\frac{d\rho}{dC}\frac{\partial C}{\partial t} = -\left(\frac{\partial(u\rho)}{\partial x} + \frac{\partial(w\rho)}{\partial z}\right) \tag{3.20}$$

where $\partial\rho/\partial C$: partial differentiation of $\rho = \rho(C, T, p)$ and represents the change in density with respect to concentration change. When this effect needs to be considered, Darcy's law should be expressed in terms of intrinsic permeability (K), which has the dimension of length squared [L^2], as;

$$u = -\frac{K}{\mu}\frac{\partial p}{\partial x}, \quad w = -\frac{K}{\mu}\left(\frac{\partial p}{\partial z} + \rho g\right) \tag{3.21}$$

3.2.2 Mass Balance Equation

The convection dispersion equation can be derived on the basis of mass conservation in the liquid phase. The liquid phase mass flux in x- and z-direction are expressed by

summing convection and dispersion effects, as follows:

$$J_{l,x} = u'C - D_{h,xx}\frac{\partial C}{\partial x} - D_{h,xz}\frac{\partial C}{\partial z}, \quad J_{l,z} = w'C - D_{h,zx}\frac{\partial C}{\partial x} - D_{h,zz}\frac{\partial C}{\partial z} \tag{3.22}$$

where $J_{l,x}$ and $J_{l,z}$ denote liquid phase mass flux in x- and z-direction, respectively, and u' and w' are real pore velocity components, defined by the following relationships.

$$u' = \frac{u}{\theta}, \quad w' = \frac{w}{\theta} \tag{3.23}$$

Similar expressions are applicable to mass transport in the gaseous phase. The total mass of pollutant dissolved in pore water in an infinitesimal control volume with sides of Δx and Δz, as shown in **Fig. 3.8**, is expressed as: $\theta \times \Delta x \times \Delta z \times C(x, z, t)$. Therefore, mass balance equation can be written as follows:

$$\frac{\partial(\theta C)}{\partial t}\Delta x \Delta z = -\frac{\partial(\theta J_{l,x})}{\partial x}\Delta x \Delta z - \frac{\partial(\theta J_{l,z})}{\partial z}\Delta x \Delta z \tag{3.24}$$

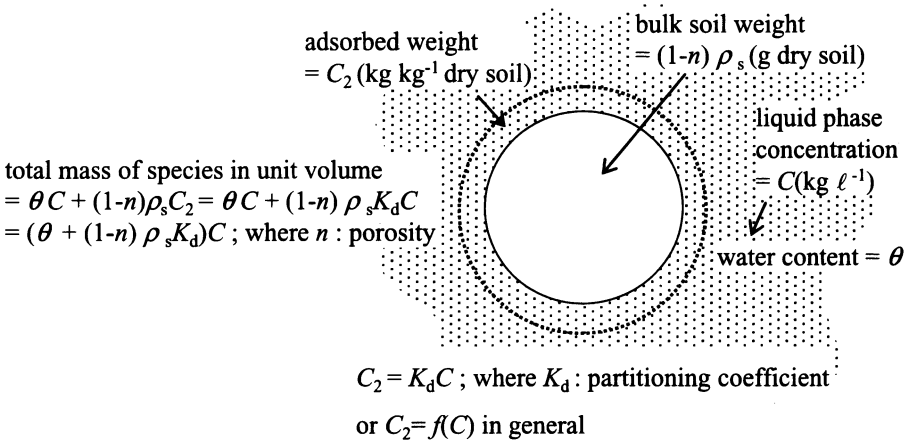

Fig. 3.9. Relationship between adsorbed material in the solid phase and dissolved species in the liquid phase

Substituting Eq. 3.22 into Eq. 3.24, we obtain the following:

$$\frac{\partial(\theta C)}{\partial t} + \frac{\partial(\theta u'C)}{\partial x} + \frac{\partial(\theta w'C)}{\partial z} = \frac{\partial}{\partial x}\left(\theta D_{h,xx}\frac{\partial C}{\partial x} + \theta D_{h,xz}\frac{\partial C}{\partial z}\right) + \frac{\partial}{\partial z}\left(\theta D_{h,zx}\frac{\partial C}{\partial x} + \theta D_{h,zz}\frac{\partial C}{\partial z}\right) \tag{3.25}$$

Using Eq. 3.16 for the left term of Eq. 3.25, the following expression is given:

$$\frac{\partial C}{\partial t} + u'\frac{\partial C}{\partial x} + w'\frac{\partial C}{\partial z} = \frac{1}{\theta}\frac{\partial}{\partial x}\left(\theta D_{h,xx}\frac{\partial C}{\partial x} + \theta D_{h,xz}\frac{\partial C}{\partial z}\right) + \frac{1}{\theta}\frac{\partial}{\partial z}\left(\theta D_{h,zx}\frac{\partial C}{\partial x} + \theta D_{h,zz}\frac{\partial C}{\partial z}\right) \tag{3.26}$$

If adsorption onto solid surfaces has to be taken into consideration, an additional mass balance equation for the solid phase should be formulated to model the effect. For example, an equation for a chemical material that obeys the linear adsorption isotherm law (the Freundlich equilibrium isotherm: adsorption mass on the solid phase is proportional to pollutant concentration), as shown in **Fig. 3.9**, is given as follows:

$$\frac{\partial(1-n)\rho_s K_d C}{\partial t} = S_{ad} \tag{3.27}$$

where ρ_s is the density of solid, K_d is the partitioning coefficient, the term S_{ad} represents the rate of adsorption in the solid phase. Equation 3.25 can be modified to take adsorption into account as:

$$\frac{\partial \theta C}{\partial t} + \frac{\partial uC}{\partial x} + \frac{\partial wC}{\partial z} = \frac{\partial}{\partial x}\left(\theta D_{h,xx}\frac{\partial C}{\partial x} + \theta D_{h,xz}\frac{\partial C}{\partial z}\right) + \frac{\partial}{\partial z}\left(\theta D_{h,zx}\frac{\partial C}{\partial x} + \theta D_{h,zz}\frac{\partial C}{\partial z}\right) - S_{ad} \tag{3.28}$$

It should be noted that the added term S_{ad} has units of [kg m^{-3}s^{-1}] whereas concentration in the dissolved phase has units of [kg m^{-3}]. Adding of Eqs. 3.27 and 3.28 so that the adsorption term S_{ad} is canceled, the following equation can be obtained.

$$\{\theta + (1-n)\rho_s K_d\}\frac{\partial C}{\partial t} + u\frac{\partial C}{\partial x} + w\frac{\partial C}{\partial z} = \frac{\partial}{\partial x}\left(\theta D_{h,xx}\frac{\partial C}{\partial x} + \theta D_{h,xz}\frac{\partial C}{\partial z}\right) + \frac{\partial}{\partial z}\left(\theta D_{h,zx}\frac{\partial C}{\partial x} + \theta D_{h,zz}\frac{\partial C}{\partial z}\right) \tag{3.29}$$

This equation shows that convection and dispersion have direct control on the changes in total mass within a unit soil volume in liquid and solid phases.

Now, the retardation factor (R_d) is defined as follows:

$$R_d = 1 + \frac{(1-n)}{\theta}\rho_s K_d \tag{3.30}$$

Then, Eq. 3.29 is rewritten as:

$$\frac{\partial C}{\partial t} + \frac{u}{\theta R_d}\frac{\partial C}{\partial x} + \frac{w}{\theta R_d}\frac{\partial C}{\partial z} = \frac{1}{\theta R_d}\frac{\partial}{\partial x}\left(\theta D_{h,xx}\frac{\partial C}{\partial x} + \theta D_{h,xz}\frac{\partial C}{\partial z}\right) + \frac{1}{\theta R_d}\frac{\partial}{\partial z}\left(\theta D_{h,zx}\frac{\partial C}{\partial x} + \theta D_{h,zz}\frac{\partial C}{\partial z}\right) \tag{3.31}$$

Thus, adsorption reduces the convection velocity and dispersion coefficient by a ratio of $1/R_d$ ($R_d > 1$), as can be seen in Eq. 3.31. This means that adsorption delays convective mass transport and that the dispersion rate becomes smaller.

3.2.3 Partitioning (or Distribution) Coefficient K_d

A partitioning (or distribution) coefficient (K_d) is defined as the mass fraction of a solution separated from the liquid phase to either another liquid phase or solid phase. It should be noted that such a partition is not necessarily linear, but varies depending on solute concentration and the characteristics of the solid surface (Young et al., 1992). Also, values of the coefficient obtained from batch tests and column tests may not be identical, because the flow velocity and soil packing condition may affect column tests.

The determination of the partitioning coefficient K_d has been investigated experimentally by several authors. Hiroshiro et al. (1996) verified that the travel time for the mean sulfate ion concentration to reach a fixed depth in a column packed with weathered granite is 1.9 times longer than that for nitrate ions, which are chemically inert in oxidizing conditions. Therefore, the retardation factor or coefficient (R_d) for sulfate ions is equal to 1.9. From Eq. 3.30, we can calculate the partitioning coefficient (K_d) as follows:

$$R_d = 1 + \frac{1-n}{\theta}\rho_s K_d \approx 1.9$$

Substituting experimental values of 0.531 for porosity (n), 0.252 for soil water content (θ), and 2.69 kg ℓ^{-1} for clay density (ρ_s), $K_d = 0.18\,\ell\,\mathrm{kg}^{-1}$ is obtained.

The partitioning coefficient of hydrophobic materials, such as trichloroethylene and tetrachloroethylene, is related to the organic carbon content of the soil as follows:

$$K_d = K_{OC}(OC) \quad \text{or} \quad \log K_d = \log K_{OC} + \log(\mathrm{OC})$$

where (OC): organic carbon content of soil, and K_{OC}: proportionality constant (Appelo C.A.J. and Postma D., 1996; Fetter C.W., 2001). The value of K_d can be estimated by measuring the (OC) mass fraction in soil and adopting the standard value of the octanol–water partitioning factor. For example, K_{OC} for tetrachloroethylene is equal to $1.0 \times 10^{2.56}$ for 0.3% (OC). Then,

$$\log K_d = \log K_{OC} + \log(\mathrm{OC}) = 2.56 + \log(0.003) = 0.037$$

and we obtain $K_d \approx 1.09\,\ell\,\mathrm{kg}^{-1}$.

Similarly, $K_d = 1200\,\ell\,\mathrm{kg}^{-1}$ for Polychlorobiphenyl (PCB) with $K_{OC} = 1.0 \times 10^{5.62}$.

3.3 One-dimensional Mass Transport with Adsorption and Decay

One-dimensional mass transport with a retardation coefficient (R_d) and a decay coefficient (λ) can be expressed by the following convection–dispersion equation.

$$\frac{\partial C}{\partial t} + \frac{u'}{R_d}\frac{\partial C}{\partial x} = \frac{D_L}{R_d}\frac{\partial^2 C}{\partial x^2} - \frac{\lambda}{R_d}C \tag{3.32}$$

where D_L: longitudinal dispersion coefficient in a uniform porous medium, which is written as $D_L = \alpha_L u'$ after neglecting molecular diffusion. The decay term $-(\lambda/R_d)C$ with R_d exhibits, for example, biodegradation of organic compounds by bacteria or radioactive degradation with adsorption.

Assume an instantaneous injection of mass ΔM within a width b at the origin of the x-axis in a confined aquifer of thickness m, that extends infinitely in the x-direction. The injection condition at time $t = 0$ can be expressed mathematically using Dirac's delta function as follows:

$$C_\delta(x,0) = \frac{\Delta M}{n \cdot m \cdot b \cdot R_d}\delta(x) \tag{3.33}$$

where the Dirac's delta function is defined as:

$$\delta(x) = \lim_{\varepsilon \to 0} \delta_\varepsilon, \quad \delta_\varepsilon = \begin{cases} 1/\varepsilon & |x| \le |\varepsilon/2| \\ 0 & |x| > |\varepsilon/2| \end{cases} \tag{3.34}$$

and ε an infinitesimal interval compared to the scale of interest, n porosity, and $R_d = 1 + (1 - n)\rho_s K_d/n$. Equation 3.33 means that the initial concentration $C_\delta(x,0)$ is given by dividing the injected mass ΔM (kg) by volume $\varepsilon \times m \times b$ (m^3), and taking into account adsorption on the solid surface. Integration of the initial concentration defined by Eq. 3.33 over the entire domain satisfies:

$$\int_{-\infty}^{\infty} b \cdot m \cdot n \cdot R_d C_\delta(x,0)dx = \Delta M \tag{3.35}$$

The boundary condition at infinity is given as:

$$C(\pm\infty, t) = 0 \tag{3.36}$$

Under these initial and boundary conditions, the following analytical solution is given as (Kinzelbach W., 1986).

$$C_\delta(x,t) = \frac{\Delta M}{2b \cdot m \cdot n \cdot R_d \sqrt{\pi \alpha_L u' t/R_d}} \cdot \exp\left(-\frac{(x - u't/R_d)^2}{4\alpha_L u' t/R_d}\right) \cdot \exp[-(\lambda/R_d)t] \tag{3.37}$$

Because of degradation effects, the peak concentration value gradually decreases with time at the rate of $\exp[-(\lambda/R_d)t]$.

Figure 3.10 shows transient concentration distributions satisfying Eq. 3.37 for two cases: conservation ($\lambda = 0$) and degradation of species ($\lambda > 0$). Adsorption apparently causes a delay in the spread of material, species are less dispersed and degraded when $R_d > 1$.

Integrating Eq. 3.37 over the entire aquifer region, we obtain,

$$\int_{-\infty}^{\infty} b \cdot m \cdot n \cdot R_d C_\delta(x,t)dx = \Delta M \exp[-(\lambda/R_d)t] \tag{3.38}$$

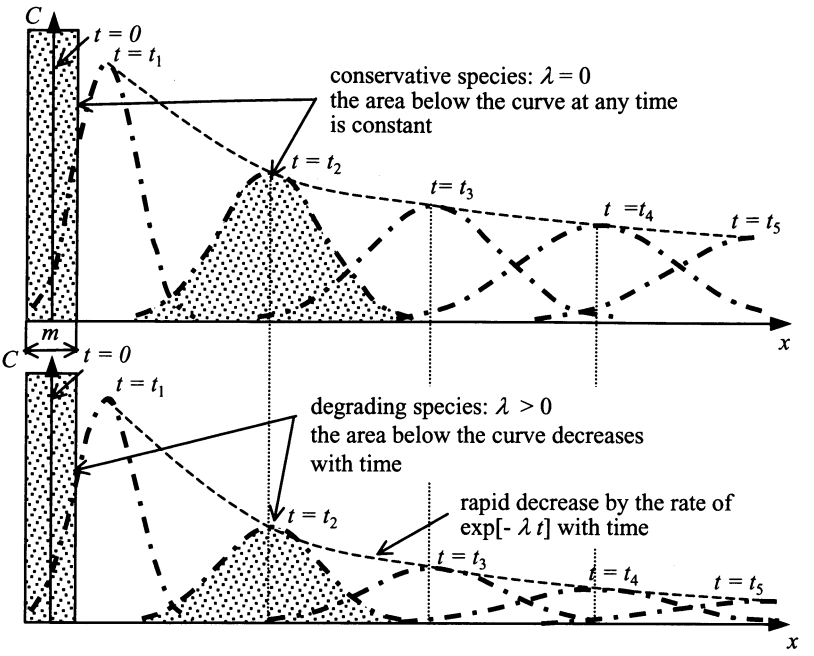

Fig. 3.10. Temporal variation of concentration distribution from Eq. 3.37 with $R_d = 1$ (original figure by Kinzelbach 1986)

This equation shows that each pollutant mass decreases with time as a result of degradation. Recently, the term natural attenuation (NA) has been used for degradable organic hydrocarbons that have been major sources of pollution in groundwater and the soil environment. The NA idea suggests that mechanical recovery of polluted groundwater and soil up to the prescribed standards is costly and a waste of time, and also that chemical and biological actions may be expected at the final stage of remediation work.

If instantaneous injection at $x = \xi$ and $t = \tau$ is considered, $(t - \tau)$ and $(x - \xi)$ should replace t and x in Eq. 3.37, respectively.

(Example 3.2)

One-dimensional mass transport as a result of convection–dispersion, and a set of initial and boundary conditions are given in Eqs. 3.39 and 3.40, respectively:

$$\frac{\partial C}{\partial t} + u' \frac{\partial C}{\partial x} = D_L \frac{\partial^2 C}{\partial x^2} \tag{3.39}$$

$$C(x,0) = 0, \quad C(0,t) = f(t), \quad C(\infty,t) = 0 \tag{3.40}$$

Analytical solution of Eq. 3.39 with the given conditions is expressed as (see Exercise 3.4, Hirano N., 1977):

$$C(x,t) = \frac{2}{\sqrt{\pi}} \exp\left(\frac{u'x}{2D_L}\right) \int_\beta^\infty f\left(t - \frac{x^2}{4D_L\lambda}\right) \cdot \exp\left[-\left(\lambda^2 + \frac{\alpha^2}{\lambda^2}\right)\right] d\lambda \tag{3.41}$$

where $f(t)$: an arbitrary function of t, $\lambda = x/2\sqrt{D_L(t-\tau)}$, u': real pore velocity, τ: variable for time, D_L: longitudinal dispersion coefficient, $\alpha = u'x/4D_L$, and $\beta = x/2\sqrt{D_L t}$.

Derive the solution when the function $f(t)$ in Eq. 3.40 is equal to a constant value C_0.

(Answer)

Replacing $f(t)$ by C_0 in Eq. 3.41 yields the following:

$$\begin{aligned} C(x,t) &= \frac{2}{\sqrt{\pi}} \exp\left(\frac{u'x}{2D_L}\right) \int_\beta^\infty f\left(t - \frac{x^2}{4D_L\lambda}\right) \cdot \exp\left[-\left(\lambda^2 + \frac{\alpha^2}{\lambda^2}\right)\right] d\lambda \\ &= \frac{2C_0}{\sqrt{\pi}} \exp\left(\frac{u'x}{2D_L}\right) I(\alpha,\beta) \end{aligned} \tag{3.42}$$

where

$$\beta = x/2\sqrt{D_L t}, \quad I(\alpha,\beta) = \int_\beta^\infty \exp\left[-\left(\lambda^2 + \frac{\alpha^2}{\lambda^2}\right)\right] d\lambda \tag{3.43}$$

To obtain an explicit expression for I, we rewrite Eq. 3.43 as:

$$\begin{aligned} I &= \int_\beta^\infty \exp\left[-\left(\lambda^2 + \frac{\alpha^2}{\lambda^2}\right)\right] d\lambda \\ &= \int_0^\infty \exp\left[-\left(\lambda^2 + \frac{\alpha^2}{\lambda^2}\right)\right] d\lambda - \int_0^\beta \exp\left[-\left(\lambda^2 + \frac{\alpha^2}{\lambda^2}\right)\right] d\lambda \\ &= I_1 - I_2 \end{aligned}$$

where

$$I_1 = \int_0^\infty \exp\left[-\left(\lambda^2 + \frac{\alpha^2}{\lambda^2}\right)\right] d\lambda, \quad I_2 = \int_0^\beta \exp\left[-\left(\lambda^2 + \frac{\alpha^2}{\lambda^2}\right)\right] d\lambda \tag{3.44}$$

Now, differentiating integral I_1 with respect to α and replacing λ by $\lambda = \alpha/\xi$ to obtain I_1, we get:

$$\frac{dI_1}{d\alpha} = -2 \int_0^\infty \exp\left[-\left(\xi^2 + \frac{\alpha^2}{\xi^2}\right)\right] d\xi = -2I_1$$

or $dI_1/I_1 = -2\,d\alpha$.

Integrating the above differential equation, we obtain:

$$I_1 = F_0 e^{-2\alpha}$$

Substituting $\alpha = 0$, the integration constant (F_0) is obtained as:

$$I_1|_{\alpha=0} = \int_0^\infty \exp[-\lambda^2]d\lambda = \frac{\sqrt{\pi}}{2} = F_0$$

Finally, the following equation is obtained.

$$I_1 = \frac{\sqrt{\pi}}{2}\exp[-2\alpha] \tag{3.45}$$

The integral I_2 can be obtained by the following procedure. Replacing ζ by $\zeta = \alpha/\lambda$, $d\lambda = -(\alpha/\zeta^2)d\zeta$, and with ∞ and α/β as the upper and lower limits of integration in I_2, then:

$$I_2 = \frac{1}{2}(I_3 + I_4) \tag{3.46}$$

where

$$\begin{aligned} I_3 &= \exp[2\alpha]\cdot\int_{\alpha/\beta}^\infty \frac{\alpha}{\zeta^2}\exp\left[-\left(\frac{\alpha}{\zeta}+\zeta\right)^2\right]d\zeta \\ &= -\exp[2\alpha]\cdot\int_{\alpha/\beta+\beta}^\infty \exp[-\kappa^2]d\kappa + \exp[2\alpha]\cdot\int_{\alpha/\beta}^\infty \exp\left[-\left(\frac{\alpha}{\zeta}+\zeta\right)^2\right]d\zeta \end{aligned} \tag{3.47}$$

$$\begin{aligned} I_4 &= \exp[-2\alpha]\cdot\int_{\alpha/\beta}^\infty \frac{\alpha}{\zeta^2}\exp\left[-\left(\frac{\alpha}{\zeta}-\zeta\right)^2\right]d\zeta \\ &= \sqrt{\pi}\cdot\exp[-2\alpha] - \exp[-2\alpha]\cdot\int_{\beta-\alpha/\beta}^\infty \exp[-\xi^2]d\xi - \exp[2\alpha] \\ &\quad\cdot\int_{\alpha/\beta}^\infty \exp\left[-\left(\frac{\alpha}{\zeta}+\zeta\right)^2\right]d\zeta \end{aligned} \tag{3.48}$$

Transforming the variable ζ into κ such that $\kappa = \zeta + \alpha/\zeta$ and $d\kappa = (1 - \alpha/\zeta^2)d\zeta$ for the integration of I_3, and also the variable ζ into ξ such that $\xi = (\alpha/\zeta) - \zeta$ and $d\xi = -(1 + \alpha/\zeta^2)d\zeta$ for the integration of I_4, simplified expression for I_2 is obtained as follows:

$$I_2 = \frac{\sqrt{\pi}}{2}\left[e^{-2\alpha} - \frac{1}{2}e^{-2\alpha}\cdot\mathrm{erfc}\left(\beta - \frac{\alpha}{\beta}\right) - \frac{1}{2}e^{2\alpha}\cdot\mathrm{erfc}\left(\beta + \frac{\alpha}{\beta}\right)\right] \tag{3.49}$$

where, $\mathrm{erf}(X) = 2/\sqrt{\pi}\int_0^X \exp[-X^2]dX$ and $\mathrm{erfc}(X) = 1 - \mathrm{erf}(X)$.

Accordingly, integration I becomes:

$$I(\alpha,\beta) = I_1 - I_2 = \frac{\sqrt{\pi}}{4}\left\{e^{-2\alpha}\cdot\mathrm{erfc}\left[\beta - \frac{\alpha}{\beta}\right] + e^{2\alpha}\cdot\mathrm{erfc}\left[\beta + \frac{\alpha}{\beta}\right]\right\} \tag{3.50}$$

Substitution of $u'x/4D_L$ for α and $x/2\sqrt{D_L t}$ for β leads to the following analytical solution for the problem with the given initial and boundary conditions.

$$\frac{C}{C_0} = \frac{1}{2}\left\{\mathrm{erfc}\left[\frac{x-u't}{2\sqrt{D_L t}}\right] + \exp\left[\frac{u'x}{D_L}\right]\cdot\mathrm{erfc}\left[\frac{x+u't}{2\sqrt{D_L t}}\right]\right\} \tag{3.51}$$

3.4 Interfaces in Coastal Aquifers

3.4.1 Ghyben–Herzberg Approximation

Groundwater overflows from inland aquifers toward sea while saltwater intrudes into the bottom of the aquifers, as depicted in **Fig. 3.11**. An interface between freshwater and saltwater lies in a mixing zone as a result of dispersion phenomena. Two approaches have been adopted for flow analysis in coastal aquifers. In the first approach, the flow of both fluids is simultaneously analyzed considering the mixing (or transition) zone between them. In the second approach, the dynamic behavior of an abrupt interface similar to the case for immiscible fluids is analyzed after the thickness of the transition zone is disregarded. The interface is called a freshwater–saltwater interface.

Several sets of field measurement data have revealed that there are many cases in which the thickness of the transition zone is smaller than the aquifer thickness. In such cases, the interface shape is analyzed using the hydrostatic pressure approximation, because groundwater flow is slow. The theory of an abrupt interface in the steady state condition is developed (Bear J., 1979).

An unconfined coastal aquifer with a sharp interface in the steady state condition is shown in **Fig. 3.11**. The freshwater seepage velocity in the vertical direction is usually negligible compared to that in the horizontal direction in coastal aquifers. Therefore, Dupuit's uniform flow approximation is applicable in this case. The pressure distribution can be considered as static hydrostatic in such a case.

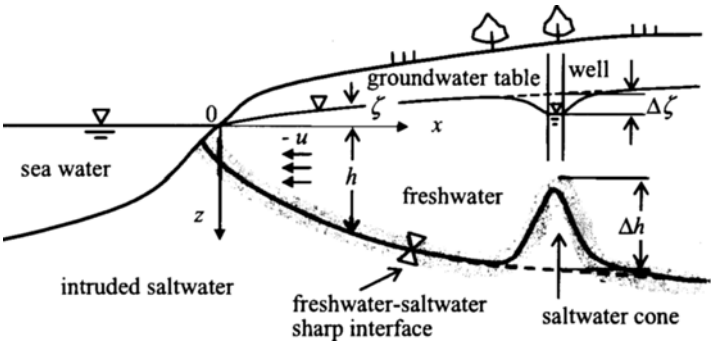

Fig. 3.11. Freshwater–saltwater interface in unconfined aquifers in the steady state

The freshwater pressure (p_f) on an interface at a depth (h) below sea level can be expressed as:

$$p_f = \rho_f g(\zeta + h) \tag{3.52}$$

where ρ_f = freshwater density, g = acceleration due to gravity, and ζ = height of groundwater table above sea level. On the other hand, the saltwater pressure (p_s)

on the interface is equal to that of seawater at depth (h) below sea level, and is expressed as:

$$p_s = \rho_s g h \tag{3.53}$$

Both pressures balance each other at the steady state. Equating them, we get the following:

$$h = \zeta \frac{\rho_f}{(\rho_s - \rho_f)} = \zeta \frac{1}{\varepsilon}, \quad \varepsilon = \frac{(\rho_s - \rho_f)}{\rho_f} \tag{3.54}$$

Equation 3.54 shows the relationship between the height of the groundwater table and the depth of the freshwater–saltwater interface in an unconfined aquifer. This relationship is called the Ghyben–Herzberg approximation.

When freshwater is pumped from a well, as shown in **Fig. 3.11**, and the water level in the well decreases by $\Delta\zeta$, then the groundwater table around the well also declines, and consequently, the freshwater–saltwater interface may rise. This rise in height of the interface (Δh) is obtained from Eq. 3.54:

$$\Delta h = \frac{\Delta\zeta}{\varepsilon} \tag{3.55}$$

For $\rho_f = 1.0\,\mathrm{g/cm^3}$ and $\rho_s = 1.025 \sim 1.03\,\mathrm{g/cm^3}$, the value of $1/\varepsilon$ is $33 \sim 40$. This means that the interface rises by up to 40 times the decrease of water level in the well. In extreme cases, the rise in the interface results in an undesirable situation in which saltwater is pumped from the well.

3.4.2 Shape of the Interface in a Two-Dimensional Vertical Aquifer

Consider the case of saltwater intrusion in a homogeneous and isotropic aquifer as shown in **Fig. 3.11** (Tamai and Shima, 1967). Let the origin of the coordinate system be at the point on the ground surface at sea level. The x-axis is taken horizontally in the inland direction while the z-axis is vertically downward. The horizontal seepage velocity of freshwater flow above the interface is u.

Freshwater discharge per unit width (q) is given by integrating u from the groundwater table to the interface, as:

$$q = \int_{-\zeta}^{h} -u\,dz = -u(h + \zeta) = -uh(1 + \varepsilon) \tag{3.56}$$

Applying Darcy's law and Dupuit's uniform flow assumption, we get:

$$u = -k\frac{d\zeta}{dx} = -k\varepsilon\frac{dh}{dx} \tag{3.57}$$

where k = permeability.

The equation of the interface is obtained by substituting Eq. 3.57 into Eq. 3.56 and integrating along the x-axis:

$$h^2 = h_1^2 + \frac{2q(x - x_1)}{k\varepsilon(1 + \varepsilon)} \tag{3.58}$$

where h_1 = depth of interface below sea level at $x = x_1$.

Substituting Eq. 3.54 into Eq. 3.58, the following is obtained:

$$\zeta^2 = \zeta_1^2 + \frac{2q(x - x_1)}{k(1 + 1/\varepsilon)} \tag{3.59}$$

where ζ_1 = height of groundwater table above sea level at $x = x_1$.

The discharge per unit width (q) is calculated using Eq. 3.59. Thus, it appears that the shape of the interface is known after the value of q is substituted in Eq. 3.58. However, Eq. 3.58 is not clear in regions near the coastline, because the height of the groundwater table coincides with sea level. Setting $x_1 = 0$ and $\zeta_1 = 0$, Eq. 3.59 becomes:

$$\zeta^2 = \frac{2qx}{k(1 + 1/\varepsilon)} \tag{3.60}$$

The equation of the interface corresponding to Eq. 3.60 is as follows,

$$h^2 = \frac{2qx}{k\varepsilon(1 + \varepsilon)} \approx \frac{2qx}{k\varepsilon} \tag{3.61}$$

Equation 3.60 satisfies the boundary condition for the groundwater table along the coastal line. However, Eq. 3.61 gives zero depth of the interface ($h = 0$), i.e., there is no exit for freshwater to flow out to sea. This shows that an error arises in interface calculation using Eqs. 3.58 and 3.61. This derives from the fact that Dupuit's assumption is not applicable in the region near the coastline; therefore, it is necessary to take the vertical seepage velocity into consideration to calculate the shape of the interface in this region.

Denoting the vertical seepage velocity by w, the continuity equation within the freshwater domain is written as:

$$\frac{\partial u}{\partial x} + \frac{\partial w}{\partial z} = 0 \tag{3.62}$$

Integrating from the groundwater table to the interface, Eq. 3.62 becomes,

$$w = -\int_{-\zeta}^{z} \frac{\partial u}{\partial x} dz + [w]_{z=-\zeta} \tag{3.63}$$

Using Eqs. 3.54, 3.56 and 3.57, we get the following:

$$\begin{aligned} \frac{\partial u}{\partial x} &= -\frac{q}{(1 + 1/\varepsilon)} \frac{d}{dx}\left(\frac{1}{\zeta}\right) = \frac{q}{(1 + 1/\varepsilon)} \frac{1}{\zeta^2} \frac{d\zeta}{dx} \\ &= \frac{q^2}{(1 + 1/\varepsilon)} \frac{1}{\zeta^2} \frac{1}{k(h + \zeta)} = \frac{q^2(1 + 1/\varepsilon)}{k} \frac{1}{(h + \zeta)^3} \end{aligned}$$

Then, Eq. 3.63 becomes:

$$w = -\frac{q^2}{k} \frac{(1 + \varepsilon)}{\varepsilon} \frac{(z + \zeta)}{(h + \zeta)^3} \tag{3.64}$$

where $[w]_{z=-\zeta} = 0$, because the change in the groundwater table is small compared to the change in the interface.

On the other hand, Darcy's law for freshwater gives w as:

$$w = -k\frac{\partial}{\partial z}\left(\frac{p_f}{\rho_f g} - z\right) \tag{3.65}$$

Equating Eqs. 3.64 and 3.65 and integrating along the vertical direction, the pressure distribution in freshwater flow is given by:

$$\frac{p_f}{\rho_f g} = z + \zeta + \frac{q^2(1+\varepsilon)}{2\varepsilon k^2}\frac{(z+\zeta)^2}{(h+\zeta)^3} \tag{3.66}$$

where $p_f = 0$ at $z = -\zeta$. The freshwater pressure on the interface can be determined from this equation while the saltwater pressure at $z = h$ is given by $p_s = \rho_s g h$. Now, using conditions $p_f = p_s$ and $\zeta = 0$ for the coastal area, the interface depth at the coastline (h_0) is expressed as:

$$h_0 = \frac{q}{k\varepsilon}\sqrt{\frac{(1+\varepsilon)}{2}} \tag{3.67}$$

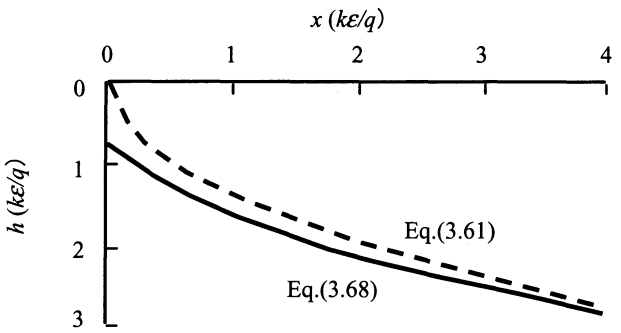

Fig. 3.12. Comparison of calculated interface shapes

The equation for the interface, taking the vertical seepage velocity into account, can be written in the following form by substituting $x_1 = 0$, $h_1 = h_0$, and $(1+\varepsilon) \approx 1$ in Eq. 3.58, and finally substituting into Eq. 3.67.

$$h^2 = \frac{q^2}{2k^2\varepsilon^2} + \frac{2qx}{k\varepsilon} \tag{3.68}$$

The shapes of the interface calculated using Eqs. 3.61 and 3.68 are shown in **Fig. 3.12**. From this figure, it is clear that the effect of the vertical seepage velocity becomes large only around the coastline and decreases inland.

These equations are derived from the analysis of freshwater flow on the upper side of the interface. Therefore, they are applicable to calculate the interface shape for flows in unconfined aquifers overlying an impervious layer, as shown in **Fig. 3.13a**. The theory using an abrupt interface also has been applied to confined aquifers and two-layered aquifers, as shown in **Fig. 3.13b** (Henry H.R., 1959; Rumer R.R. and Harleman D.R.F., 1963) and **Fig. 3.13c** (Sugio S. and Mori K., 1989), respectively. Darcy's law and Dupuit's assumption have been applied to the interface in two-dimensional horizontal planes (Strack O.L.D., 1976). All these authors derived the interface equation for the steady state condition. Solutions for unsteady conditions have been obtained by numerical simulations using the Finite Difference Method (Kawatani T., 1975) and the Boundary Element Method (Fujino K., 1985).

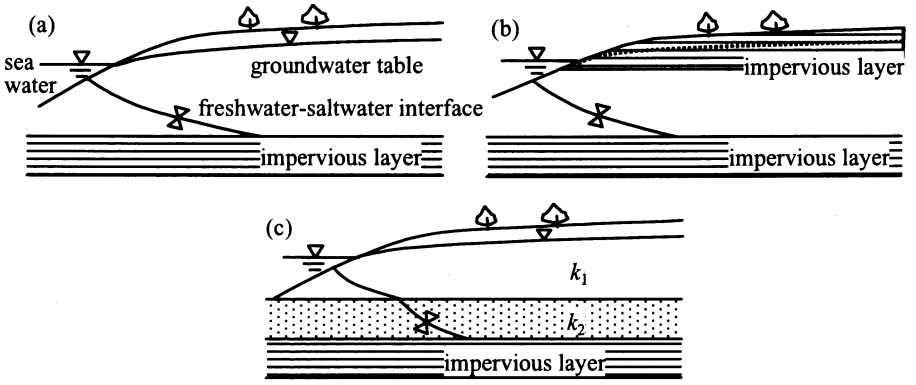

Fig. 3.13. Saltwater intrusion in various aquifers

Exercises

[Ex. 3.1]
How is the coefficient of transverse dispersion (D_T) determined experimentally?

[Ex. 3.2]
Explain the physical meaning of molecular diffusion.

[Ex. 3.3]
Explain the reason why microscopic and macroscopic dispersions should be distinguished.

[Ex. 3.4]
Solve the following partial differential equation with D = constant,

$$\frac{\partial C}{\partial t} + u' \frac{\partial C}{\partial x} = D \frac{\partial^2 C}{\partial x^2} \qquad \text{(E3.4.1)}$$

with initial condition:

$$C(x, 0) = 0 \tag{E3.4.2}$$

and boundary conditions:

$$C(0, t) = f(t) \quad \text{and} \quad C(\infty, t) = 0 \tag{E3.4.3}$$

[Ex. 3.5]
In **Fig. 3.13a,** H denotes the height of sea level from the impervious layer, and the groundwater level ζ is $0.02H$ at a distance $10H$ from the seashore. Calculate the shape of the freshwater–saltwater interface for $(1/\varepsilon) = 40$.

References

Appelo CAJ, Postma D (1996) Geochemistry, groundwater and pollution. Balkema Rotterdam, pp 341–344, 349–367

Aris R (1956) On the dispersion of a solute in a fluid flowing through a tube. Proc R Soc, A 235: 76

Bear J (1979) Hydraulics of groundwater. McGraw-Hill New York, pp 379–435

Bear J, Verruijt A (1987) Modeling groundwater flow and pollution. Reidel Dordrecht, pp 153–167

Fetter CW (2001) Applied hydrogeology, Prentice-Hall New Jersey, pp 407–414

Fujino K (1985) Numerical analysis of groundwater density flow with boundary element method and the effect of an impervious wall against saltwater intrusion. J JAGH, 27(2): 51–60

G De Josselin De Jong (1958) Longitudinal and transverse diffusion in granular deposit. Transactions, AGU, Vol 139, No 1, pp 67–74

Harleman DRF, Rumer BR (1963) Longitudinal and lateral dispersion in an isotropic porous medium. J Fluid Mech 16: 385–394

Henry HR (1959) Salt intrusion into fresh-water aquifers. J Geophys Res. 64(11): 1911–1919

Hirano N (1977) Diffusion of backwashing water in the upper region of sand infiltration (in Japanese). Masters thesis, Graduate School of Engineering, Kyushu University

Hiroshiro Y, Jinno K, Yokoyama T, et al (1996) Transport properties of anions through weathered granite (in Japanese). Tech rep Eng Fac Kyushu Univ 69(5): 677–682

Huyakorn PS, Pinder GF (1983) Computational method in subsurface flow. Academic, New York

Josselin DJ (1959) Longitudinal and transverse diffusion in granular deposit. Trans AGU 139(1): 67–74

Kawatani T (1975) Numerical analysis of the groundwater mound and fresh-salt water interface in a coastal aquifer (in Japanese). Proc JSCE 238: 89–98

Kinzelbach W (1986) Groundwater modeling. Elsevier Amsterdam, pp 120, 188–202

Nakagawa K, Jinno K (2000) Evaluation of the transition characteristics of macroscopic dispersion and estimation on the non-uniform hydrogeological structure. IAHS Publ, No 265, pp 110–116

Nakagawa K, Jinno K, Hosokawa T et al (1998) Seepage flow and mass transport in heterogeneous porous media. Groundwater Hydrol 40(1) 1–6

Rumer BR, Harleman DRF (1963) Intruded saltwater wedge in porous media. J Hyd Div ASCE 89(6): 193–220

Saffman P G (1959) A theory of dispersion in a porous medium. J Fluid Mech, No 6, pp 321–349

Strack OLD (1976) A single-potential solution for regional interface problem in coastal aquifers. Water Resource Res 12(6): 1165–1174

Sugio S, Mori K (1989) Seawater intrusion in two-layered unconfined aquifers (in Japanese). Proceedings of the 33rd Japanese Conference on Hydraulics, JSCE, Tokyo, pp 199–204

Tamai N, Shima S (1967) Saltwater wedge in unconfined coastal aquifers (in Japanese). Proc JSCE 139: 31–38

Taylor G (1952) Dispersion of soluble matter in solvent flowing slowly through a tube, Proc R Soc, A 219: 186–203

Young RN, Mohamed AMO, Warkentin BP (1992) Principles of contaminant transport in soils. Elsevier, pp 280–284

4

Groundwater Flow under a Temperature Gradient

Summary

In recent years, the behaviour of subsurface water with a temperature gradient has generated considerable interest. Dynamic approaches to the phenomenon are founded on simultaneous mass and heat transport in porous media. Most problems are classified into two areas: one is natural and forced convection of fluids in saturated porous media and the other is such mass and heat transfer in unsaturated porous media, as encounterd in processes such as drying/vaporization, and pollutant migration.

Heat exchange between atmosphere and ground surface or between groundwater and soils/rock masses may generate new local flows and temperature gradients within the saturated zone. Thus, the heat transfer may make the analysis of groundwater flow more complicated because of addtional flow caused by non-uniform temperature distributions. Buoyancy effect caused by fluid density differences and exchange between fluid and solid phases are essential factors.

Moisture transfer with a temperature gradient induces heat transfer and changes in phase between liquid and vapor; therefore, it is very important to understand heat and moisture transfer in porous media to gain a better insight into unsaturated flow.

The basic theories of heat and fluid transfer in saturated and unsaturated soil are discussed in this chapter. Typical examples of heat and moisture transfer in closed and open systems are also presented.

4.1 Heat Transfer in Saturated Soil

4.1.1 Mode of Heat Transfer

Temperature gradients (or geothermal differences) in groundwater can be caused by geothermal energy, heat sources or well recharge for heat storage purposes and pose scientific and technical problems as a result of natural or forced convection in saturated pore spaces. Prior to a detailed discussion on the hydraulic formulation, the modes of heat transfer will be introduced.

K. Sato et al. (eds.), *Groundwater Hydraulics*

There are three basic mechanisms for heat transfer: (1) Heat transfer through the molecules of a continuous solid or liquid medium is known as conduction. (2) Convection refers to heat transfer caused by the movement of a fluid medium from one point to another. Convective flow may be classified into two types: natural and forced convection. Fluid density differences resulting from temperature gradients cause natural convection, whereas mechanical forces such as well pumping and injection account for forced convection. (3) Energy transfer in the form of electromagnetic waves from various states of matter is known as thermal radiation. Conduction and convection are usually taken into account for heat transfer in saturated and unsaturated porous media, whereas the thermal radiation can be ignored.

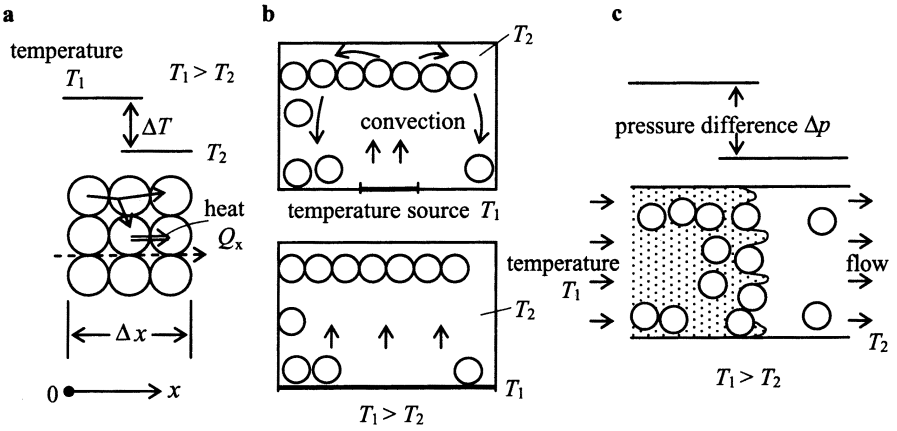

Fig. 4.1 a–c. Examples of heat propagation in saturated porous media. **a** Heat conduction, **b** natutal convection, and **c** forced convection

Heat transfer modes in saturated media are schematically shown in **Fig. 4.1**. The governing equations in saturated media comprise heat conservation, Fourier's law, and other auxiliary equations, in addition to the mass conservation equation and Darcy's law.

4.1.2 Heat Transfer Mechanism

Figure 4.2 shows heat transfer associated with convection when a fluid with temperature T_1 infiltrates into saturated soil with temperature T_2 ($T_2 < T_1$). The heat transfer consists of (1) conduction between soil particles, (2) conduction in pore water, (3) heat exchange resulting from conduction between soil particles and pore water, and (4) convection as a result of fluid flow through the pores. The cumulative heat of conduction from (1) to (4) is expressed as the product of the equivalent thermal conductivity and temperature gradient. As the soil dries, the heat flux associated with conduction becomes dominant.

4.1.3 Basic Equations of Heat and Moisture Transfer

The heat transfer equation will be derived with reference to the flows and transfers shown in **Figs. 4.1** and **4.2**.

4.1.3 (a) Laws of Heat Transfer

A porous medium, shown in **Fig. 4.1a**, has an infinitesimal dimension Δx and the two ends are kept at temperatures T_1 and T_2. The heat flux (Q_{hx}) resulting from conduction in the x-direction can be written in the form of Fourier's law:

$$Q_{hx} = -\lambda \frac{\Delta T}{\Delta x} A \tag{4.1}$$

where λ = thermal conductivity (W/mK), T = temperature, and A = cross-sectional area.

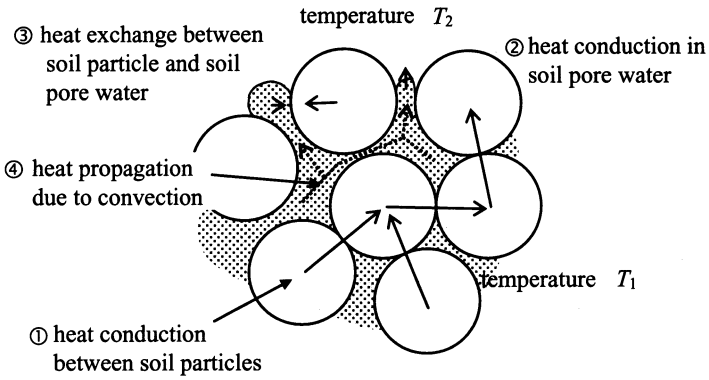

Fig. 4.2. Heat propagation mechanisms resulting from convection of a fluid with temperature T_1 infiltrating a saturated soil at temperature T_2

In Eq. 4.1, the conduction heat flux is proportional to the temperature gradient and the thermal conductivity, where the value of λ depends greatly on the kind of material involved, as shown in **Table 4.1**.

Convective heat transfer relates to the bulk movement of fluid over a solid surface. The convective heat flux (Q_h) is described according to Newton's law of cooling as:

$$\frac{Q_h}{A} = \alpha(T_s - T_f) \tag{4.2}$$

where α = coefficient of heat transfer (W/m^{2}K), T_s = solid surface temperature, T_f = fluid temperature, and A = surface area.

Table 4.1. Thermal properties of matter (at 20 °C)

Materials	Thermal conductivity, λ (W/(m·K))	Specific heat, c_p (kJ/(kg·K))
Water	0.60	4.18
Air	0.026	1.0
Sand	0.30	0.80
Concrete	0.8 ~ 0.9	0.84
Steel	15 ~ 54	0.46
Granite	1.80	0.80

4.1.3 (b) Equations of Heat and Liquid Water Transfer

Consider a control volume as shown in **Fig. 4.3**. The basic equations consist of the continuity equation, the motion equation, the energy equation, and auxiliary equations between the density and temperature or pressure of the fluid.

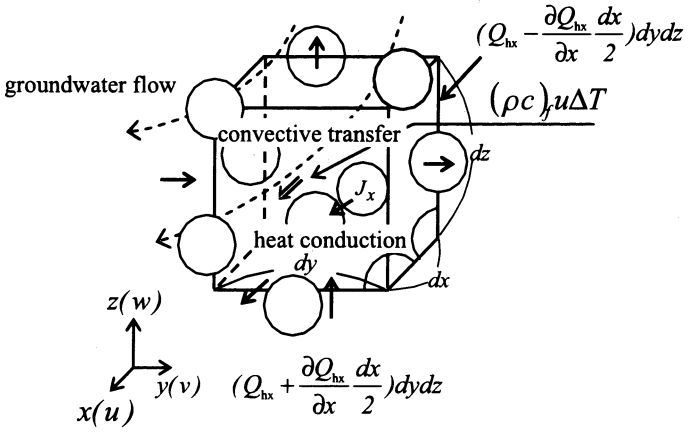

Fig. 4.3. Heat propagation in control volume

The continuity equation is the mass conservation equation, which was discussed in Chap. 2, and written as $-\nabla\rho\mathbf{q} = \partial(n\rho)/\partial t$, where ρ = density of the fluid; $\mathbf{q} = (u, v, w)$; u, v, w = Darcy velocity components in the x-, y- and z-directions, respectively; n = porosity; and $\nabla = (\partial/\partial x, \partial/\partial y, \partial/\partial z)$. Assuming ρ to be constant, the continuity equation becomes $-\nabla\mathbf{q} = 0$. The motion equation can be derived from the Navier-Stokes equation and expressed as $(\rho/n)\partial\mathbf{q}/\partial t = -\text{grad}\, p + \rho\mathbf{g} - (\mu/K)\mathbf{q}$,

where grad $= (\partial/\partial x, \partial/\partial y, \partial/\partial z)$; $\mathbf{g}(0, 0, -g)$ is the gravity vector; μ = viscosity of the fluid; K = intrinsic permeability (dim. L^2); and p = pressure.

The total heat flux ($\mathbf{Q}_h$) per unit area and time is obtained by summing the heat of conduction and convection. For example, the heat flux in the x-direction (Q_{hx}) is expressed as:

$$Q_{hx} = J_x + (\rho c)_f u(T - T_0) \tag{4.3}$$

where J_x = conduction heat flux and $(\rho c)_f u(T - T_0)$ = sensible heat flux resulting from bulk motion with velocity u, and c_f = specific heat of the fluid.

The net heat flux per unit time along the x-direction in the control volume is given by:

$$\left(Q_{hx} - \frac{\partial Q_{hx}}{\partial x}\frac{dx}{2}\right)dy\,dz - \left(Q_{hx} + \frac{\partial Q_{hx}}{\partial x}\frac{dx}{2}\right)dy\,dz = -\frac{\partial Q_{hx}}{\partial x}dx\,dy\,dz$$

The rate of net heat flux entering the control volume is conserved according to the first law of thermodynamics, so the equation for net total heat flux is obtained by summing the components in the three directions as:

$$\frac{\partial Q_{hx}}{\partial x} + \frac{\partial Q_{hy}}{\partial y} + \frac{\partial Q_{hz}}{\partial z} + (\rho c)_e \frac{\partial T}{\partial t} = \nabla \mathbf{Q}_h + (\rho c)_e \frac{\partial T}{\partial t} = 0 \tag{4.4}$$

Substituting Eq. 4.3, $Q_{hy} = J_y + (\rho c)_f v(T - T_0)$, $Q_{hz} = J_z + (\rho c)_f w(T - T_0)$, and Fourier's law into Eq. 4.4 yields the following:

$$(\rho c)_e \frac{\partial T}{\partial t} = \lambda_e \,\mathrm{div}(\mathrm{grad}\, T) - (\rho c)_e \mathbf{q} \cdot \mathrm{grad}\, T \tag{4.5}$$

where λ_e and $(\rho c)_e$ are, respectively, the equivalent thermal conductivity and the volumetric heat capacity of wetted soil.

The thermodynamic fluid properties are evaluated using the correlation between fluid density and temperature at constant pressure. The correlation is approximated as $\rho = \rho_0[1 - \beta(T - T_0)]$, where ρ_0 = fluid density at an arbitrary reference temperature T_0 and β = thermal expansion coefficient.

Finally, the basic equations of groundwater flow under a temperature gradient are expressed as follows:

$$\nabla \mathbf{q} = 0 \tag{4.6}$$

$$\frac{\rho}{n}\frac{\partial \mathbf{q}}{\partial t} = -\,\mathrm{grad}\, p + \rho \mathbf{g} - \frac{\mu}{K}\mathbf{q} \tag{4.7}$$

$$(\rho c)_e \frac{\partial T}{\partial t} = \lambda_e \,\mathrm{div}(\mathrm{grad}\, T) - (\rho c)_f \mathbf{q} \cdot \mathrm{grad}\, T \tag{4.8}$$

$$\rho = \rho_0[1 - \beta(T - T_0)] \tag{4.9}$$

where $(\rho c)_f$ = volumetric heat capacity of the fluid.

It should be noted that the second term on the right-hand side of Eq. 4.7 expresses the buoyancy effect in the energy conservation equation. This idea for

buoyancy effect is also called Boussinesq's approximation. The main interest in solving Eqs. 4.6–4.8 is whether convective flow is generated or not (see Rees, 2002) and if it is generated, its shape, size and numbers are interested in (Combanous and Bories, 1975).

Nondimensional quantities in the basic equations 4.6–4.9 are very important when discussing experimental data and nondimensional basic equations. Before being rendered nondimensional, the equations have dimension as follows: the mass conservation equation for incompressible fluids Eq. 4.6 has unit of $[T^{-1}]$ (s^{-1} in the SI unit system), the equation of fluid motion Eq. 4.7 has unit of $[kg\,m^{-2}s^{-2}]$, and the conservation equation Eq. 4.8 has unit of $[W\,m^{-3}]$.

Rewriting Eqs. 4.7 and 4.8 in a nondimensional form by introducing nondimensional velocity $q^* = q/q_0$; length $s^* = s/s_0$; and time $t^* = vt/s_0^2$; in which q_0 = a representative velocity, s_0 = a representative length, and v = kinematic viscosity (μ/ρ).

Focusing on the vertical component (z: positive upward) of Eq. 4.7, by putting $\mathbf{g} = -g$, we get:

$$\frac{\partial w}{\partial t} = -\frac{n}{\rho}\left(\frac{\partial p}{\partial z} + \rho g\right) - \frac{n\mu}{\rho K}w. \tag{4.10}$$

Because groundwater flow with a temperature gradient or convective flow with a thermal effect is inactive, $\partial p/\partial z = -\rho_0 g$ under hydrostatic pressure $p = -\rho_0 gz + C$ (= constant) at temperature T_0. Thus, substituting Eq. 4.9 into Eq. 4.7, Eq. 4.10 is written as:

$$\frac{\partial w}{\partial t} = \frac{n}{\rho}\rho_0\beta\,\Delta T g - \frac{n\mu}{\rho K}w, \quad \Delta T = (T - T_0). \tag{4.11}$$

The nondimensional form of the equation of motion for the vertical component using $w^* = w/q_0$ and $t^* = vt/s_0^2$ reduces to:

$$\frac{\partial w^*}{\partial t^*} = \frac{n}{\rho}\frac{s_0^2 g\beta\rho_0\,\Delta T}{q_0 v} - \frac{ns_0^2}{K}w^*. \tag{4.12}$$

The first term on the right-hand side is dependent on the temperature difference.

The first term without $n\rho_0/\rho$ on the right-hand side multiplied by the Reynolds number $R_e = q_0 s_0/v$ is called Grashof number (G_r). G_r multiplied by Prandtl number (P_r) is the Rayleigh number (R_a). Nondimensional quantities deduced from the equation of motion are:

$$\left.\begin{aligned} G_r &= \frac{s_0^3 g\beta\,\Delta T}{v^2}, \quad P_r = \frac{(\mu c)_f}{\lambda_e} \\ R_a &= G_r \cdot P_r = g\frac{\beta(\rho c)_f}{v}\frac{K}{\lambda_e}\Delta T s_0, \quad \frac{s_0^2}{K}, \quad n \end{aligned}\right\} \tag{4.13}$$

Equation 4.8 in dimensionless form becomes,

$$\frac{\partial T}{\partial t^*} = \frac{\lambda_e}{(\rho c)_e v}\,\mathrm{div}(\mathrm{grad}\,T) - \frac{(\rho c)_f}{(\rho c)_e}\frac{\boldsymbol{q}s_0}{v}\,\mathrm{grad}\,T, \tag{4.14}$$

with

$$\frac{\lambda_e}{(\rho c)_e v} = \left(\frac{1}{P_r}\right), \quad \frac{(\rho c)_f}{(\rho c)_e}, \quad R_e = \frac{qs_0}{v}. \tag{4.15}$$

4.2 Unsaturated Flow under a Temperature Gradient

4.2.1 Modeling of Unsaturated Flow with Heat Transfer

The governing equations of unsaturated flow in soil under a temperature gradient consist of simultaneous heat and moisture transport equations. Soil moisture exists mainly in two phases: liquid and vapor. In frost phenomena, solid phase ice will appear in topsoil below the freezing temperature.

It should be noted that the physical properties of water, such as density, viscosity, surface tension, and thermal conductivity are strongly dependent on temperature. Therefore, the theory of heat and moisture transport is somewhat complicated and the governing equations are nonlinear.

Based on the types of boundary conditions, simultaneous heat and moisture transport can be divided into two categories: closed and open systems. There is no heat and moisture transfer across the boundaries in closed systems while transfer does occur in open systems. The ground surface is a typical example of an open system. Its interaction with the atmosphere involves heat and moisture exchange in terms of radiation, sensible heat, latent heat, evaporation, and precipitation. Latent heat is the heat added as a result of phase change between liquid and water vapor (evaporation or condensation). Sensible heat is dependent on wind velocity, roughness of the ground surface, and the stability of atmospheric conditions.

4.2.2 Basic Equations of Heat and Moisture Transport in Unsaturated Porous Media

Philip and de Vries (1957) and de Vries (1958) originally formulated a comprehensive theory of heat and moisture movement in unsaturated porous media. In their theory, moisture movement is considered to take place in the vapor and liquid phases, and internal vaporization and condensation mutually compensate through mass exchange between these two phases. Therefore, the volumetric moisture content is interpreted as the sum of the volumetric liquid and vapor contents. The theory can explain liquid and vapor movement under temperature and moisture gradients.

4.2.2 (a) Moisture Transport Equation

Consider a representative elementary control volume (dx, dy, dz), as shown in **Fig. 4.4**.

Liquid Water Transport

Applying Darcy's law to liquid water transport in unsaturated porous media, the flux transport ($\mathbf{q}_\ell$) per unit area and time can be written as follows:

$$\frac{\mathbf{q}_\ell}{\rho_\ell} = k\nabla h_c, \quad h_c = \frac{p_c}{\rho_\ell g} + z = \psi + z \tag{4.16}$$

where h_c = piezometric head, p_c = matric potential (capillary pressure), z = vertical ordinate, and k = unsaturated hydraulic conductivity. Now, taking surface tension (σ)

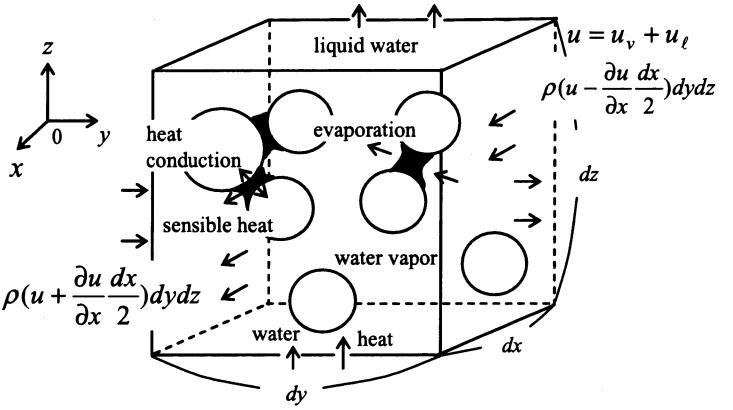

Fig. 4.4. Control volume for unsaturated flow under a temperature gradient

into account for determining p_c, the matric potential head ($p_c/\rho_\ell g$) may be rewritten as $\psi(\theta, T)$.

Thus, the spatial gradient of h_c is written as $\nabla h_c = (\partial\psi/\partial T)\nabla T + (\partial\psi/\partial\theta_\ell)\nabla\theta_\ell + \nabla z$, and considering that $\partial\psi/\partial T = (\psi/\sigma)d\sigma/dT$, Eq. 4.16 finally becomes:

$$\frac{\mathbf{q}_\ell}{\rho_\ell} = -D_{T\ell}\nabla T - D_{\theta\ell}\nabla\theta - k\,\mathbf{i} \tag{4.17}$$

$$D_{T\ell} = \frac{k}{\sigma}\frac{d\sigma}{dT}\psi; \quad D_{\theta\ell} = k\frac{\partial\psi}{\partial\theta_\ell} \tag{4.18}$$

where $D_{T\ell}$ = thermal liquid diffusivity, $D_{\theta\ell}$ = isothermal liquid diffusivity and $\mathbf{i}$ = the unit vector.

Water Vapor Transport

The transport mass flux of water vapor in soil per unit area and time ($\mathbf{q}_v$) can be written by combining the equation of state and a Fickian type diffusion equation as:

$$\mathbf{q}_v = -D^*\nabla\rho_v; \quad D^* = D_{atm} f\eta a \tag{4.19}$$

where $\mathbf{q}_v$ = mass flux density of water vapor (kg/m^{2}s), D^* = vapor diffusivity in soil pores (m^2/s), D_{atm} = vapor diffusivity in the atmosphere (m^2/s), f = mass flow factor (ratio of gas pressure to partial pressure of dry air = 1.02), η = tortuosity ($2/\pi = 0.67$, $\pi = 3.14$), and a = volumetric air content. It is to be noted that D_{atm} is a function of temperature.

Water vapor density (ρ_v) may be expressed as a function of T and ψ (< 0) using Kelvin's relation as:

$$\rho_v = \rho_{v0}H_r; \quad H_r = e^{\frac{\psi g}{RT}} \tag{4.20}$$

$$\nabla\rho_v = H_r\nabla\rho_{v0} + \rho_{v0}\nabla H_r \tag{4.21}$$

where ρ_{v0} = density of saturated water vapor, H_r = relative humidity, R = gas constant of water vapor, and g acceleration due to gravity. Assuming that the temperature effect on H_r is very small, and that ρ_{v0} is a function of T only, Eq. 4.21 can be written as:

$$\nabla\rho_v = H_r\frac{d\rho_{v0}}{dT}\nabla T + \rho_{v0}\frac{dH_r}{d\theta}\nabla\theta = H_r\frac{d\rho_{v0}}{dT}\nabla T + \frac{\rho_v g}{RT}\frac{\partial\psi}{\partial\theta}\nabla\theta \tag{4.22}$$

Substituting Eq. 4.22 into Eq. 4.19 gives the following:

$$\frac{\mathbf{q}_v}{\rho_\ell} = -D_{Tv}\nabla T - D_{\theta v}\nabla\theta \tag{4.23}$$

where $D_{Tv} = D^*(H_r/\rho_\ell)(d\rho_{v0}/dT)$, $D_{\theta v} = (\rho_v g/\rho_\ell RT)(\partial\psi/\partial\theta)$ and D_{Tv} and $D_{\theta v}$ are called thermal and isothermal vapor diffusivities, respectively.

Total moisture flux ($\mathbf{q}$) can be obtained by summing the liquid and vapor fluxes as $\mathbf{q} = \mathbf{q}_v + \mathbf{q}_\ell$. Now, adding Eqs. 4.17 and 4.23, the following equation is obtained:

$$\frac{\mathbf{q}}{\rho_\ell} = -D_\theta\nabla\theta - D_T\nabla T - k\mathbf{i} \tag{4.24}$$

where $D_T = D_{Tv} + D_{T\ell}$, $D_\theta = D_{\theta v} + D_{\theta\ell}$, and D_T and D_θ are called the thermal and isothermal moisture diffusivities, respectively.

Mass Conservation Equation

Applying the principle of mass conservation in the control volume ($dV = dx\,dy\,dz$) shown in **Fig. 4.4**, the x-component of the total net mass flux across an infinitesimal area ($dy \times dz$) per unit time is as follows:

$$\begin{aligned} q_{\ell x} &= \rho_\ell\left(u_\ell - \frac{\partial u_\ell}{\partial x}\frac{dx}{2}\right)dy\,dz - \rho_\ell\left(u_\ell + \frac{\partial u_\ell}{\partial x}\frac{dx}{2}\right)dy\,dz \\ &= -\rho_\ell\frac{\partial u_\ell}{\partial x}dx\,dy\,dz \end{aligned} \tag{4.25}$$

where $q_{\ell x}$ = net mass flux in the x-direction. The first and the second terms on the right-hand side of Eq. 4.25 are incoming and outgoing mass fluxes at $(x - dx/2)$ and $(x + dx/2)$, respectively. The net mass fluxes in the y- and z-directions can be similarly expressed.

The total net mass flux in the control volume can be obtained by using the flux equations in the x-, y-, and z-directions as:

$$-\rho_\ell\left(\frac{\partial u_\ell}{\partial x} + \frac{\partial v_\ell}{\partial y} + \frac{\partial w_\ell}{\partial z}\right)dx\,dy\,dz = -\nabla\mathbf{q}_\ell\,dx\,dy\,dz$$

In addition, mass transfer from the liquid to the vapor phase associated with evaporation should be included in the above equation. The evaporation rate (E) in the control volume can be defined as $E\rho_\ell\,dx\,dy\,dz$, and is negative for condensation. The rate of change of mass of liquid water stored in the control volume is given by $dx\,dy\,dz\,\partial(\rho_\ell\theta_\ell)/\partial t$. The mass conservation equation for liquid water may be expressed as:

$$\frac{\partial \theta_\ell}{\partial t} = -\nabla\left(\frac{\mathbf{q}_\ell}{\rho_\ell}\right) - E \tag{4.26}$$

Substitution of Eq. 4.17 into Eq. 4.26 yields the following:

$$\frac{\partial \theta_\ell}{\partial t} = \nabla(D_{\theta\ell}\nabla\theta_\ell) + \nabla(D_{T\ell}\nabla T) + \frac{\partial k}{\partial z} - E \tag{4.27}$$

The mass conservation equation for vapor phase water can be similarly derived as:

$$\frac{\partial \theta_v}{\partial t} = -\nabla\left(\frac{\mathbf{q}_v}{\rho_\ell}\right) + E \tag{4.28}$$

Evaporation plays an important role in the source term of Eq. 4.28. Equation 4.28 can be written in the following form after substituting Eq. 4.23 into it:

$$\frac{\partial \theta_v}{\partial t} = \nabla\left(D_{\theta v}\nabla\theta_v\right) + \nabla(D_{Tv}\nabla T) + E \tag{4.29}$$

Since total moisture flux and volumetric water content are defined as the sum of the corresponding values in the liquid and vapor phases, the mass conservation equation for moisture can be obtained by adding Eqs. 4.27 and 4.29 as:

$$\frac{\partial \theta}{\partial t} = -\nabla\left(\frac{\mathbf{q}}{\rho_\ell}\right) = \nabla(D_\theta\nabla\theta) + \nabla(D_T\nabla T) + \frac{\partial k}{\partial z} \tag{4.30}$$

The second term on the right-hand site of Eq. 4.30 represents flow induced by the temperature gradient. We can obtain Klute's equation for the isothermal state when $T = 0$ in Eq. 4.30 as:

$$\frac{\partial \theta}{\partial t} = \nabla(D_\theta\nabla\theta) + \frac{\partial k}{\partial z} \tag{4.31}$$

4.2.2 (b) Heat Transport Equation

Total heat flux $\mathbf{Q}_h(Q_{hx}, Q_{hy}, Q_{hz})$, as represented by a vector in **Fig. 4.3**, can be expressed as follows:

$$\mathbf{Q}_h = -\lambda_e\nabla T + c_v(T - T_0)\mathbf{q}_v + c_\ell(T - T_0)\mathbf{q}_\ell \tag{4.32}$$

Equation 4.32 shows that the total heat flux in an unsaturated porous media is the summation of the conduction heat flux and the sensible heat fluxes resulting from liquid and vapor phase moisture movement. It should be noted that thermal conductivity correlates with volumetric water content, as depicted in **Fig. 4.5**.

The x-component of the total net heat flux stored in the control volume (dV) may be expressed as $-(\partial Q_{hx}/\partial x)dx\,dy\,dz$ using Taylor's expansion. Here, $dy\,dz$ represents the boundary area of the control volume element normal to the x-axis. In a similar fashion, heat fluxes in the y- and z-directions are given as $-(\partial Q_{hy}/\partial y)dx\,dy\,dz$ and $-(\partial Q_{hz}/\partial z)dx\,dy\,dz$, respectively.

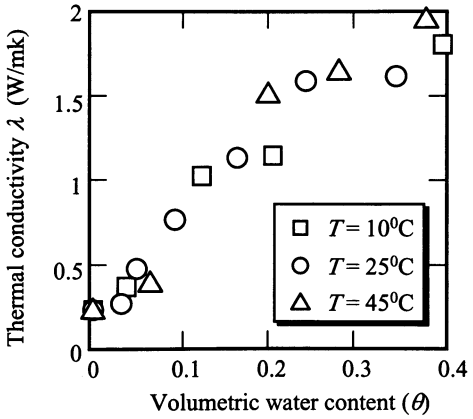

Fig. 4.5. Changes in thermal conductivity (λ) with volumetric water content (θ) for fine sand

Applying the principle of energy conservation in the control volume shown in **Fig. 4.3**, the rate of change in internal energy within the volume, $[\partial\{(\rho c)_{sw}(T - T_0)\}/\partial t]dV$, equals the sum of the total net heat flux stored and the heat of evaporation ($LE\,dx\,dy\,dz$). Therefore, the heat conservation equation becomes:

$$\frac{\partial[(\rho_{sw}c_{sw})(T - T_0)]}{\partial t} = -\nabla \mathbf{Q}_h - LE \tag{4.33}$$

where ρ_{sw} = density of wetted porous media, c_{sw} = specific heat of wetted porous media, and L = rate of heat in vaporization. The volumetric heat capacity (c) of the control volume is calculated using the following equation:

$$c = (\rho_{sw}c_{sw}) = \rho_s c_s(1 - n) + \rho_\ell c_\ell \theta_\ell + \rho_v c_v \theta_v \tag{4.34}$$

where n = porosity and the suffixes s, ℓ and v represent solid, liquid and vapor phases, respectively.

Substituting Eq. 4.32 into Eq. 4.33, and assuming T_0 to be constant yields,

$$\frac{\partial[(\rho_{sw}c_{sw})T]}{\partial t} = \nabla(\lambda \nabla T) - \nabla(c_\ell q_\ell T) - \nabla(c_v q_v T) - LE \tag{4.35}$$

4.3 Examples of Heat and Moisture Transport

Two experimental results will be presented in this section to help readers to better understand heat and moisture transport in unsaturated soils with closed and open boundary conditions.

4.3.1 A Closed System

A stainless steel column packed with fine sand is shown in **Fig. 4.6a**. The volumetric water content of the sand throughout the column is 0.10. The top and bottom of the

column ($z = 0$ and $z = -z_0$, respectively) are maintained at two different constant temperatures, while the curved outer surface is completely insulated. The temperature gradient in the radial direction is negligibly small and the boundary condition for mass transport can be written as $(\partial\psi/\partial z)]_{z=0,-z_0} = 0$. Therefore, the total moisture volume in the column is given by, $\left(A\int_{z=-z_0}^{z=0}\theta\,dz\right)$ where A = cross-sectional area, is always the same as the initial value.

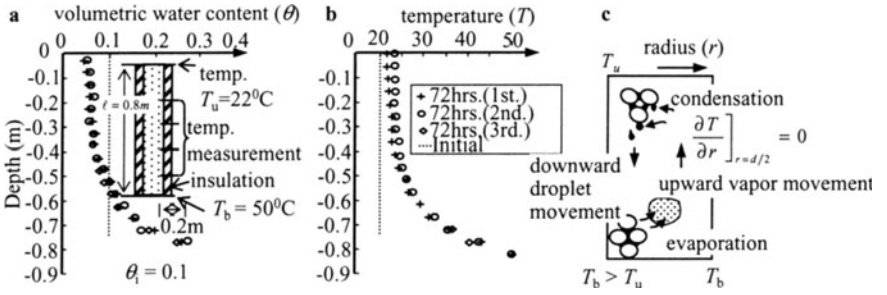

Fig. 4.6 a–c. Examples of water content and temperature profiles in a closed unsaturated soil column under a temperature gradient. (Sato et al., 2001). **a** Water content (θ), **b** temperature (T), and **c** mechanism of moisture movement and phase change

Figure 4.6b shows the temperature distribution inside the soil column in the steady state condition. The temperature increases from the cold end (top) to the hot end (bottom) in a nonlinear fashion. This temperature gradient is attributed to the locality of the thermal conductivity and volumetric heat capacity, which are dependent on soil water content.

Figure 4.6c depicts the phase change and moisture movement processes in the column. Liquid phase transport and vapor phase transport take place simultaneously. Although the initial water content θ_i throughout the column is uniform, in the steady state, the water content increases toward the hot end because gravity produces downward percolation, as shown in **Fig. 4.6a**. Liquid water vaporizes at the hotter lower end, traverses through air-filled pores, and condenses in the top low-temperature zone. Although the movement of water vapor is much smaller than the liquid phase flow, it becomes appreciable for the relatively dry soil layer. After vapor condensation, the total pressure head gradient (hydraulic gradient) drives liquid water from cold upper end to the hot lower end. Thus, the temperature gradient ultimately affects moisture movement. Similar experimental results were reported by Bories (1991), and Prunty and Horton (1994).

4.3.2 An Open System

The boundary conditions for heat and moisture transport in an open system may be more complicated than those for a closed system because of interaction with the

above-ground environment. The exchange of heat and moisture between the ground surface and the atmosphere is a typical example of an open system.

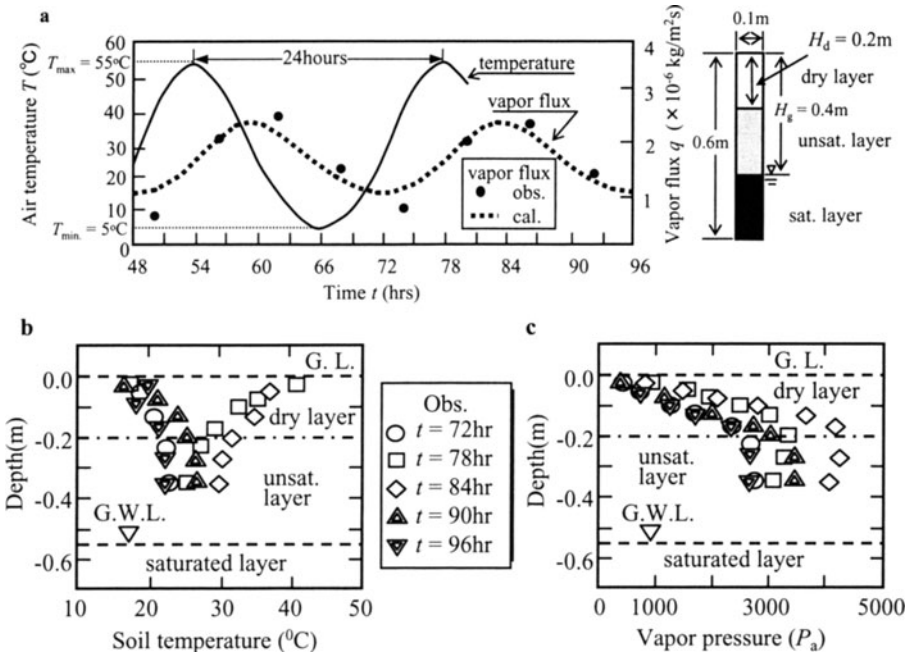

Fig. 4.7. Temporal variation of temperature and vapor flux density. Temporal and depth variation of **b** temperature and **c** vapor pressure (Fukuhara et al., 1994)

Consider heat and moisture transport within a soil column in a room with periodical temperature variation $T_{max} \sim T_{min}$ in daily cycle, as shown in **Fig. 4.7a**. The soil in the column consists of sand with a uniform diameter 0.20 mm. The saturated water level is initially fixed at H_g below the soil surface and the volumetric water content profile remains steady because of the constant water level. As a result, the top of soil H_d remains dry.

The temporal variation of soil temperature over three (72 h) to four cycles (96 h) is presented in **Fig. 4.7b**. The diurnal variation is evident, and positive and negative temperature gradients occur periodically. The vapor pressure profiles are, however, similar all the time, as shown in **Fig. 4.7c**. The maximum water vapor density appears below the soil surface, and its position corresponds to the interface between the dry layer and the unsaturated layer beneath it. It can be observed that upward and downward movements of water vapor originate at the interface. The water vapor is eventually released to the atmosphere. It is observed that vapor density profiles in the dry layer are approximately linear, and therefore, Eq. 4.19 in discretized form can be written as:

$$q_v \approx -D^* \frac{\rho_{v\,sur} - \rho_{v\,int}}{L_D} \tag{4.36}$$

where $\rho_{v\,sur}$ = vapor density at the top surface, $\rho_{v\,int}$ = vapor density at the interface, and L_D = thickness of the dry layer.

Equation 4.36 indicates that the evaporation rate is approximately proportional to the vapor density difference in the dry layer, and in inverse proportion to the thickness of the dry layer. The applicability of Eq. 4.36 is shown in **Fig. 4.7** through comparison of the measured vapor flux with values calculated using Eq. 4.36. The evaporation flux at the interface has a distinct diurnal variation as a result of air temperature variations.

Exercises

[Ex. 4.1]
Prove that the relationship between vapor density (ρ_v) and relative humidity (H_r) (see Eq. 4.20) in unsaturated porous media is expressed by the following equation:

$$\rho_v = \rho_{v0} H_r \quad \text{and} \quad H_r = \exp\left(\frac{h_c g}{RT}\right) \tag{E4.1.1}$$

where h_c = capillary head, g = acceleration due to gravity, T = temperature, and R = the gas constant.

[Ex. 4.2]
Formulate an influenced temperature effect upon the permeability (hydraulic conductivity) in saturated and unsaturated flow.

References

Bories SA (1991) Fundamentals of drying of capillary-porous bodies. Convective heat and mass transfer in porous media. Edited by Kakac et al., Kluwer Aca. Pub., The Netherlands, pp 391–434

Combarnous MA, Bories SA (1975) Hydrothermal convection in saturated porous media. Advances in Hydroscience edited by Ven te Chow, Vol. 10, Academic Press, New York, pp 231–307

de Vries DA (1958) Simultaneous transfer of heat and moisture in porous media. Trans Am Geophys Union 39: 909–916

Fukuhara T, Takano Y, Sato K (1994) Evaporation in a sand column under diurnal temperature variation. Annual J of Hydraulic Eng (JSCE) 38: 119–124

Phillip JR, de Vries DA (1957) Moisture movement in porous materials under temperature gradients. Trans Am Geophys Union 38: 222–232

Rees DAS (2002) Recent advances in the instability of free convective boundary layers in porous media. Transport Phenomena in Porous Media II edited by Derek B. Ingham and Ioan Pop, Pergamon, Amsterdam, pp 54–81

Prunty L, Horton R (1994) Steady-state temperature distribution in nonisothermal, unsaturated closed soil cells. Soil Sci. Soc. Am. J., 58: pp 1358–1363

Sato K, Resurrection AC (2001) Solute transport characteristics under temperature gradients in a closed unsaturated fine sand column. Proceedings of the 1st groundwater seminar between China, Korea and Japan, Fukuoka. pp 25–32

5

Numerical Methods in Groundwater Flow Analysis

Summary

Numerical techniques are popular in solving groundwater flow problems. The basic concepts of the methods for solving problems are briefly discussed at the beginning of this chapter. The finite-element and finite-difference methods are featured because of their wide application in this field. Discretization and formulation techniques in these two methods are well illustrated in problems such as one-dimensional flow, saturated/unsaturated conditions, and steady/unsteady flows. Because the finite element method is preferred to the finite difference technique in making choices of flexible finite element geometry, the former is discussed in more detail.

5.1 Solution Methods for Groundwater Flow Problems

The solution methods for groundwater flow problems are classified into three categories: (a) analytical methods, (b) analog model methods (Bear, 1972, 1979), and (c) numerical methods.

Figure 5.1a demonstrates an aquifer model with groundwater recharge, pumping wells, boundary conditions, groundwater hydrology, and a finite element or mesh (cf. Chap. 1). Numerical methods are aimed at solving groundwater motion in unsaturated and saturated zones that meet specific boundary conditions. Groundwater problems have been classified into three areas: groundwater hydraulic quantity for water resource development, groundwater quality to solve pollution problems, and groundwater environments. In **Fig. 5.1b**, the approaches to solving groundwater problems are summarized based on theoretical and practical methods. These are characterized as follows.

Analytical methods are preferable in understanding the nature of the studied phenomena whenever such solutions are possible. They show how characteristics of flow domains and/or boundary conditions lie behind the phenomena. In groundwater flow study, however, the use of analytical methods is not always possible because

K. Sato et al. (eds.), *Groundwater Hydraulics*

of domain heterogeneity and/or the complexity of the boundary. Additionally, nonlinearity in phreatic groundwater flow, unsaturated flow, and density flow bring about difficulty in analysis.

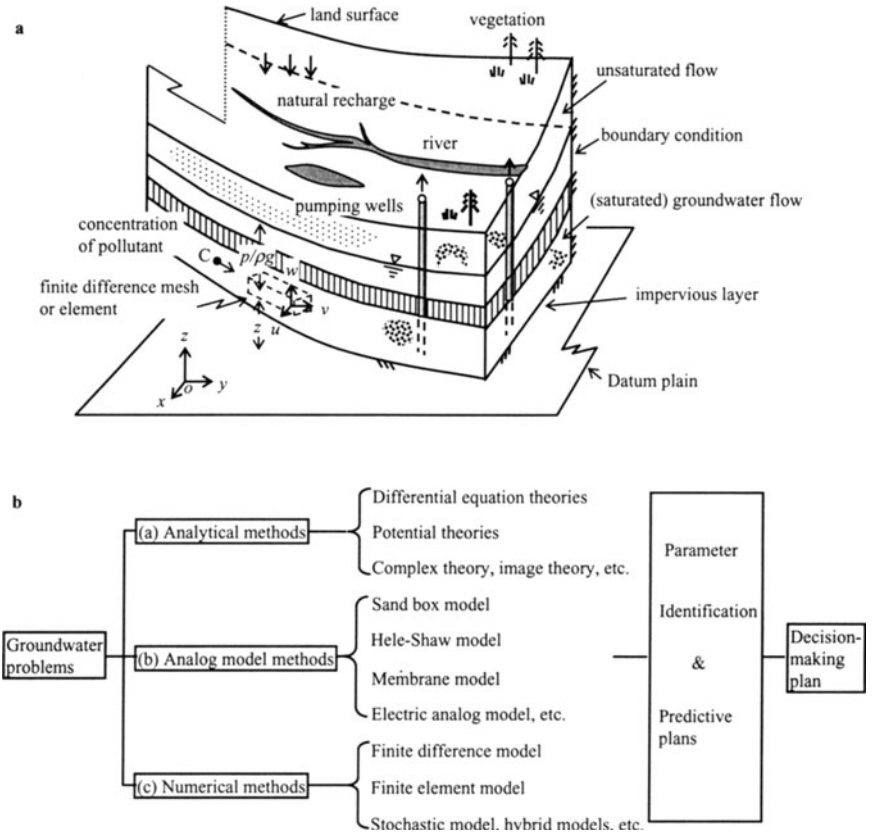

Fig. 5.1. a Aquifer modeling for numerical methods and **b** techniques applied

The analog model method is used to study phenomena in prototype aquifer systems, where the governing equations for both the prototype and model systems are similar. Well-known analog models are: (a) the sand box model, (b) the Hele-Shaw model, (c) the membrane analog, (d) the electric analog, and (e) the capillary tube analog. A suitable analog model is chosen to study an encountered groundwater phenomenon in which the geometry, parameters and boundary conditions are definitely specified. Because analog methods often require expert skill and have narrow applicability, they currently have few advantages.

Simulation and numerical methods are currently the most practical and useful approaches for studying groundwater flow phenomena. Once a simulation scheme is set up, simulation can be performed for flow domains of various geometries, param-

eters and boundary conditions. Because simulation models are deterministic, predictive quantities can be obtained by running simulations for various conditions.

Numerical simulation methods can be divided into two groups. The first group is based on the discretization of differential equations, whereas the second is based on the discretization of integral equations, and the best-known methods are finite-difference and finite-element methods, respectively. These two methods are discussed in the following sections.

5.2 Finite Difference Method

The finite difference method is a numerical approximation technique that has been employed for solving differential equations in boundary-value problems. Because partial differential equations are frequently encountered in groundwater flow problems, the finite difference scheme for the one-dimensional diffusion equation is introduced as a basic formulation for finite difference discretization.

5.2.1 Finite Difference Approximation

When a function $f(x)$ and its derivatives are single-valued, finite, and continuous functions of x, then by Taylor's theorem:

$$f(x+\Delta x) = f(x) + \frac{df(x)}{dx}\Delta x + \frac{1}{2}\frac{d^2f(x)}{dx^2}(\Delta x)^2 + \frac{1}{6}\frac{d^3f(x)}{dx^3}(\Delta x)^3 + \cdots + \frac{1}{n!}\frac{d^nf(x)}{dx^n}(\Delta x)^n + \cdots \tag{5.1}$$

$$f(x-\Delta x) = f(x) - \frac{df(x)}{dx}\Delta x + \frac{1}{2}\frac{d^2f(x)}{dx^2}(\Delta x)^2 - \frac{1}{6}\frac{d^3f(x)}{dx^3}(\Delta x)^3 + \cdots + \frac{1}{n!}\frac{d^nf(x)}{dx^n}(-\Delta x)^n + \cdots \tag{5.2}$$

Addition and subtraction of these expansions give Eqs. 5.3 and 5.4, respectively, as follows:

$$\frac{d^2f(x)}{dx^2} = \frac{f(x+\Delta x) - 2f(x) + f(x-\Delta x)}{(\Delta x)^2} + O\{(\Delta x)^2\} \tag{5.3}$$

$$\frac{df(x)}{dx} = \frac{f(x+\Delta x) - f(x-\Delta x)}{2\Delta x} + O\{(\Delta x)^2\} \tag{5.4}$$

where $O\{(\Delta x)^2\}$ means the terms containing the second and higher orders of Δx. Approximation of Eqs. 5.3 and 5.4 after ignoring the second and higher derivative terms results to a truncation error of the order of $(\Delta x)^2$.

Equations 5.1 and 5.2 can be approximated by the first derivative with a truncation error of order Δx, respectively, as follows:

$$\frac{df(x)}{dx} = \frac{f(x+\Delta x) - f(x)}{\Delta x} + O\{\Delta x\} \tag{5.5}$$

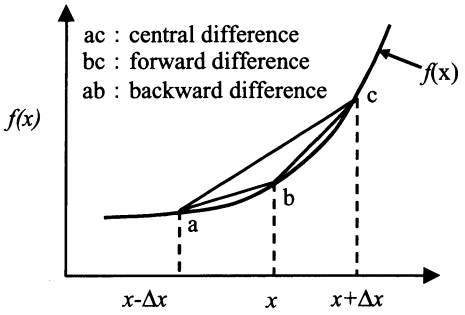

Fig. 5.2. Finite difference approximation

$$\frac{df(x)}{dx} = \frac{f(x) - f(x - \Delta x)}{\Delta x} + O\{\Delta x\} \tag{5.6}$$

The finite difference approximations given by Eqs. 5.4, 5.5 and 5.6 with the terms for truncation error are called the central difference, the forward difference, and the backward difference formulas, respectively (Smith, 1965). **Figure 5.2** shows a graphical formulation on these approximations.

5.2.2 Finite Difference Formulation of the One-Dimensional Diffusion Equation

Consider the finite difference approach to the one-dimensional diffusion equation.

$$\frac{\partial C}{\partial t} = D\frac{\partial^2 C}{\partial x^2} \tag{5.7}$$

where C = concentration and D = diffusion coefficient. C_i^k denotes concentration for $x = i\,\Delta x$ and $t = k\,\Delta t$.

A finite difference approximation to Eq. 5.7, in which the time derivative is expressed by the forward-difference formula, whereas the space derivative is expanded in terms of concentrations at $t = k\,\Delta t$ using the central difference formula, is given as:

$$\frac{C_i^{k+1} - C_i^k}{\Delta t} = D\frac{C_{i+1}^k - 2C_i^k + C_{i-1}^k}{(\Delta x)^2} \tag{5.8}$$

or

$$C_i^{k+1} = C_i^k + D\frac{\Delta t}{(\Delta x)^2}(C_{i+1}^k - 2C_i^k + C_{i-1}^k) \tag{5.9}$$

Hence, Eq. 5.9 gives the unknown pivotal value of concentration C_i^{k+1} at $t = (k+1)\Delta t$ in terms of known concentrations at $t = k\,\Delta t$. A scheme, such as Eq. 5.9, which expresses one unknown pivotal value directly in terms of known values, is called an

explicit scheme. Because finite difference approximation to the space derivative is based on values at $t = k\Delta t$ in Eq. 5.8, the approximation to the time derivative is also based on values at $t = k\Delta t$, and hence is regarded as a forward difference. Thus, Eq. 5.8 itself is called a forward difference scheme.

Although the explicit method is computationally simple, it has one serious defect, namely that a numerical solution of the difference equation Eq. 5.9 becomes inaccurate and unstable (Smith, 1965) when:

$$D\frac{\Delta t}{(\Delta x)^2} > \frac{1}{2} \tag{5.10}$$

To guarantee reasonable accuracy and stability in the explicit method, the time step and space interval must be carefully determined.

On the other hand, the finite difference approximation with respect to time at $t = (k + 1)\Delta t$ gives:

$$\frac{C_i^{k+1} - C_i^k}{\Delta t} = D\frac{C_{i+1}^{k+1} - 2C_i^{k+1} + C_{i-1}^{k+1}}{(\Delta x)^2} \tag{5.11}$$

or

$$-\frac{D\,\Delta t}{(\Delta x)^2}C_{i-1}^{k+1} + \left(1 + \frac{2D\,\Delta t}{(\Delta x)^2}\right)C_i^{k+1} - \frac{D\,\Delta t}{(\Delta x)^2}C_{i+1}^{k+1} = C_i^k \tag{5.12}$$

Because Eq. 5.12 contains three unknowns on the left hand side, this kind of formulation necessitates solution of a set of simultaneous equations, which consists of finite-difference formulas for $i = 1, 2, \ldots, M$, i.e., for all space-mesh points. A method like this is called an implicit method. In addition, formulas, such as Eq. 5.11, in which finite approximations to both space and time derivatives are based on unknown values at $t = (k + 1)\Delta t$, are known as backward-difference formula. The implicit method is valid for all finite values of $D\,\Delta t/(\Delta x)^2$, but large time steps will result in an inaccurate approximation for the time derivative.

5.2.3 Initial and Boundary Conditions

A partial differential equation is a mathematical statement, but provides no particular solution to any specific problem. A particular solution of a partial differential equation can be found only when initial and boundary conditions for the problem are known. Initial conditions, for a diffusion problem, for example, would be to specify the concentrations at all points within the domain at a certain initial time, i.e., $t = 0$.

Generally, there are three kinds of boudary conditions for (partial) differential equations in mathematics: the Dirichlet condition (or the boundary condition of the first kind) in which the values of the dependent variables only are prescribed on the boudary; the Neumann condition (or the boundary condition of the second kind) in which the values of the derivatives in the direction normal to the boundary only are specified; and the Robin condition (or the boundary condition of the third kind) is

a combination of the first and the second ones. Most of the boundary conditions encountered in groundwater flow are either Dirichlet or Neumann conditions.

Consider finite difference formulation of the following equation with the second type boundary condition.

$$-D\frac{\partial C}{\partial x} = q_{CB} \tag{5.13}$$

where q_{CB} = the prescribed flux across the boundary. Denoting the end mesh point with M (= 1, 2, 3, ..., M), the central-difference approximation to Eq. 5.13 is written as:

$$\frac{C_{M+1} - C_{M-1}}{2\Delta x} = -\frac{q_{CB}}{D} \tag{5.14}$$

or

$$C_{M+1} = C_{M-1} - 2\Delta x\frac{q_{CB}}{D} \tag{5.15}$$

where C_{M+1} = the fictitious concentration at the extra mesh point when the domain is imagined to be extended by Δx. By substituting Eq. 5.15 into the central-difference formula for a second-order space derivative, such as the terms on right hand side of Eq. 5.8 or 5.11, the boundary condition of the prescribed flux is introduced. This is the same with respect to the fictitious concentration C_{-1}.

When a boundary is impervious, (i.e., $q_{CB} = 0$), $C_{M+1} = C_{M-1}$ from Eq. 5.15. The finite-difference approximation to the second-order space derivative is written as:

$$\frac{\partial^2 C}{\partial x^2} \cong \frac{C_{M+1} - 2C_M + C_{M-1}}{(\Delta x)^2} = -\frac{2(C_M - C_{M-1})}{(\Delta x)^2} \tag{5.16}$$

5.2.4 Two-Dimensional Horizontal Flow

Consider horizontal flow in a confined aquifer. The aquifer is assumed to be homogeneous and isotropic with constant depth. Equation 2.29 governs the flow:

$$\frac{S}{T}\frac{\partial h}{\partial t} = \frac{\partial^2 h}{\partial x^2} + \frac{\partial^2 h}{\partial y^2} \tag{5.17}$$

where h = piezometric head, S = storage coefficient, and T = transmissivity.

Applying the explicit method to Eq. 5.17, we obtain the following finite difference formula:

$$\frac{S}{T}\frac{h_{i,j}^{k+1} - h_{i,j}^{k}}{\Delta t} = \frac{h_{i+1,j}^{k} - 2h_{i,j}^{k} + h_{i-1,j}^{k}}{(\Delta x)^2} + \frac{h_{i,j+1}^{k} - 2h_{i,j}^{k} + h_{i,j-1}^{k}}{(\Delta y)^2} \tag{5.18}$$

or

$$h_{i,j}^{k+1} = h_{i,j}^{k} + \frac{T}{S}\Delta t\left\{\frac{h_{i+1,j}^{k} - 2h_{i,j}^{k} + h_{i-1,j}^{k}}{(\Delta x)^2} + \frac{h_{i,j+1}^{k} - 2h_{i,j}^{k} + h_{i,j-1}^{k}}{(\Delta y)^2}\right\} \tag{5.19}$$

where $h^k_{i,j}$ = piezometric head at a point ($i\Delta x$, $j\Delta y$, $k\Delta t$, $i, j, k = 1, 2, 3, \ldots$). Using Eq. 5.19, we can explicitly calculate the unknown piezomtric head h^{k+1} for each node ($i\Delta x$, $j\Delta y$) from the known values h^k. The criterion to obtain a converging and stable solution for this case (Smith, 1965) is given by:

$$\frac{T}{S}\Delta t\left\{\frac{1}{(\Delta x)^2}+\frac{1}{(\Delta y)^2}\right\}\leq\frac{1}{2} \tag{5.20}$$

This condition necessitates extremely small values for Δt.

Unlike for the one-dimensional case, the ordinary implicit method for Eq. 5.17 leads to a large set of simultaneous algebraic equations, which require a large amount of computational capacity for their solution. A more efficient and unconditionally stable method is the alternating direction implicit (ADI) method (Smith, 1965). The advantage of the ADI method is that the large set of simultaneous equations to be handled in the ordinary implicit method is reduced to a small set.

The ADI method consists of replacing only one of the second-order space derivatives (e.g., the one in the x-direction) by an implicit difference approximation in terms of unknown values of h at time level $t = (k + 1)\Delta t$, whereas the second-order derivative in the y-direction is replaced by an explicit method using known values at $t = k\,\Delta t$. Then, the difference equation is written as:

$$\frac{S}{T}\frac{h^{k+1}_{i,j}-h^k_{i,j}}{\Delta t}=\frac{h^{k+1}_{i+1,j}-2h^{k+1}_{i,j}+h^{k+1}_{i-1,j}}{(\Delta x)^2}+\frac{h^k_{i,j+1}-2h^k_{i,j}+h^k_{i,j-1}}{(\Delta y)^2} \tag{5.21}$$

or

$$-\gamma_x h^{k+1}_{i+1,j}+(1+2\gamma_x)h^{k+1}_{i,j}-\gamma_x h^{k+1}_{i-1,j}=\gamma_y h^k_{i,j+1}+(1+2\gamma_y)h^k_{i,j}+\gamma_y h^k_{i,j-1} \tag{5.22}$$

where

$$\gamma_x=\frac{T}{S}\frac{\Delta t}{(\Delta x)^2},\quad \gamma_y=\frac{T}{S}\frac{\Delta t}{(\Delta y)^2} \tag{5.23}$$

The advancement of the solution from $t = (k + 1)\Delta t$ to $t = (k + 2)\Delta t$ is achieved by replacing the derivative in the y-direction by an implicit finite difference approximation, while replacing the one in the x-direction by an explicit approximation. The corresponding difference equation is:

$$\frac{S}{T}\frac{h^{k+2}_{i,j}-h^{k+1}_{i,j}}{\Delta t}=\frac{h^{k+1}_{i+1,j}-2h^{k+1}_{i,j}+h^{k+1}_{i-1,j}}{(\Delta x)^2}+\frac{h^{k+2}_{i,j+1}-2h^{k+2}_{i,j}+h^{k+2}_{i,j-1}}{(\Delta y)^2} \tag{5.24}$$

or

$$-\gamma_y h^{k+2}_{i,j+1}+(1+2\gamma_y)h^{k+2}_{i,j}-\gamma_y h^{k+2}_{i,j-1}=\gamma_x h^{k+1}_{i+1,j}+(1+2\gamma_x)h^{k+1}_{i,j}+\gamma_x h^{k+1}_{i-1,j} \tag{5.25}$$

Equation 2.31, given below, governs flow in a homogeneous and isotropic phreatic aquifer with an impervious horizontal bottom.

$$n_e \frac{\partial h}{\partial t} = \frac{\partial}{\partial x}\left(kh\frac{\partial h}{\partial x}\right) + \frac{\partial}{\partial y}\left(kh\frac{\partial h}{\partial y}\right) \tag{5.26}$$

where n_e: effective porosity.

Equation 5.26 is nonlinear, and hence linearization is required for the solution of an implicit difference equation. In actual computations, because the phreatic surface moves slowly with only small fluctuations at each step, the transmissivity ($T \cong kh$) at time $t = (k + 1)\Delta t$ is calculated using the known value of h at $t = k\,\Delta t$. For example, the difference equation using the ADI method at time $t = (k + 1)\Delta t$ is written as:

$$n_e \frac{h_{i,j}^{k+1} - h_{i,j}^{k}}{\Delta t} = T_{i,j}^{k} \frac{h_{i+1,j}^{k+1} - 2h_{i,j}^{k+1} + h_{i-1,j}^{k+1}}{(\Delta x)^2} + T_{i,j}^{k} \frac{h_{i,j+1}^{k} - 2h_{i,j}^{k} + h_{i,j-1}^{k}}{(\Delta y)^2} \tag{5.27}$$

where $T_{i,j}^{k} = kh_{i,j}^{k}$.

5.3 Finite Element Method

Inhomogeneous and anisotropic aquifers with complex boundary shapes are often encountered in numerical simulations of groundwater flow. The finite element method (FEM) is quite flexible and powerful for dealing with such situations (Zienkiewicz and Taylor, 2000a; Pinder and Gray, 1977). This method is advantageous when dividing a portion of the flow domain into smaller elements to study flow patterns in detail.

The concept and formulation of the FEM and examples of its application for saturated groundwater flow and convection–dispersion phenomena are discussed in this section.

5.3.1 Interpolation Function

The interpolation function (or shape function) plays a most important role in the FEM. Consider a two-dimensional horizontal flow in a groundwater basin as shown in **Fig. 5.3a**. The first step of discretization in the FEM is to divide the basin into a number of elements. The elements are assumed to be interconnected at a discrete number of nodal points situated on their boundaries and occasionally in their interior. In analysis of two-dimensional flow, the geometry of the finite elements is generally triangular or quadrilateral to accord with an arbitrarily shaped boundary, and the nodes are located on their vertices (i.e. three or four nodes for each element, as depicted in **Fig. 5.3b**).

The interpolation function (or shape function) is defined as a function that uniquely gives piezometric head over each element domain in terms of nodal heads, as depicted in **Fig. 5.4** (Zienkiewicz and Taylor, 2000a; Pinder and Gray, 1977; Connor and Brebbia, 1976). Let $N_n(x, y)$ be an interpolation function defined for node n. Then, the head at any point in the flow domain is approximated by a function $\tilde{h}$, which is composed of a linear combination of interpolation functions with nodal heads as follows:

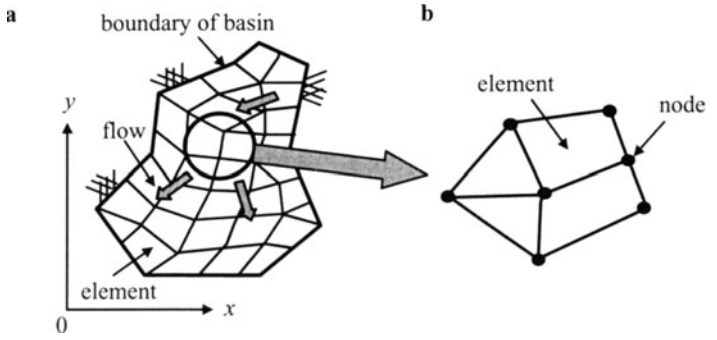

Fig. 5.3 a, b. Flow domain divided into finite elements. **a** Groundwater flow and **b** elements and nodes

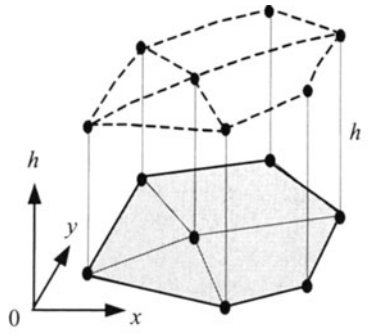

Fig. 5.4. Piezometric heads at nodes

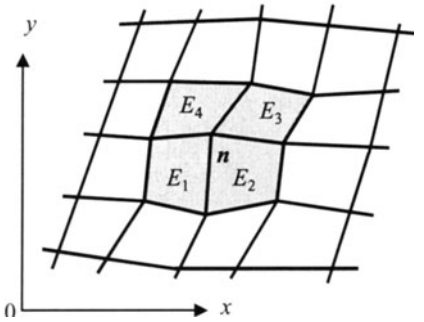

Fig. 5.5. Domain over which N_n is defined

$$\tilde{h} = \sum_{n=1}^{M} h_n N_n(x, y) \tag{5.28}$$

where h_n = piezometric head at node n, and M = total number of nodes.

The interpolation function is defined as nonzero when the node concerned is on the finite element. If node n is not within the element, then $N_n(x, y) = 0$. For the case shown in **Fig. 5.5**, $N_n(x, y) \neq 0$ on elements E_1, E_2, E_3, and E_4 and $N_n(x, y)$ is dependent on the element shape. Thus, it becomes:

$$N_n(x, y) = \bigcup_{E_e} N_n^e(x, y) \tag{5.29}$$

where $N_n^e(x, y)$ = function defined in the element E_e, and $\bigcup_{E_e}$ denotes the set sum over all the elements. For example, in the case of a quadratic element with four nodes as shown in **Fig. 5.6**, the head ($\tilde{h}_p$) at a point $P(x_p, y_p)$ is approximated in terms of the heads at four nodes (h_1, h_2, h_3, h_4) as:

$$\tilde{h}_p = h_1 N_1^e(x_p, y_p) + h_2 N_2^e(x_p, y_p) + h_3 N_3^e(x_p, y_p) + h_4 N_4^e(x_p, y_p) \tag{5.30}$$

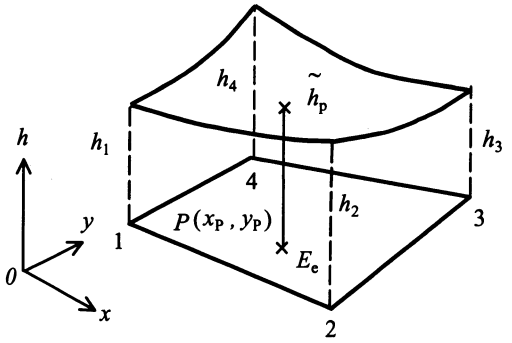

Fig. 5.6. Piezometric head approximation over a guadratic element

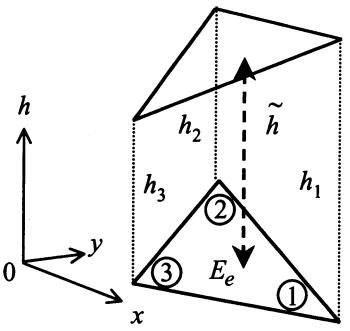

Fig. 5.7. Piezometric head approximation over a triangular element

It is understood from Eq. 5.30 that function $N_n^e(x, y)$ should satisfy the following conditions:

$$N_n^e(x_n, y_n) = 1 \tag{5.31}$$

$$N_n^e(x_m, y_m) = 0 \quad (m \neq n) \tag{5.32}$$

For a triangular element with three nodes, the piezometric head distribution within the element is given by a plain triangle, which contains heads h_1, h_2 and h_3 at the three nodes, as shown in **Fig. 5.7**. Thus, the interpolation function $N_k^e(x, y)$ for node k is a linear function written as:

$$N_k^e = a_k^e x + b_k^e y + c_k^e \quad (k = 1, 2, 3) \tag{5.33}$$

Applying the conditions of Eqs. 5.31 and 5.32 to Eq. 5.33, the constants a_k^e, b_k^e, c_k^e are written as:

$$\begin{aligned} a_1^e &= (y_2 - y_3)/2\Delta_e, & b_1^e &= (x_3 - x_2)/2\Delta_e, & c_1^e &= (x_2 y_3 - x_3 y_2)/2\Delta_e \\ a_2^e &= (y_3 - y_1)/2\Delta_e, & b_2^e &= (x_1 - x_3)/2\Delta_e, & c_2^e &= (x_3 y_1 - x_1 y_3)/2\Delta_e \\ a_3^e &= (y_1 - y_2)/2\Delta_e, & b_3^e &= (x_2 - x_1)/2\Delta_e, & c_3^e &= (x_1 y_2 - x_2 y_1)/2\Delta_e \end{aligned} \tag{5.34}$$

where Δ_e = the area of the element E_e given by:

$$2\Delta_e = \begin{vmatrix} x_1 & y_1 & 1 \\ x_2 & y_2 & 1 \\ x_3 & y_3 & 1 \end{vmatrix} \tag{5.35}$$

Although interpolation functions for quadratic elements of arbitrary shape are not always defined, the case for a rectangular element with four nodes in local coordinates (ξ, η), as shown in **Fig. 5.8**, is given by:

$$
\begin{aligned}
N_1^e &= (1-\xi)(1-\eta)/4 \\
N_2^e &= (1+\xi)(1-\eta)/4 \\
N_3^e &= (1+\xi)(1+\eta)/4 \\
N_4^e &= (1-\xi)(1+\eta)/4
\end{aligned}
\tag{5.36}
$$

Each element with irregular shape in a global Cartesian coordinate system (x, y) can be transformed into a rectangular element in a local coordinate system (ξ, η) using an interpolation function. Then, derivatives in global coordinates (x, y) in a finite element analysis are transformed into local coordinates (ξ, η). In the transformation, the x- and y-coordinates are expressed as:

$$
x = \sum_{k=1}^{4} x_k N_k^e, \quad y = \sum_{k=1}^{4} y_k N_k^e \tag{5.37}
$$

where N_k^e = an interpolation function given in terms of local coordinates (ξ, η). If the interpolation functions used in coordinate transformation are identical with those used for variable approximation, (e.g., piezometric head: $\tilde{h} = \sum_{k=1}^{4} h_k N_k^e$), then the element is called isoparametric.

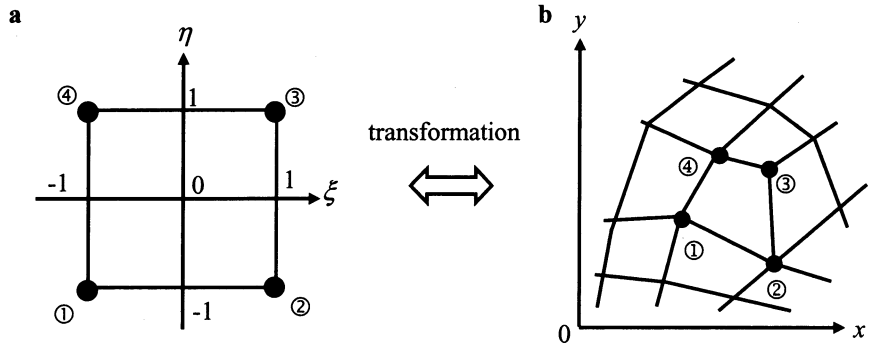

Fig. 5.8 a, b. Transformation of an element between global and local coordinate systems. **a** Element in local coordinates (ξ, η) and **b** correspoding element in global coordinates (x, y)

5.3.2 Governing Equations and Boundary Conditions for Saturated Groundwater Flow

The concept and formulation of the FEM are applied to a two-dimensional vertical saturated flow as an example.

The following governing equation can be introduced from the continuity equation and Darcy's law, as:

$$S_s \frac{\partial h}{\partial t} = \frac{\partial}{\partial x}\left(k_x \frac{\partial h}{\partial x}\right) + \frac{\partial}{\partial z}\left(k_z \frac{\partial h}{\partial z}\right) \tag{5.38}$$

where S_s = specific storage.

A prescribed piezometric head as the boundary condition is given by:

$$h = h_b(x, z, t) \tag{5.39}$$

where $h_b(x, z, t)$ is a known function that describes the head h on the boundary.

On the other hand, the boundary condition for a prescribed discharge is written as:

$$-\left\{k_x \frac{\partial h}{\partial x} n_x + k_z \frac{\partial h}{\partial z} n_z\right\} = q_b(x, z, t) \tag{5.40}$$

where $q_b(x, z, t)$ is a known function that gives flux through the boundary, and n_x, n_z = x-, z-components of the unit vector normal to the boundary.

For phreatic groundwater flow, the following conditions should be satisfied on the free water surface.

$$h = z_f(x, t) \tag{5.41}$$

and

$$-\left\{k_x \frac{\partial h}{\partial x} n_x + k_z \frac{\partial h}{\partial z} n_z\right\} = \left(n_e \frac{\partial z_f}{\partial t} - N\right) n_z \tag{5.42}$$

where z_f = height of the free surface from a datum line (or surface), N = rate of accretion per unit area and time, and n_e = effective porosity. In addition, the condition on seepage face is:

$$h = z \tag{5.43}$$

because the pressure head becomes zero.

5.3.3 Finite Element Formulation

The governing equation in the case of steady flow is written from Eq. 5.38 as:

$$\frac{\partial}{\partial x}\left(k_x \frac{\partial h}{\partial x}\right) + \frac{\partial}{\partial z}\left(k_z \frac{\partial h}{\partial z}\right) = 0 \tag{5.44}$$

Substitution of the approximated piezometric head (which is called the trial function) $\tilde{h}$, which satisfies the boundary conditions mentioned above, into h produces an error $\varepsilon(x, z)$, called the residual:

$$\frac{\partial}{\partial x}\left(k_x \frac{\partial \tilde{h}}{\partial x}\right) + \frac{\partial}{\partial z}\left(k_z \frac{\partial \tilde{h}}{\partial z}\right) = \varepsilon(x, z) \neq 0 \tag{5.45}$$

Thus, the best approximation of h requires that an integration of $\varepsilon(x, z)$ with a weighting function over the flow domain equals zero, as follows:

$$\int_E \varepsilon(x,z) W \, dE = 0 \tag{5.46}$$

where W = a set of space-weighting functions and E = flow domain. The type of finite element formulation based on Eq. 5.46 is called the weighted residual method (Zienkiewicz and Taylor, 2000a). The Galerkin method is a popular weighted-residual method in which the interpolation function is used as the weighting function.

Applying the Galerkin procedure to Eq. 5.45, the following integral equation holds:

$$\int_E \left\{ \frac{\partial}{\partial x}\left(k_x \frac{\partial \tilde{h}}{\partial x}\right) + \frac{\partial}{\partial z}\left(k_z \frac{\partial \tilde{h}}{\partial z}\right) \right\} N_m \, dE = 0 \tag{5.47}$$

where the interpolation function N_m is used as a weighting function. Integration of Eq. 5.47 by parts (Green's theorem: $\int_\Gamma (n_x X + n_z Z) d\Gamma = \int_E (\partial X/\partial x + \partial Z/\partial z) dE$, in which X and Z are functions) leads to the following equation which consists of only the first derivatives:

$$\begin{aligned} &\int_\Gamma \left\{ \left(k_x \frac{\partial \tilde{h}}{\partial x}\right) n_x + \left(k_z \frac{\partial \tilde{h}}{\partial z}\right) n_z \right\} N_m \, d\Gamma \\ &- \int_E \left\{ \left(k_x \frac{\partial \tilde{h}}{\partial x}\right) \frac{\partial N_m}{\partial x} + \left(k_z \frac{\partial \tilde{h}}{\partial z}\right) \frac{\partial N_m}{\partial z} \right\} dE = 0 \end{aligned} \tag{5.48}$$

where Γ = the boundary of domain E.

Because the trial function $\tilde{h}$ is chosen to satisfy the boundary conditions, the integral in the first term of the above equation has to be replaced by Eq. 5.40 as:

$$\left\{ k_x \frac{\partial \tilde{h}}{\partial x} n_x + k_z \frac{\partial \tilde{h}}{\partial z} n_z \right\} = -q_b \tag{5.49}$$

Then, Eq. 5.48 becomes:

$$\int_E \left\{ \left(k_x \frac{\partial \tilde{h}}{\partial x}\right) \frac{\partial N_m}{\partial x} + \left(k_z \frac{\partial \tilde{h}}{\partial z}\right) \frac{\partial N_m}{\partial z} \right\} dE = -\int_\Gamma q_b N_m \, d\Gamma \tag{5.50}$$

The summation convention is employed to avoid repetition of the summation symbol and subscripts hereafter. For example, Eq. 5.28 is expressed as:

$$\tilde{h} = \sum_{n=1}^{M} h_n N_n = h_n N_n \tag{5.51}$$

Substitution of Eq. 5.51 into Eq. 5.50 leads to an equation with respect to unknown piezometric head (h_n) at node n as follows:

$$A_{mn} h_n = r_m \tag{5.52}$$

where

$$A_{mn} = \int_E \left\{ \left(k_x \frac{\partial N_n}{\partial x}\right) \frac{\partial N_m}{\partial x} + \left(k_z \frac{\partial N_n}{\partial z}\right) \frac{\partial N_m}{\partial z} \right\} dE \tag{5.53}$$

$$r_m = -\int_{\Gamma} q_b N_m \, d\Gamma \tag{5.54}$$

Coefficient A_{mn} and the right hand side term r_m are determined by integrating and summing them over all elements, i.e.,

$$A_{mn} = \sum_{E_e} \int_{E_e} \left\{ k_x^e \frac{\partial N_m^e}{\partial x} \frac{\partial N_n^e}{\partial x} + k_z^e \frac{\partial N_m^e}{\partial z} \frac{\partial N_n^e}{\partial z} \right\} dE_e \tag{5.55}$$

$$r_m = -\sum_{E_e} \int_{\Gamma_e} q_b^e N_m^e \, d\Gamma_e \tag{5.56}$$

where E_e = domain of an element; Γ_e = boundary of an element, k_x^e and k_z^e = hydraulic conductivities in the x- and z-directions, respectively, within an element; and q_b^e = prescribed flux through Γ_e.

Taking the interpolation functions of M elements $N_1, N_2, \ldots, N_m, \ldots, N_M$ as weighting function W in the Galerkin procedure, simultaneous algebraic equations with M unknowns provide for M values of piezometric heads at the nodes. It must be noted again that these solutions give the best approximation when adhering to Eq. 5.46.

5.3.4 Calculation of Coefficient A_{mn}

Equations 5.55 and 5.56 can be integrated if interpolation functions are defined for each element. For a triangular element with nodes at its vertices, the interpolation functions are given by Eq. 5.33, and hence the coefficients are written as:

$$\begin{aligned} A_{mn} &= \sum_{E_e} \int_{E_e} \left\{ k_x^e \frac{\partial N_m^e}{\partial x} \frac{\partial N_n^e}{\partial x} + k_z^e \frac{\partial N_m^e}{\partial z} \frac{\partial N_n^e}{\partial z} \right\} dE_e \\ &= \sum_{E_e} \int_{E_e} \left(k_x^e a_m^e a_n^e + k_z^e b_m^e b_n^e \right) dE_e \\ &= \sum_{E_e} (k_x^e a_m^e a_n^e + k_z^e b_m^e b_n^e) \int_{E_e} dE_e = \sum_{E_e} (k_x^e a_m^e a_n^e + k_z^e b_m^e b_n^e) \Delta_e \end{aligned} \tag{5.57}$$

where a_n and b_n are given by Eq. 5.34.

For a quadratic element with four nodes at its vertices, integration is performed by transforming derivatives from global to local coordinates (Zienkiewicz and Taylor, 2000a). The usual rule of partial differentiation can be applied for the derivatives of Eqs. 5.36 and 5.37 in the two coordinate systems as follows:

$$\frac{\partial N_n^e}{\partial \xi} = \frac{\partial N_n^e}{\partial x} \frac{\partial x}{\partial \xi} + \frac{\partial N_n^e}{\partial z} \frac{\partial z}{\partial \xi}, \quad \frac{\partial N_n^e}{\partial \eta} = \frac{\partial N_n^e}{\partial x} \frac{\partial x}{\partial \eta} + \frac{\partial N_n^e}{\partial z} \frac{\partial z}{\partial \eta}$$

and also in matrix form as:

$$\begin{Bmatrix} \frac{\partial N_n^e}{\partial \xi} \\ \frac{\partial N_n^e}{\partial \eta} \end{Bmatrix} = \begin{bmatrix} \frac{\partial x}{\partial \xi} & \frac{\partial z}{\partial \xi} \\ \frac{\partial x}{\partial \eta} & \frac{\partial z}{\partial \eta} \end{bmatrix} \begin{Bmatrix} \frac{\partial N_n^e}{\partial x} \\ \frac{\partial N_n^e}{\partial z} \end{Bmatrix} = [J] \begin{Bmatrix} \frac{\partial N_n^e}{\partial x} \\ \frac{\partial N_n^e}{\partial z} \end{Bmatrix} \tag{5.58}$$

The matrix $[J]$ above is known as the Jacobian matrix, and can easily be calculated using Eq. 5.37, i.e.,

$$[J] = \begin{bmatrix} \frac{\partial x}{\partial \xi} & \frac{\partial z}{\partial \xi} \\ \frac{\partial x}{\partial \eta} & \frac{\partial z}{\partial \eta} \end{bmatrix} = \begin{bmatrix} x_i \frac{\partial N_i^e}{\partial \xi} & z_i \frac{\partial N_i^e}{\partial \xi} \\ x_i \frac{\partial N_i^e}{\partial \eta} & z_i \frac{\partial N_i^e}{\partial \eta} \end{bmatrix} \tag{5.59}$$

where the summation convention is applied with subscript i. Thus, global derivatives are written from Eq. 5.58 as:

$$\begin{Bmatrix} \frac{\partial N_n^e}{\partial x} \\ \frac{\partial N_n^e}{\partial z} \end{Bmatrix} = [J]^{-1} \begin{Bmatrix} \frac{\partial N_n^e}{\partial \xi} \\ \frac{\partial N_n^e}{\partial \eta} \end{Bmatrix} \tag{5.60}$$

and the inverse matrix of $[J]$ is given by:

$$[J]^{-1} = \frac{1}{J} \begin{bmatrix} \frac{\partial z}{\partial \eta} & -\frac{\partial z}{\partial \xi} \\ -\frac{\partial x}{\partial \eta} & \frac{\partial x}{\partial \xi} \end{bmatrix} = \frac{1}{J} \begin{bmatrix} z_i \frac{\partial N_i^e}{\partial \eta} & -z_i \frac{\partial N_i^e}{\partial \xi} \\ -x_i \frac{\partial N_i^e}{\partial \eta} & x_i \frac{\partial N_i^e}{\partial \xi} \end{bmatrix} \tag{5.61}$$

where J denotes the determinant of $[J]$, i.e.,

$$J = \begin{vmatrix} \frac{\partial x}{\partial \xi} & \frac{\partial z}{\partial \xi} \\ \frac{\partial x}{\partial \eta} & \frac{\partial z}{\partial \eta} \end{vmatrix} = \frac{\partial x}{\partial \xi}\frac{\partial z}{\partial \eta} - \frac{\partial x}{\partial \eta}\frac{\partial z}{\partial \xi} = \begin{vmatrix} x_i \frac{\partial N_i^e}{\partial \xi} & z_i \frac{\partial N_i^e}{\partial \xi} \\ x_i \frac{\partial N_i^e}{\partial \eta} & z_i \frac{\partial N_i^e}{\partial \eta} \end{vmatrix} \tag{5.62}$$

Therefore, from Eqs. 5.60 and 5.61, derivatives of the interpolation function in global coordinates in terms of local coordinates (ξ, η) are rewritten as:

$$\begin{aligned} \frac{\partial N_n^e}{\partial x} &= \frac{1}{J}\left\{\left(z_i \frac{\partial N_i^e}{\partial \eta}\right)\frac{\partial N_n^e}{\partial \xi} - \left(z_i \frac{\partial N_i^e}{\partial \xi}\right)\frac{\partial N_n^e}{\partial \eta}\right\} \\ \frac{\partial N_n^e}{\partial z} &= \frac{1}{J}\left\{\left(x_i \frac{\partial N_i^e}{\partial \xi}\right)\frac{\partial N_n^e}{\partial \eta} - \left(x_i \frac{\partial N_i^e}{\partial \eta}\right)\frac{\partial N_n^e}{\partial \xi}\right\} \end{aligned} \tag{5.63}$$

For the surface integral on an element in two-dimensional analysis, it can be shown that the differential area transforms to the following:

$$dE_e \ (= dx\, dz) = J\, d\xi\, d\eta \tag{5.64}$$

This is also evaluated in terms of local coordinates.

To perform integration of the coefficient A_{mn}, Gaussian quadrature, which is a numerical integration technique for choosing the best integrating intervals and their weighting coefficients, is frequently used (Zienkiewicz and Taylor, 2000a; Connor and Brebbia, 1976). In this technique, the definite integral of $f(\xi, \eta)$ over the square domain $(-1 \le \xi \le 1, -1 \le \eta \le 1)$, as shown in **Fig. 5.8**, is written as:

$$\int_{-1}^{1}\int_{-1}^{1} f(\xi, \eta)\, d\xi\, d\eta = \sum_{i=1}^{M_g}\sum_{j=1}^{M_g} H_i H_j f(\xi_i, \eta_j) \tag{5.65}$$

Table 5.1. Gauss-point locations and weighting coefficients

M_g	$\pm\xi$, $\pm\eta$	H_i
2	0.57735 02692	1.00000 00000
3	0.77459 66692 0.00000 00000	0.55555 55555 0.88888 88888
4	0.86113 63116 0.33998 10436	0.34785 48451 0.65214 51549

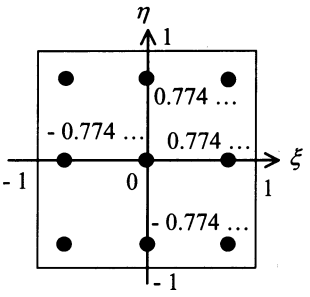

Fig. 5.9. Gauss points for $M_g = 3$

where H_i and H_j = weighting coefficients, $f(\xi_i, \eta_j)$ = value of the function at the specified point called the Gauss point, and M_g = number of Gauss points in the numerical integration.

On the other hand, coefficient A_{mn} is a function of ξ and η as expressed in Eqs. 5.63 and 5.64. Thus, when the integrand in Eq. 5.55 is written as:

$$f(\xi,\eta) = \left\{ k_x^e \frac{\partial N_m^e}{\partial x}\frac{\partial N_n^e}{\partial x} + k_z^e \frac{\partial N_m^e}{\partial z}\frac{\partial N_n^e}{\partial z} \right\} J \tag{5.66}$$

then the coefficient A_{mn} is rewritten as follows:

$$A_{mn} = \sum_{E_e} \int_{E_e} f(\xi,\eta)\, d\xi\, d\eta \tag{5.67}$$

which can be evaluated using the Gaussian quadrature technique expressed in Eq. 5.65. The Gauss-point locations and weighting factors for $M_g = 2, 3, 4$ are listed in **Table 5.1**. The locations and weighting coefficients for n Gauss points can be obtained explicitly in terms of Legendre polynomials (Abramowitz and Stegum, 1965; Zienkiewicz and Taylor, 2000a). **Figure 5.9** shows nine Gauss points for $M_g = 3$ in a square region.

5.3.5 Calculation of the Right Hand Side Term (r_m)

For a prescribed flux boundary, the term r_m on the right hand side of Eq. 5.52 is given by Eq. 5.56 and is evaluated as follows:

Let q_1 and q_2 be prescribed fluxes through outer boundaries Γ_1 and Γ_2 of elements E_1 and E_2, respectively, as shown in **Fig. 5.10**. The interpolation function N_m is linear along the boundaries Γ_1 and Γ_2. Thus, $N_m = 1$ at node m, and $N_m = 0$ at the other ends.

Hence, integration of Eq. 5.56 with respect to the elements E_1 and E_2, results in:

$$r_m = -(q_1\Gamma_1 + q_2\Gamma_2)/2 \tag{5.68}$$

which is equal to half the discharge through the boundaries Γ_1 and Γ_2 and is regarded as the concentrated discharge at node m, as shown in **Fig. 5.10**.

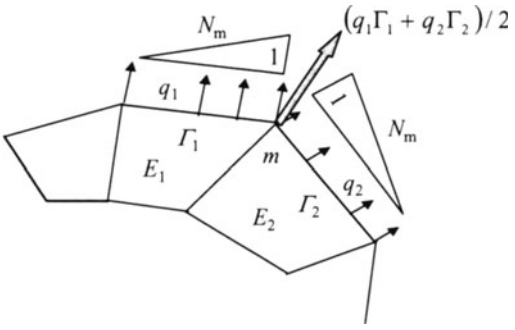

Fig. 5.10. Prescribed flux boundary conditions

For a prescribed head boundary, when the piezometric head at node m is specified as $h_m = h_{bm}$, A_{mn} and r_m in Eq. 5.52 are written as:

$$A_{mn} = \begin{cases} 1 & (n = m) \\ 0 & (n \neq m) \end{cases} \quad \text{and} \quad r_m = h_{bm} \tag{5.69}$$

5.3.6 Treatment of Free Surface

The location of the free water surface is unknown in finite-difference and finite-element numerical analyses for saturated groundwater flow. This means that the domain which is divided into elements and over which integrations of A_{mn} and r_m are performed in the FEM is not specified a priori.

The location of the free surface is determined by taking the following two steps in iterative computations (Neuman and Witherspoon, 1970).

Step-1:

1.1 The free surface and seepage face are assumed.
1.2 Both the free surface and seepage face are regarded as prescribed head boundaries given by Eqs. 5.41 and 5.43.
1.3 After head h_n at the node is solved by Eq. 5.52, discharge at the node on the seepage face is found by r_m.

Step-2:
2.1 Both the free surface and seepage face are regarded as prescribed-flux boundaries. The condition on the free surface is given by Eq. 5.42, in which $\partial z_f/\partial t = 0$ for steady flow. The discharge specified for the seepage face is already calculated in step 1.3.
2.2 Piezometric head h_n at the node is given by solving Eq. 5.52. In most cases, the head at a node on the free surface is not equal to the height of the free surface, i.e., the boundary condition of Eq. 5.41 is not satisfied.
2.3 The new height z_f' of the free surface is chosen as:

$$z_f' = (z_f + h_f)/2 \tag{5.70}$$

where z_f' = a new height for the free surface, z_f = height at the previous step, and h_f = piezometric head on the free surface as calculated in step 2.2. Then the process is repeated from step 1.2 until the boundary condition of Eq. 5.41 is reasonably satisfied.

5.3.7 Unsteady Saturated Flow

In the finite element formulation of governing Eq. 5.38 given by Eq. 5.28, the time derivative reduces to:

$$\int_E S_s \frac{\partial \tilde{h}}{\partial t} N_m \, dE = \left\{ \int_E S_s N_m N_n \, dE \right\} \frac{dh_n}{dt} = \left\{ \sum_{E_e} \int_{E_e} S_s^e N_m^e N_n^e \, dE_e \right\} \frac{dh_n}{dt} \tag{5.71}$$

where S_s^e = specific storage of an element E_e.

On the other hand, the finite element formulation of the space derivatives on the right hand side of Eq. 5.38 leads to the integral term on the left hand side of Eq. 5.48. By separating the boundary into the free surface (denoted by Γ_f) and the remaining boundary (denoted by Γ_0), the Neumann condition on Γ_f is given by Eq. 5.42, whereas that on Γ_0 is given by Eq. 5.40. Hence, the integral term of Eq. 5.48 is written as:

$$\begin{aligned} &\int_\Gamma \left\{ k_x \frac{\partial \tilde{h}}{\partial x} n_x + k_z \frac{\partial \tilde{h}}{\partial z} n_z \right\} N_m \, d\Gamma \\ &\quad = -\int_{\Gamma_f} \left(n_e \frac{\partial z_f}{\partial t} - N \right) n_z N_m \, d\Gamma_f - \int_{\Gamma_0} q_b N_m \, d\Gamma_0 \end{aligned} \tag{5.72}$$

Therefore, the finite element formula of Eq. 5.38 is expressed as:

$$B_{mn} \frac{dh_n}{dt} + A_{mn} h_n = E_m + F_m + G_m \tag{5.73}$$

In the above equation, coefficient A_{mn} is found from Eq. 5.55, and

$$B_{mn} = \sum_{E_e} \int_{E_e} S_s^e N_m^e N_n^e \, dE_e \tag{5.74}$$

$$E_m = -\sum_{R^e} \int_{\Gamma_f^e} n_e^e \frac{\partial z_f}{\partial t} n_z^e N_m^e \, d\Gamma_f^e \tag{5.75}$$

$$F_m = \sum_{E_e} \int_{\Gamma_f^e} N^e n_z^e N_m^e \, d\Gamma_f^e \tag{5.76}$$

$$G_m = -\sum_{E_e} \int_{\Gamma_0^e} q_b^e N_m^e \, d\Gamma_0^e \tag{5.77}$$

where superscript e denotes the value for an element E_e. In Eq. 5.73, the coefficients and terms are functions of time, because the flow domain changes with time.

A finite difference scheme is employed for time integration, in general (Neuman and Whitherspoon 1971). Because the specific storage (S_s) is negligibly small compared with the effective porosity (n_e) for unconfined flow, $B_{mn} = 0$. In addition, because $z_f = h = h_n N_n$ on the free surface, E_m in Eq. 5.75 is rewritten as:

$$E_{mn} = -\left(\sum_{E_e} \int_{\Gamma_f^e} n_e^e N_m^e N_n^e n_z^e \, d\Gamma_f^e \right) \frac{dh_n}{dt} = -E'_{mn} \frac{dh_n}{dt} \tag{5.78}$$

Substitution of Eq. 5.78 and $B_{mn} = 0$ into Eq. 5.73 leads to:

$$E'_{mn} \frac{dh_n}{dt} + A_{mn} h_n = F_m + G_m \tag{5.79}$$

The forward-difference approximation with respect to time step k to the above equation is written as:

$$E'^{(k)}_{mn} \frac{h_n^{(k+1)} - h_n^{(k)}}{\Delta t} + A_{mn}^{(k)} h_n^{(k)} = F_m^{(k)} + G_m^{(k)} \tag{5.80}$$

or

$$E'^{(k)}_{mn} h_n^{(k+1)} = (E'^{(k)}_{mn} - \Delta t \, A_{mn}^{(k)}) h_n^{(k)} + \Delta t (F_m^{(k)} + G_m^{(k)}) \tag{5.81}$$

where values with superscript k denote those at $t = k\,\Delta t$. In the simultaneous Eq. 5.81, only $h_n^{(k+1)}$ is an unknown variable, whereas the coefficients and the right hand side terms are known because they were evaluated at $t = k\,\Delta t$. Although Eq. 5.81 is easily solved for $h_n^{(k+1)}$, the criterion for numerical stability and convergence requires that element sizes (Δx, Δz) correspond to Eq. 5.20.

The backward-difference approximation of Eq. 5.79 can be written as:

$$E'^{(k+1/2)}_{mn} \frac{h_n^{(k+1)} - h_n^{(k)}}{\Delta t} + A_{mn}^{(k+1/2)} h_n^{(k+1)} = F_m^{(k+1/2)} + G_m^{(k+1/2)} \tag{5.82}$$

or

$$(E'^{(k+1/2)}_{mn} + \Delta t\, A^{(k+1/2)}_{mn})h^{(k+1)}_n = E'^{(k+1/2)}_{mn} h^{(k)}_n + \Delta t(F^{(k+1/2)}_m + G^{(k+1/2)}_m) \qquad (5.83)$$

where values with superscript $(k + 1/2)$ denote those at time $t = (k + 1/2)\Delta t$, defined as the average value for $t = k\,\Delta t$ and $(k + 1)\Delta t$. Because the coefficients and terms with superscript $(k + 1/2)$ are unknown in Eq. 5.83, the numerical solution for $h^{(k+1)}_n$ requires an iteration process in which coefficients and terms at $t = (k + 1)\Delta t$ are modified for the newest flow domain. This approach is stable regardless of element size and time increment.

5.3.8 Saturated–Unsaturated Flow

The saturated-unsaturated flow analysis can be delt using a merged groundwater system with two saturated zones as shown in **Fig. 5.11**. It is also possible to follow a transient seepage process through an earth dam, as depicted in **Fig. 5.12**, in which saturated and unsaturated zones exist together. The analytical domain is the whole dam, and the phreatic surface (or free surface) is defined as an internal boundary between positive and negative pore pressure zones.

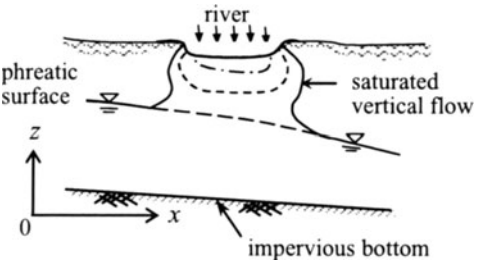

Fig. 5.11. Merger of two saturated zones

The governing equation for two-dimensional flow is given by:

$$\left(n_e \frac{dS_w}{d\psi} + S_w S_s\right)\frac{\partial \psi}{\partial t} - \left[\frac{\partial}{\partial x}\left(k_r k_x \frac{\partial \psi}{\partial x}\right) + \frac{\partial}{\partial z}\left\{k_r k_z\left(\frac{\partial \psi}{\partial z} + 1\right)\right\}\right] = 0 \qquad (5.84)$$

where ψ = pressure head (i.e., $\psi = p/\rho g$), S_w = degree of saturation, k_r = relative permeability, k_x and k_z = hydraulic conductivities at $S_w = 1$ in the x- and z-directions, respectively, and $n_e(dS_w/d\psi)$ is called the specific moisture capacity. Clearly, $\psi \geq 0$ in the saturated zone while $\psi < 0$ in the unsaturated zone. The specific moisture capacity is defined only in the unsaturated zone.

The prescribed head boundary condition is written as:

$$\psi = \psi_b \qquad (5.85)$$

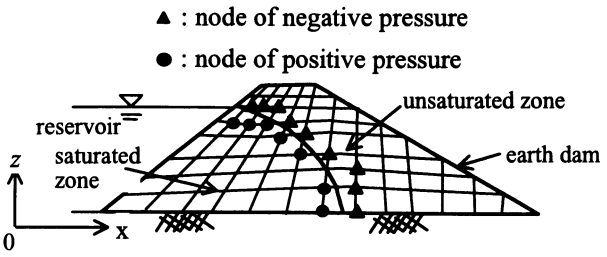

Fig. 5.12. Seepage analysis in an earth dam

and the prescribed flux boundary condition is given by:

$$-\left[k_r k_x \frac{\partial \psi}{\partial x} n_x + k_r k_z \left(\frac{\partial \psi}{\partial z} + 1\right) n_z\right] = q_b \tag{5.86}$$

where ψ_b = specified head, q_b = specified flux, and n_x and n_z are the x- and z-components of the unit vector normal to the boundary.

Using a similar derivation process, the Galerkin formulation of Eq. 5.84 presented by Neuman and Witherspoon, 1973 is:

$$B_{mn} \frac{d\psi_n}{dt} + A_{mn}\psi_n = D_m + G_m \tag{5.87}$$

where

$$A_{mn} = \sum_{E_e} \int_{E_e} k_r^e \left\{k_x^e \frac{\partial N_m^e}{\partial x} \frac{\partial N_n^e}{\partial x} + k_z^e \frac{\partial N_m^e}{\partial z} \frac{\partial N_n^e}{\partial z}\right\} dE_e \tag{5.88}$$

$$B_{mn} = \sum_{E_e} \int_{E_e} \left(n_e^e \frac{dS_w^e}{d\psi} + S_w^e S_s^e\right) N_m^e N_n^e \, dE_e \tag{5.89}$$

$$D_m = -\sum_{E_e} \int_{E_e} k_r k_z \frac{\partial N_m^e}{\partial z} dE_e \tag{5.90}$$

$$G_m = -\sum_{E_e} \int_{\Gamma_e} q_b^e N_m^e \, d\Gamma_e \tag{5.91}$$

Integration of Eq. 5.87 with respect to time is realized by replacing the time derivative with a finite difference, as in the case of transient saturated flow. The time-centered scheme endorses good integration results if the original flow domain remains unsaturated all the time or if $S_s \neq 0$ in the saturated zone.

If $S_s = 0$ in the saturated zone, coefficient B_{mn} vanishes, and the governing equation becomes an elliptic type Laplace equation. In this case, ψ is no longer a continuous function over all finite elements because a part of the flow domain is saturated, and so a fully implicit backward difference scheme must be adopted to overcome this difficulty.

Regardless of the integration scheme, the coefficients are evaluated at $t = (k + 1/2)\Delta t$ to make Eq. 5.87 quasilinear and their accuracy is improved by iteration.

5.3.9 Numerical Scheme for Advection-dispersion Phenomena

Analysis of the advection-dispersion equation is necessary for solution of groundwater pollution problems. A difficulty often encountered in numerical analyses of advection-dispersion phenomena is instability when advection is large compared with dispersion. The upwind method can get over this difficulty and ensure an accurate solution.

The advection-dispersion equation for a heterogeneous flow domain in x-z coordinates is written as:

$$\frac{\partial C}{\partial t} - \frac{\partial}{\partial x}\left(D_{xx}\frac{\partial C}{\partial x} + D_{xz}\frac{\partial C}{\partial z}\right) - \frac{\partial}{\partial z}\left(D_{zx}\frac{\partial C}{\partial x} + D_{zz}\frac{\partial C}{\partial z}\right) + u'\frac{\partial C}{\partial x} + w'\frac{\partial C}{\partial z} = 0 \quad (5.92)$$

where C = concentration defined as mass of a solute per unit mass of water; D_{xx}, D_{xz}, D_{zx} and D_{zz} = components of dispersion coefficient tensor, and u' and w' are x- and z-components of the average pore velocity components. As will be discussed in Chap. 6, the dispersion coefficients are given by:

$$D_{xx} = \alpha_l\frac{u'^2}{q'} + \alpha_t\frac{w'^2}{q'} + D_M \quad (5.93)$$

$$D_{zz} = \alpha_t\frac{u'^2}{q'} + \alpha_l\frac{w'^2}{q'} + D_M \quad (5.94)$$

$$D_{xz} = D_{zx} = (\alpha_l - \alpha_t)\frac{u'w'}{q'} \quad (5.95)$$

where $q' = \sqrt{u'^2 + w'^2}$; α_l and α_t = longitudinal and transverse dispersivities with different length dimensions, respectively; and D_M = coefficient of molecular diffusion.

Let us discuss how to deal with the advective term to get numerical accuracy in computational processes using the one-dimensional equation in the x-direction ($0 \le x \le L$) for the steady state:

$$u'\frac{dC}{dx} - \frac{d}{dx}\left(D\frac{dC}{dx}\right) = 0 \quad (5.96)$$

where D = dispersion coefficient, u' = average pore velocity, and both are assumed to be constant.

The central finite difference approximation to Eq. 5.96 becomes:

$$u'\frac{C_{i+1} - C_{i-1}}{2\Delta x} - D\frac{C_{i+1} - 2C_i + C_{i-1}}{(\Delta x)^2} = 0 \quad (5.97)$$

or

$$-(Pe + 1)C_{i-1} + 2C_i + (Pe - 1)C_{i+1} = 0 \quad (5.98)$$

where Δx = mesh interval, C_i = concentration at $x = x_i = i\,\Delta x$, and

$$Pe = \frac{u' \Delta x}{2D} \tag{5.99}$$

In Eq. 5.99, Pe is called the element Peclet number in the finite difference analysis. The Galerkin formulation of Eq. 5.96 employing a linear interpolation function also leads to Eq. 5.97. The accuracy of the solution by Eq. 5.98 deteriorates as Pe increases. The solution oscillates when Pe becomes quite large. This oscillation is attenuated if the advection term is replaced with an upwind finite difference, as shown below:

$$u' \frac{dC}{dx} \approx u' \frac{C_i - C_{i-1}}{\Delta x} \tag{5.100}$$

This approach is based on the fact that solute transport as a result of advection occurs, in reality, from upstream to downstream, not in the opposite direction.

The upwind finite difference approximation to Eq. 5.97 can be rewritten in a central difference form similar to Eq. 5.97 as follows:

$$u' \frac{C_{i+1} - C_{i-1}}{2\Delta x} - D(1 + Pe) \frac{C_{i+1} - 2C_i + C_{i-1}}{(\Delta x)^2} = 0 \tag{5.101}$$

Comparing Eq. 5.97 with Eq. 5.101, the difference is that D becomes $D(1 + Pe)$, and $Pe\, D = u' \Delta x/2$ is called the artificial diffusion or balancing diffusion.

Equation 5.101 suggests that the upwind finite formulation is attained by applying the Galerkin method to the advection-dispersion equation, in which the dispersion coefficient (D) is replaced with $(1 + Pe)D$. Thus, the upwind Galerkin formulation of Eq. 5.96 leads to the following:

$$\int_0^L N_i u' \frac{dN_j}{dx} dx\, C_j + D(1 + Pe) \int_0^L \frac{dN_i}{dx} \frac{dN_j}{dx} dx\, C_j = 0 \tag{5.102}$$

or

$$\left\{ \int_0^L \left(N_i + \frac{\Delta x}{2} \frac{dN_i}{dx} \right) u' \frac{dN_j}{dx} dx \right\} C_j + D \left\{ \int_0^L \frac{dN_i}{dx} \frac{dN_j}{dx} dx \right\} C_j = 0 \tag{5.103}$$

Equation 5.103 indicates that the same equation can be derived when the weighted residual formulation is applied to Eq. 5.96 with the following weighting function:

$$W = N_i + \frac{\Delta x}{2} \frac{dN_i}{dx} \tag{5.104}$$

In other words, the upwind finite-element formulation can be obtained using Eq. 5.104 as weighting functions in the weighted residual method (Zienkiewicz and Taylor, 2000b).

Equation 5.101 is rewritten as:

$$-(2Pe + 1)C_{i-1} + (2Pe + 2)C_i - C_{i+1} = 0 \tag{5.105}$$

and the solution is known not to oscillate even if the Peclet number becomes infinitely large. However, this does not mean that the solution is accurate; in fact, the accuracy depends on the Peclet number.

Hence, to achieve an accurate solution for various values of Peclet number, the weighting function is modified as follows:

$$W = N_i + \alpha \frac{\Delta x}{2} \frac{dN_i}{dx} \tag{5.106}$$

where

$$\alpha = \coth |Pe| - \frac{1}{|Pe|} \tag{5.107}$$

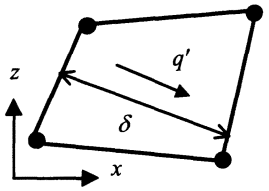

Fig. 5.13. Element size (δ) in the upwind finite-element method

Now, taking the flow direction into account for a two-dimensional flow, the weighting function is given by,

$$W = N_i + \alpha \frac{\delta}{2q'} \left(u' \frac{\partial N_i}{\partial x} + w' \frac{\partial N_i}{\partial z} \right) \tag{5.108}$$

where δ = element size in the direction of flow as shown in **Fig. 5.13**. Then, using this weighting function, the residual weighted formulation of the dispersion terms in Eq. 5.92 leads to the following:

$$\int_E \left\{ \frac{\alpha \delta u'}{2q'} \left(u' \frac{\partial N_j}{\partial x} + w' \frac{\partial N_j}{\partial z} \right) \frac{\partial N_i}{\partial x} + \frac{\alpha \delta w'}{2q'} \left(u' \frac{\partial N_j}{\partial x} + w' \frac{\partial N_j}{\partial z} \right) \frac{\partial N_i}{\partial z} \right\} dE\, C_j \tag{5.109}$$

From the above equation, the balancing diffusion (or dispersion) coefficients are defined as:

$$\tilde{D}_{xx} = \frac{\alpha \delta u'^2}{2q'}, \quad \tilde{D}_{xz} = \tilde{D}_{zx} = \frac{\alpha \delta u' w'}{2q'}, \quad \tilde{D}_{zz} = \frac{\alpha \delta w'^2}{2q'} \tag{5.110}$$

The residual weighted methods with weighting functions different than the interpolation function are called the Petrov-Galerkin method. The method using the weighting function defined along the flow direction, such as Eq. 5.106 or 5.108, is called the streamline upwind Petrov-Galerkin (or SUPG) method. For a two-dimensional element, element size (δ) in **Fig. 5.13** is not always defined, but usually the average length of the element is measured in flow direction.

For analysis of unsteady advection-dispersion phenomena, the explicit characteristic-Galerkin method is known to be effective and stable under certain conditions fot the time interval Δt (Zienkiewicz and Taylor, 2000b). This formulation employs a weighting function as follows:

$$W = N_i + \frac{\Delta t}{2}\left(u'\frac{\partial N_i}{\partial x} + w'\frac{\partial N_i}{\partial z}\right) \tag{5.111}$$

Then, in the Petrov-Galerkin method, this weighting function is applied to the governing equation, excluding the time derivative terms, which are formulated using the Galerkin method.

Exercises

[Ex. 5.1]
Calculate the maximum possible time step for an explicit finite difference method if the unconfined groundwater depth = 20 m, permeability = 1.0 m/day, effective porosity (n_e) = 0.20, and grid interval ($\Delta x = \Delta y$) = 5 m.

[Ex. 5.2]
Groundwater heads at nodes ① through ④ are 1.5, 2.0, 3.0, and 2.6 m, respectively, as shown in **Fig. E5.1**. Calculate the approximate head at point a ($\xi = -0.8$, $\eta = 0.5$).

[Ex. 5.3]
Show interpolation functions for each node for the triangular element shown in **Fig. E5.2**. Also, express the simultaneous equation for a finite element formulation of the Laplace equation using the Galerkin method, where h_n denotes the unknowns at each node.

[Ex. 5.4]
The groundwater heads at the nodes of the triangular element shown in **Fig. E5.2** are 2.0, 3.0, and 1.5 m, respectively. Calculate Darcy's velocities q_x and q_z.

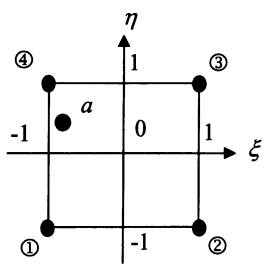

Fig. E5.1 A square element

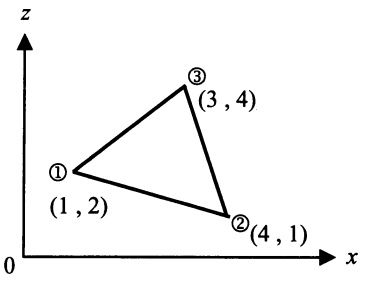

Fig. E5.2 A triangular element

References

Abramowitz N, Stegun IA (1965) Handbook of mathematical functions. Dover, New York

Bear J (1972) Dynamics of fluids in porous media. American Elsevier, New York, pp 665–727

Bear J (1979) Hydraulics of groundwater. McGraw-Hill, New York, pp 125–128

Connor JJ, Brebbia CA (1976) Finite element techniques for fluid flow. Butterworth, London

Neuman SP (1973) Saturated-unsaturated seepage by finite elements. Proc ASCE, J Hydraul Div 99(12): 2233–2250

Neuman SP, Witherspoon PA (1970) Finite element method of analyzing steady seepage with a free surface. Water Resources Res 6(3): 889–897

Neuman SP, Witherspoon PA (1971) Analysis of non-steady flow with a free surface using the finite element method. Water Resources Res 7(3): 611–623

Pinder GF, Gray WG (1977) Finite element simulation in surface and subsurface hydrology. Academic Press, New York

Smith GD (1965) Numerical solution of partial differential equations. Oxford University Press, New York

Zienkiewicz OC, Taylor RL (2000a) The finite element method, 5th edn, vol 1. Butterworth-Heinemann, Oxford

Zienkiewicz OC, Taylor RL (2000b) The finite element method, 5th edn, vol 3. Butterworth-Heinemann, Oxford

6

Groundwater Investigation

Summary

Groundwater investigation can be generally divided into two types: investigation of water quantity and water quality; nevertheless, investigation priorities depend on project requirements and objectives. Investigation techniques, in-situ tests for determining hydraulic coefficients, and groundwater quality are discussed in this chapter. The first half of the chapter outlines the performances and details of groundwater investigation and gives typical examples. Such information will help readers to understand groundwater investigation processes and priorities.

For quantitative groundwater study, it is essential to measure not only groundwater level/hydraulic head but also the hydraulic parameters of an aquifer, such as conductivity. The viability of groundwater sources and exploitation methods depend on the water quality. Therefore, investigation of groundwater quality and result assessment and interpretation are very important in deciding management policy. The latter half of this chapter describes basic measurement methods for hydraulic quantities and groundwater quality.

Groundwater is regarded as contaminated if it contains substances harmful to human health and the biological environment. The characteristics of soil and groundwater contamination and some technical approaches are also discussed in this chapter.

6.1 Definition of Groundwater Investigation

Unlike surface water (rivers, lakes, and the ocean), groundwater lies in soil aquifers and rocks. Direct observation and monitoring of groundwater without underground surveys are, therefore, not possible. Thus, groundwater needs to be investigated using methods different from those for surface water. The main tasks in groundwater investigation are directed at (1) topographical and geological aspects of the basin, (2) groundwater movement, (3) the groundwater environment, (4) the hydrological conditions, and (5) management optimization. Additional investigations are often required according to the situation.

K. Sato et al. (eds.), *Groundwater Hydraulics*

Groundwater investigation is conducted with the purpose of resource development, recharge schemes, environmental protection, construction work, and ground stability, as depicted in **Table 6.1**. The investigation process differs depending on the purpose, as demonstrated in the table.

6.2 Groundwater Investigation Techniques

Groundwater investigation generally consists of three types of study: preliminary, main, and follow-up studies, as shown in **Fig. 6.1**. Since investigation process varies with the focus and objectives of the study, its standard procedure is discussed along with the following steps.

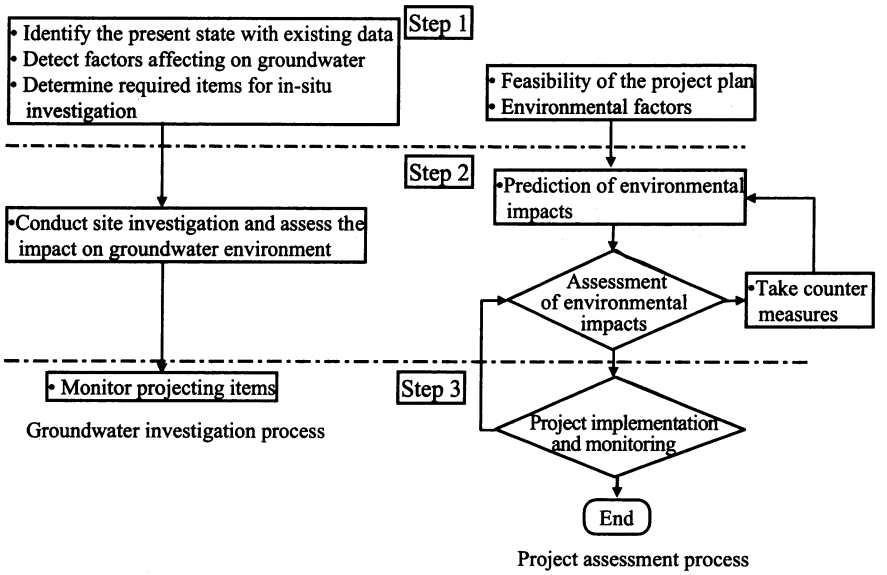

Fig. 6.1. Groundwater investigation processes and procedures involved in land development and groundwater resource development/environment protection

6.2.1 Preliminary Investigation

A desk-based study is available to identify the existing groundwater situation of the site as a preliminary investigation. Data, mainly on hydrogeological conditions and groundwater use, are collected at this stage. The effects on groundwater of the planned projects, such as land development, groundwater resource development, and engineering work are then assessed. The scope of the in-situ investigation is then decided for quantitative and qualitative evaluation of the planned project.

Table 6.1. Summary of items in groundwater investigation

Objectives			Images	Investigation items			
Category 1	Category 2			Topography and geology[a]	Groundwater hydraulic quantity[b]	Groundwater quality[c]	Contamination and remediation[d]
Groundwater resources and groundwater recharge	Groundwater resources by pumping		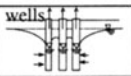	1, 2	1 - 3	1	1, 2
	Rainfall infiltration		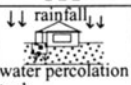	1, 2	1 - 3	2	-
	Irrigation and drainage		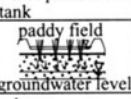	-	1, 3	2	1
	Groundwater resources in arid areas		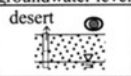	1 - 3	1 - 3	1	1
Groundwater environment protection	Ground subsidence	Prediction and monitoring of ground subsidence	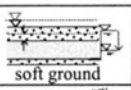	1, 2	1, 2	3	-
	Water landscape	Preservation of springs	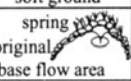	1, 2	1 - 4	3	3
		Preservation of base flow	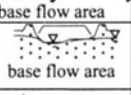	1, 2	1 - 4	4	3
	Water quality	Groundwater quality (natural condition)	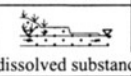	1	1, 2	3	3
		Contamination and remediation	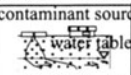	1	1, 2, 5	4	2
Construction work and ground stability	Excavation (open-cut)		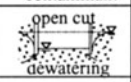	1	1, 2, 4	3, 4	3
	Excavation (tunnel,cavern)		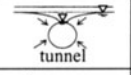	1, 2	1, 2, 4	3	3
	Stability of embankment or slope		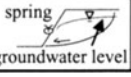	1	1, 2, 4	4	-

a)Topography and geology : 1, Geologic profile/hydrogeologic condition/topographic condition; 2, groundwater/surface water use; 3, remote sensing

b) Groundwater hydraulic quantity: 1, Groundwater level/piezometric head; 2, hydraulic conductivity (transmissivity)/storativity; 3, groundwater recharge rate/infiltration rate; 4, spring discharge/runoff discharge; 5, parameters related to contamination

c) Groundwater quality: 1, Water quality examination corresponding to the purpose; 2, clean water is required for recharge or use; 3, water quality investigation in case of necessity; 4, groundwater quality investigation or tracer tracking

d) Contamination and remediation: 1, Water quality examination; 2, water quality examination according to contaminant standards; 3, water quality investigation as occasion demands

6.2.2 Main Investigation

The main investigation includes a geological survey, boring at various sites, groundwater observation, impacts on the present situations like springs and wells, the hydrological water balance, and a feasibility study.

Surface geological information, such as stratum formation, unconformity, dips and strikes of layers, and the impermeable base, are studied through geological reconnaissance. The conditions of soil water, spring water, and water from ravines are also available. This information is summarized on a geologic map of the area being investigated.

Geophysical exploration and electric and seismic prospects are effective methods for indirect sounding of subsurface geological structure and its physical properties. Boring exploration is important to study the geological and groundwater conditions through borehole logs, giving information on subsurface geology, groundwater depth, and basic data on aquifers. Geophysical logging and other tests are conducted through boreholes whenever required.

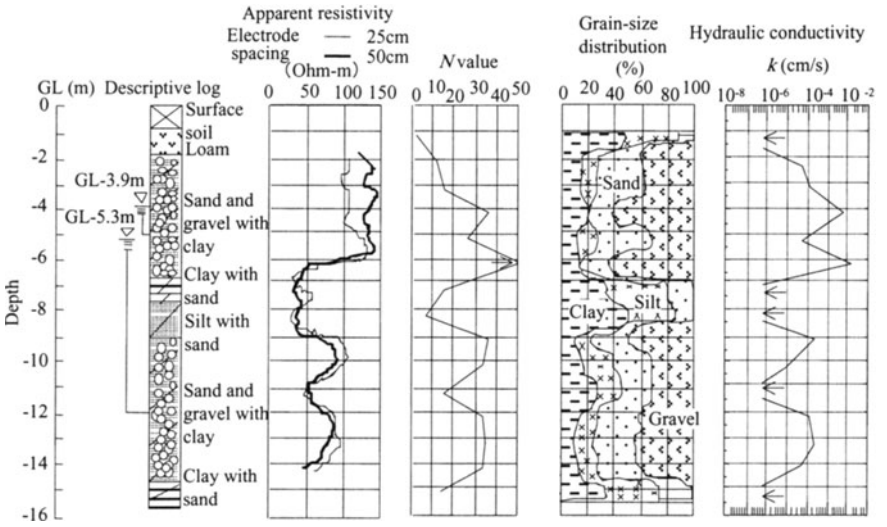

Fig. 6.2. Typical sample of geologic surveys. Electrode spacing is the distance between electrodes inserted in the borehole during resistivity measurement. Grain size distribution is, for the sample, obtained during standard penetration tests. Of the soil samples used in mechanical analysis, those of grain size d_{20} were used and the hydraulic conductivity was estimated based on a table proposed by Creager et al. (1945) to indicate the d_{20}–k relationship

Figure 6.2 demonstrates a set of examples of geophysical logging and tests. It indicates that soil resistivity is higher when it contains high proportions of gravel and sand, and lower for high clay and silt contents. The tendency is similar for the N value obtained from standard penetration test (to measure the resistance of the soil

to penetration through the N value) and hydraulic conductivity (k) at depths greater than 5 m below the surface.

Flow identification based on hydraulic head measurement is essential in groundwater investigation. The hydraulic head is obtained by measuring the groundwater head in observation wells. Information on springs, in which the groundwater head is exposed at the surface, is also useful.

The impacts of groundwater resource development and underground developments on the groundwater environment are predicted using groundwater simulation modeling. Necessary countermeasures should be taken if undesirable impacts are expected.

6.2.3 Follow-up Investigation

Changes in groundwater head and quality during and after development must be continuously monitored. Usually, boreholes and observation wells drilled during the main investigation are used. Land subsidence and settlement will be monitored in addition if groundwater drawdown is predicted.

(Example 6.1)
Assuming that several new deep wells are bored to facilitate the development of groundwater resources, explain the necessary investigation and tests.

(Answer)
Table 6.2 shows the typical process for groundwater investigation. The investigation is carried out in the following steps.

Table 6.2. Groundwater investigation with multiple deep wells

Investigation items		Images	Investigation items		Images
(i) Existing data review (as basic information)		Scale: 1/5000 existing data	Groundwater hydraulic quantity and water quality	(iv) Environmental impact assessment	existing wells -15 -10 newly installed well -5 -20
Topography and geology	(ii) In-situ investigation	platform land groundwater table low land		(v) Location and specifications of new wells	valve pumping pipe grout casing filter well screen
	(iii) Geophysical explorations including electric surveys, and borehole logging	unconfined aquifer confined aquifer confined aquifer		(vi) Pumping test and water quality examination	drawdown pumping rate water quality

Preliminary Investigation
Existing groundwater data is collected and reviewed to plan subsequent investigation and analyses. Useful data, such as topography, geology, the conditions of nearby wells and aquifers, and pumping regulation are thoroughly assessed.

Main Investigation
Necessary in-situ tests and procedures for determining groundwater behavior are planned. Optimal stations are determined for geophysical explorations and borehole logging. The geological formation and structure are identified by geophysical explorations. Boring logs are available for analyzing permeability, grain size, and aquifer thickness. Main aquifers for groundwater extraction are determined using these practical data.

Environmental Impact Assessment and Management
Allocation and specifications of new wells are determined based on the results of preceding investigations. Screen depths are determined by referring to mud logging and electrical resistivity tests during well construction. Pumping tests are carried out after the completion of each well to sound out the pumping capacity based on the relationship between pumping rate and groundwater head drawdown during the tests. Water quality examination is also carried out through water sampling. The impact of new wells on the groundwater environment and safety with regard to land settlement are assessed as required. A well-oriented management policy is established for sustainable groundwater utilization based on the results of the above tests.

6.3 In-Situ Measurement of Hydraulic Coefficients

Popular methods for measuring hydraulic coefficients, e.g., hydraulic conductivity (k) or transmissivity (T) and specific storage (S_s) or storativity (S), are discussed in this section.

It is very important to measure the groundwater table and hydraulic head to understand groundwater flow. Observation wells and boreholes have been used for measuring the water table and hydraulic head. There are two types of measurement system, those which use of a float and those which use a water pressure gauge in the observation well. Generally, a groundwater basin is composed of more than one confined aquifer with different hydraulic heads; therefore, care must be taken while measuring the hydraulic head of a particular aquifer. Watertight seals should be used to avoid undesired water inflow into the designated aquifer, especially if the observation well is used to collect groundwater samples.

Table 6.3 summarizes the methods for determining in-situ hydraulic conductivity k (or T) and S_s (or S). A suitable method should be adopted according to the purpose and the geologic conditions of the aquifer. The Lugeon test is available for determining the permeability of the rock masses.

Methods for determining hydraulic coefficients, as demonstrated in **Table 6.4**, are conducted under a constant pumping rate in both steady and unsteady conditions. These methods require pumping time (t) and drawdown data [$s(r, t) = H - h(r, t)$] measured in observation wells during pumping tests (i.e., t–s data) in the unsteady state or in the steady state, the radial distance to the well (r) and drawdown data (i.e., r–s data). The notation used here is defined in the conceptual figures shown in **Table 6.3**.

Table 6.3. In-situ determination of k and S_s

k	S_s	Category	Method	Description and image
✓	×	Measurement of groundwater velocity	The direction and rate of groundwater flow are measured by tracer methods. Pigments or electrolytes are used as tracers	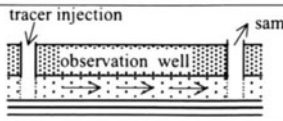
✓	✓	Pumping/ injection tests	Steady state/unsteady state pumping test using constant rate pumping well and observation wells Steady state/unsteady state injection test using constant rate injection well and observation wells	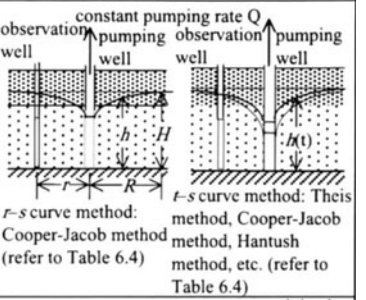
✓	×	Rock permeability test	Lugeon test: water injection test in borehole (refer to Ex. 6.1)	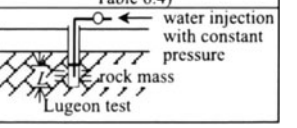

Figure 6.3 shows groundwater flow into a pumping well within a confined and unconfined aquifer. The same analytical method can be applied as long as the pumping well drawdown is less than 25% of the initial aquifer thickness, i.e. $s < 0.25H$ (Marino and Luthin, 1982). The typical methods proposed for confined aquifers are described below.

Theis (1935) solved the basic equation for a well under given initial and boundary conditions, as derived in Chap. 2. If drawdown (s) is small, then the solution is also applicable to unconfined aquifers, as shown in Eqs. 6.1 and 6.2:

$$s = \frac{Q}{4\pi kb}\int_u^\infty \frac{e^{-u}}{u}du, \quad S = n_e = \frac{4Ttu}{r^2} = \frac{4(kb)tu}{r^2} \tag{6.1}$$

$$s = \frac{Q}{4\pi kb}W(u),$$

$$W(u) = \left[-0.5772 - \log u + u - \frac{u^2}{2\cdot 2!} + \frac{u^3}{3\cdot 3!} - \frac{u^4}{4\cdot 4!} + \frac{u^5}{5\cdot 5!} - \cdots\right] \tag{6.2}$$

where kb (or kh) = T = transmissivity, $u = r^2S/4kbt$ for a confined aquifer and $u = r^2n_e/4kht$ for an unconfined aquifer, r = distance to the observation well, S = storativity, n_e = effective porosity, and t = time. Using the well function $W(u)$, $s = (Q/4\pi kb)W(u)$. The well function is equivalent to the value of the brackets in Eq. 6.2. Theis proposed a graphical method using a type curve with respect to the $W(u)$–u relationship based on s/Q and r^2/t obtained from a pumping test, as shown in **Fig. 6.4**.

Table 6.4. Determination of k and S_s by pumping tests

Type of aquifer	Steady or unsteady state	Data used	Proposed methods
Unconfined	Steady	$r-s$	Thiem-Dupuit method (Thiem 1906)
	Unsteady	$t-s$	Neuman method (Neuman 1972,1973a, 1973b,1975; Dawson and Istok 1991)
Confined (without leakage)	Steady	$r-s$	Thiem method (Thiem 1906)
	Unsteady	$t-s$	① Jacob method (Cooper and Jacob 1946) ② Theis method (Theis 1935)
		$r-s$	Jacob method (Cooper and Jacob 1946)
Partially confined (with leakage)	Steady	$r-s$	Hantush-Jacob method (Hantush and Jacob 1955; Hantush 1956,1964)
	Unsteady	$t-s$	Walton method (Walton 1962)

r, Distance from the pumping well to the observation well (coordinates); s, drawdown of the observation well; t, continuous pumping time

On the other hand, Jacob's method (Cooper and Jacob, 1946) makes it possible to plot a set of t–s data from a pumping test on arithmetic–logarithmic paper for analysis assuming that the third and subsequent terms on the right hand side of Eq. 6.2 can be ignored for u values less than 0.02. As described later in Exercise 6.2, a linear relationship with $\Delta s \sim \log_{10}(t_2/t_1) = \log_{10}(10) = 1.0$ is obtained except for an initial log cycle after the data are plotted. T, S, and n_e are calculated using the following equations:

$$T = kb = \frac{2.303Q}{4\pi s}\log_{10}\left(\frac{t_2}{t_1}\right) = \frac{0.183Q}{\Delta s} \tag{6.3}$$

$$S = n_e = \frac{2.25kbt_0}{r_i^2} \tag{6.4}$$

where Δs = drawdown over one log cycle of t [from $\log t_1$ to $\log(10 \times t_1)$, e.g., from 100 min to 1000 min], and t_0 = the intercept between the line obtained and the axis representing a drawdown of $s = 0$.

When two or more observation wells are located at different distances (r_1, r_2), then the r–s line (straight) is given by data with time t. Then, T and S are calculated from the following equations.

$$T = kb = \frac{2.303Q}{2\pi s}\log_{10}\left(\frac{r_2}{r_1}\right) = \frac{0.366Q}{\Delta s} \tag{6.5}$$

$$S = n_e = \frac{2.25kbt}{r_i^2} \tag{6.6}$$

where Δs = drawdown over one log cycle of r, and r_i = the intercept radial distance between the straight line obtained and the axis representing a drawdown of $s = 0$.

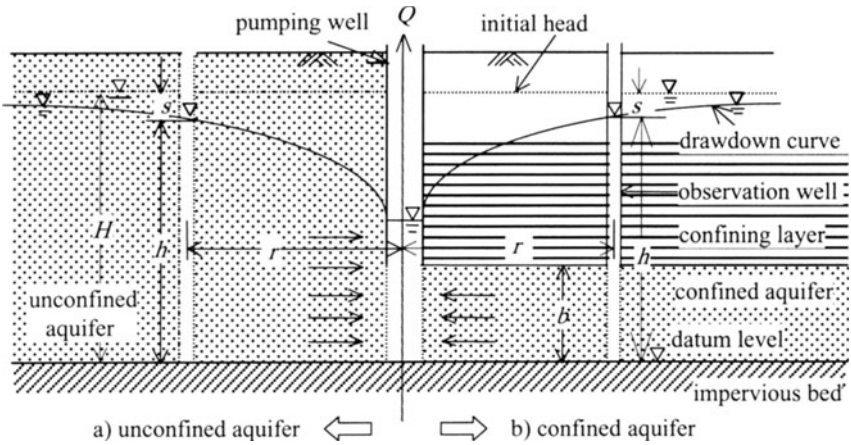

Fig. 6.3. Groundwater flow into a pumping well. Q, constant pumping rate; r, distances from the pumping well; H, depth between datum level and original piezometric surface; h, heads above the datum level at distances r and from the pumping well; s, drawdown from initial head at distances r and from the pumping well; b, aquifer thickness

6.4 Groundwater Quality Investigation

6.4.1 Objectives

Groundwater quality depends on various factors, e.g., sources of aquifer recharge, geologic formation, and the mineral constituents of the aquifer and the surrounding area. The important factors involved in groundwater quality are: (1) the variety of mineral constituents in the aquifer and their mineralization (2) the variety of chemical reactions among the constituents in the aquifer, and (3) the deterioration of groundwater quality. There are two main objectives of groundwater quality examination: (a) whether the quality is suitable for drinking purpose or other uses, and (b) to trace groundwater behavior by specifying quality components.

The theory, investigation techniques, and data evaluation procedures for groundwater quality will be discussed in the following section.

6.4.2 Chemical Constituents and Quality Examination

Groundwater quality measurement has two purposes: (1) to check the suitability and environmental adaptability of water in accordance with quality standards and (2) to elucidate the hydrologic behavior, the interaction between groundwater and surface water, and the stagnant age of the groundwater aquifer. Accordingly, the test items for groundwater quality are not always the same as those for water quality examination.

The main parameters in groundwater quality investigation are listed in **Table 6.5**. These consist of cations (Na^+, K^+, Ca^{2+}, and Mg^{2+}), anions (HCO_3^-, Cl^-, SO_4^{2-},

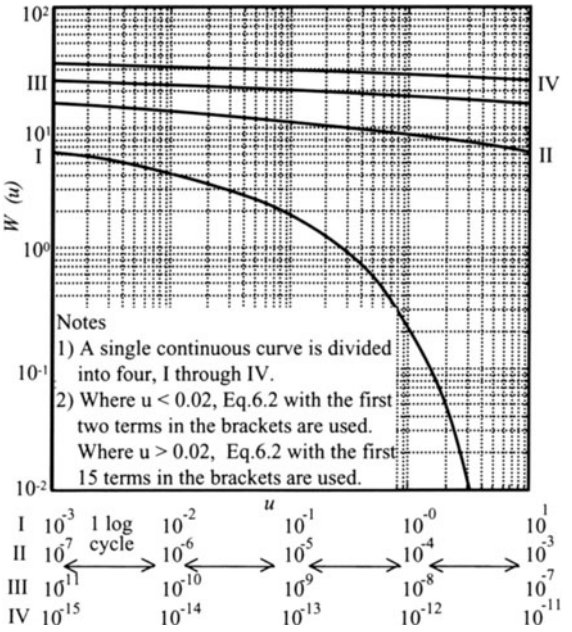

Fig. 6.4. Theoretical relationship between $W(u)$ and u

and NO_3^-), and nondissolvable ions (SiO_2). Human activity and precipitation greatly affect the concentrations of these ions in the groundwater environment.

There are 46 parameters in total to be examined in groundwater quality investigation for drinking/tap water in Japan. Of these, 29 parameters are related to toxicity, public health, and disease, and the remaining 17 are related to physical properties. The concept of quality examination is based on the guidelines of the World Health Organization (WHO), which are intended to ensure public health if people consume 2 l of water daily throughout their life.

To extract the required information from the analyses of groundwater quality investigation, physical and chemical tests have to be conducted unlike in conventional water quality examination, in which only physical tests are required. When interpreting and analyzing results, hydrologic travel on and below the ground surface and the geological formation processes of water quality should be taken into consideration.

6.4.3 Hydrologic Cycle and Water Quality

Precipitation (e.g., rain and snow) and runoff processes in the hydrologic cycle are shown in **Fig. 6.5**. Once it reaches the ground surface, precipitation gets divided into four main components (② to ⑤), as shown in the figure. Part of it infiltrates the ground surface and gets accumulated in aquifers as groundwater. The modes of

Table 6.5. Water quality parameters in groundwater investigation

Components	Units	Equivalent[d)]
Water temperature	°C	
Electric conductivity (EC)	mS /m(25°C)	
pH[a)]		
Sodium ion (Na^+)	mg/ l,me/ l	22.99
Potassium ion (K^+)	mg/ l,me/ l	39.10
Calcium ion (Ca^{2+})	mg/ l,me/ l	20.04
Magnesium ion (Mg^{2+})	mg/ l,me/ l	12.16
Iron ion (Fe^{2+})[b)]	mg/ l,me/ l	27.93
Manganese ion (Mn^{2+})[b)]	mg/ l,me/ l	27.47
Ammonium ion (NH_4^+)[b)]	mg/ l,me/ l	18.04
Total cations	me/ l	
Bicarbonate ion (HCO_3^-)	mg/ l,me/ l	61.02
Chloride ion (Cl^-)	mg/ l,me/ l	35.45
Sulfate ion (SO_4^{2-})	mg/ l,me/ l	48.04
Nitrate ion (NO_3^-)	mg/ l,me/ l	52.01
Total anions	me/ l	
Silica (SiO_2)[c)]	me/ l , mmol / l	(60.09)

a) pH is defined as the negative logarithm of hydrogen ion concentration (pH=-log[H^+]). Value of dissociation constant of water of 10^{-14} leads to [H^+][OH^-] = 10^{-14}. For neutral water, pH = 7 based on [H^+],[OH^-] = 10^{-7}

b) Concentrations of substances in parentheses are small in surface water and groundwater at shallow levels

c) SiO_2 is a nondissociating constituent and the figure in parentheses is molecular weight

d) The quantity of an element that can combine with or be replaced by one mole of hydrogen atoms or a half mole of oxygen atoms, expressed in grams

transport for precipitation are indicated by arrows in the figure. The chemical characteristics of rainwater and other types of water are summarized in **Table 6.6**, and enable us to trace the hydrologic process and understand the basics of the interactions between soil and water.

Generally, the quality of rainwater is close to that of pure water. However, it tends to adsorb salinity near coastal areas and atmospheric pollutants in urban areas. Surface waters, such as rivers and lakes, are highly susceptible to pollution as a result of wastewater discharge and atmospheric pollutants in urban areas. On the other hand, unsaturated soil water and groundwater can become polluted as a result of their long stagnation below ground and as a result of chemical and biological exchanges between soils/rock masses and groundwater. Typical groundwater quality parameters are summarized in **Table 6.5**, and these are also called groundwater quality items.

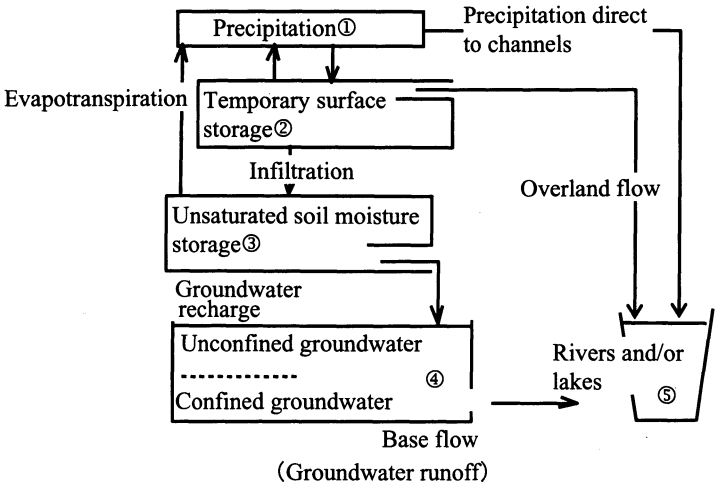

Fig. 6.5. Precipitation and runoff into the ocean

The following chemical and biochemical reactions in the groundwater environment provide important knowledge in geohydrology.

6.4.3 (a) Cation Exchange

Because trivalent aluminum (Al^{3+}) partially replaces tetravalent silicon (Si^{4+}) in clay mineral crystals, the minerals are negatively charged resulting in a capability to absorb cations to some extent. The absorption potential depends on the characteristics of the cations, as shown in **Table 6.6 3b)**. A groundwater softening phenomenon is often observed in confined aquifers because of fully developed ionic exchange in clay minerals, as shown in **Table 6.7 (i)**.

6.4.3 (b) Biochemical Reactions

Possible ionic change in water quality under high and low dissolved oxygen conditions (oxidizing and reducing conditions, respectively) are shown in **(3d)** and **(3e)** of **Table 6.6**. Because water near the ground surface is in contact with the atmosphere, it contains a large amount of dissolved oxygen. When rainwater infiltrates the subsurface, the dissolved oxygen of the infiltrating water is consumed in the decomposition of organic substances, which produces carbon dioxide (CO_2). Activities of microorganisms in pore water bring water quality change in oxidizing (or aerobic) as well as reducing (or anaerobic) conditions. Item (ii) in **Table 6.7** gives three biochemical reactions and their impacts on water quality (Morel, 1983).

However, it should be noted that the reactions described in Sects. 6.4.3 a, b result not only in changes in concentration, but also in water quality composition. Nitrogen sbstance is converted into anion from cation by nitrification. Cation is absorbed

Table 6.6. Hydrologic processes and water quality parameters

(1) Precipitation
a) Addition of constituents from condensation nuclei to which water vapor is attracted **Na^+, Ca^{2+}, Mg^{2+}, Cl^-, SO_4^{2-}**, and NO_3^-
b) Absorption of atmospheric constituents (N_2, O_2, Ar, and CO_2)
(2) Temporary storage near the ground surface
a) Reaction between CO_2 containing water and rock-forming minerals (chemical weathering)
Cations - Silicate + CO_2 + H_2O = Clay minerals + cations* + HCO_3^- + SiO_2
***Na**$^+$, **K^+**, **Ca^{2+}**, **Mg^{2+}**, and (Fe^{2+})
b) Leaching from cohesive soil layers
i) Leaching of soluble salts from marine clay layers of younger horizon
ii) Leaching of H^+ and SO_4^{2-} from sulfide-containing soil layers by oxidation
(3) Soil water and unconfined groundwater
a) Increases of CO_2 in the soil atmosphere encourage progress of 2a
b) Changes in cation composition resulting from capacity for cation exchange: $H^+ > Ca^{2+} > Mg^{2+} > K^+ > Na^+$
c) Condensation of salts resulting from evaporation from the ground surface, and their precipitation
d) Higher level of dissolved oxygen (DO) content promotes oxidation
i) Reaction 2b(ii)
ii) Insolubilization of iron ($Fe^{2+} \rightarrow Fe^{3+}$)
iii) Decomposition of organic substances ($\rightarrow CO_2$)
iv) Nitrification ($NH_4^+ \rightarrow NO_3^-$)
e) Lack of DO accelerates reduction
i) Solubilization of iron ($Fe^{3+} \rightarrow Fe^{2+}$)
ii) Reduction of nitrate (denitrification) ($NO^-_3 \rightarrow N_2$)
iii) Sulfate reduction ($SO_4^{2-} \rightarrow H_2S$ and HS^-)
(4) Confined groundwater
a) Progress of cation exchange: water softening
b) Progress of reduction: progress of 3e
c) Squeezing out from confined layers by consolidated drainage- $\rightarrow$ Increase in concentrations of HCO_3^-, NH_4^+ and PO_4-P
d) Inflow of connate water $\rightarrow$ Increase in concentration of Cl^-

Bold indicates major dissolved chemical species

rather than anion by soil. Nitrogen is apt to be released into groundwater from soil. Decrease or disappearance of NO_3^- and SO_4^{2-} resulting from chemical reduction brings about changes in composition as HCO_3^- is generated in their place.

6.4.4 Presentation of Water Quality Data

Solute concentration in groundwater is expressed in milligrams per liter (mg/l) or milligram per kilogram (mg/kg). The former is employed for water with a specific gravity of more or less unity (e.g., drinking water), whereas the latter is adopted for water with high salt concentration and specific gravity more than unity (e.g., seawater and hot spring water). The mg/kg unit is identical to parts per million (ppm).

Table 6.7. Chemical reactions involved in groundwater quality change

Chemical reactions	Remarks
(i) Cation exchange Na_2-(clay) + Ca^{2+} = Ca-(Clay) + $2Na^+$ (Clay with Na^+)(Ca^{2+} in water)	The chemical reaction shown on the left represents a process in water quality change in confined aquifers. This process is known as groundwater softening.
(ii) Biochemical reaction	Biochemical reactions can be classified into: nitrification, denitrification, and sulfate reduction as a result of microbial activities.
(a) Nitrification $NH_4^+ + 2O_2 = NO_3^- + 2H^+ + H_2O$	NH_4^+ from chemical fertilizers and sewage gets partially oxidized as shown on the left of the equation. This chemical reaction results in increase in pH (or HCO_3^- concentration increase). The exchange with H^+ increases cation concentration including Ca^{2+}.
(b) Denitrification $4NO_3^- + 5CH_2O + 4H^+ = 2N_2 + 5CO_2 + 7H_2O$	In reducing conditions, NO_3^- gives rise to N_2 as shown in the equation. CH_2O in the equation represents organic substances, which are nutrients for microorganisms. A condition: $CO_2 + H_2O \leftrightarrows H^+ + HCO_3^-$ in the reaction possibly increases HCO_3^- concentration.
(c) Sulfate reduction $SO_4^{2-} + 2CH_2O + 2H^+ = H_2S + 2H_2O + 2CO_2$	SO_4^{2-} is reduced with progressing reduction as shown in the equation. Reduction of one mole of SO_4^{2-} gives rise to two moles of HCO_3^- resulting to an increase of pH. Hydrogen sulfide (H_2S) is recognizable due to its offensive odor. In reducing conditions, H_2S is often fixed as FeS because iron present in soil turns into Fe^{2+}.

In water quality examination, solute concentration is often measured in terms of chemical equivalent, such as milliequivalents per liter (me/l) or equivalent per million (epm). Concentration in milliequivalents per liter is obtained by dividing the concentration in mg/l by its equivalent, shown in **Table 6.5**. The pH of a neutral solution $\approx$ 7.0, and summation of cations ($\sum C$) and anions ($\sum A$) should be almost the same. However, actual analyses may have some errors, and hence the $\sum C / \sum A$ ratio should be carefully maintained within 0.95–1.05.

Graphical representation methods are frequently adopted in water quality data analyses and are very useful in hydrologic characterization. Changes in water quality include variations in the composition of constituents and their concentrations. Graphical representations are expressed in terms of time series data, aerial distribution, vertical profiles, and the correlation between two different constituents.

6.4.4 (a) Concentration Diagrams (me/l)

Several techniques for expressing water quality data have been used in field investigations. **Figures 6.6a, b** show ionic concentration values (Cl^-, HCO_3^-, SO_4^{2-}, Na^+, K^+, Ca^{2+} and Mg^{2+}) on a bar graph and radial diagram, respectively. Similarly, another graphic method shown in **Fig. 6.6c** presents ionic concentrations plotted along three horizontal axes. These are called hexadiagrams because of their hexagonal shape. They are also called Stiff diagrams after the name of the developer Stiff (1951). These diagrams are very useful in understanding water quality composition.

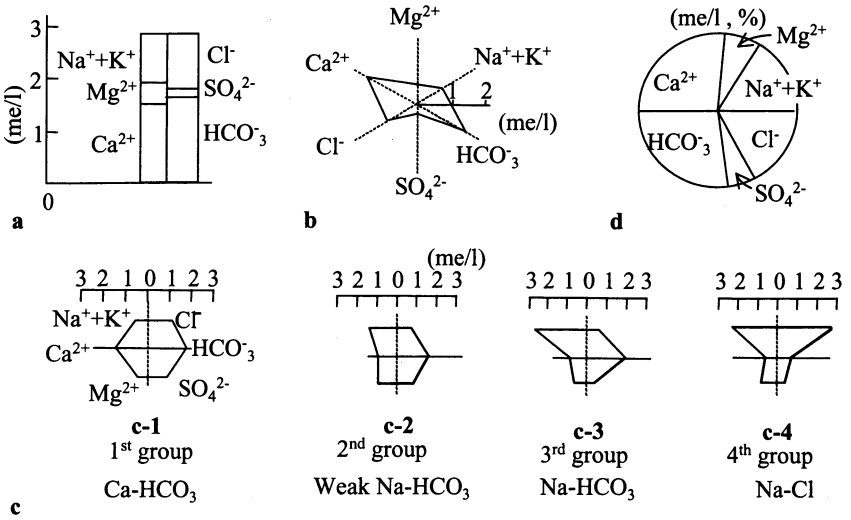

Fig. 6.6 a–d. Graphical representations of water quality data. **a** Bar graph, **b** radial diagram, **c** Stiff diagram, **d** circular diagram

6.4.4 (b) Percentage Diagram in Milliequivalents (me)

The percentage concentration of an ion (cation or anion) in milliequivalents (me/l % or epm %) can be defined as the ratio of the ion concentration to the total concentration of that type of ion ($\sum C$ or $\sum A$). The obtained percentage can be used for making a circular diagram, as shown in **Fig. 6.6**d.

Moreover, water quality data with more than one component can also be presented in a diamond-shaped diagram, as shown in **Fig. 6.7**. The figure consists of a diamond with two cations and anions each, and two triangles with three cations and anions in each. This is known as a trilinear diagram.

Recently, multivariate analysis methods, especially principal factor analysis and cluster analysis methods, have been widely employed for water quality analysis because of the increasing use of computers.

6.5 Investigation of Soil and Groundwater Pollution

Field investigation for soil and groundwater pollution/contamination and remediation has been carried out since the early 1980s. The fundamental features of groundwater pollution and the technical approaches in solving these problems are briefly discussed in this section.

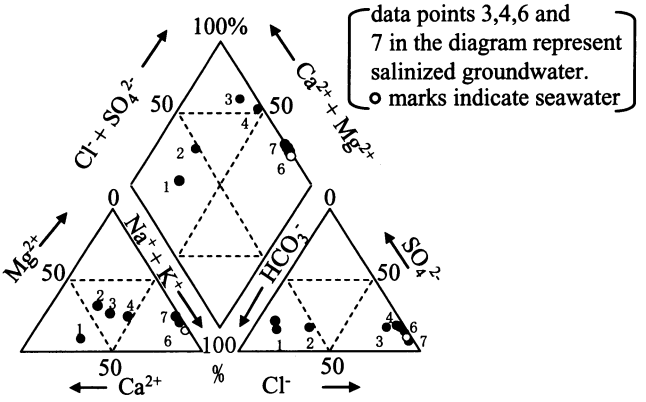

Fig. 6.7. Example of a trilinear diagram

6.5.1 Definition of Pollution and Water Quality Standards

Pollution/contamination of groundwater is defined as water in which pollutant concentrations are above the existing standards. The origin of contaminants can be broadly classified into two categories: (a) those existing naturally, for example geologically accumulated fluorine and (b) those originating from human activity (chemicals produced for various purposes, such as agriculture). Some chemicals, like heavy metals, get accumulated in the subsurface environment in the process of geologic formation, and this is natural background contamination. Groundwater contaminants and their sources are summarized in **Table 6.8**.

Table 6.8. Classification of groundwater contaminants

Contaminant	Examples	Sources
Inorganic substances	Hexavalent chromium, mercury, cyanide, and cadmium	Plants
Pathogenic microorganisms	Coliform bacillus, dysentery bacillus, viruses and etc.	Individuals and groups
Organic chemicals	Tetrachloroethylene, trichloroethylene, simazine, benzene, and many other constituents	Manufacturing processes, insecticides and herbicides, and landfill waste
Radioactive nuclides	Strontium and cesium	Eutrophication at nuclear facilities
Salts	Nitrate nitrogen and inorganic phosphorus	Fertilizers and pesticides

Soil is a key environmental component in material cycles, along with water and air; therefore, the soil ecosystem cannot be disregarded in the discussion of contamination. Contaminants in soil get dissolved in pore water and infiltrate into groundwater through the unsaturated zone, which ultimately results to groundwater contamination. **Table 6.9** shows drinking water quality standards promulgated by the World Health Organization and the Japanese Welfare and Labor Ministry.

Table 6.9. Drinking water quality standards

Group	Substance	WHO[a)] (mg/l)	Japan[b)] (mg/l)
Inorganic substances	Arsenic	0.01	0.01
	Cadmium	0.003	0.01
	Cyanide	0.07	0.01
	Fluorine	1.5	0.8
	Lead	0.01	0.05
	Total mercury	0.001	0.0005
	Selenium	0.01	0.01
Organic substances	Carbon tetrachloride	0.002	0.002
	Dichloromethane	0.02	0.02
	Trichloroethylene	0.07	0.03
	Tetrachloroethylene	0.04	0.01
	Benzene	0.01	0.01
Pesticides	1,3-Dichloropropene	0.02	0.002
	Simazine	0.002	0.003

a) WHO drinking water quality guidelines
b) Drinking water quality standards of Japan

Social and economic activities depend on various industries, in which some materials are hazardous to health and the environment. The inappropriate handling of chemicals has led to various contamination problems.

6.5.2 Hydraulic Characteristics of Contamination

Generally, contaminant transport in soil and the groundwater environment occurs as a result of water movement both in dissolved and nondissolved phases. In other words, contaminant migration and dispersion result from soil water and groundwater movement. The contaminant transport rate strongly depends on the seepage velocity and the travel path in the unsaturated zone and aquifers. Solubility, adsorption and contaminant dispersivity influence this transport.

Contaminant transport in soil occurs downward as a result of vertical unsaturated flow. Horizontal contaminant movement as a result of capillarity in the unsaturated zone is relatively small. However, in the saturated zone, horizontal movement is, in

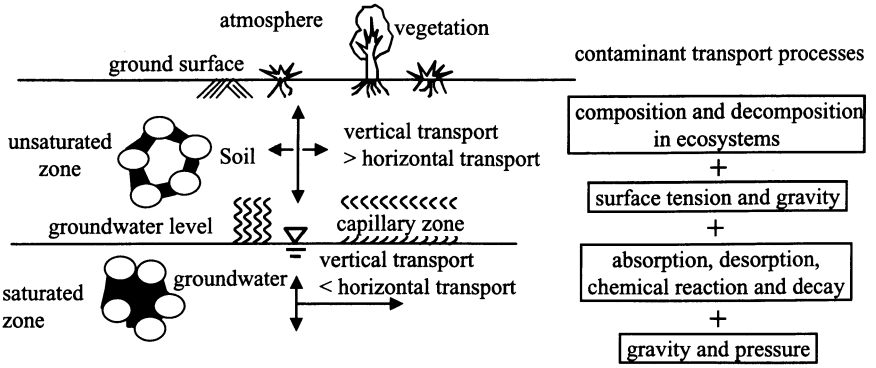

Fig. 6.8. Contaminant transport in soil and groundwater

general, predominant. **Fig. 6.8** demonstrates a conceptual view of contaminant transport in soil and the groundwater environment. Soil particles adsorb dissolved contaminants once the groundwater is contaminated. Then, the contaminants undergo various chemical reactions making their remediation difficult. Remediation of contaminated soils, in general, is time consuming and requires a lot of resources.

6.5.3 Investigation of Contamination and Remedial Measures

Investigation of soil and groundwater contamination is required not only to detect the contaminant source and identify the contamination scenario, but also to take remedial measures and verify their effectiveness. **Fig. 6.9** shows an investigation process for identification and remediation of soil and groundwater contaminants and monitoring of the remediation techniques.

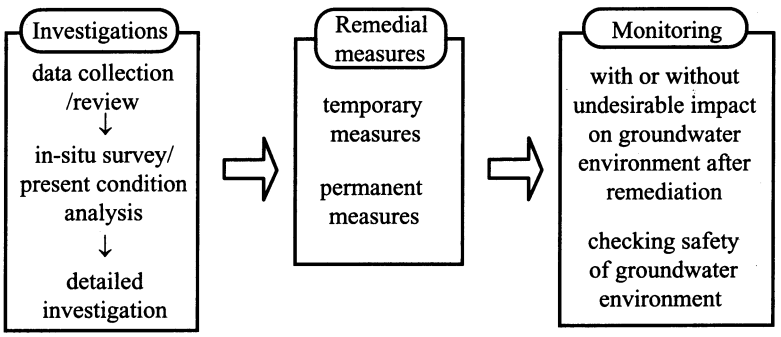

Fig. 6.9. Investigation and remediation processes in soil and groundwater

Investigation is accomplished in the following steps: data collection/review, in-situ survey/analysis of current conditions, and detailed investigation for taking remedial measures. The investigation task starts with data collection on groundwater behavior, toxic contaminants, and industrial practices. If contamination is a concern in water quality analysis, then in-situ and detailed investigations are started. Data sampling density (number of sampling points) and sampling frequency (number of samples) at a specified depth are decided based on the contaminant source and the extent of contamination. In the process, numerical simulations are carried out to predict dynamic behaviors such as velocity and contaminant dispersion. The results indicate the best remediation/recovery technique after the investigation is conducted.

Remedial measures are divided into two types: (1) emergency measures to prevent further spreading of contaminants and (2) permanent measures for long-term management. In remediation work, the contaminants are detoxified (various techniques are applied depending on the type of contaminant) and removed (e.g., extraction of soil gas from sites contaminated with volatile organic compounds and the pumping and treatment of contaminated groundwater). Monitoring for undesirable impact on the surrounding environment is indispensable while taking these measures; monitoring is required to watch for effects on the surrounding atmosphere and groundwater. Additionally, precautions must be taken in pumping and treatment methods to prevent an excessive decrease in the water level, which may result in subsidence or the drying of wells. Therefore, the monitoring of groundwater level and the measurement of ground subsidence are very important in this process. Water quality investigation may also be carried out depending on the situation. The management policy must be verified after remedial measures have been carried out.

Exercises

[Ex. 6.1]

Lugeon test was proposed by Maurice Lugeon (Barrages et Géologie, 1932) to survey rock mass permeability in the field. 1 Lugeon value is defined by injected water volume (liter) per unit time (minute) and borehole length (m) under acting water pressure of $10\,\mathrm{kgf/cm^2}$, i.e. 1 l/min/m/$10\,\mathrm{kgf/cm^2}$. This value approximately corresponds to permeability coefficient 10^{-5} cm/s if Eq. E6.1.1 is applied.

$$k = 2.3\frac{\rho g Q}{(2\pi L p)}\log_{10}\left(\frac{R}{r_0}\right) \tag{E6.1.1}$$

Find the Lugeon value L_u and its permeability coefficient k when the injected water discharge $Q = 5\,\mathrm{l/min}$ ($= 8.33 \times 10^{-5}\,\mathrm{m^3/sec}$), the borehole length $L = 5.0\,\mathrm{m}$, acting water pressure $p = 10\,\mathrm{kgf/cm^2}$ ($= 9.81 \times 10^2\,\mathrm{kN/m^2}$), radius of the borehole $r_0 = 4.5 \times 10^{-2}\,\mathrm{m}$, the water weight of volume $\rho g = 9.81\,\mathrm{kN/m^3}$, and the influence radius of injected borehole $R = 100\,\mathrm{m}$.

[Ex. 6.2]

A pumping test was carried out in a confined aquifer 10 m in width and with a constant discharge (Q) of $0.34\,\mathrm{m^3/min}$, as shown in **Fig. E6.1**. Head loss data of the two

observation wells (no. 1 and 2) are presented in **Table E6.1**. Determine the permeability (k) and the coefficient of specific storage (S_s).

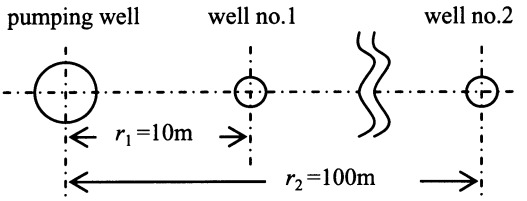

Note: Constant pumping rate $Q = 0.34 m^3/min$.
Confined aquifer thickness $b = 10m$.

Fig. E6.1 Location of pumping and observation wells, and pumping conditions

Table E6.1 Drawdown in wells no. 1 and 2

Time (min)	Drawdown in well no.1(m)	Drawdown in well no.2 (m)	Time (min)	Drawdown in well no.1 (m)	Drawdown in well no.2 (m)
1	0.870	0.025	80	1.485	0.588
2	0.900	0.038	100	1.529	0.652
3	0.940	0.075	150	1.608	0.730
4	0.965	0.105	200	1.665	0.791
5	0.995	0.127	300	1.744	0.852
6	1.010	0.144	400	1.800	0.920
8	1.080	0.180	500	1.844	0.981
10	1.118	0.210	600	1.879	1.020
15	1.148	0.282	800	1.935	1.068
20	1.225	0.340	1000	1.979	1.108
30	1.272	0.410	1500	2.058	1.195
40	1.334	0.461	2000	2.115	1.242
50	1.394	0.510	3000	2.194	1.324
60	1.429	0.539	4000	2.250	1.328

Wells no.1 and no.2 are 10m and 100m from the pumping well

References

Cooper HH, Jacob CE (1946) A generalized graphical method for evaluating formation constants and summarizing well field history. Trans Am Geophys Union 27: 526–534

Creager WP, Justin JD, Hinds J (1945) Engineering for dams Vol III, earth, rock-fill, steel and timber dams. Wiley, New York, pp 648–649

Dawson KJ, Istok JD (1991) Aquifer testing design and analysis of pumping and slug tests. Lewis, Boca Raton, Florida, pp 257–276

Hantush MS, Jacob CE (1955) Non-steady radial flow in an infinite leaky aquifer. Trans Am Geophys Union 36: 95–100

Hantush MS (1956) Analysis of data from pumping tests in leaky aquifers. Trans Am Geophys Union 37: 702–714

Hantush MS (1964) Hydraulics of wells. In: VT Chow (editor). Advances in hydroscience, Academic, New York, 1: pp 281–432

Lugeon M (1932) Barrages et géologie. imprimé par poligrafico pedrazzini, locarno, Suisse Montreux (1979), pp 7–136

Marino MA, Luthin JN (1982) Seepage and groundwater. Elsevier, Amsterdam-Oxford-New York, p 301

Morel FMM (1983) Principles of aquatic chemistry. Wiley, New York, pp 151–155

Neuman SP (1972) Theory of flow in unconfined aquifers considering delayed response of the water table. Water Resource Res 8: 1031–1045

Neuman SP (1973a) Calibration of distributed parameter groundwater flow models viewed as a multiple-objective decision process under uncertainty. Water Resource Res 9: 1006–1021

Neuman SP (1973b) Supplementary comments on theory of flow in unconfined aquifers considering delayed response of the water table. Water Resource Res 9: 1102–1103

Neuman SP (1975) Analysis of pumping test data from anisotropic unconfined aquifers considering delayed gravity response. Water Resource Res 11: 329–342

Stiff HA (1951) The interpretation of chemical water analyses by means of patterns. J Petrol Tech 3(10): 15–17

Theis CV (1935) The relation between the lowering of the piezometric surface and the rate and duration of discharge of a well using groundwater storage. Trans Am Geophys Union 16: 519–524

Thiem G (1906) Hydrogische methoden. Gebhardt Leipzig, p 56

Walton WC (1962) Selected analytical methods for well and aquifer evaluation. Illinois State Water Survey Bulletin, Urbana, No 49, p 81

7

Groundwater Resource Management

Summary

Groundwater resources have traditionally been used all over the world from ancient times. Some characteristics of groundwater resources, and a short history are reviewed in the first part of this chapter. Then, the geologic forms of potential groundwater reserves are classified and the present situation of groundwater resource utilization is briefly discussed. Excessive and reckless use of groundwater resources cause their depletion and land subsidence in all alluvial and diluvial plains, and seawater intrusion into coastal aquifers; therefore, sustainable groundwater resource management and development policies are mentioned in the latter part of this chapter.

7.1 Features of Groundwater Resources and Their Uses

Traditionally, groundwater has been used as an important water resource. Hydrogeologic conditions, such as the scale of a groundwater basin, the storage volume, natural recharge, aquifer thickness, and permeability are greatly related to groundwater resource reservoir.

Groundwater, as a water resource, has the following main features:

1. Groundwater temperature is stable regardless of the atmospheric temperature changes (temperature stability).
2. Water quality is suitable for drinking purposes (safe water quality).
3. Expected pumping volume is kept sustainable and stable within a groundwater budget (qualitative stability).
4. Groundwater extraction costs are low because of simple pumping facilities (economical water resource development).
5. Few legal regulations and ownership criteria are imposed on groundwater developers.

Groundwater resources have been used for such purposes as agriculture (irrigation), industry, city water supply, fish farming, and snow melting. In Japan, from

K. Sato et al. (eds.), *Groundwater Hydraulics*

ancient times, people have embraced the idea that groundwater is pure and holy to purify the body and soul. In some countries, groundwater and spring water are used in religious ceremonies.

A historical perspective on technological development and national laws concerning groundwater in Japan are shown in **Fig. 7.1**.

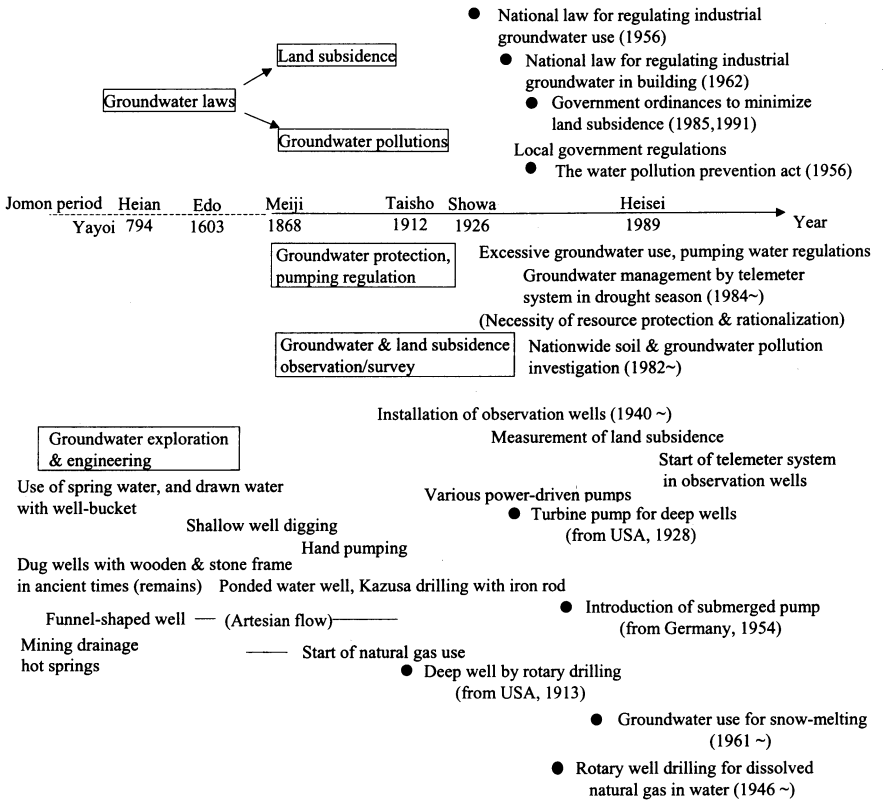

Fig. 7.1. History of groundwater resources in Japan (National Land Agency 2000)

In Japan, most human remains from the Jomon period (before 3BC) have been found near flat land adjacent to gushing primitive springs. Wells built with wooden or stone walls were discovered from the Yayoi period (before 3AD).

In the Middle Ages, various types of wells were dug, and specialists in well-digging appeared in the Edo (old Tokyo after 1603) period. At this time, water supply services were started in some big cities. In the late Edo period, the percussion type deep well drilling technique, called the Kazusa drilling method, was developed and became popular. Rotary well drilling machines were imported from United States to dig deep wells in the early decades of the 20th century.

Traditionally, well water was drawn using buckets. Hand pumps were popularized in the Meiji period (after 1868). Rotary well drilling machinery was imported and pumping techniques were improved in the Taisho period (after 1912). The introduction of submersible pumps brought a new revolution in groundwater pumping techniques after the Second World War (1945).

An increase in deep well exploitation and excessive pumping caused land subsidence, groundwater depletion, and saltwater intrusion into coastal aquifers. These consequences gave the alarm bells indicating unsustainable groundwater use.

Land subsidence was observed in Osaka and Tokyo in the 1930s. Observation stations for measuring groundwater head and land subsidence were established in these areas to consider a counter plan against land subsidence in the 1940s. In the 1950s, rapid industrial growth demanded further increases in water supply leading to more land subsidence and secondary damage. As a result, land subsidence was recognized officially as a public nuisance and groundwater use for industrial and domestic purposes was regulated. To cope with such serious problems, numerical simulation techniques were introduced to help forecast optimal groundwater production as well as subsidence prevention.

The land subsidence problem gradually decreased after the implementation of groundwater pumping regulations and water resource conservation plans. However, water shortages in the summer months resulted in increased pumping and land subsidence (e.g., during the serious droughts of 1994 and 1996). Therefore, a monitoring system for hydraulic heads and land subsidence using telemeters was introduced in 1997 for groundwater management in dry periods.

Such groundwater pollutants as volatile organic compounds (VOCs), and heavy metals have been a social problem since the 1980s. Therefore, new state and local government laws for preventing/improving soil and groundwater pollution as well as groundwater quality standards have been put into force to maintain safe groundwater quality.

7.2 Aquifer Types and the Groundwater Environment

Hydrogeologic knowledge of groundwater is essential in field investigations and groundwater resource utilization planning for engineers. Basic knowledge on the quality of typical aquifers with natural recharge and topographic and geologic conditions is discussed in the following sections.

7.2.1 Chronology of Groundwater Basins

Much groundwater is used in plain areas such as seashores and alluvial and diluvial basins. Sediment strata are composed of geologic deposits with varying grain size, and gravel and sand-rich deposits have a high porosity of around 40%.

The period from two million years ago is known as the Quaternary based on the evidence of human civilization and remains (see **Table 7.1**). It was marked by climate change with repetition of glacial and interglacial epochs over geologic time.

Table 7.1. Geologic chronology

Formation process of strata	**Comments**: The sea level changes bring about sedimentary environments. Fluvial deposit, Land, Low sea level erosion, High sea level erosion, marine deposit												
	Alluvium				Diluvium								
Age of man	Neanthropic man				Paleo-man			Proto-man				Man-ape	
Sea level change	The sea level has come to the present stage after a small rise				Marine regression	— Repetition of sea level falls and rises —							
Glacial epoch	Late glacial epoch	Late	Middle	Early	Last inter-glacial epoch	Riss glacial stage	Inter-glacial epoch	Mindel glacial stage	Inter-glacial epoch	Günz glacial stage	Diastrophism		
		Würm glacial stage											
Geologic time	10^4 year				10^5 year					10^6 year		2×10^6 year	
	Holocene	Late Pleistocene				Middle Pleistocene				Early Pleistocene		Pliocene	
	Quaternary											Tertiary	

As shown in **Table 7.1**, changes in seawater level favored the geologic formation of groundwater basins over multiple glacial and interglacial epochs. During the interglacial epochs, marine deposits accumulated thickly because of higher sea levels, whereas fluvial deposits built up because of active erosion and sedimentation during the lower sea levels of the glacial epochs.

Sea levels in glacial epoch were the lowest about 18 000 years ago. The strata of the Quaternary period are divided into diluvium and alluvium, accumulated ealier and later in the period, respectively. Fairly consolidated diluvium is distributed over many sedimentary plains, and much groundwater is stored in the pore spaces of the gravel and sand layers. Layers that can store and supply abundant water are called aquifers.

Alluvium also forms aquifers, but it is weakly consolidated and contains soft clay layers, and so pumping causes land subsidence as a result of water level decline and compaction of clay layers.

7.2.2 Geologic Features of Groundwater Basins

The concept of a water balance is indispensable for groundwater management. A groundwater basin consists of a large single aquifer or a group of aquifers depending on the geographic and geologic features. A coastal plain faces the seashore, as shown in **Table 7.2**. The stratum is composed of gravels, sand, clay and rocks buried in a valley-shaped basement.

An alluvial fan is formed by a stream originating in a mountain area passing through plains and sediment load as a result of velocity decrease. The sediment is deposited on riverbank and decreases in flow velocity result in meanders (changes in

Table 7.2. Geologic features of groundwater basins

	Geographic and geologic features	Conceptual illustrations
Coastal plain	A coastal plain results from upheaval of submarine sediment below sea level or marine regression. Excessive pumping results in land subsidence and seawater intrusion although such plains contain abundant groundwater resources	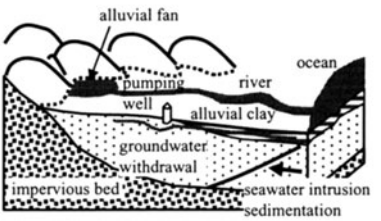
Alluvial fan	An alluvial fan has a half-circular cone. The area has discharge and intake zones with abundant groundwater resources	
Sedimentary basin	A sedimentary basin is formed by upheaval of sedimentary deposits above a submerging basement. The basin abounds in groundwater resources	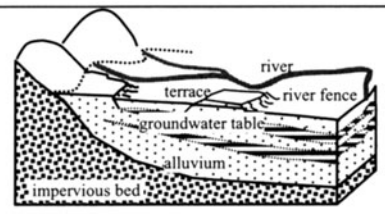
Terrace	Strata are classified into fluviatile and marine deposits and lacustrine sediment in its original formation. Many springs sometimes are found on the terrace scarp	
Volcano foot area	A volcano consists of such volcanic products as lava, lapilli, and pyroclastic materials. Abundant groundwater resources and springs are found in those areas	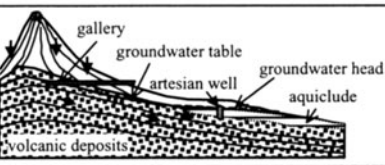
Limestone area	A limestone area consists of biological remains with calcium carbonate ($CaCO_3$). It can form stalactites, caves and sinkholes depending on corrosion. Groundwater resources in limestone areas are very useful	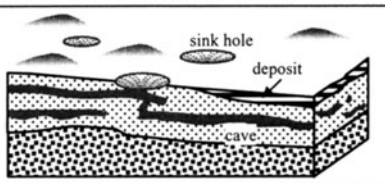
Arid zone and oasis	Groundwater in oases is very precious. There is no surface water because precipitation is returned to the atmosphere as a result of evapotranspiration	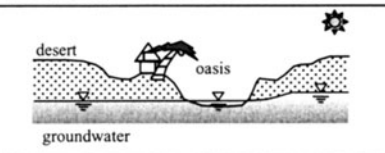

river channel). The deposition is spread over a wide area, often in a fan shape, and is called an alluvial fan.

A sedimentary basin is formed of gravel, sand, and clay deposition after a basement upheaval. It is characterized by thick layers covering a large area. A terrace consists of a stair-shaped surface and scarp situated in the center and sides of a sedimentary basin, as shown in **Table 7.2.** Strata at the foot of a volcano are composed of lava and volcanic debris, which are permeable and often form major aquifers. Springs are found near the foot of volcanic mountains (e.g., Mt. Fuji).

Most calcium carbonate aquifers consist of limestone and dolomite. Carbonate rocks are composed of calcium and magnesium carbonates in varying proportions

often mixed with clay and siliceous components. Oases are fertile spots in a desert where the groundwater table is exposed at the surface in a lowland area. It is an important water resource in arid regions.

7.2.3 Negative Impacts on Groundwater Aquifers

Reckless and excessive groundwater utilization brings undesirable impacts on the groundwater environment by affecting the hydrologic balance between groundwater extraction and natural recharge. Skills for managing groundwater resources and environments stress the avoidance of negative impacts on the groundwater environment. Some typical undesirable impacts on the groundwater environment are outlined in **Table 7.3**, and discussed briefly in this section.

Well drying is a phenomenon in which groundwater pumping must be discontinued because of the decline in groundwater level. The occurrence of this phenomenon is related to the pumping discharge rate.

Soft clay layers settle following groundwater level decline as a result of excessive pumping and this is known as land subsidence. Excessive pumping increases the effective stress in the soil particles resulting to its settlement and compaction. Land subsidence mostly occurs in alluvial lowland areas that have underlying intercalated soft clay beds. Sometimes, groundwater extraction poses serious subsidence problems in the exploitation of dissolved natural gas.

Oxygen deficient air in the unsaturated zone sometimes causes catastrophic accidents in below-ground excavation work. The withdrawal of groundwater results in higher oxygen consumption in the pore spaces of gravel layers and the movement of oxygen-deficient air after pressure changes are the causes of this problem.

Groundwater salinization problems are mostly observed in coastal plains. Seawater gradually intrudes into coastal aquifers when the balance between seawater and freshwater pressure is upset by excessive groundwater pumping. Once the intrusion takes place, it is not easy to remedy the problem completely, even after the aquifer water level recovers.

Rapid rises in groundwater level caused by recharge or other factors, also pose problems. Most problems will affect various underground facilities; however high groundwater levels are directly linked with the liquefaction phenomenon. The danger increases with increasing groundwater levels in conjunction with the shock of earthquakes. Therefore, it is very important to maintain groundwater at optimum levels.

Toxic substances used in industry, agriculture and other human activities spread in the saturated/unsaturated subsurface environment resulting in groundwater pollution. The pollution may prevent groundwater use as a result of declining water quality.

7.3 Trends in Groundwater Resource Use

The total amount of freshwater used in Japan was 87.0 km^3 in 2000. The total volume of groundwater resources used in 2000 was 12.9 km^3, of which industry used

Table 7.3. Undesirable impacts on the groundwater environment

Impacts	Explanations	Conceptual illustrations
Groundwater withdrawal	Pumping wells run dry or can not operate because of low water levels	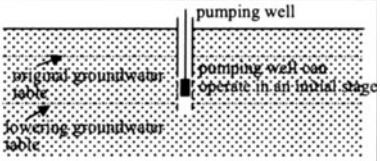
Land subsidence	Land subsidence is due to consolidation of clay layers and compaction of substrata by lowering groundwater head	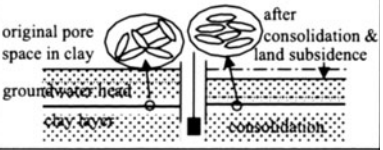
Oxygen deficient air in the unsaturated zone	Oxidation of organic materials and the iron with simultaneous groundwater head lowering results in oxygen deficit air in the unsaturated zone. There is a risk of workers death due to suffocation if oxygen deficient air flows into excavation sites	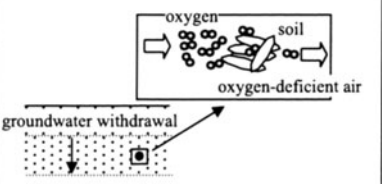
Seawater intrusion	Seawater intrusion is common in coastal aquifers due to density differences between fresh and seawater ($\rho_s > \rho_f$, where ρ_s, ρ_f = densities of seawater and freshwater, respectively). Pumping wells near coasts cause seawater intrusion	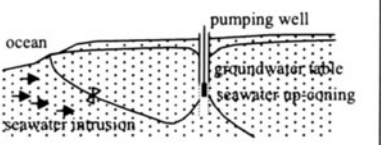
Unexpected groundwater recovery/rise	Unexpected groundwater rise brings instability in underground spaces and structures, which may result in ground liquefaction if an earthquake occurs	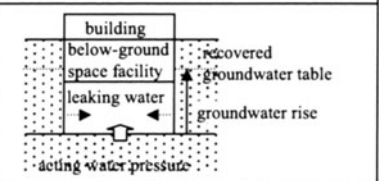
Groundwater pollution	Groundwater pollution poses a threat to groundwater resource	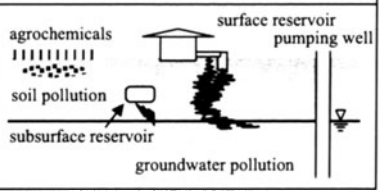

3.97 km^3 (31%), agriculture and fish farming used 4.63 km^3 (36%), and towns and cities used 4.31 km^3 (33%) (Ministry of Land, Infrastructure and Transport, Japan, 2003). The percentage of groundwater used in the total water use of 87.0 km^3 was 15%.

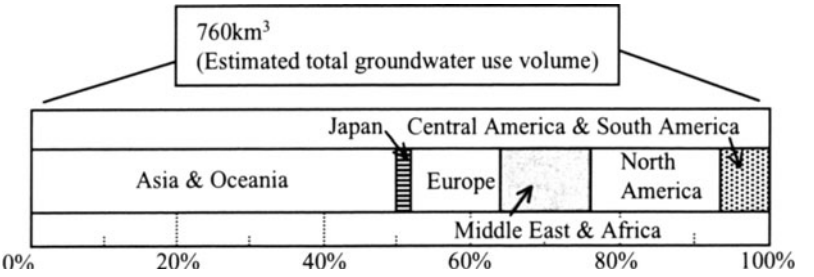

Fig. 7.2. World groundwater use in the world (UNDP, 2001)

The amount of freshwater used around the world was approximately 3500 km^3 in 1990 (UNDP, 2001). Of this amount, 760 km^3, about 20%, was groundwater. The amount of groundwater used in Asia and Oceania (excluding Japan) was just under 400 km^3, around 50% of the total groundwater used (**Fig. 7.2**). The amount of groundwater used in North America was over 100 km^3, or less than 20% of the total. The total sum of groundwater used in Europe, Middle East and Africa was around 100 km^3, or more than 10% each. The amount of groundwater used in Central America and South America, was estimated at about 50 km^3, or about 5% or more.

7.4 Groundwater Management Policies and Planning

Groundwater originates as precipitation as part of the hydrologic cycle. All peoples have been closely related to groundwater in daily life and productivity regardless of their natural and social situations. Traditionally, groundwater has been used as a water resource, but since the mid-1900s, groundwater decline, land subsidence, and salinization of groundwater in coastal areas due to excessive groundwater use have posed a social problem with advances in drilling and pumping technology. The problems occurred as a result of a rapid increase of water resource utilization in developed countries. Today, the same problems are evident in developing countries. In the late 1990s, soil and groundwater pollution became a serious problem in developed countries as a result of industrialization. Groundwater pollution has emerged as a new area of concern and by the end of the 1990s, disturbance of the groundwater environment caused by urbanization and industrialization has been reported throughout the world.

It is necessary to manage both quantity and quality in facing the present problems and in ensuring the sustainable utilization of groundwater (Friedman et al.,

1984; Schaible et al., 1999). There is a pressing need for integrated management policies for groundwater basin scaling (from hydraulic basins to regional basins and hydrologic basins) and there is an urgent need to frame management guidelines in three areas: water resources, water quality, and the groundwater environment.

Various problems related to groundwater resources or pollution occurred in the 19th century, and many are still unsolved. Our action plan to achive an integrated management policy for groundwater will be carried out in the following three steps: (1) Research and planning, (2) practice and management, and (3) monitoring and maintenance.

These steps need to be applied to the following three subjects: (1) Groundwater resources, (2) groundwater quality, and (3) conservation of the groundwater environment.

The focus of groundwater resources is recharge and storage and determination of the allowable pumping volume in accordance with the scale of the basin. The allowable pumping volume can be set for each area under criteria of groundwater levels.

Preserving groundwater quality in keeping with the water quality standards requires sound policies for groundwater conservation. Conservation of the groundwater environment is urged to avoid groundwater deterioration such as the disappearance of springs or spouted ponds as a result of urbanization and construction.

7.4.1 Groundwater Management Policies

Optimal groundwater management is essential for sustainable extraction and to minimize related socioenvironmental problems such as land subsidence, groundwater pollution, and drought. The concept of groundwater management is discussed in the following section.

Many groundwater management-related problems are solved using numerical models under managing constraints. Decision variables and constraints have to be defined in this technique. The quantity of water to be developed and the required water and its head have been dealt with under imposed constraints (Wanakule et al., 1986; Magnouni & Treichel, 1994). Then, the optimum groundwater pumping rate, recharge rate, and distributions in the basin have been estimated by solving groundwater flow equations numerically (Bear, 1979). Financial aspects and risk can also be examined by management constraints (Karatzas & Pinder, 1996; Schaible, 1999). Impacts of contaminated water recharge and dispersion into an aquifer can be estimated using the finite-element method. Then, optimal recharge/exploitation rates and schedules can be decided based on the groundwater quality response (Willis, 1979; Reed et al., 2000).

Human activities can have negative impacts on the groundwater environment, which may ultimately result in serious consequences to us, and bring about ecological imbalances. Groundwater resource management is a tool to minimize and prevent groundwater-related problems. The most efficient and economical management plan is called "the best policy" (see **Fig. 7.3a**). The managing criteria and constraints, as well as the goal period, are some of the factors that must be duly con-

sidered in deciding the best policy. Management decides the factors to be controlled, e.g., installation capacities and pumping rates. Water quality in aquifers, streams, lakes, and their surroundings are controlled to protect the groundwater environment. These are called the decision variables in groundwater management.

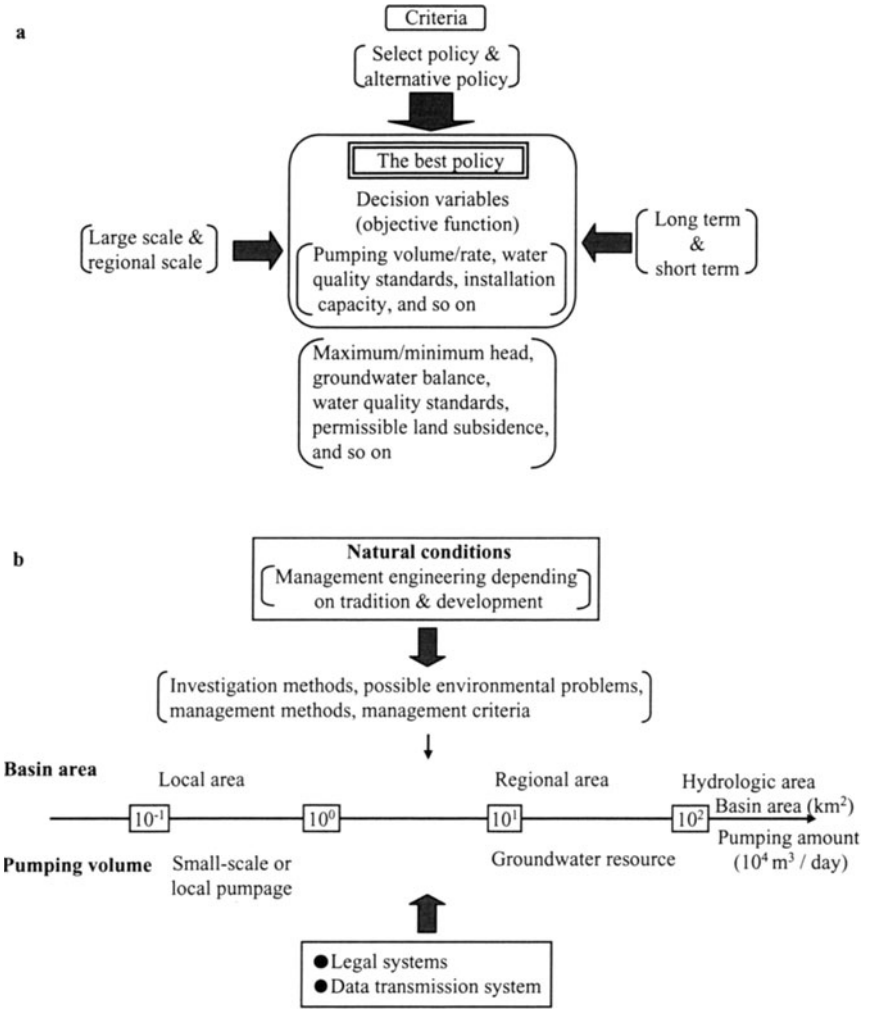

Fig. 7.3 a, b. Concept of groundwater management policy. **a** process of groundwater management, **b** scaling of groundwater management

Limitation constraints have a direct influence on deciding the best policy, and these determine the optimum levels of the variables to be decided. Laws regulate maximum/minimum groundwater heads, spring discharges, tolerable land subsidence,

and water quality standards as limitation constraints. The policy of groundwater management is dependent upon whether the planning period is longterm or shortterm. Similarly, it relates to the expansion of basins based on hydrological conditions as shown in **Fig. 7.3b**.

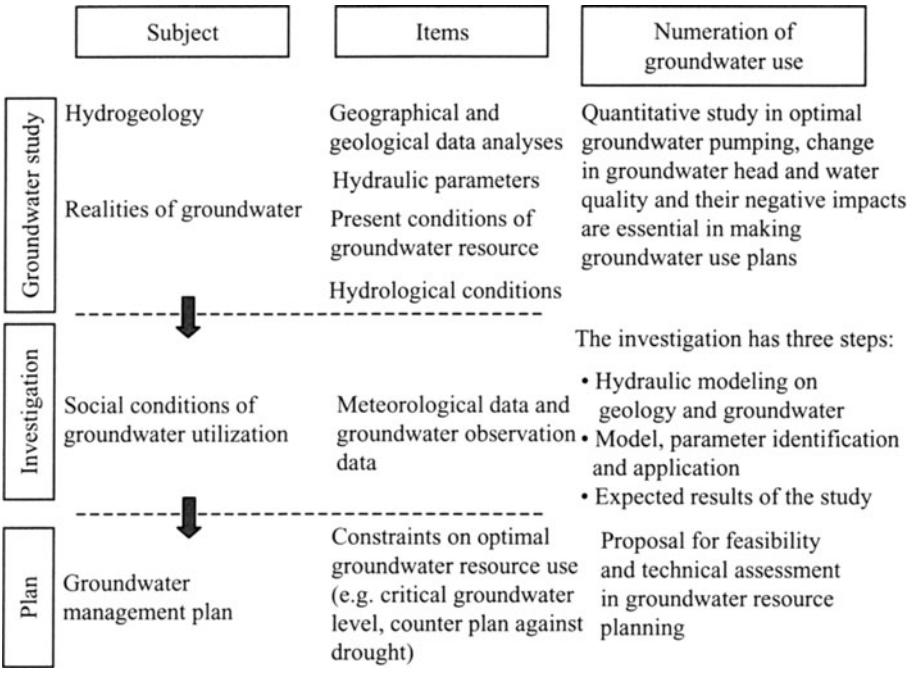

Fig. 7.4. Groundwater investigation and planning processes

Three different scales for groundwater basins are considered: local basins with a size of several hundred meters, regional basins with a size of tens of kilometers, and hydrological basins that stretch over several hundreds of kilometers. The allowable pumping volumes in these basins are estimated at several thousand cubic meters per day, more than a hundred thousand cubic meters per day, and millions of cubic meters per day, respectively. Management engineering, i.e., management methods and criteria, and legal systems will depend on tradition, developmental goals, and hydrogeological view point.

(a) Groundwater Investigation and the Planning Process

The actual groundwater state in a basin is related to geographic, geologic, weather, and land-use conditions of the area. Therefore, groundwater development plans should be made for individual basins. The quantity of water to be drawn and local hydrogeologic conditions must be known beforehand. A groundwater development plan

mainly consists of three stages: surveying, prediction and feasibility study, as shown in **Fig. 7.4**. The estimation of field characteristics, the collection of observed groundwater head data, and the setting of conditions for optimal groundwater use are carried out in sequence.

(b) Optimization in Groundwater Management

Research on the prevailing conditions, the management approach, and planning proceeds from assessing whether the present groundwater use is optimal or not in quantity and quality. Focusing policy on future prospects is indispensable in making the groundwater management plan. Some typical groundwater optimization techniques are briefly discussed here.

A mathematical optimization approach gives the optimal pumping volume and its distribution over a basin. Environmental conservation and political and financial aspects have to be duly considered in the process. In this approach, optimization is carried out using governing equations with mass conservation and Darcy's law under given conditions to maximize/minimize an objective function. A simulation management model coupled with linear programming consists of (a) aquifer and groundwater flow models, (b) constraints, (c) the objective function, and (d) boundary conditions.

Hydraulic models of multiple-well systems, cell models, and numerical simulation models are adopted to optimize well theory and regional allocation of pumping volume. Numerical simulation is employed to estimate groundwater flow. Optimization based on these models has to satisfy imposed conditions such as critical head and allowable pumping volume.

A typical mathematical formulation for groundwater flow is as follows:

$$\frac{\partial}{\partial x}\left(k_x \frac{\partial h}{\partial x}\right) + \frac{\partial}{\partial y}\left(k_y \frac{\partial h}{\partial y}\right) + \frac{\partial}{\partial z}\left(k_z \frac{\partial h}{\partial z}\right) = S_s \frac{\partial h}{\partial t} + W \tag{7.1}$$

where h = hydraulic head, k_x, k_y, k_z = permeability in the x-, y-, and z-directions, respectively; S_s = specific storage; t = time; and W = summation of pumping, recharge, and leakage in unit time and area. Equation 7.1 reduces to a set of simultaneous equation with n unknowns (from finite-difference/finite element analysis) at the steady state ($\partial/\partial t = 0$).

(c) Linear Programming

Linear programming is used for solving an optimal allocation problem of limited resources. The optimizing principle is to minimize (or maximize) an objective function (z), which is obtained by summing decision variables (x_i) with weighting constants $c_1, c_2, c_3, \ldots, c_n$ in a set of equations. The objective function (z) can be written as follows (Bear, 1979):

$$z = c_1x_1 + c_2x_2 + c_3x_3 + \cdots + c_nx_n \rightarrow \begin{matrix}\text{minimize}\\ \text{or}\\ \text{maximize}\end{matrix} \tag{7.2}$$

The constraint equations are:

$$\begin{aligned} &a_{i1}x_1 + a_{i2}x_2 + \cdots + a_{ir}x_r \begin{pmatrix} \geq \\ = \\ \leq \end{pmatrix} b_i, \quad i = 1, 2, \ldots, m \\ &x_j \geq 0, \quad j = 1, 2, \ldots, r \quad \text{(nonnegative condition)} \end{aligned} \tag{7.3}$$

where a_{ij}, b_i and c_i are constants whose values are known. The simplex method is often employed to solve linear programming problems.

The management constraints are distinguished from initial and boundary conditions in groundwater motion. Some typical constraints, for example, are:

$$Q_{it(\min)} \leq Q_{it} \leq Q_{it(\max)}, \quad q_{it(\min)} \leq q_{it} \leq q_{it(\max)} \tag{7.4}$$

$$\begin{aligned} Q_t &= Q_{1t} + Q_{2t} + Q_{3t} + \cdots + Q_{Nt} = \sum Q_{it} \\ &= A_1 q_{1t} + A_2 q_{2t} + A_3 q_{3t} + \cdots + A_N q_{Nt} = \sum A_i q_{it} \end{aligned} \tag{7.5}$$

where Q_{it}, $q_{it} \geq 0$, Q_t = total pumping/recharge rate at time (t), Q_{it} = pumping rate in the ith sub-basin at time (t), A_i = area of ith sub-basin, q_{it} = pumping/recharge rate in unit area in time (t), and the subscripts min/max are for specified minimum/maximum values. The constraints show that total pumping rate (Q_t) at time (t) is obtained by summing pumping rates (Q_{it}) in all the sub-basins with the $Q_{it(\min)} \leq Q_{it} \leq Q_{it(\max)}$ condition.

Furthermore, the following condition has to be satisfied to introduce additional constraints with respect to hydraulic head in sub-basin (i):

$$h_{c(it)} \leq h_{it} \leq h_{it(\max)} \tag{7.6}$$

where $h_{c(it)}$ = specified critical hydraulic head.

The constraints of Eq. 7.5 and the objective function will be the same if the pumping rate (Q_{it}) in the former is replaced by pumping cost ($C_t = a_{it}Q_{it}$, where a_{it} = conversion rate of pumping cost corresponding to pumping rate). The objective function can be written as:

$$C_t = a_{1t}Q_{1t} + a_{2t}Q_{2t} + a_{3t}Q_{3t} + \cdots + a_{Nt}Q_{Nt} \rightarrow \min. \tag{7.7}$$

Thus, the total distributed optimal groundwater pumping rate in a basin can be obtained by solving the governing flow equation and objective function under the given constraints.

7.5 Groundwater Resource Management for Large Basins

Investigation results and observed data are very important in choosing pertinent techniques, such as numerical analysis, in addition to imposing evaluation criteria. An example of the fluctuation patterns in hydraulic head and land subsidence as shown in **Fig. 7.5a** is presented here.

Annual changes in pumping rate have an impact on groundwater head over long periods, and short-term changes give seasonal variations because of recharge and pumping. Both long- and short-term changes in groundwater head, pumping rate, and recharge are responsible for well drying and land subsidence/rebounding.

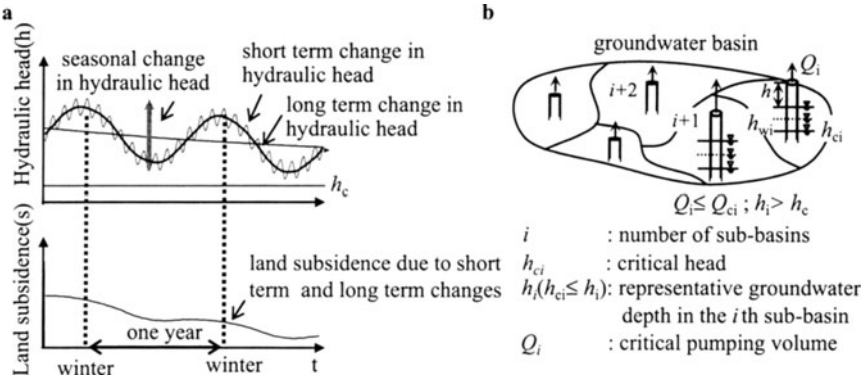

Fig. 7.5. Typical field data (a) and optimal groundwater resource allotment (b)

Long-term changes in groundwater head reveal the trend in land subsidence year by year. However, short-term changes, especially during drought, result in severe land subsidence even if the annual groundwater head is maintained at the average level. Therefore, control of groundwater head fluctuation within tolerable limits in both the long and short-term is the best preventive measure against land subsidence.

Techniques based on practical experience, statistical analysis, numerical simulation, or combinations there are very useful in maintaining groundwater head fluctuations within tolerable limits. These techniques can be applied to the allotment of optimal pumping rates in a target basin. The target basin is divided into small sub-basins and a critical head (h_{ci}) is set for each. **Fig. 7.5b** shows an illustration of optimal pumping distribution in a basin.

Warning and critical heads are set to limit regional water demand so as to minimize seasonal and annual land subsidence. An online system of head and land subsidence monitoring using telemeters is an effective technique in groundwater management as shown in **Fig. 7.6** (Sato, 2000). The telemeter system records data collected by groundwater head and land subsidence measuring methods, data is processed by personal computer, and information is transmitted to facilitate groundwater extraction regulation.

Many numerical simulation codes for planning and managing groundwater resource have been proposed with the popularization of personal computers. For example, MODFLOW (McDonald and Harbaugh, 1988; Harbaugh and McDonald, 1996a and 1996b) was developed in USA. PMPATH (Chiang and Kinzelbach, 1994 and 1998), MT3D (Zheng, 1996) for contaminant transport and PEST (Doherty et al., 1994) for parameter optimization based on MODFLOW were developed. These

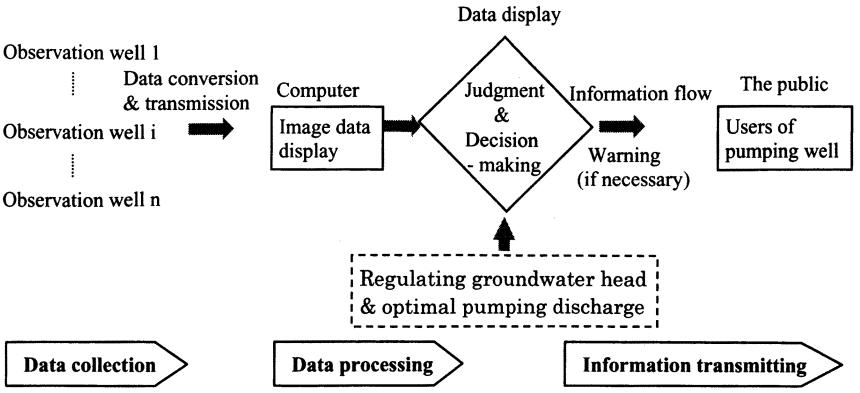

Fig. 7.6. System flow diagram for groundwater resource protection and land subsidence prevention

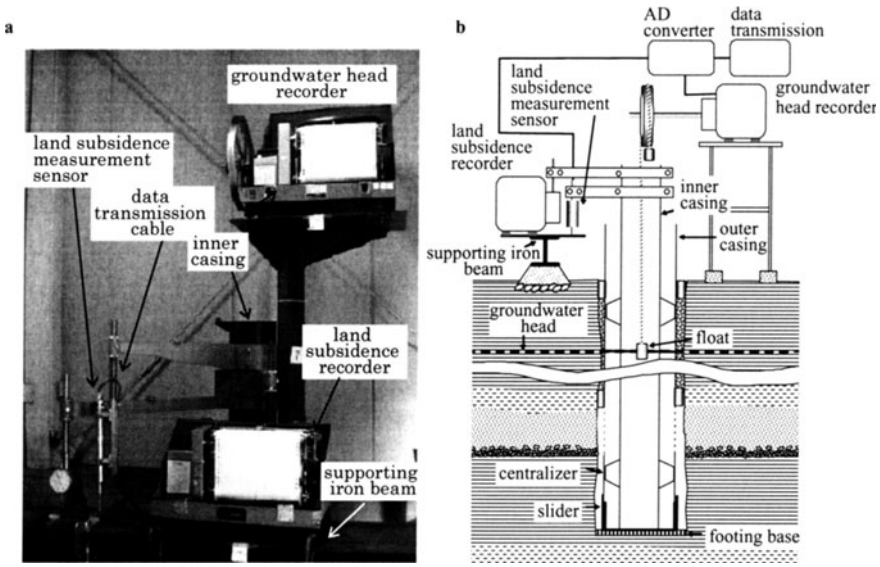

Fig. 7.7 a, b. An example of observation well (Koshigaya, Saitama, Japan). **a** Picture of observation well and measurement system, **b** Structure of groundwater well and data recording and transmission devices

codes have been used for solving problems of groundwater management from the end of the 1990s in Japan.

7.6 Monitoring

Monitoring groundwater data, such as head levels, land subsidence, and water quality, is very important in realizing sustainable groundwater management. A large number of observation wells (more than 1000) have been drilled in Japan for monitoring, as shown in **Fig. 7.8**. Many observation wells are located in those regions where groundwater-related problems such as land subsidence, and seawater intrusion have had serious impacts.

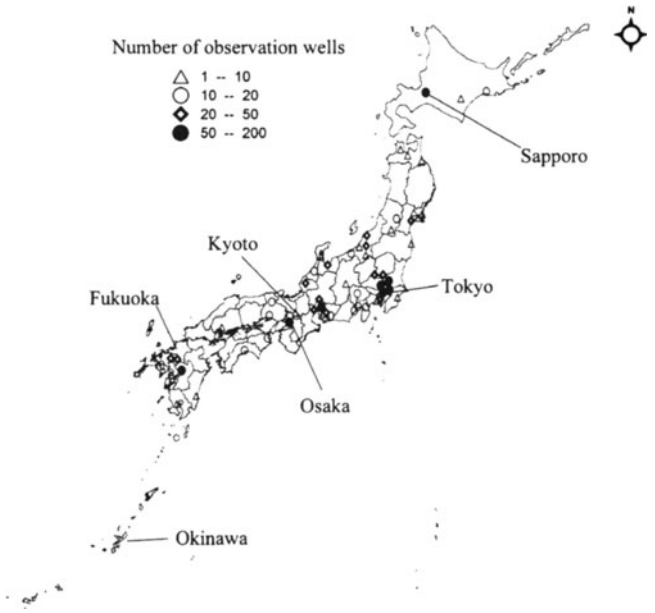

Fig. 7.8. Distribution of observation wells in Japan to monitor hydraulic head and land subsidence (The Ministry of the Environment, Japan 2001)

Exercises

[Ex. 7.1]
Figure E7.1 shows some observed time series in groundwater head throughout the year at three different sites. Discuss the characteristics of these data and the possibility of land subsidence.

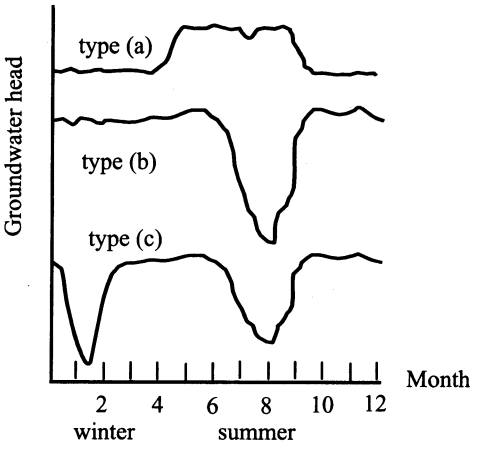

Fig. E7.1 Changes in groundwater head (or table) throughout the year

[Ex. 7.2]
The groundwater discharge rate, water head and land subsidence at a pumping station site for the last one-decade are shown in **Fig. E7.2** and **Table E7.1**. Answer the following questions based on the information given in the figure and table.

1. Present a correlation between minimum groundwater head and land subsidence in graphical form. Also, estimate the minimum groundwater head for zero land subsidence.
2. Show a graphical correlation between discharge and land subsidence and determine the discharge rate when land subsidence is zero.
3. Show a graphical correlation between discharge and minimum groundwater head.

References

Bear J (1979) Hydraulics of groundwater. McGraw-Hill, N.Y., pp 491–512
Chiang WH and Kinzelbach W (1994) PMPATH for Windows. User's manual. Scientific Software Group, Washington DC

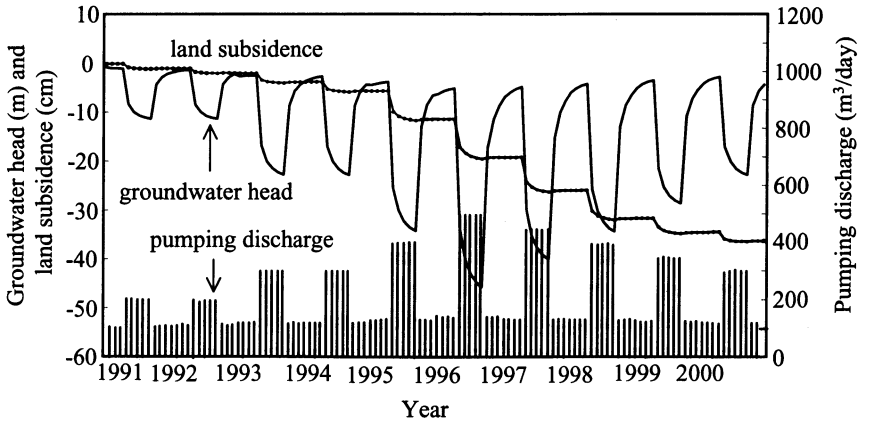

Fig. E7.2 Change in pumping discharge, groundwater head and land subsidence throughout the last decade

Table E7.1 Transition in pumping discharge, groundwater head, and land subsidence throughout a decade

Year	Discharge (m^3/year)	Minimum groundwater head (m)	Total land subsidence (cm)	Land subsidence (cm/year)
1991	53,838	−11.401	−1.140	−1.140
1992	53,838	−11.426	−2.047	−0.907
1993	71,175	−22.827	−4.033	−1.986
1994	71,175	−22.852	−5.848	−1.814
1995	88,513	−34.253	−11.751	−5.904
1996	105,850	−45.678	−19.566	−7.815
1997	97,181	−40.003	−26.191	−6.625
1998	88,513	−34.291	−31.858	−5.667
1999	79,844	−28.578	−34.774	−2.917
2000	71,175	−22.865	−36.522	−1.747

Chiang WH and Kinzelbach W (1998) PMPATH 98. An advective transport model for processing MODFLOW,U.S. Geological Survey, USA

Doherty J, Brebber L and Whyte P (1994) PEST Model-independent parameter estimation. User's manual. Watermark Computing, Australia

Friedman R, Ansell C, Diamond S and Haimes YY (1984) The use of models for water resources management, planning and policy. Water Resource Res 20: 793–802

Harbaugh AW and McDonald MG (1996a) User's documentation for MODFLOW-96, an update to the U.S. Geological Survey modular three-dimensional finite differences groundwater flow model, U. S. Geological Survey, Open-file report, pp 96–485

Harbaugh AW and McDonald MG (1996b) Programmer's documentation for MODFLOW-96, an update to U.S. Geological Survey modular three-dimensional finite differences groundwater flow model. U. S. Geological Survey, Open-file report, pp 96–486

Karatzas GP and Pinder GF (1996) The solution of groundwater quality managemnet problems with a nonconvex feasible reasion using a cutting plane optimization technique. Water Resource Res 32: 1091–1100

McDonald MG and Harbaugh AW (1988) MODFLOW, A modular three-dimensional finite difference groundwater flow model, U. S. Geological Survey, Open-file report, pp 83–875, Chapter A1

Magnouni SE and Treichel W (1994) A multicriterion approach to groundwater management. Water Resource Res 30: 1881–1895

The Ministry of the Environment, Japan (2001) Homepage:http://www.env.go.jp/water/jiban/index.html

The Ministry of Land, Infrastructure and Transport, Japan (2003) Water resources in Japan (in Japanese)

National Land Agency, Japan (2000) Interim report of committee on groundwater use (in Japanese), p 29

Reed P. Minsker B and Valocchi AJ (2000) Cost-efective long-term groundwater monitoring design using a genetic algorithm and global mass interpolation. Water Resource Res 36: 3731–3741

Wanakule N N, Mays LW, and Lasdon LS (1986) Optimal management of large-scale aquifers, Methodology and applications. Water Resource Res 22: 447–465

Willis R (1979) A planning model for the management of groundwater quality. Water Resource Res 15: 1305–1312

Sato K (2000) A new control system of groundwater resource. Groundwater updates. Springer, Tokyo, p 15

Schaible GD (1999) The Edwards Aquifer water resource conflict: USDA farm program resource-use incentives. Water Resource Res 35: 3171–3183

United Nations Development Program Report (2001) World Resources.

Zheng C (1996) MT3D Version DOD-1.5. A modular three-dimensional transport model. The Hydrogeology Group, University of Alabama

Answers

Chapter 1

[Ans. 1.1]
The hydrologic balance is realized in:

$$(1-h)\times(0.15-0.1)+h(0.4-0.1)=0.04\times 2$$
$$\therefore \quad h=0.12\,\mathrm{m}$$

[Ans. 1.2]
The continuity equation for the tank model is given by:

$$Q\,dt=-n_eA\,dh \tag{A1.2.1}$$

where A = tank cross-section, $h(t)$ = water level, Q = discharge, n_e = effective porosity.

Assuming that the discharge Q is proportional to h:

$$Q=\lambda h, \quad \lambda=\text{constant} \tag{A1.2.2}$$

Combining Eqs. A1.2.1 and A1.2.2, we get the following:

$$\lambda h\,dt=-n_eA\,dh \quad \text{or} \quad -(n_eA/\lambda)dh/h=dt$$
$$\therefore \quad -(n_eA/\lambda)\log h=t+C$$

Assuming $h=h_0$, $Q=Q_0$ ($Q_0>Q$) for $t=t_0$, the following equation is obtained:

$$-(n_eA/\lambda)\log h_0=t_0+C$$
$$\therefore \quad t-t_0=(n_eA/\lambda)\log(h_0/h)=(n_eA/\lambda)\log(Q_0/Q)$$
$$\therefore \quad Q(t)=Q_0e^{-\frac{\lambda}{n_eA}(t-t_0)} \tag{A1.2.3}$$

Equation A1.2.3 shows the basis of the hydrograph (the relationship between discharge and time).

Chapter 2

[Ans. 2.1]

Bernoulli's theorem can be extended for seepage flow as shown here. The equation of motion is expressed as follows (see **Fig. A2.1**):

$$\left\{p-\left(p+\frac{\partial p}{\partial s}ds\right)\right\}A-\rho\,ds\,Ag\frac{\partial z}{\partial s}-\rho\,ds\,Ag\frac{\partial h_r}{\partial s}$$
$$=-\frac{\partial p}{\partial s}ds\,A-\rho\,ds\,Ag\frac{\partial z}{\partial s}-\rho\,ds\,Ag\frac{\partial h_r}{\partial s} \qquad \text{(A2.1.1)}$$

where p = pressure, ds = infinitesimal length of a stream tube, A = sectional area of stream tube, ρ = density of fluid, g = acceleration due to gravity, z = elevation, h_r = frictional head loss.

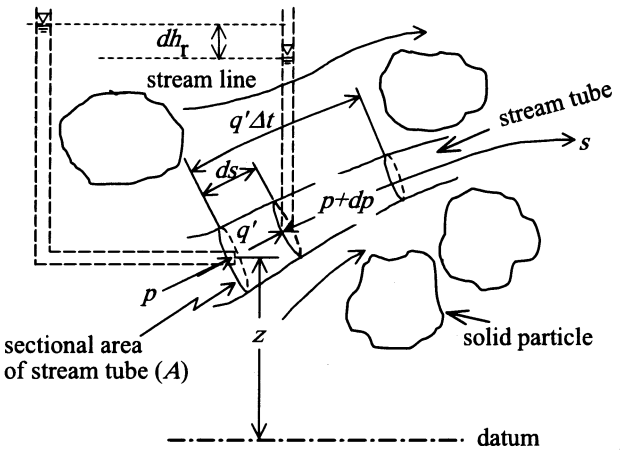

Fig. A2.1 Fluid flow in saturated porous media

Acceleration α_s is derived from the total differential of velocity $q'(s,t)$ as follows:

$$\alpha_s=\lim_{\Delta t\to 0}\frac{\Delta q'}{\Delta t}=q'\frac{\partial q'}{\partial s}+\frac{\partial q'}{\partial t} \qquad \text{(A2.1.2)}$$

Therefore, the equation of motion is written as:

$$\rho\,ds\,A\alpha_s=-\frac{\partial p}{\partial s}ds\,A-\rho\,ds\,Ag\frac{\partial z}{\partial s}-\rho\,ds\,Ag\frac{\partial h_r}{\partial s}$$
$$\therefore\quad \frac{1}{g}\frac{\partial q'}{\partial t}+\frac{\partial}{\partial s}\left(\frac{q'^2}{2g}\right)+\frac{1}{\rho g}\frac{\partial p}{\partial s}+\frac{\partial z}{\partial s}+\frac{\partial h_r}{\partial s}=0 \qquad \text{(A2.1.3)}$$

As the flow velocity is very small ($q'^2/2g \to 0$), then for steady flow:

$$\frac{d}{ds}\left(\frac{p}{\rho g}+z\right)=-\frac{dh_r}{ds},\quad \left(\frac{p_1}{\rho g}+z_1\right)-\left(\frac{p_2}{\rho g}+z_2\right)=\Delta h_r \tag{A2.1.4}$$

[Ans. 2.2]

If $u\,dx+v\,dy=0$ is an exact differential equation, then

$$u\,dx+v\,dy=\frac{\partial\psi}{\partial x}dx+\frac{\partial\psi}{\partial y}dy\quad\left(u=\frac{\partial\psi}{\partial x},\ v=\frac{\partial\psi}{\partial y}\right)$$

$$\therefore\quad \frac{\partial u}{\partial y}=\frac{\partial^2\psi}{\partial y\partial x}=\frac{\partial^2\psi}{\partial x\partial y}=\frac{\partial v}{\partial x} \tag{A2.2.1}$$

Equation A2.2.1 is the necessary condition.

Meanwhile, if $\partial u/\partial y=\partial v/\partial x$ and the integral of u in $y=$ constant, then, let $F=\int u\,dx$ [where $F(x,y)$ is an arbitrary function].

$$\frac{\partial F}{\partial x}=u,\quad \frac{\partial^2 F}{\partial y\partial x}=\frac{\partial u}{\partial y}=\frac{\partial v}{\partial x}$$

Therefore,

$$\frac{\partial}{\partial x}\left[\frac{\partial F}{\partial y}-v\right]=0,\quad \frac{\partial F}{\partial y}-v=f(y),\quad v=\partial F/\partial y-f(y)$$

$$\therefore\quad u\,dx+v\,dy=\frac{\partial F}{\partial x}dx+\left[\frac{\partial F}{\partial y}-f(y)\right]dy$$

$$=dF-f(y)dy=d\left[F-\int f(y)dy\right] \tag{A2.2.2}$$

Equation A2.2.2 is the sufficient condition for $u\,dx+v\,dy=0$ to be an exact differential equation.

[Ans. 2.3]

Differentials of $\phi(x,y)=$ constant and $\psi(x,y)=$ constant with respect to x are:

$$\frac{\partial\phi}{\partial x}+\frac{\partial\phi}{\partial y}\left(\frac{\partial y}{\partial x}\right)_\phi=0,\quad \frac{\partial\psi}{\partial x}+\frac{\partial\psi}{\partial y}\left(\frac{\partial y}{\partial x}\right)_\psi=0 \tag{A2.3.1}$$

while the Cauchy Riemann equation is given as:

$$\frac{\partial\phi}{\partial x}=\frac{\partial\psi}{\partial y},\quad \frac{\partial\phi}{\partial y}=-\frac{\partial\psi}{\partial x}$$

$$\therefore\quad \frac{\partial\phi}{\partial x}\frac{\partial\psi}{\partial x}=\frac{\partial\psi}{\partial y}\frac{\partial\psi}{\partial x},\quad \frac{\partial\phi}{\partial y}\frac{\partial\psi}{\partial y}=-\frac{\partial\psi}{\partial x}\frac{\partial\psi}{\partial y} \tag{A2.3.2}$$

Then,

$$\frac{\partial\phi}{\partial x}\frac{\partial\psi}{\partial x}+\frac{\partial\phi}{\partial y}\frac{\partial\psi}{\partial y}=0 \tag{A2.3.3}$$

Substituting Eq. A2.3.1 into Eq. A2.3.3, we get the following:

$$\frac{\partial\phi}{\partial y}\frac{\partial\psi}{\partial y}\left[\left(\frac{\partial y}{\partial x}\right)_{\phi}\left(\frac{\partial y}{\partial x}\right)_{\psi}+1\right]=0$$

$$\therefore \quad \left(\frac{\partial y}{\partial x}\right)_{\phi}\cdot\left(\frac{\partial y}{\partial x}\right)_{\psi}=-1 \tag{A2.3.4}$$

Equation A2.3.4 shows that the directional cosine of $\phi(x, y)$ = constant and $\psi(x, y)$ = constant cross each other at right angles.

[Ans. 2.4]

The static forces acting on a dam shown in **Fig. E2.1** are: total water pressure (P), weight of the dam (W), and uplift (F_y). The stability of the dam should be examined as follows:

1. Resistance to sliding force: $F_x > P$
2. $W > F_y$
3. $M = Wx_1 - (Py_1 + F_y x_2)$, $M > 0$
4. Anti-sand boiling measures at the tail of the dam (for example, a filter layer)

The water pressure distribution (p_u) to the dam bottom and uplift force (F_y) are expressed as follows:

$$\frac{p_u}{\rho g}=h_2+\frac{H}{\pi}\cos^{-1}\left(\frac{x}{L}\right)\approx\frac{H}{\pi}\cos^{-1}\left(\frac{x}{L}\right)$$

$$\frac{F_y}{\rho g}=\int_{-L}^{L}p_u\,dx\approx HL, \quad p_u = \text{uplifting water pressure}$$

where $y_1 = h_1/3 \approx H/3$, $x_2 \approx 2L/3$, $x_1 \approx 2L/3$.

[Ans. 2.5]

From the principle of linear superposition, velocity potential $\phi(x, y)$ at an arbitrary point $P(x, y)$ is given as:

$$\phi = kh = \sum_{i=1}^{n}\frac{Q_i}{2\pi b}\log\frac{r}{r_i}+\text{constant}, \quad r=\sqrt{(x-x_i)^2+(y-y_i)^2} \tag{A2.5.1}$$

where k = permeability, h = head, and b = thickness of confined aquifer.

In the vicinity of the jth well:

$$\phi_j = kh_j = \sum_{i=1}^{\tilde{n}}\frac{Q_i}{2\pi b}\log\frac{r_{ij}}{r_i}+\text{constant} \tag{A2.5.2}$$

where $\sum_{i=1}^{\tilde{n}}$ = summation of $i = 1, 2, 3, \ldots, n$ (except $i = j$).

Assuming the head at R ($\gg r$) to be H, we obtain the following:

$$\phi_{r\to R} = kH = \sum_{i=1}^{n}\frac{Q_i}{2\pi b}\log\frac{R}{r_i}+\text{constant} \tag{A2.5.3}$$

From Eqs. A2.5.2 and A2.5.3, we get the following:

$$k(H - h_j) = \sum_{i=1}^{n} \frac{Q_i}{2\pi b} \log \frac{R}{r_i} - \sum_{i=1}^{n} \frac{Q_i}{2\pi b} \log \frac{r_{ij}}{r_i} \tag{A2.5.4}$$

Equation A2.5.4 can be written as follows for $n = 2$:

$$2\pi bk(H - h_1) = Q_1 \log \frac{R}{r_1} + Q_2 \log \frac{R}{r_{21}}$$
$$2\pi bk(H - h_2) = Q_1 \log \frac{R}{r_{12}} + Q_2 \log \frac{R}{r_2}$$

Q_1 and Q_2 are determined by solving the simultaneous equations.

[Ans. 2.6]

1. Piezometric head (h_B) at point B:

$$Q_1 = b_1 k_1 \frac{(h_1 - h_B)}{h_1} \sin\theta_1, \quad Q_2 = b_2 k_2 \frac{(h_B - h_2)}{h_2} \sin\theta_2$$

where Q_1 and Q_2 are discharges between fault AB and BC, respectively.

From the continuity relationship ($Q = Q_1 = Q_2$):

$$h_B = \frac{h_1(1+f)}{\left(1 + f\frac{h_1}{h_2}\right)}, \quad f = \frac{b_2 k_2 \sin\theta_2}{b_1 k_1 \sin\theta_1}$$

2. The conditions for the spring to persisting are as follows:

$$Q > 0, \quad h_1 > h_2, \quad Q = Nb_1$$

where N = natural recharge rate per unit area and time.

Chapter 3

[Ans. 3.1]

Saltwater concentration $C(x, y)$ is measured using an electric conductivity meter, as shown in **Fig. A3.1**. The measured relative concentration values (C/C_0, where C_0 is initial concentration) are plotted at $x = x_1$ in the figure. The dispersion equation at the steady state is written as follows:

$$u' \frac{\partial C}{\partial x} = D_T \frac{\partial^2 C}{\partial y^2} \tag{A3.1.1}$$

The boundary conditions are:

$$\left.\begin{aligned} &C(0, y) = C_0, && -\infty < y \le 0 \\ &C(0, y) = 0, && 0 < y < +\infty \\ &\frac{\partial C}{\partial y} = 0, && y = \pm\infty \end{aligned}\right\} \tag{A3.1.2}$$

Solution of the above equation is given by:

$$\frac{C}{C_0} = \frac{1}{2}\,\mathrm{erfc}\left(\frac{y}{2\sqrt{D_T x/u'}}\right) \tag{A3.1.3}$$

where erfc X = 1 − erf X, erf X = error function, D_T = coefficient of transverse dispersion, u' = real pore velocity in the x-direction. D_T is identified from the best fit solution curve with measured C/C_0 values.

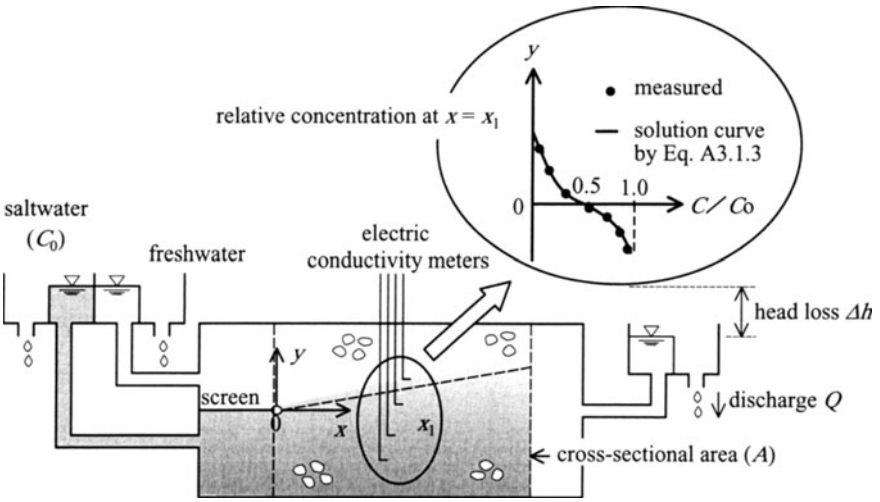

Fig. A3.1 Experimental determination of transverse dispersion coefficient

[Ans. 3.2]

Gas and liquid molecules have continuous random movement (**Fig. A3.2**). The velocity of the molecules increases with rises in temperature (T) or pressure (p).

When some solute molecules are injected into a groundwater flow field, solute molecules gradually scatter as a result of collisions with water molecules. This phenomenon is called molecular diffusion, which occurs both in gas and water. Einstein's diffusion equation is expressed as:

$$\frac{\partial C}{\partial t} = D_M \frac{\partial^2 C}{\partial x^2} \tag{A3.2.1}$$

where C = concentration and D_M = coefficient of molecular diffusion.

[Ans. 3.3]

The coefficient of longitudinal dispersion (D_L) is proportional to the product of grain size (d_m) and pore velocity (u') in a homogeneous aquifer ($D_L \propto d_m q'$) for $q' \approx u'$. Similarly, $D_T \propto d_m v'$.

The dispersion phenomenon in a homogeneous aquifer is called mechanical dispersion to distinguish it from molecular diffusion (refer to **Ex. 3.2**). However, an

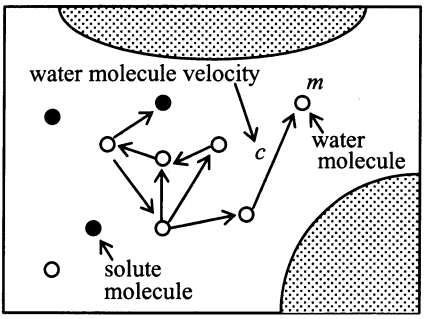

Fig. A3.2 Mechanism of solute diffusion

inhomogeneous aquifer consists of several layers with different grain diameter; therefore, pore velocity (q') and dispersion coefficients (D_L and D_T) vary in each layer.

This is the reason why microscopic and macroscopic dispersions should be distinguished. This relates to the expression of representative velocity (q' or Darcy velocity q). For a homogeneous aquifer: $n_e q' = q$, where n_e = effective porosity. Since the porosity varies in composed layers of an inhomogeneous aquifer, it is rational to express each representative velocity in terms of the real pore velocity.

[Ans. 3.4]

The basic equation is:

$$\frac{\partial C}{\partial t} + u' \frac{\partial C}{\partial x} = D \frac{\partial^2 C}{\partial x^2} \tag{A3.4.1}$$

Initial and boundary conditions are as follows:

$$C(x, 0) = 0 \tag{A3.4.2}$$

$$C(0, t) = f(t) \tag{A3.4.3}$$

$$C(\infty, t) = 0 \tag{A3.4.4}$$

The variable transformation is considered by:

$$C(x, t) = \Gamma(x, t) \cdot \exp[ax + bt] \tag{A3.4.5}$$

Substituting Eq. A3.4.5 into Eq. A3.4.1:

$$\frac{\partial \Gamma}{\partial t} + (u' - 2aD)\frac{\partial \Gamma}{\partial x} + (au' + b - a^2 D)\Gamma(x, t) = D \frac{\partial^2 \Gamma}{\partial x^2}. \tag{A3.4.6}$$

In Eq. A3.4.6, the values of constants a and b are obtained by solving equations: $u' - 2aD = 0$ and $au' + b - a^2 D = 0$:

$$a = \frac{u'}{2D} \quad \text{and} \quad b = -\frac{u'^2}{4D} \tag{A3.4.7}$$

Then Eq. A3.4.5 is transformed to:

$$C(x,t) = \Gamma(x,t) \cdot \exp\left(\frac{u'x}{2D} - \frac{u'^2 t}{4D}\right) \tag{A3.4.8}$$

Thus, the following equation holds from Eqs. A3.4.1 and A3.4.8

$$\frac{\partial \Gamma}{\partial t} = D\frac{\partial^2 \Gamma}{\partial x^2} \tag{A3.4.9}$$

Now, substituting Eq. A3.4.2 into Eq. A3.4.8:

$$\Gamma(x,0) \cdot \exp\left[\frac{u'x}{2D}\right] = 0$$

Then, it requires initial condition:

$$\Gamma(x,0) = 0 \tag{A3.4.10}$$

Substituting Eq. A3.4.2 into Eq. A3.4.8:

$$\Gamma(0,t) \cdot \exp\left[-\frac{u'^2 t}{4D}\right] = f(t)$$

$$\Gamma(0,t) = f(t) \cdot \exp\left[\frac{u'^2 t}{4D}\right] \tag{A3.4.11}$$

Similarly, substituting Eq. A3.4.4 into Eq. A3.4.8:

$$\Gamma(\infty,t) = 0 \tag{A3.4.12}$$

As a result, Eqs. A3.4.1–A3.4.4 are transformed into Eqs. A3.4.9–A3.4.12.

Let us derive a required solution of Eq. A3.4.9 by superposing linearly an elementary solution (a response function) satisfying a unit step function $\Gamma_0(0,t) = 1$ on given boundary condition $\Gamma(0,t) = f(t)\exp[u'^2 t/4D]$ (Duhamel theorem).

Initial condition:	$\Gamma_0(x,0) = 0$	(A3.4.13)
Boundary conditions:	$\Gamma_0(0,t) = 1$	(A3.4.14)
	$\Gamma_0(\infty,t) = 0$	(A3.4.15)

where the subscript 0 denotes initial and boundary conditions for a unit step function.

Laplace transformation of Eq. A3.4.9 is given by:

$$\mathcal{L}[\Gamma_0] = \int_0^\infty \Gamma_0(x,t)e^{-st}\,dt = Y(x,s)$$

$$\mathcal{L}\left[\frac{\partial \Gamma_0}{\partial t}\right] = s\mathcal{L}[\Gamma_0] - \Gamma_0(x,0) = sY(x,s) - \Gamma_0(x,0) = sY(x,s)$$

Now, using the following equation:

$$\mathcal{L}\left[D\frac{\partial^2 \Gamma_0}{\partial x^2}\right] = D\frac{d^2 Y}{dx^2}$$

Laplace transformation of Eqs. A3.4.9, A3.4.14, and A3.4.15 are:

$$D\frac{d^2Y}{dx^2} - sY = 0 \tag{A3.4.16}$$

$$Y(0,s) = \int_0^\infty \Gamma_0(0,t)e^{-st}\,dt = \int_0^\infty 1 \cdot e^{-st}\,dt = 1/s \tag{A3.4.17}$$

$$Y(\infty,s) = \int_0^\infty \Gamma_0(\infty,t)e^{-st}\,dt = \int_0^\infty 0 \cdot e^{-st}\,dt = 0 \tag{A3.4.18}$$

The general solution of Eq. A3.4.16 is as follows:

$$Y(x,s) = c_1(s)e^{-qx} + c_2(s)e^{qx} \tag{A3.4.19}$$

where $q = \sqrt{s/D}$.

From Eq. A3.4.18, $c_2(s) = 0$, and $c_1(s) = 1/s$ from Eq. A3.4.17.

$$\therefore \quad Y(x,s) = (1/s)e^{-qx} \tag{A3.4.20}$$

Now, using the equation, $\mathcal{L}^{-1}[Y(x,s)] = \mathcal{L}^{-1}[(1/s)e^{-\sqrt{s/D}\,x}]$, the inverse Laplace transformation of Eq. A3.4.20 is given by:

$$\Gamma_0(x,t) = 1 - \mathrm{erf}(x/2\sqrt{Dt}) = \mathrm{erfc}(x/2\sqrt{Dt}) = \frac{2}{\sqrt{\pi}}\int_{x/2\sqrt{Dt}}^\infty e^{-\eta^2}d\eta \tag{A3.4.21}$$

Equation A3.4.21 is regarded as a response function to a unit step input in time.

Thus, required solution of Eq. A3.4.9 under Eqs. A3.4.10, A3.4.11 and A3.4.12 is written by Duhamel theorem as:

$$\Gamma(0,t) = g(t) = f(t) \cdot e^{\frac{u'^2 t}{4D}} \tag{A3.4.22}$$

$$\begin{aligned}\Gamma(x,t) &= \int_0^t g(\tau)\frac{\partial \Gamma_0(x,t-\tau)}{\partial t}d\tau \\ &= \int_0^t f(\tau)\cdot e^{\frac{u'^2\tau}{4D}}\cdot\left[\frac{\partial}{\partial t}\left\{1 - \mathrm{erf}\left(\frac{x}{2\sqrt{D(t-\tau)}}\right)\right\}\right]d\tau \\ &= \int_0^t f(\tau)\cdot e^{\frac{u'^2\tau}{4D}}\cdot\left[\frac{\partial}{\partial t}\int_{x/2\sqrt{D(t-\tau)}}^\infty \frac{2}{\sqrt{\pi}}\cdot e^{-\eta^2}d\eta\right]d\tau\end{aligned} \tag{A3.4.23}$$

Now, using the following equation:

$$\frac{\partial}{\partial t}\int_{x/2\sqrt{D(t-\tau)}}^\infty \frac{2}{\sqrt{\pi}}\cdot e^{-\eta^2}d\eta = \frac{x}{2\sqrt{\pi D}(t-\tau)^{3/2}}\cdot\exp\left(-\frac{x^2}{4D(t-\tau)}\right)$$

Eq. A3.4.23 can be written as follows:

$$\Gamma(x,t) = \int_0^t f(\tau)\cdot\frac{x}{2\sqrt{\pi D}(t-\tau)^{3/2}}\cdot\exp\left(\frac{u'^2\tau}{4D} - \frac{x^2}{4D(t-\tau)}\right)d\tau \tag{A3.4.24}$$

Introducing a new parameter $\lambda = x/2\sqrt{D(t-\tau)}$,

$$\tau = t - \frac{x^2}{4D\lambda^2}, \quad d\tau = \frac{4\sqrt{D}}{x}(t-\tau)^{3/2}\,d\lambda.$$

Then, Eq. A3.4.24 can be written as:

$$\Gamma(x,t) = \frac{2}{\sqrt{\pi}}\int_{x/2\sqrt{Dt}}^{\infty} f\left(t - \frac{x^2}{4D\lambda^2}\right)\cdot \exp\left[\frac{u'^2}{4D}\left(t - \frac{x^2}{4D\lambda^2}\right)\right]\cdot e^{-\lambda^2}\,d\lambda$$
$$= \frac{2}{\sqrt{\pi}}\exp\left(\frac{u'^2 t}{4D}\right)\int_{x/2\sqrt{Dt}}^{\infty} f\left(t - \frac{x^2}{4D\lambda^2}\right)\cdot \exp\left[-\left(\lambda^2 + \frac{u'^2 x^2}{16D^2\lambda^2}\right)\right]d\lambda$$

Let $\alpha = u'x/4D$ and $\beta = x/2\sqrt{Dt}$, then:

$$\Gamma(x,t) = \frac{2}{\sqrt{\pi}}\exp\left(\frac{u'^2 t}{4D}\right)\int_{\beta}^{\infty} f\left(t - \frac{x^2}{4D\lambda^2}\right)\cdot \exp\left[-\left(\lambda^2 + \frac{\alpha^2}{\lambda^2}\right)\right]d\lambda \qquad \text{(A3.4.25)}$$

Substituting Eq. A3.4.25 into Eq. A3.4.8, we have the following:

$$C(x,t) = \frac{2}{\sqrt{\pi}}\exp\left(\frac{u'x}{2D}\right)\int_{\beta}^{\infty} f\left(t - \frac{x^2}{4D\lambda^2}\right)\cdot \exp\left[-\left(\lambda^2 + \frac{\alpha^2}{\lambda^2}\right)\right]d\lambda \qquad \text{(A3.4.26)}$$

Equation A3.4.26 is the solution of the basic Eq. A3.4.1 (after N. Hirano, 1977).

[Ans. 3.5]

Substituting $x = 10H$ and $\zeta = 0.02H$ in Eq. 3.60, we get:

$$q/k = \{H(1 + 1/\varepsilon)\}/50\,000$$

The shape of the interface between freshwater and saltwater is calculated using Eqs. 3.61 and 3.68 as shown below in **Table A3.1**.

Table A3.1 Freshwater saltwater interface

(x/H)		0	2	4	6	8	10
(h/H)	Eq. 3.61	0	0.362	0.512	0.627	0.724	0.810
	Eq. 3.68	0.023	0.363	0.513	0.628	0.725	0.810

Chapter 4

[Ans. 4.1]

Figure A4.1 shows a liquid water island between two solid particles in unsaturated medium. Water molecules evaporate from the boundary surface until the vapor pressure (p_v) becomes equal to the saturated vapor pressure (p_{v0}).

Static balance between pressure difference ($p - p_v$) and surface tension σ becomes: $(p - p_v) = 2\sigma/r$, where p = water pressure, σ = surface tension, and r = curvature radius. Now, using the gas law ($p_v v_{mv} = RT$) at temperature T, the energy balance is:

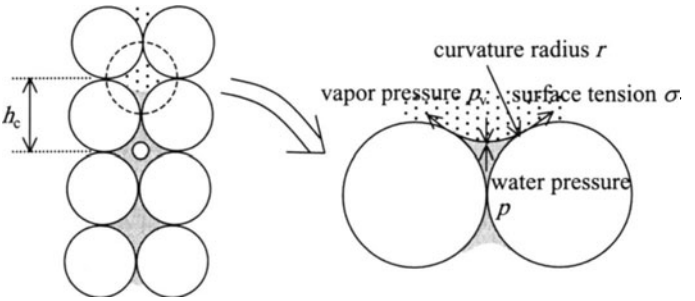

Fig. A4.1 Relationship between water pressure and surface tension

$$(2\sigma/r)v_{mw} = \int_{p_{v0}}^{p_v} v_{mv}\,dp = RT\log(p_v/p_{v0}) \tag{A4.1.1}$$

where v_{mv} = molar volume of vapor, R = gas constant, v_{mw} = molar volume of liquid water. Lord Kelvin (1824~1907) derived Eq. A4.1.1. Then, putting $(p_v/p_{v0}) = (\rho_v/\rho_{v0})$ and $h_c = (p_c/\rho g) = (p - p_v)/\rho g$, ρ = liquid water density, Eq. A4.1.1 is written by:

$$\rho_v = \rho_{v0}\exp(h_c g/RT) \tag{A4.1.2}$$

where ρ_v, ρ_{v0} = density of vapor at p_v and p_{v0}, respectively.

[Ans. 4.2]

Let us introduce saturated and unsaturated viscous fluid flows in capillary pipe models as shown in **Fig. A4.2**. Averaged velocity u_m for saturated viscous fluid flow is given by Poiseuille's law:

$$u_m = ki, \quad k = a^2\rho g/8\mu, \quad i = -(1/\rho g)dp/dx \tag{A4.2.1}$$

where k: hydraulic conductivity, a: radius of pipe, ρ: fluid density, μ: fluid viscosity, p: pressure, g: acceleration of gravity, and i: hydraulic gradient.

On the other hand, averaged velocity u_{um} of unsaturated flow within circular radius a and a_1 becomes (using unsaturated conductivity k_u):

$$u_{um} = k_u i, \quad k_u = \frac{\rho g}{8\mu}a^2\left[1 + (a_1/a)^2 - \frac{1-(a_1/a)^2}{\log(a/a_1)}\right] = \frac{\rho g}{8\mu}f(\theta) \tag{A4.2.2}$$

$$i = -\frac{1}{\rho g}\frac{dp}{dx}$$

$$f(\theta) = 2 - \theta - \theta/\log(1/\sqrt{1-\theta}), \quad \theta = 1 - (a_1/a)^2$$

In both hydraulic conductivities k and k_u, it has to be noted that temperature dependency on fluid viscosity μ is bigger than one of fluid density ρ in possible circumstance. Thus:

$$k = k_0\frac{\nu(T_0)}{\nu(T)}, \quad k_u = k_{u0}\frac{\nu(T_0)}{\nu(T)}, \quad \nu = \mu/\rho \quad \text{and} \quad k_u = k_0\frac{\nu(T_0)}{\nu(T)}f(\theta) \tag{A4.2.3}$$

where k_0, k_{u0}: k and k_u at reference temperature T_0 respectively.

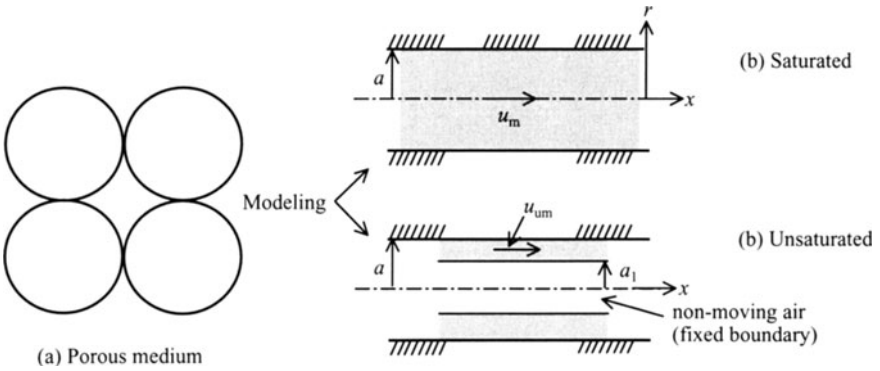

Fig. A4.2 Saturated and Unsaturated Flows in Capillary Pipe Model

Chapter 5

[Ans. 5.1]
The maximum possible time step is calculated using Eq. 5.20 as:

$$\Delta t \le \frac{1}{2}\frac{S}{kh}\left[1\Big/\left\{\frac{1}{(\Delta x)^2}+\frac{1}{(\Delta y)^2}\right\}\right] = \frac{1}{2}\left(\frac{0.2}{1.0\times 20}\right)\left[1\Big/\left\{\frac{1}{(5)^2}+\frac{1}{(5)^2}\right\}\right]$$
$$= (1/2)\,0.01\,(25/2) \approx 0.06\,\text{day}$$

[Ans. 5.2]
The interpolation functions at point $a(-0.8, 0.5)$ are obtained by using Eq. 5.36, as shown below.

$$N_1^e = (1/4)(1+0.8)(1-0.5) = 0.225, \quad N_2^e = (1/4)(1-0.8)(1-0.5) = 0.025$$
$$N_3^e = (1/4)(1-0.8)(1+0.5) = 0.075, \quad N_4^e = (1/4)(1+0.8)(1+0.5) = 0.675.$$

Therefore,

$$h_a = \sum_{k=1}^{4} h_k N_k^e = h_1 N_1^e + h_2 N_2^e + h_3 N_3^e + h_4 N_4^e$$
$$= 1.5\times 0.225 + 2\times 0.025 + 3\times 0.075 + 2.6\times 0.675$$
$$= 0.3375 + 0.05 + 0.225 + 1.755 = 2.3675\,\text{m}$$

[Ans. 5.3]
Referring to Eqs. 5.33–5.35, two times of element area $2\Delta_e$ is:

$$2\Delta_e = \begin{vmatrix} 1 & 2 & 1 \\ 4 & 1 & 1 \\ 3 & 4 & 1 \end{vmatrix} = (1-4) + 2\times(3-4) + (16-3) = 8$$

$a_1 = (1-4)/8 = -3/8, \quad b_1 = (3-4)/8 = -1/8, \quad c_1 = (4\times 4 - 3\times 1)/8 = 13/8$

$a_2 = (4-2)/8 = 2/8, \quad b_2 = (1-3)/8 = -2/8, \quad c_2 = (3\times 2 - 1\times 4)/8 = 2/8$

$a_3 = (2-1)/8 = 1/8, \quad b_3 = (4-1)/8 = 3/8, \quad c_3 = (1\times 1 - 4\times 2)/8 = -7/8$

Therefore, the interpolation functions are:

$$N_1 = -(3/8)x - (1/8)z + 13/8, \qquad N_2 = (2/8)x - (2/8)z + 2/8,$$
$$N_3 = (1/8)x + (3/8)z - 7/8$$

The coefficients in the simultaneous equations are calculated using Eq. 5.57 ($k_x = k_z = 1.0$) as follows:

$$A_{mn} = \int_R \left\{ \frac{\partial N_m}{\partial x}\frac{\partial N_n}{\partial x} + \frac{\partial N_m}{\partial z}\frac{\partial N_n}{\partial z} \right\} dR = (a_m a_n + b_m b_n) \int_R dR = (a_m a_n + b_m b_n)\Delta_e$$

For example:

$$A_{12} = [(-3/8)(2/8) + (-1/8)(-2/8)] \times 8 = -(4/8) = A_{21}$$

Therefore, the simultaneous equations for $r_m = 0$ are written as follows:

$$1/8\{10h_1 - 4h_2 - 6h_3\} = 0, \quad 1/8\{-4h_1 + 8h_2 - 4h_3\} = 0,$$
$$1/8\{-6h_1 - 4h_2 + 10h_3\} = 0$$

Note that these simultaneous equations are indeterminate since the boundary conditions are unknown.

[Ans. 5.4]

The groundwater head in the element is given by Eq. 5.51:

$$h = \sum_{n=1}^{3} N_n h_n$$

Therefore,

$$q_x = -k_x(\partial h/\partial x) = -k_x \sum_{n=1}^{3} (\partial N_n/\partial x) h_n$$
$$= -1[(-3/8)\,2 + (2/8)\,3 + (1/8)\,1.5] = -(1.5/8)\,\text{m/day}$$
$$q_z = -k_z(\partial h/\partial z) = -k_z \sum_{n=1}^{3} (\partial N_n/\partial z) h_n$$
$$= -0.5[(-1/8)\,2 + (-2/8)\,3 + (3/8)\,1.5] = (1.75/8)\,\text{m/day}$$

Note that for the squared element, as shown in **Fig. E5.1**, $(\partial N_n/\partial \xi) \neq$ constant, $(\partial N_n/\partial \eta) \neq$ constant, and their velocities are not constant but dependent on their position.

Chapter 6

[Ans. 6.1]
In the Lugeon test, when the injected water rate Q/L = 5 l/min/5 m = 1.0 l/min/m, then Lugeon value is 1 Lu. The permeability equivalent to it becomes:

$$k = [(2.3 \times 9.81 \times 8.33 \times 10^{-5})/(2 \times 3.14 \times 5 \times 9.81 \times 10^{2})] \times \log_{10}\{100/(4.5 \times 10^{-2})\}$$
$$= 2.04 \times 10^{-7}\ \text{m/s} = 2.04 \times 10^{-5}\ \text{cm/s}$$

[Ans. 6.2]
1. Theis' method:

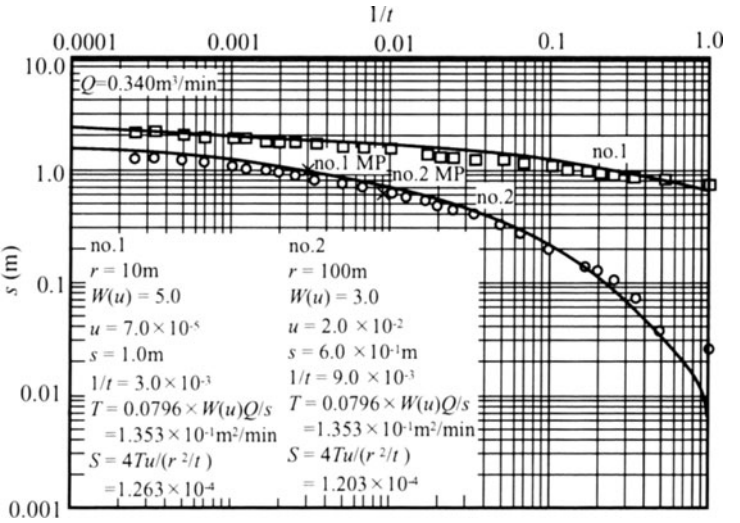

Fig. A6.1 Best fit of observed data using Theis' method

The observed data are plotted in **Fig. A6.1**. The match point (MP) of no. 1 well is found from the best fit curve [$u \sim W(u)$]. The values $W(u)$ = 5.0, $u = 7.0 \times 10^{-5}$, s = 1.0 m, $1/t = 3.0 \times 10^{-3}$ are then determined. Thus, T and S are given by the following calculation from Eq. 6.2:

$$T = (1/4\pi)QW(u)/s = (0.0796 \times 0.340 \times 5.0)/1.0 = 1.353 \times 10^{-1}\ (\text{m}^2/\text{min}),$$

and from Eq. 6.1,

$$S = 4Tu/(r^2/t) = (4 \times 1.353 \times 10^{-1} \times 7.0 \times 10^{-5})/(10^2 \times 3.0 \times 10^{-3})$$
$$= 1.263 \times 10^{-4}$$

Then, $k = 1.35 \times 10^{-2}$ m/min, $S_s = 1.26 \times 10^{-5}$/m. In a similar way, MP of well no. 2 is found, and $T = 1.353 \times 10^{-1}$ m^2/min, $S = 1.203 \times 10^{-4}$.

2. Jacob's method (*t*-*s* data)

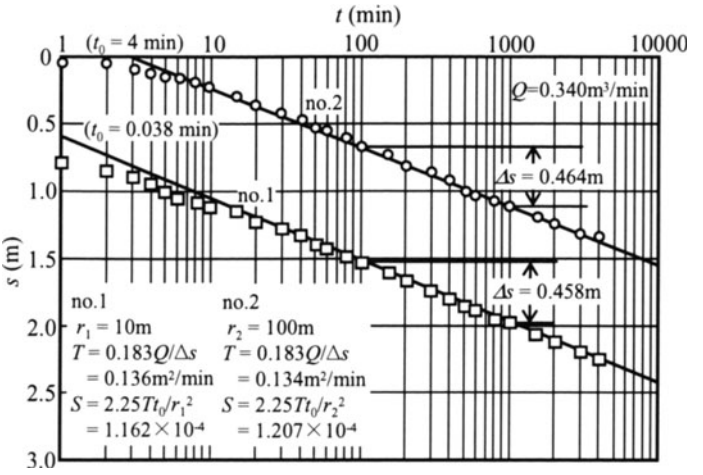

Fig. A6.2 Best fit of observed data using Jacob's method (*t*-*s* data)

The observed data are plotted as shown in **Fig. A6.2**. $\Delta s = 0.458$ m and $t_0 = 0.038$ min for no. 1 well. Then, from Eq. 6.3:

$$T = (0.183Q)/\Delta s = (0.183 \times 0.340)/0.458 = 0.136\,\text{m}^2/\text{min}$$

Similarly, from Eq. 6.4:

$$S = (2.25Tt_0)/r_{i=1}^2 = (2.25 \times 0.136 \times 0.038)/(10)^2 = 1.162 \times 10^{-4}$$

Then, $k = 1.36 \times 10^{-2}$ m/min, $S_s = 1.16 \times 10^{-5}$/m. By the same procedure for no. 2 well, $T = 0.134$ m^2/min, $S = 1.207 \times 10^{-4}$.

3. Jacob's method (*r*-*s* data)

The observed data at $t = 100$ min are plotted as shown in **Fig. A6.3**. Then, $\Delta s = 0.878$ m and $r_{i=2} = 550$ m. From Eq. 6.5:

$$T = (0.366Q)/\Delta s = (0.366 \times 0.340)/0.878 = 1.42 \times 10^{-1}\,\text{m}^2/\text{min}$$

Similarly, from Eq. 6.6:

$$S = (2.25Tt)/r_{i=2}^2 = (2.25 \times 1.42 \times 10^{-1} \times 100)/(550)^2 = 1.06 \times 10^{-4}$$

and $k = 1.42 \times 10^{-2}$ m/min, $S_s = 1.06 \times 10^{-5}$/m.

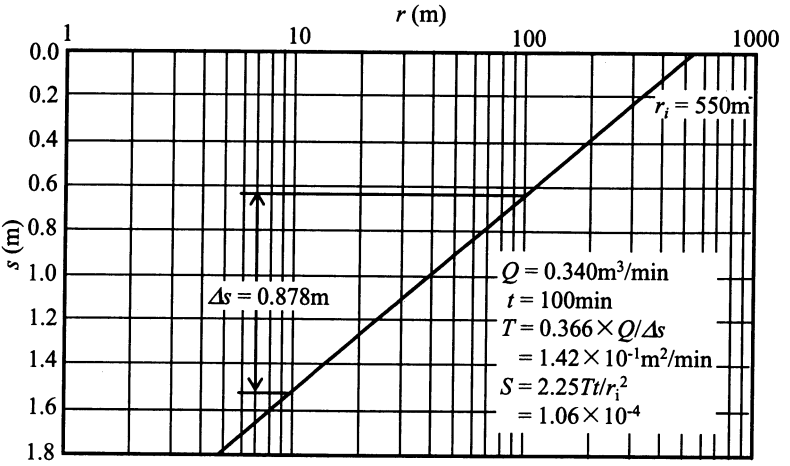

Fig. A6.3 Best fit of observed data using Jacob's method (r-s data)

Chapter 7

[Ans. 7.1]

Type (a): There will be often observed in an unconfined shallow aquifer, because groundwater level synchronizes with natural recharge in rainy season. No land subsidence will occur in such a case.

Type (b): Confined aquifers with much groundwater pumping in summer results in a water head reduction. Land subsidence possibly appears.

Type (c): The trend in summer is similar to type (b); groundwater head depression in winter is also observed. Land subsidence may be accelerated due to double depression.

[Ans. 7.2]

1. Land subsidence does not appear when the minimum groundwater head is about 2 m, as shown in **Fig. A7.1**.
2. The land subsidence becomes zero when a discharge of 36 000 m^3/year is realized, as shown in **Fig. A7.2**.
3. As seen in **Fig. A7.2**, a linear relationship is found between pumping discharge and minimum groundwater head.

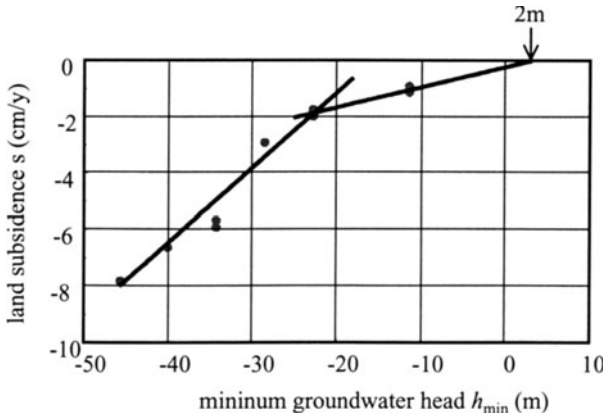

Fig. A7.1 Relationship between minimum groundwater head and land subsidence

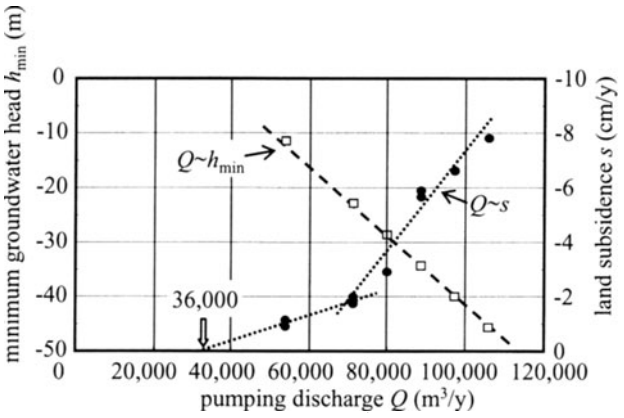

Fig. A7.2 Relationship between pumping discharge and groundwater head as well as land subsidence

Index